

LAWRENCE TECHNOLOGICAL UNIVERSITY

A. Leon Linton Department of Mechanical Engineering

New Approaches to Predict Fatigue Parameters of Steels from Monotonic Properties and Estimation of Elasto-Plastic Localized Stresses and Strains

Submitted in partial fulfillment of the requirements for the degree of

Doctor of Engineering in Mechanical Engineering (DEME)

by

Rafaa M. R. Esmaael



DEME COMMITTEE

Dr. Vernon Fernandez, Associate Prof, Academic Advisor Mechanical Engineering.

Dr. Chris Riedel, Associate Professor, Mechanical Engineering.

Dr. Giscard Kfoury, Associate Professor, Mechanical Engineering.

Dr. Abolhassan Khosrovaneh, Adjunct Faculty, General Motors Corporation (GM).

Dr. Changgong Zhou, Associate Professor, Department of Natural Science.

July, 2015

I

ProQuest Number: 3726480

All rights reserved

INFORMATION TO ALL USERS

The quality of this reproduction is dependent upon the quality of the copy submitted.

In the unlikely event that the author did not send a complete manuscript and there are missing pages, these will be noted. Also, if material had to be removed, a note will indicate the deletion.



ProQuest 3726480

Published by ProQuest LLC (2015). Copyright of the Dissertation is held by the Author.

All rights reserved.

This work is protected against unauthorized copying under Title 17, United States Code
Microform Edition © ProQuest LLC.

ProQuest LLC.
789 East Eisenhower Parkway
P.O. Box 1346
Ann Arbor, MI 48106 - 1346

LAWRENCE TECHNOLOGICAL UNIVERSITY

A. Leon Linton Department of Mechanical Engineering

New Approaches to Predict Fatigue Parameters of Steels from Monotonic Properties and Estimation of Elasto-Plastic Localized Stresses and Strains

Submitted in partial fulfillment of the requirements for the degree of

Doctor of Engineering in Mechanical Engineering (DEME)

by

Rafaa M. R. Esmaael



Approved by:

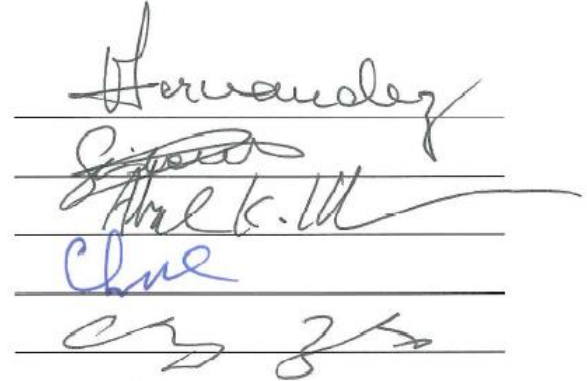
Dr. Vernon Fernandez, (Academic Advisor)

Dr. Giscard Kfoury

Dr. Abolhassan Khosrovaneh

Dr. Chris Riedel

Dr. Changgong Zhou



ABSTRACT

Fatigue strain - life prediction model depends on six material fatigue parameters, fatigue strength coefficient σ'_f , fatigue strength exponent b , fatigue ductility coefficient ϵ'_f , fatigue ductility exponent c , cyclic strength coefficient K' , and cyclic strain hardening exponent n' .

In this study, a new nonlinear correlation between the Brinell hardness HB and ultimate tensile strength is proposed. The prediction results obtained from this model were compared with the results obtained using Roessle-Fatemi's method and experimental data. The correlation factor in the proposed model is higher than that found in the current literature.

The ultimate tensile strength is replaced by an equivalent Brinell hardness HB expression in the Modified Universal Slopes strain-life prediction model. This change results in σ'_f and ϵ'_f fatigue parameters these parameters predicted using Brinell hardness HB. The new fatigue life prediction model was compared with the original Modified Universal Slopes model, and experimental data in the literature.

This model is valid for steels with hardness that ranges from 150HB to 660HB. The model is compared qualitatively and quantitatively with the Modified Universal Slopes life fatigue prediction model and experimental data. Different types of steels were employed to validate this model. The results show that the proposed model provides better fatigue life prediction when compared to the Modified Universal Slopes model, and experimental data. An accurate prediction of elasto-plastic cyclic deformation becomes extremely important in design optimization by providing accurate fatigue life prediction and that results in weight savings. Notch root stress-strain prediction is controlled by the two material parameters K' and n' . In this study a two-stage notch root prediction method is proposed. This was implemented using a correction factor to Neuber's rule notch strain amplitude as the first stage, and a linear interpolation scheme, between the results obtained from the first stage and elastic finite element analysis, as the second stage. The accuracy of this method is assessed by comparing the predicted results with the results obtained from elasto-plastic finite element analysis and Neuber's rule results. Various steels with different yield strengths were used in this study. Notch deformation behavior under cyclic fully reversed

as well as variable amplitude loading conditions was monitored for a double notched flat plate and a circumferentially notched round bar to cover plane stress and plane strain conditions. Elastic as well as elasto-plastic finite element analyses were performed. Notch strain amplitudes in addition to fatigue life predictions obtained using the proposed method are in good agreement with the elasto-plastic finite element analysis when compared to predictions obtained using Neuber's rule. ABAQUS 6.13 software was used for elastic and elasto-plastic finite element analysis. Analytical methods together with fe-safe 6.5 software were used to obtain fatigue life under each loading condition.

*Dedicated To my Parents, Wife, Kids
and Siblings
This humble work is a sign of my love
to you!*

Copyright 2015, Rafea Esmaael

All right reserved

v

Acknowledgments

I would never have been able to finish my dissertation without the helpful guidance of several individuals whose contribution and assistance aided in the preparation of this research study. First and foremost, I would like to express my sincere gratitude to my advisor Dr. Vernon Fernandez, my academic supervisor for his encouragement patience, motivation, enthusiasm and support throughout this research.

Besides my advisor, I would like to thank my thesis committee: Dr. Abolhassan Khosrovaneh, GM, Dr. Chris Riedel, Associate Professor, Mechanical Engineering, Dr. Gischarad Kafury, Associate Professor, Mechanical Engineering, Dr. C. Zhou, Associate Professor, Department of Natural Sciences, for their encouragement and insightful comments. I would like to express my deepest gratitude to Dr. Badih Jawad, Department Chair for his excellent guidance, caring, patience.

1 TABLE OF CONTENTS

1.	INTRODUCTION	1
1.1	FATIGUE	1
1.2	HARDNESS	3
1.3	STRESS- STRAIN BEHAVIOR UNDER CYCLIC DEFORMATION	6
1.4	FATIGUE TESTS.....	11
1.4.1	Fatigue loading.....	11
1.5	STRESS-LIFE (S-N) APPROACH.....	12
1.5.1	Mean Stress Effect on S-N Behavior	14
1.5.2	Factors that Affect the S-N Behavior.....	15
1.5.3	S-N Approximations	15
1.6	THE STRAIN-LIFE (ϵ -N) APPROACH.....	16
1.6.1	Mean Stress Effects on Strain-Life Approach	18
1.7	NOTCH EFFECT	19
1.7.1	Stress Concentration Factor	19
1.7.2	Plane Stress and Plane Strain.....	24
1.7.2.1	Plane Stress	24
1.7.2.2	Plane Strain	24
1.8	MOTIVATION	25
2	LITERATURE SEARCH:.....	26
2.1	CORRELATIONS BETWEEN CYCLIC DEFORMATIONS WITH TENSILE PROPERTIES....	26
2.1.1	Existing methods that estimate ultimate tensile strength	26
2.1.1.1	For Steels	26
2.1.1.2	For Non-Ferrous Materials	29
2.1.2	Existing Correlations between Monotonic Tensile Properties and Fatigue Cyclic Deformation Properties.	30
2.1.3	Estimation of Fatigue Parameters using Monotonic Tensile Properties.	33
2.1.4	Commonly Used Notch Stress-Strain Models	37
2.1.4.1	Linear rule.....	37

2.1.4.2	Neuber's Rule	38
2.1.4.3	Glinka's Rule	41
2.2	PLASTICITY	49
2.2.1	Failure Theories	50
2.2.1.1	Von Mises	50
2.2.1.2	Maximum Shear Stress Theory (Tresca)	56
2.2.2	Isotropic and Kinematic Hardening	58
2.2.2.1	Isotropic Hardening	58
2.2.2.2	Kinematic Hardening	59
2.2.2.3	Prager Rule.....	60
2.2.2.4	Armstrong and Frederick	61
2.2.2.5	Mroz Model	62
2.2.2.6	Garud.....	63
2.2.2.7	Wang and Ohno	64
2.2.2.8	Chaboche.....	64
2.2.2.9	Initial Hardening Modulus.....	65
2.2.2.10	Nonlinear Recall Parameters.....	67
2.2.2.11	Multiple Kinematic Hardening Models	68
2.2.3	Identification of Parameter	69
2.2.4	Combined Kinematic-Isotropic Hardening Model	72
2.2.5	Multiaxial State of Stress	73
2.2.6	Finite Element Analysis	73
3	STATEMENT OF PROBLEM AND THEORY	75
3.1	THE STRAIN-LIFE PREDICTION MODEL.....	75
3.1.1	Objectives	76
3.2	NOTCH STRAIN PREDICTION MODELS.....	77
3.2.1	Notch Geometry.....	78
4	PERFORMING PREDICTION METHODS.....	79
4.1	PERFORM FATIGUE PROPERTIES ESTIMATION MODEL	79
4.1.1	Correlations Among Tensile Data	79

4.1.2	Evaluation of the Proposed Strain-Life Estimation Method.....	85
4.1.2.1	Qualitative Evaluation	85
4.1.2.2	Quantitative Evaluation	89
4.2	THE NOTCH ROOT STRAIN PREDICTION MODEL TECHNIQUE.....	91
4.2.1	Methodology.....	94
4.2.2	Developing a Prediction Method.	96
4.2.3	Evaluation of the Proposed Method.....	100
5	RESULTS AND DISCUSSIONS.....	102
5.1	ULTIMATE TENSILE STRENGTH HB CORRELATION MODEL.....	102
5.2	STRAIN-LIFE PREDICTION PROPOSED METHOD	102
5.3	NOTCH ROOT PREDICTION MODEL	107
6	CONCLUSIONS	119
7	APPENDIX A.....	122
8	APPENDIX B.....	142
9	APPENDIX C.....	171
	Fatigue test machines.....	171
	Fatigue Test Specimens	172
10	REFERENCES	176

LIST OF TABLES

Table 1 Correlation between Strain Hardening Exponent and Material's Behavior [21].	33
Table 2 Estimation Methods for Coffin-Manson's Parameters.....	35
Table 3 Ranking of Estimation Methods in Total Predictability for each Material Group [18].....	37
Table 4 Summary of Von Mises Criterion at Different Stress Conditions.....	57
Table 5 Ultimate Tensile Strength Values Obtained from Proposed Method and Rossel-Fatemi Compared with Experimental Data.....	81
Table 6 Estimated Ultimate Tensile Strength Quantitative Analysis	84
Table 7 Strain-Life Quantitative Analysis	90
Table 8 Fatigue Parameters Obtained from the Proposed and Modified Universal Slopes Methods.....	103
Table 9 Root Stress-Strain for Flate Plate under Completely Reversed Cyclic Loading	107
Table 10 Results Obtained from RQC-100 under Completely Reversed Nominal Stress.	109
Table 11 Results Obtained from SAE1045 under Completely Reversed Nominal Stress.	110
Table 12 Results Obtained from SAE1050M under Completely Reversed Nominal Stress.	111
Table 13 Results Obtained from SAE1050M under Completely Reversed Nominal Stress.	112
Table 14 Ultimate Tensile Strength Obtained from Proposed, Roessle-Fatemi $S_u - HB$ Correlation Models Compared with Experimental Data.	122
Table 15 Results Obtained from SAE1141V under Variable Amplitudes	142
Table 16 Results Obtained from RQC-100 under Variable Amplitudes	143
Table 17 Results Obtained from SAE1038 under Variable Amplitudes	144
Table 18 Results Obtained from SAE1050M under Variable Amplitudes.....	145
Table 19 Results Obtained from SAE1117 under Variable Amplitudes	146
Table 20 Results Obtained from SAE15V24 under Variable Amplitudes	147

Table 21 Results Obtained from SAE1141Nb under Variable Amplitudes	148
Table 22 Results Obtained from SAE1045 under Variable Amplitudes	149
Table 23 Results Obtained from SAE1141”A ₂ ” under Variable Amplitudes	150

TABLE OF FIGURES

Figure 1 Elastic, Plastic and Total Strain [1]	2
Figure 2 True Stress vs True Strain for 11V41 Steel [1].	3
Figure 3 Formulas and the Indentation Geometry of Brinell Hardness [3].	5
Figure 4 Representation of Bauschinger Effect (a) Specimen under Tension (b) Specimen under Compression (c) Tension Followed by Compression.	7
Figure 5 Stress-Strain Relationship for Copper under Cyclic Strain-Controlled Axial Load (a) Fully Annealed (b) Partially Annealed (c) Cold Worked [1].	7
Figure 6 Variation of Stress under Constant Strain Amplitude (a) Cyclic Hardening Condition (b) Cyclic Softening Condition	8
Figure 7 Stabilized Cyclic Stress-Strain Hysteresis Loop	9
Figure 8 Stable hysteresis loop for determining the cyclic stress-strain curve and comparison with the monotonic stress-strain curve for Man-Ten steel [1].	10
Figure 9 Cyclic and Monotonic Stress-Strain Curves for Different Materials [5]	10
Figure 10. Typical S-N Diagram	12
Figure 11 Relation between Rotating Bending Endurance Limit and Tensile Strength of Wrought Steel [6].	13
Figure 12 Mean Stress Effect on S-N Behavior [1].	14
Figure 13 Basquin S-N Curve [1]	15
Figure 14 Typical Strain-Life Curve for SAE 1141 VFG	17
Figure 15 Density of Internal Force Lines around the Hole	19
Figure 16 Stress Distribution on a Tension Plate with Hole.	20
Figure 17 Maximum and minimum stress in rectangular notched bar under axial tension.	21
Figure 18 Maximum and minimum stress for a notched shaft under axial tension	22
Figure 19 Variation of K_t with r/w Ratio [12].	23
Figure 20 Schematic Representations of Notch Root Plane Stress and Plane Strain	24
Figure 21 Ultimate Tensile Strength vs. Brinell Hardness [15].	27

Figure 22 Comparison of the Predicted and Experimental S_u for (a) Unalloyed Steel (b) Low-Alloy Steel (c) High-alloy Steels [18].	29
Figure 23 Comparison of Stress Ratio at 1-Percent Strain with Virgin Tensile Properties [19].	30
Figure 24 Comparison of Predicted and Experimental Fatigue Lives for low-alloy Steel [18].	34
Figure 25, Average Prediction Ratio versus Strain Amplitude [32].	36
Figure 26 Determination of Monotonic Notch Strain using Neuber's Rule	39
Figure 27 Cyclic Notch Stress-Strain Determination for Constant Amplitude using Neuber's Rule.	40
Figure 28 Planes Passing through Point P in a body under Applied Surface Forces.	51
Figure 29 Von Mises/Tresca Yield Surfaces in Principal Stress Coordinates [59].	56
Figure 30 Schematic Representation of Isotropic Hardening "same shape, different size"	58
Figure 31 Kinematic Hardening Representation "same shape, same size"	59
Figure 32 Isotropic and Kinematic Hardening under Cyclic Loading.	60
Figure 33 Schematic Representation of Linear Kinematic Hardening	66
Figure 34 Stress-Strain Behavior of Linear Kinematic Hardening Model.	66
Figure 35 Small Strain	67
Figure 36 High Strain.	68
Figure 37 Effect of Kinematic Hardening Parameters Numbers	69
Figure 38 Half Cycle of Stress-Strain Data	70
Figure 39 Identification of Coefficients C and γ from Three Tension-Compression Cycles of Different Strain Amplitudes.	72
Figure 40 Some Types of Elements in ABAQUS	74
Figure 41 Notched Configurations (a) Notched Plate with 2.77 mm Radius (b) Circumference Notched Round bar with 1.588 mm Radius	78
Figure 42 Predicted vs Experimental Ultimate Tensile Strength.	82
Figure 43 Estimated, Experimental Data Ratio versus Brinell Hardness (HB)	82

Figure 44 Comparison between Four Prediction Approaches for SAE 4140, HB409 Steel	86
Figure 45 Comparison between Four Prediction Approaches for SAE 1141, HB277 Steel	87
Figure 46 Comparison between Four Prediction Approaches for SAE 1070, HB280 Steel	87
Figure 47 Comparison Between four Prediction Approaches for SAE H-11, HB660 Steel	88
Figure 48 Comparison of the Predicted and Experimental Fatigue Lives for Different Alloys	89
Figure 49 One-Fourth of Flat Plate Finite Element Model.....	92
Figure 50 Mesh Configuration for the Area around Notched Plate.....	92
Figure 51 Axisymmetric two Dimensional Model for Round Bar.	93
Figure 52 Mesh Distribution around the Round Bar Notch.....	93
Figure 53 Cyclic Stress-Strain Curves for Different Steels	95
Figure 54 Variation of $\delta\varepsilon$ with Different m Values	97
Figure 55 Variation of δ with K' at Fixed Value of m & S	98
Figure 56 Interpolation Assumption by Calladine [73]	99
Figure 57 Applied Nominal Stress for Different Geometries.....	101
Figure 58 Actual/ Predicted Fatigue Strength Ratio vs Actual Values.....	104
Figure 59 Comparison of Predicted Fatigue Ductility Coefficient with Experimental Data	105
Figure 60 Local Strain Obtained from Elasto-Plastic FEA, Neuber Rule and Proposed Method	113
Figure 61 Local Strain Obtained from Elasto-Plastic FEA, Neuber Rule and Proposed Method	113
Figure 62 Local Strain Obtained from Elasto-Plastic FEA, Neuber Rule and Proposed Method	114
Figure 63 Local Strain Obtained from Elasto-Plastic FEA, Neuber Rule and Proposed Method	114

Figure 64 Local Strain Obtained from Elasto-Plastic FEA, Neuber Rule and Proposed Method	115
Figure 65 Local Strain Obtained from Elasto-Plastic FEA, Neuber Rule and Proposed Method	115
Figure 66 Local Strain Obtained from Elasto-plastic FEA, Neuber Rule and Proposed Method	116
Figure 67 Local Strain Obtained from Elasto-Plastic FEA, Neuber Rule and Proposed Method	116
Figure 68 Snapshot from ABAQUS Viewer for Strain Contours of Flat Plate under Tensile Cyclic Load.	117
Figure 69 Snapshot using fe-safe/ABAQUS Viewer for Fatigue Life Contours of Flat Plate under Tensile Cyclic Load.	117
Figure 70 Snapshot from ABAQUS Viewer for Strain Contours of Round Bar under Tensile Cyclic Load.	118
Figure 71 Snapshot using fe-safe/ABAQUS Viewer Fatigue Life Contours of Round Bar under Tensile Cyclic Load.....	118
Figure72 Comparison between Three Prediction Approaches for SAE 15B35, HB286 Steel.....	129
Figure 73 Comparison between Three Prediction Approaches for SAE 1141, HB223 Steel	129
Figure 74 Comparison between Three Prediction Approaches for SAE 8620,HB326 Steel	130
Figure75 Comparison between Three Prediction Approaches for SAE A538C,HB480 Steel.....	130
Figure 76 Comparison between Three Prediction Approaches for SAE1015,HB130 Steel	131
Figure77, Comparison between Three Prediction Approaches for SAE41B17, HB277 Steel.....	131
Figure 78 Comparison between Three Prediction Approaches for SAE 1090, HB309 Steel	132

Figure79 Comparison between Three Prediction Approaches for SAE1050M,HB220 Steel.....	132
Figure 80 Comparison between Three Prediction Approaches for SAE 1541,HB195 Steel	133
Figure 81 Comparison between Three Prediction Approaches for SAE4340,HB350 Steel	133
Figure 82 Comparison between Three Prediction Approaches for SAE1090,HB259 Steel	134
Figure 83 Comparison between Three Prediction Approaches for SAE1117,HB193 Steel	134
Figure 84 Comparison between Three Prediction Approaches for SAE1141V,HB217 Steel.....	135
Figure 85 Comparison between Three Prediction Approaches for SAE1151V,HB251 Steel.....	135
Figure 86 Comparison between Three Prediction Approaches for SAE1541,HB180 Steel	136
Figure 87 Comparison between Three Prediction Approaches for SAE1541,HB250 Steel	136
Figure 88 Comparison between Three Prediction Approaches for SAE4620,HB289 Steel	137
Figure 89 Comparison between Three Prediction Approaches for SAE1045,HB222 Steel	137
Figure 90 Comparison between Three Prediction Approaches for SAE5150,HB245 Steel	138
Figure 91 Comparison between Three Prediction Approaches for SAE8620,HB430 Steel	138
Figure 92 Comparison between Three Prediction Approaches for AISI-310,HB145 Steel	139
Figure 93 Comparison between Three Prediction Approaches for AISI-Ni8,HB170 Steel	139

Figure 94 Comparison between Three Prediction Approaches for AISI304,HB327 Steel	140
Figure 95 Comparison between Three Prediction Approaches for Man-Ten,HB150 Steel	140
Figure 96 Comparison between Three Prediction Approaches for VAN-80,HB225 Steel	141
Figure 97 Comparison between Three Prediction Approaches for AM-350,HB325 Steel	141
Figure 98 Notch Root Strain Amplitude vs Reversals for Flat Plate of SAE1141V	151
Figure 99 Notch Root Strain Amplitude vs Reversals for Round Bar of SAE1141V	151
Figure 100 Cycles to Failure vs Strain Range and Mean Stress for SAE1141V	152
Figure 101 Cycles to Failure vs Strain Range and Mean Stress for SAE1141V	152
Figure 102 Notch Root Strain Amplitude vs Reversals for Flat Plate of RQC-100	153
Figure 103 Notch Root Strain Amplitude vs Reversals for Round Bar of RQC-100	153
Figure 104 Cycles to Failure vs Strain Range and Mean Stress for RQC-100 Flat Plate	154
Figure 105 Cycles to Failure vs Strain Range and Mean Stress for RQC-100 Round Bar	154
Figure 106 Notch Root Strain Amplitude vs Reversals for Flat Plate of SAE1038	155
Figure 107 Notch Root Strain Amplitude vs Reversals for Round Bar of SAE1038	155
Figure 108 Cycles to Failure vs Strain Range and Mean Stress for SAE1038 Flat Plate	156
Figure 109 Cycles to Failure vs Strain Range and Mean Stress forSAE1038 Round Bar	156
Figure 110 Notch Root Strain Amplitude vs Reversals for Flat Plate of SAE1050M	157
Figure 111 Notch Root Strain Amplitude vs Reversals for Round Bar of SAE1050M	157
Figure 112 Cycles to Failure vs Strain Range and Mean Stress for SAE1050M Flat Plate	158
Figure 113 Cycles to Failure vs Strain Range and Mean Stress forSAE1050M Round Bar	158

Figure 114 Notch Root Strain Amplitude vs Reversals for Flat Plate of SAE1117	159
Figure 115 Notch Root Strain Amplitude vs Reversals for Round Bar of SAE1117.....	159
Figure 116 Cycles to Failure vs Strain Range and Mean Stress for SAE1117 Flat Plate	160
Figure 117 Cycles to Failure vs Strain Range and Mean Stress for SAE1117 Round Bar	160
Figure 118 Notch Root Strain Amplitude vs Reversals for Flat Plate of SAE15V24	161
Figure 119 Notch Root Strain Amplitude vs Reversals for Round Bar of SAE15V24..	161
Figure 120 Cycles to Failure vs Strain Range and Mean Stress for SAE15V24 Flat Plate	162
Figure 121 Cycles to Failure vs Strain Range and Mean Stress for SAE15V24 Round Bar	162
Figure 122 Notch Root Strain Amplitude vs Reversals for Flat Plate of SAE1141Nb ..	163
Figure 123 Notch Root Strain Amplitude vs Reversals for Round Bar of SAE1141Nb	163
Figure 124 Cycles to Failure vs Strain Range and Mean Stress for SAE1141Nb Flat Plate	164
Figure 125 Cycles to Failure vs Strain Range and Mean Stress for SAE1141Nb Round Bar.....	164
Figure 126 Notch Root Strain Amplitude vs Reversals for Flat Plate of SAE1045	165
Figure 127 Notch Root Strain Amplitude vs Reversals for Round Bar of SAE1045.....	165
Figure 128 Cycles to Failure vs Strain Range and Mean Stress for SAE1045 Flat Plate	166
Figure 129 Cycles to Failure vs Strain Range and Mean Stress for SAE1045 Round Bar	166
Figure 130 Notch Root Strain Amplitude vs Reversals for Flat Plate of SAE1141	167
Figure 131 Notch Root Strain Amplitude vs Reversals for Round Bar of SAE1141.....	167
Figure 132 Cycles to Failure vs Strain Range and Mean Stress for SAE1141 Flat Plate	168
Figure 133 Cycles to Failure vs Strain Range and Mean Stress for SAE1141 Round Bar	168

Figure 134 Hysteresis loops for RQC-100 Flat Plate	169
Figure 135 Hysteresis Loops for SAE1141V Flat Plate	169
Figure 136 Hysteresis loop for SAE1050M Flat Plate	170
Figure 137 Nonuniform bending moment machine.....	173
Figure 138 Uniform bending moment machine.....	173
Figure 139 Constant deflection amplitude cantilever bending machine.....	174
Figure 140 Axial loaded fatigue test machine	174
Figure 141 Closed-loop Servohydraulic test system including personal computer [74].	175
Figure 142 different types of fatigue test specimens [1].....	175

1. INTRODUCTION

1.1 FATIGUE

Fatigue is defined as a material failure under cyclic loading. At least half of all mechanical failures are due to fatigue. Estimates state that 50 to 90 percent of all mechanical failures are fatigue failures; most of these failures are unexpected [1]. Fatigue failures usually happen with little or no warning.

The American Society for Testing and Materials (ASTM), define fatigue as the progressive, localized, and permanent structural change that occurs in a material subjected to repeated or fluctuating strain at nominal stresses with maximum values less than the tensile strength of the material [1]. For fatigue to occur a cyclic plastic deformation should occur at stress concentration regions where the stress is greater than the material tensile strength despite the nominal stress still in the elastic region.

The yield point in the stress-strain curve is defined as the point at which plastic deformation occurs and Hook's law no longer holds true. The yield criterion is defined as the elastic limit of elasticity under a combination of stresses. For some materials the yield point is not easily defined, in such cases, the offset method is used; this method is based on using a 0.2% strain (.002in/in), a line parallel to the initial straight-line portion of stress-strain curve is drawn, the yield point is the point where this line intersect the curve, the stress at this point of intersection is called the yield strength of material. An increase in stress past the yield point results in a curve that rises continuously but becomes flatter until it reaches a maximum stress referred to as the ultimate stress, σ_u . the rise in the curve in this manner is called strain hardening of the material [2].

Total engineering strain (ϵ) is a combination of the two components: elastic strain, $\epsilon_e = \sigma/E$, and plastic strain ϵ_p . Figure 1, shows schematic of elastic and plastic strain curve

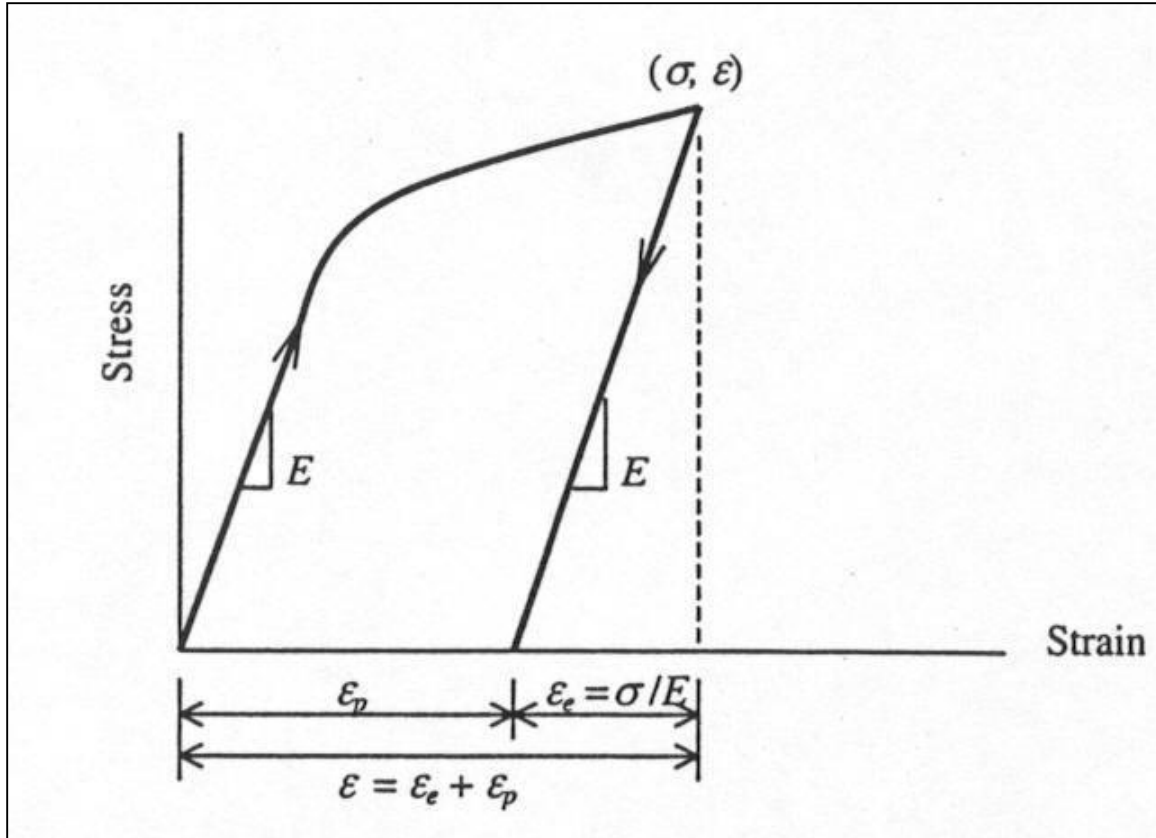


Figure 1 Elastic, Plastic and Total Strain [1]

The relationship between true plastic stress as a function of true plastic strain is a power function equation given by:

$$\sigma = K(\epsilon_p)^n \quad (1)$$

Where (k) and (n) are the strength coefficient and strain hardening exponent of the material respectively.

A plot of true plastic stress versus true plastic strain on a log-log scale results in a linear curve shown in Figure 2 for 11V41 steel.

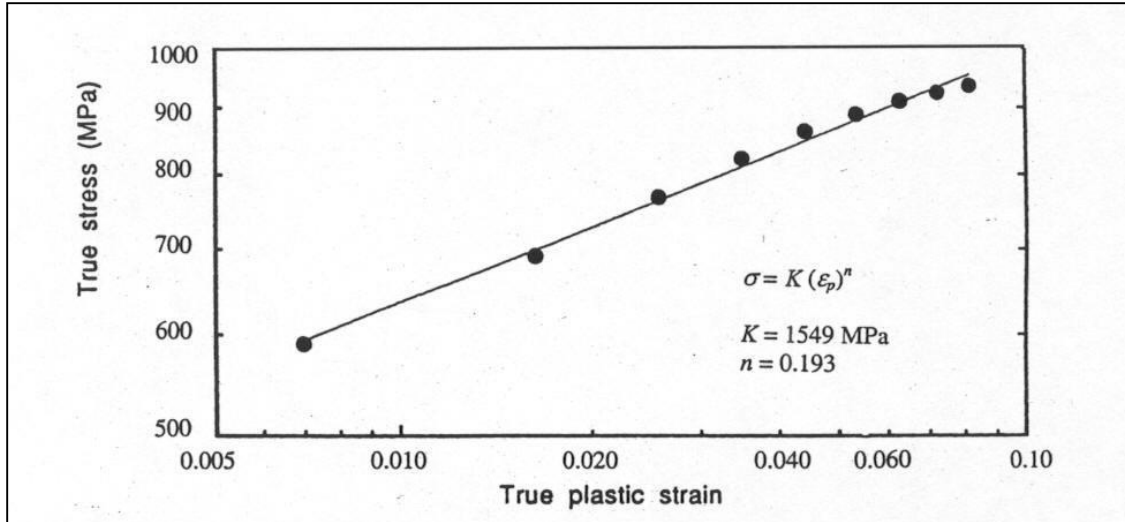


Figure 2 True Stress vs True Strain for 11V41 Steel [1].

Combining elastic and plastic true strain equations results in the total strain equation given by:

$$\varepsilon = \varepsilon_e + \varepsilon_p = \frac{\sigma}{E} + \left(\frac{\sigma}{K}\right)^{\frac{1}{n}} \quad (2)$$

The value of (n) represents the ability of the material to work harden and ranges from 0 to 0.5 for steels.

1.2 HARDNESS

Hardness is defined as the resistance of solid material to a permanent shape change when pressure is applied on its surface. Hardness depends generally on many material properties such as, ductility, strength, toughness, and plasticity.

Three types of measurements are commonly used for hardness, Scratch hardness, Indentation hardness and Rebound hardness.

- a) Scratch hardness, is the measure of the resistance of the material surface to fracture due to friction of a sharp object.

- b) Rebound hardness, sometimes called ‘dynamic hardness’ measure the height of the “bound” of a diamond-tipped hammer dropped from a fixed height on to the material surface.
- c) Indentation hardness is the resistance of a material surface to a constant compression load. The test is based on measuring of indentation left by a specifically dimensioned indenter. There are four common indentation hardness scales, Rockwell, Shore, Vickers and Brinell.

Brinell hardness scale was proposed by Swedish engineer Johan August Brinell in 1900. The typical test is based on using 10 mm diameter steel ball with 3000 kgf. The Brinell hardness calculations is calculated using the equation:

$$BHN = \frac{2P}{\pi D(D - \sqrt{D^2 - d^2})} \quad (3)$$

Where:

- P = applied force (kgf)
- D = diameter of indenter (mm)
- d = diameter of indentation (mm)

Figure 3 shows the geometrics and specifications for hardness testing.

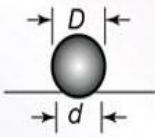
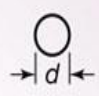


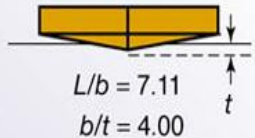

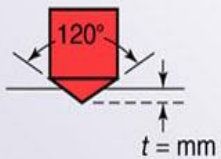

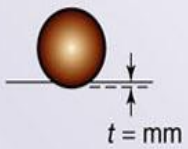

Test	Indenter	Shape of indentation		Load, P	Hardness number
		Side view	Top view		
Brinell	10-mm steel or tungsten carbide ball			500 kg 1500 kg 3000 kg	$HB = \frac{2P}{(\pi D)(D - \sqrt{D^2 - d^2})}$
Vickers	Diamond pyramid			1-120 kg	$HV = \frac{1.854P}{L^2}$
Knoop	Diamond pyramid			25 g-5 kg	$HK = \frac{14.2P}{L^2}$
Rockwell					
A } C } D }	Diamond cone			60 kg 150 kg 100 kg	HRA } HRC } HRD } = 100 - 500t
B } F } G }	$\frac{1}{16}$ - in. diameter steel ball			100 kg 60 kg 150 kg	HRB } HRF } HRG } = 130 - 500t
E	$\frac{1}{8}$ - in. diameter steel ball			100 kg	HRE }

Figure 3 Formulas and the Indentation Geometry of Brinell Hardness [3].

1.3 STRESS- STRAIN BEHAVIOR UNDER CYCLIC DEFORMATION

The stress-strain behavior under a monotonic test is different from the behavior under cyclic test. This difference was observed by Bauschinger in 1886. He discovered that the yield strength in tension or compression is reduced after applying a load of opposite sign which cause inelastic deformation.

This can be clearly seen in Figure 4, where the yield strength in compression is significantly reduced prior yielding in tension [1].

Morrow [4] carried out tests on three copper specimens heat treated as: (a) fully annealed condition (b) partially annealed, and (c) cold worked (hardened). In each case the stress-strain curve is continuously monitored during cyclic strain- controlled testing, as shown in Figure 5. The hysteresis loops started with a monotonic tensile stress-strain solid curve from the origin to the first reversal, the last hysteresis loop is also represented by a solid line. The remaining curves represent the change in the stress-strain curves during plastic cyclic straining. The fully annealed (soft) specimen (a) is cyclically hardened where the stress range is increased to reach the constant amplitude strain range. On the other hand, the cold worked specimen (c) is cyclically softened which appear a stress decrease. The partially annealed specimen (b) initially appears cyclic hardening followed by cyclic softening behavior. The cyclic hardening or softening is related to the density, movement and arrangement of the dislocation.

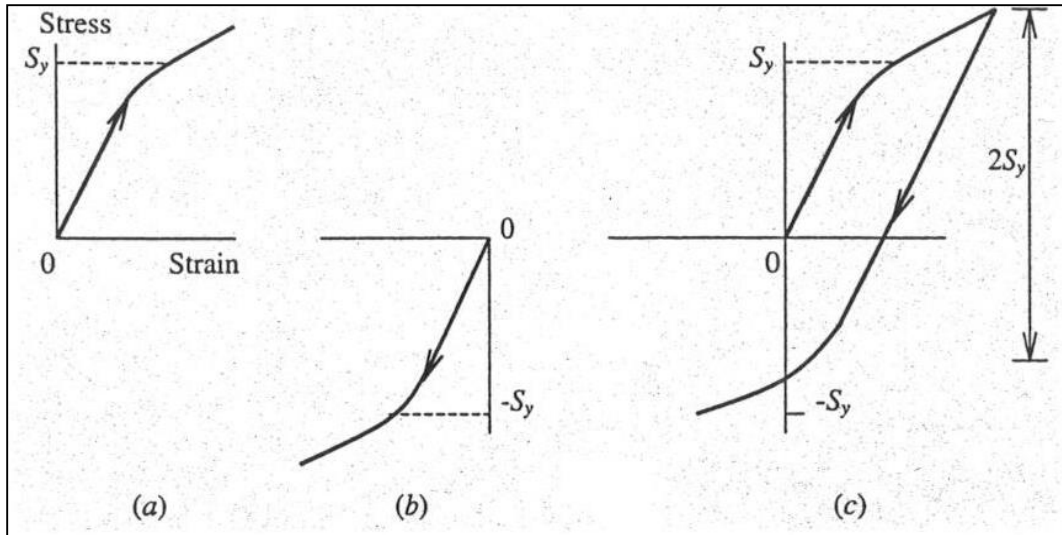


Figure 4 Representation of Bauschinger Effect (a) Specimen under Tension (b) Specimen under Compression (c) Tension Followed by Compression.

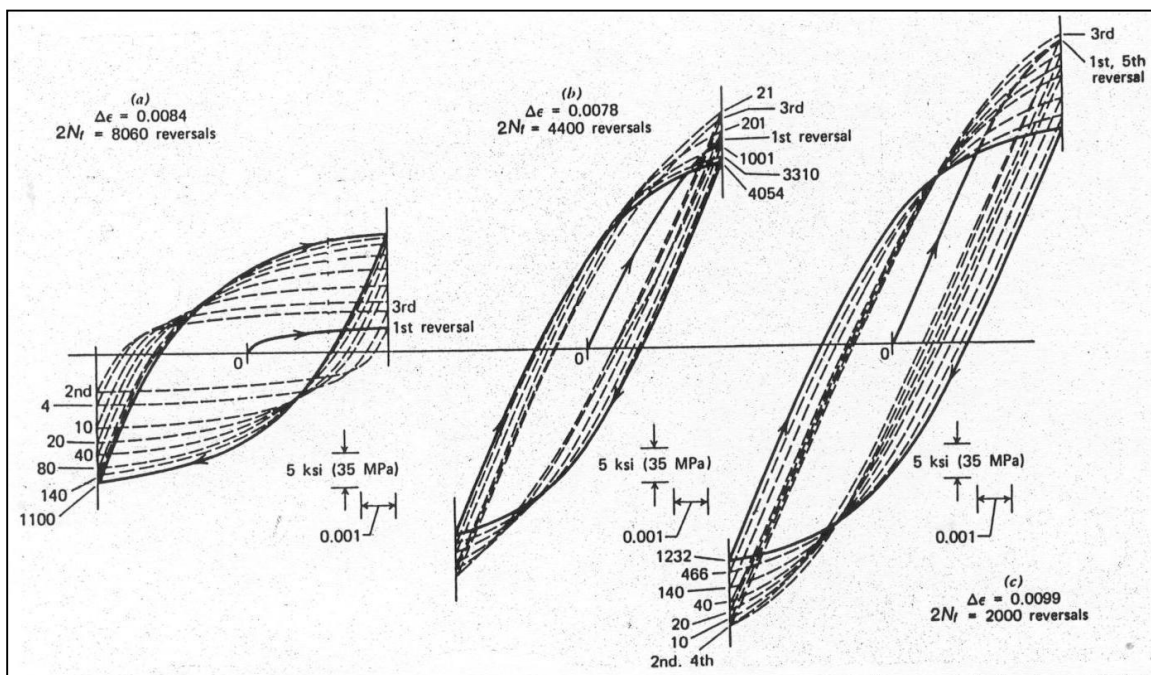


Figure 5 Stress-Strain Relationship for Copper under Cyclic Strain-Controlled Axial Load (a) Fully Annealed (b) Partially Annealed (c) Cold Worked [1].

A representation of cyclic hardening or softening behavior under a condition of strain-controlled testing can be done by plotting of stress variation as a function of the number of cycles, as shown in Figure 6. In the case of cyclic hardening the resistance to deformation increases as the number of cycles increases (Figure 6a), the opposite occurs in the case of cyclic softening where the resistance to deformation decreases by increasing the number of cycles, (Figure 6b).

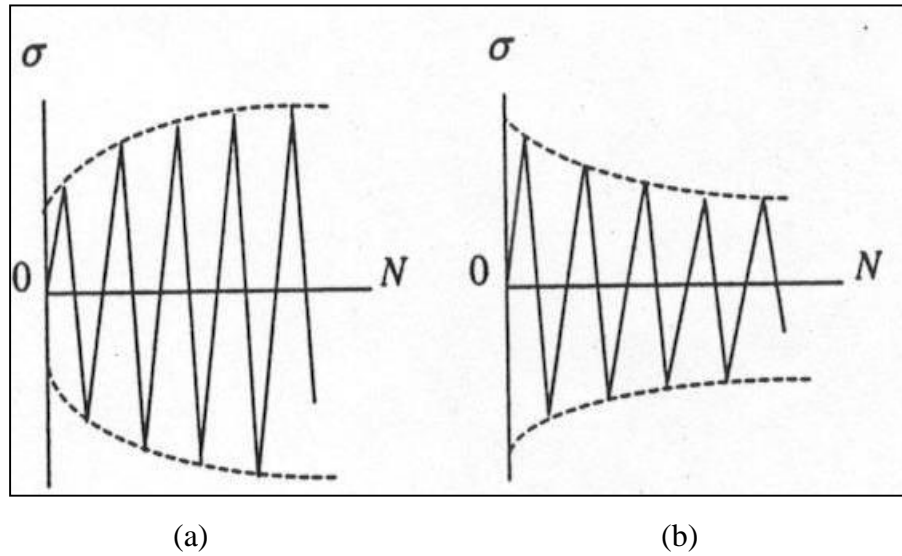


Figure 6 Variation of Stress under Constant Strain Amplitude (a) Cyclic Hardening Condition (b) Cyclic Softening Condition

Usually within 10 to 40 percent of the total fatigue life the stress variation reaches a state of cyclic stabilization which is referred to as “cyclic transient behavior” it is often a hysteresis loop at half of fatigue life chosen which represent the steady-state cyclic stress-strain behavior of the material. Figure 7 shows the stable cyclic stress-strain hysteresis loop.

The relationship between total true strain $\Delta\varepsilon$, true stress range $\Delta\sigma$, elastic strain range $\Delta\varepsilon_e$, and plastic true strain range $\Delta\varepsilon_p$, is given by the equation:

$$\Delta\varepsilon = \Delta\varepsilon_e + \Delta\varepsilon_p = \frac{\Delta\sigma}{E} + \Delta\varepsilon_p \quad (4)$$

The difference between true and engineering strain values is usually negligible since the strain levels during the cyclic loading are below 2 percent. These values are much lower than the strain values in the case of monotonic loading.

In order to obtain a cyclic stress-strain curve for a given material a family of hysteresis loops can be connected as shown in Figure 8 for (Man-Ten steel).

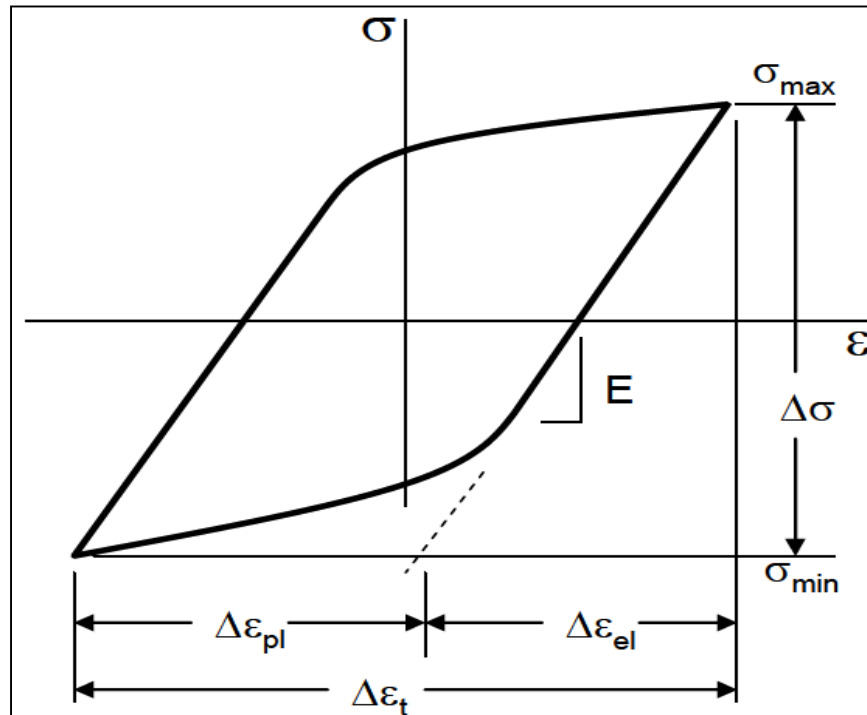


Figure 7 Stabilized Cyclic Stress-Strain Hysteresis Loop

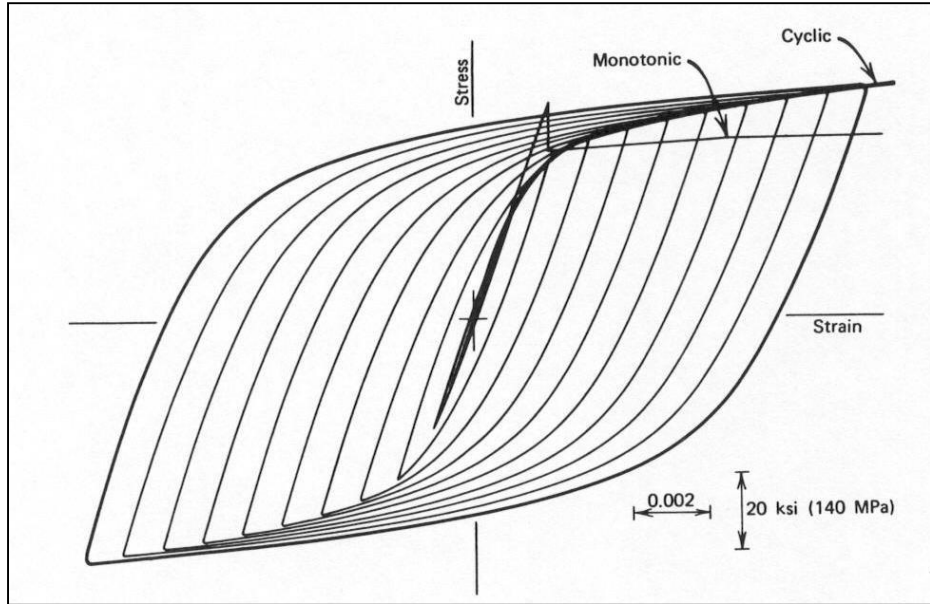


Figure 8 Stable hysteresis loop for determining the cyclic stress-strain curve and comparison with the monotonic stress-strain curve for Man-Ten steel [1].

Langraf, Morrow, and Endo [5] presented the monotonic and cyclic stress-strain curves for different materials including softening and hardening. They demonstrated that soft materials tends to harden under cyclic loading whereas hard materials have an opposite behavior. They tend to soften under cyclic loading, as shown in Figure 9.

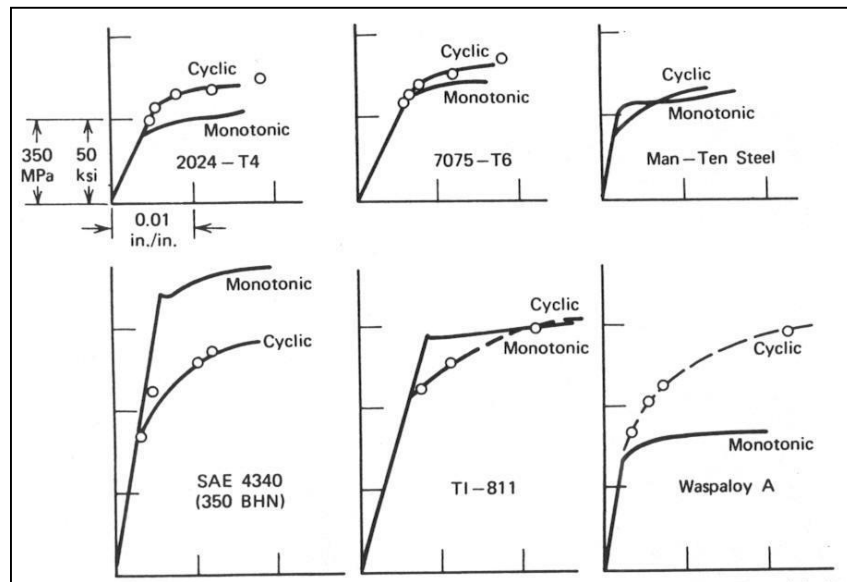


Figure 9 Cyclic and Monotonic Stress-Strain Curves for Different Materials [5]

A plot of plastic stress amplitude, $\Delta\sigma/2$, versus plastic strain amplitude, $\Delta\varepsilon_p/2$, in a log-log scale results in the relationship:

$$\sigma_a = K' \left(\frac{\Delta\varepsilon_p}{2} \right)^{n'} \quad (5)$$

Where K' and n' are the cyclic strength coefficient and cyclic strain hardening exponent, respectively. Eq. (5) can be written in a different form using Eq. (4) as:

$$\varepsilon_a = \frac{\Delta\varepsilon}{2} = \frac{\Delta\varepsilon_e}{2} + \frac{\Delta\varepsilon_p}{2} = \frac{\Delta\sigma}{2E} + \left(\frac{\Delta\sigma}{2K'} \right)^{1/n'} = \frac{\sigma_a}{E} + \left(\frac{\sigma_a}{K'} \right)^{1/n'} \quad (6)$$

The range of n' values is smaller than for monotonic it ranges from .05 to .25 for most of metals. The value for cyclic yield strength is often defined at 0.2 percent strain offset of plastic strain amplitude.

1.4 FATIGUE TESTS

1.4.1 Fatigue loading

Structures and components are usually subjected to alternating load histories which are sometimes simple and repetitive. However, in most cases these histories are completely random and may contain high loading peaks that exceed the elastic limit of the material.

To understand material fatigue behavior and its properties, it is convenient to start with a constant amplitude loading. Some real-life load histories can be modeled as constant amplitude.

$R = S_{min}/S_{max}$, is called stress ratio and is commonly used as a test condition to obtain fatigue properties, When S_{min} equal $-S_{max}$, $R = -1$ this condition is called “fully reversed” condition. In the case where $S_{min} = 0$ this condition is called “pulsating tension”. In fatigue studies it is convenient to use reversal instead of a complete cycle, in which case one cycle equals two reversals. Description of fatigue testing and loading is shown in appendix C.

1.5 STRESS-LIFE (S-N) APPROACH

The stress-life method is the oldest approach used to understand and quantify behavior of metal fatigue. This method is used when the elastic strain is dominant and no significant plastic strain is encountered

A plot of alternating stress, S_a versus number of cycles to failure, N_f in a log-log scale results in a diagram called Wholer or S-N diagram shown in Figure 10.

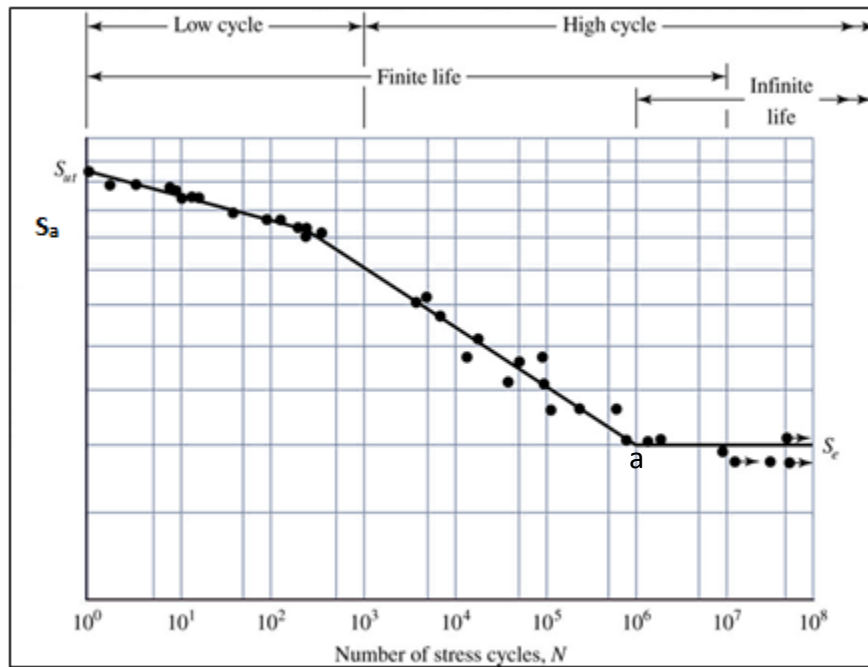


Figure 10 Typical S-N Diagram

The main disadvantage of this method is that it does not include the true stress-strain behavior and considers all strains as elastic strains, the crack initiation is usually occurs under plastic deformation state.

When the S-N data is plotted on a log-log scale, the actual line represents the mean data. Most body center cubic (BCC) crystal structure materials (Steel) show a discontinuity or “knee” indicated as point **a** in the S-N curve, the nominal stress at knee point is defined as fatigue strength or fatigue limit, below this point the material has infinite number of cycles to failure. This knee is between 10^6 and 10^7 cycles under noncorrosive environment. In general, most materials do not have a knee.

Fatigue typically consists of three stages, crack nucleation, crack growth, and final fracture. Figure 10, does not facilitate between these stages its gives only the total fatigue life. There are certain general empirical relationships between the fatigue properties of steel and the less expensively monotonic tension and hardness properties [6].

There is a ratio called “fatigue ratio (S_f/S_u)” this ratio ranges from 0.35 to 0.6. For most steels with a tensile strength below 1400 MPa (200 ksi) the fatigue ratio is 0.5. Carbide inclusions formed during the tempering of martensitic steels with an ultimate tensile strength of more than 1400 MPa (200 ksi) becomes a source of crack initiation points and effectively reduces the fatigue limit. The fatigue limit for these materials is approximated by a constant value of 700 MPa (100 ksi), this behavior is shown in Figure 11, where the ultimate tensile strength is plotted versus the endurance limit.

For steels the ultimate tensile strength (S_u) can be approximated using Brinell hardness (HB) given by Eq. (7):

$$S_u \approx 3.45HB \quad \text{MPa (200 ksi)} \quad (7)$$

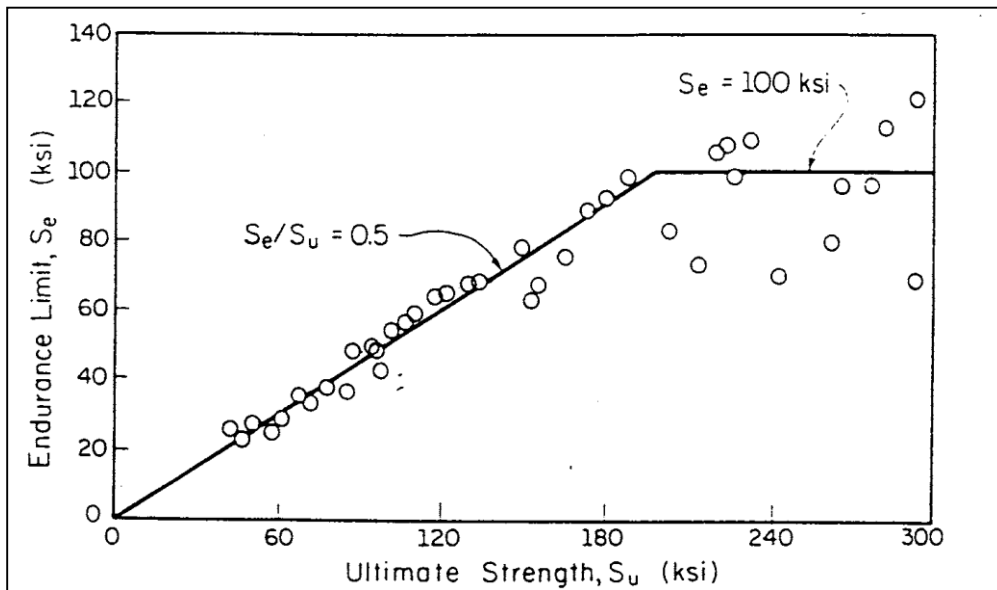


Figure 11 Relation between Rotating Bending Endurance Limit and Tensile Strength of Wrought Steel [6].

1.5.1 Mean Stress Effect on S-N Behavior

Fatigue behavior is strongly affected by the mean stress, S_m , this effect is shown in Figure 12, where the stress amplitude, S_a is plotted against the number of cycles to failure, N_f , for varying mean stresses. In general as shown in the figure compressive mean stresses are beneficial, on the other hand, the tensile mean stresses are detrimental this can be observed by the intercepts of the three vertical lines with the fatigue life line N_{fc} , N_{fo} and N_{ft} .

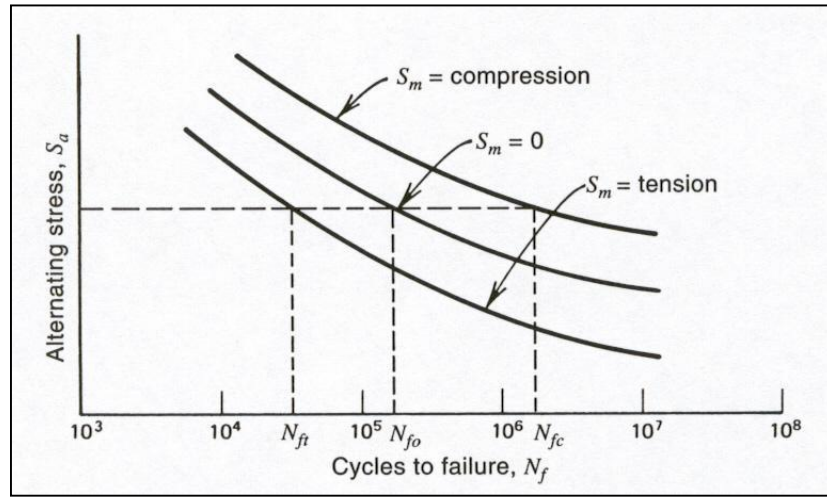


Figure 12 Mean Stress Effect on S-N Behavior [1].

The tensile mean stress effect for uniaxial state can be represented in the following equations:

Modified Goodman equation
$$\frac{S_a}{S_f} + \frac{S_m}{S_u} = 1 \quad (8)$$

Gerber equation
$$\frac{S_a}{S_f} + \left(\frac{S_m}{S_u}\right)^2 = 1 \quad (9)$$

Morrow equation
$$\frac{S_a}{S_f} + \frac{S_m}{\sigma_f} = 1 \quad (10)$$

Where, S_a , S_m , S_f , S_u , σ_f , are stress amplitude, mean stress, fatigue strength, tensile strength and fracture strength respectively.

1.5.2 Factors that Affect the S-N Behavior

There are three main factors that affect the behavior of S-N including, microstructure, size of the test specimen, and surface finish. Details are shown in appendix C.

1.5.3 S-N Approximations

When experimental fatigue data is not available in data handbooks, design codes, or from the test data, there is another option which is a prediction model. There are many prediction models, these models usually imply a median fatigue life.

Figure 13 shows S-N median fatigue curves based on a straight-line log-log approximation.

Basquin in 1910 [7] suggested a log-log straight line S-N approximation in Eq. (11):

$$S_a = A(N_f)^B \quad (11)$$

Where, S_a alternating stress at $R = -1$, N_f number of cycles, A is the coefficient its the value at the intercept at N_f equal one, and B is the slope of log-log S-N curve.

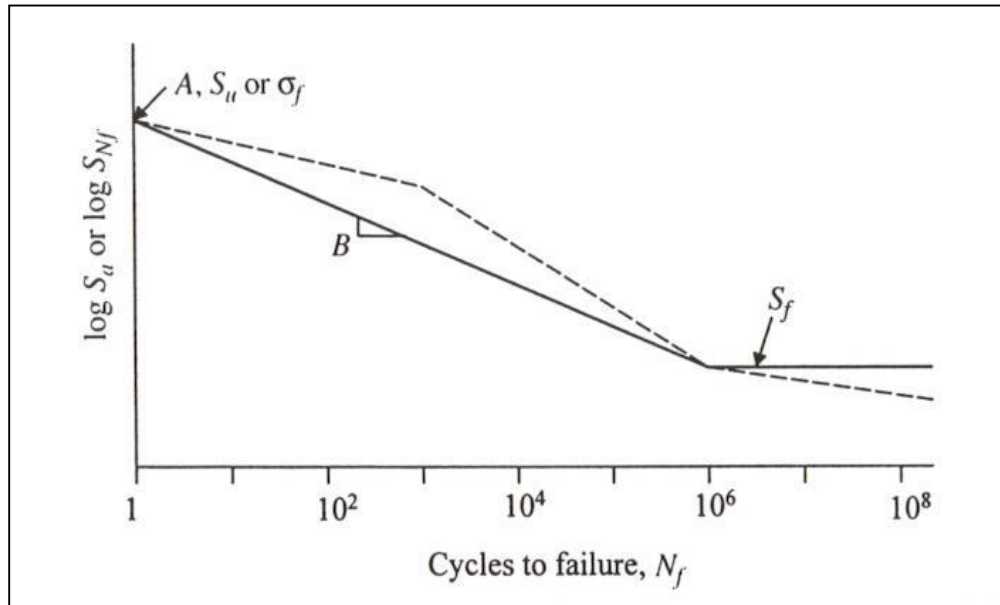


Figure 13 Basquin S-N Curve [1]

1.6 The Strain-Life (ϵ -N) Approach.

Fatigue philosophy has changed from one based on an endurance limit method to one based upon a more precise assessment of fatigue, the strain-life (ϵ -N) approach has gained wide acceptance, particularly in the ground vehicle industry [8]. This approach combines the localized highest measured/design strains applied to the structure and the material's fatigue properties. The material's fatigue properties are characterized by the strain-life curves, obtained from strain-controlled fatigue testing of smooth specimens [9]. Total strain amplitude is divided in two components, elastic ($\Delta\epsilon_e/2$) and plastic ($\Delta\epsilon_p/2$) strain amplitudes and given by:

$$\frac{\Delta\epsilon}{2} = \frac{\Delta\epsilon_e}{2} + \frac{\Delta\epsilon_p}{2} \quad (12)$$

Where, $\Delta\epsilon/2$, $\Delta\epsilon_e/2$, $\Delta\epsilon_p/2$ is the total, elastic and plastic strain amplitudes respectively. The elastic strain-life relation can be considered as the stress-life relationship divided by the modulus of elasticity given by:

$$\frac{\Delta\sigma}{2E} = \frac{\Delta\epsilon_e}{2} = \frac{\sigma'_f}{E} (2N_f)^b \quad (13)$$

Where, $\Delta\sigma/2$ is the stress amplitude; $2N_f$ is the reversal to failure; σ'_f is the fatigue strength coefficient which is the intercept of the $\log(\Delta\sigma/2)$ versus $\log(2N_f)$ plot for $2N_f$ equal one, b is called fatigue strength exponent which is the slope of the elastic curve, and E is the modulus of elasticity. Plastic strain-life relationship can be written as:

$$\frac{\Delta\epsilon_p}{2} = \epsilon'_f (2N_f)^c \quad (14)$$

Where, ϵ'_f is the fatigue ductility coefficient taken as the intercept of the plastic curve for $2N_f$ equal one and c is the fatigue ductility exponent which is the slope of the plastic curve.

Combining the elastic and plastic components results in a form of strain-life relationship given by Eq.(15) and shown in Figure 14 for 1141 VFG steel

$$\frac{\Delta\varepsilon}{2} = \frac{\sigma'_f}{E}(2N_f)^b + \varepsilon'_f(2N_f)^c \quad (15)$$

The four fatigue parameters needed in this relationship are the fatigue strength coefficient (σ'_f), fatigue strength exponent (b), fatigue ductility coefficient (ε'_f) and fatigue ductility exponent (c)

The strain-life approach considers the plastic deformation that occurs at localized regions where the crack nucleation usually occurs. This approach is also known the comprehensive approach.

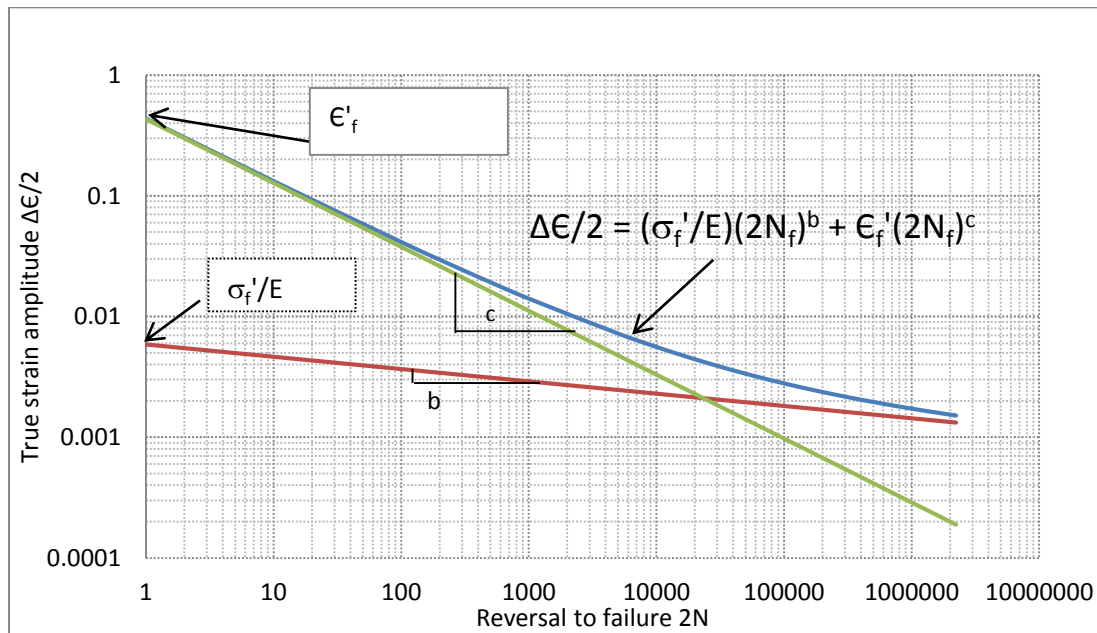


Figure 14 Typical Strain-Life Curve for SAE 1141 VFG

1.6.1 Mean Stress Effects on Strain-Life Approach

The effect of mean stress in the case of strain-life fatigue behavior is complex. There are many models proposed for strain-life fatigue, one of these models called “Morrow’s mean method”, in this method the fatigue strength coefficient is replaced with $(\sigma'_f - \sigma_m)$ in the strain-life approach Eq (15).

$$\frac{\Delta\varepsilon}{2} = \frac{(\sigma'_f - \sigma_m)}{E} (2N_f)^b + \varepsilon'_f (2N_f)^c \quad (16)$$

Where σ_m is the mean stress.

When the σ_m is positive it refers to a positive tensile value while when σ_m is negative it refers to a compressive value. According to this equation the tensile mean stress is detrimental while the compressive mean stress is beneficial to fatigue life.

An alternative version of Morrow’s mean stress parameter where both the elastic and plastic terms are affected by the mean stress is given by Eq. (17), [10].

$$\frac{\Delta\varepsilon}{2} = \left(\frac{\sigma'_f - \sigma_m}{E} \right) (2N_f)^b + \varepsilon'_f \left(\frac{\sigma'_f - \sigma_m}{\sigma'_f} \right)^{c/b} (2N_f)^c \quad (17)$$

Another equation has been suggested by Smith, Watson, and Topper [11], this equation is usually known as “SWT parameter” and given by:

$$\sigma_{max} \varepsilon_a E = (\sigma'_f)^2 (2N_f)^{2b} + \sigma'_f \varepsilon'_f E (2N_f)^{b+c} \quad (18)$$

Where $\sigma_{max} = \sigma_m + \sigma_a$ and ε_a is the alternating strain.

1.7 NOTCH EFFECT

Threads, holes, grooves, and welds cannot be avoided when designing structures or mechanical components. These geometrical discontinuities are generally termed as notches [12]. When the component is loaded, local stress and strain are induced at these locations which in most cases exceeds the elastic limit of the material in the region around the notch root even when the nominal stress is still within the elastic limit. When the material subjected to a cyclic loading, the cyclic plastic deformation in these highly stressed locations can cause a high reduction in the component life. Cyclic plastic strains at the notch root can be a location for crack initiation and subsequent propagation which then leads to component failure.

Stress - strain state at the notch root is extremely important in fatigue life calculations. In order to define the local stress-strain state at the notch root the local stress σ has to be related to the nominal stress S . There are many models to relate the nominal stress to local stress and strain as described in the following sections. The factor used in such situation is called stress concentration factor and represented by K .

1.7.1 Stress Concentration Factor

The stress concentration also known as stress raisers, it is a location on a component where the stress concentrated. When a flat plate with a center hole loaded such as in Figure 15, to meet the equilibrium condition the internal force lines become denser around the hole.

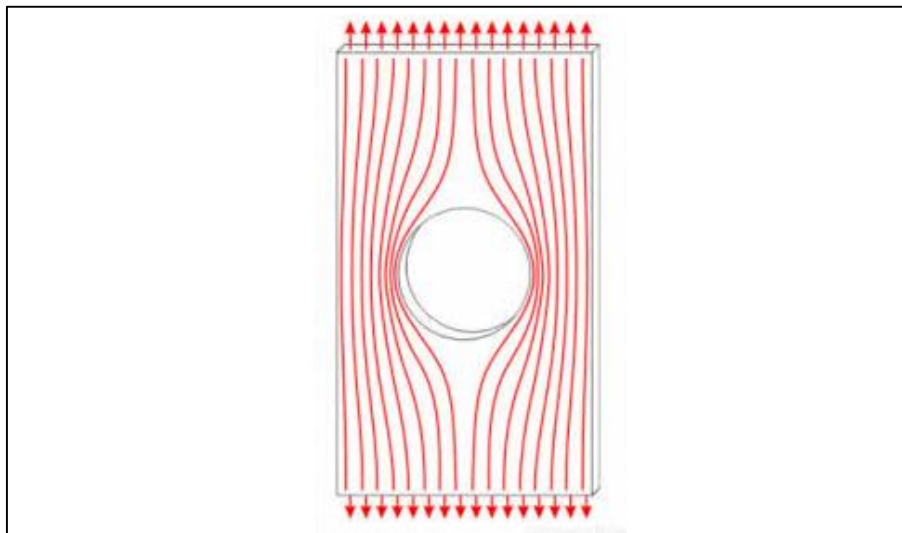


Figure 15 Density of Internal Force Lines around the Hole

The stress concentration factor K can be defined as the ratio of the maximum stress in the body to some other stress taken as a reference stress [13].

$$\text{For tension or bending} \quad K_t = \frac{\sigma_{max}}{\sigma_{nom}} \quad (19)$$

$$\text{For torsion} \quad K_t = \frac{\tau_{max}}{\tau_{nom}} \quad (20)$$

Where, σ_{max} , τ_{max} , are the maximum stresses expected on the component and σ_{nom} , τ_{nom} , the normal and shear stresses. The subscript t refers to the theoretical stress concentration factor.

For a tension plate with a hole in center, the maximum stress occurs at point A in Figure 16. The stress distribution is also shown in Figure 16. The reference stress is based on the net cross sectional area and is defined in Eq. (21) as:

$$\sigma_n = \frac{P}{(H - d)h} \quad (21)$$

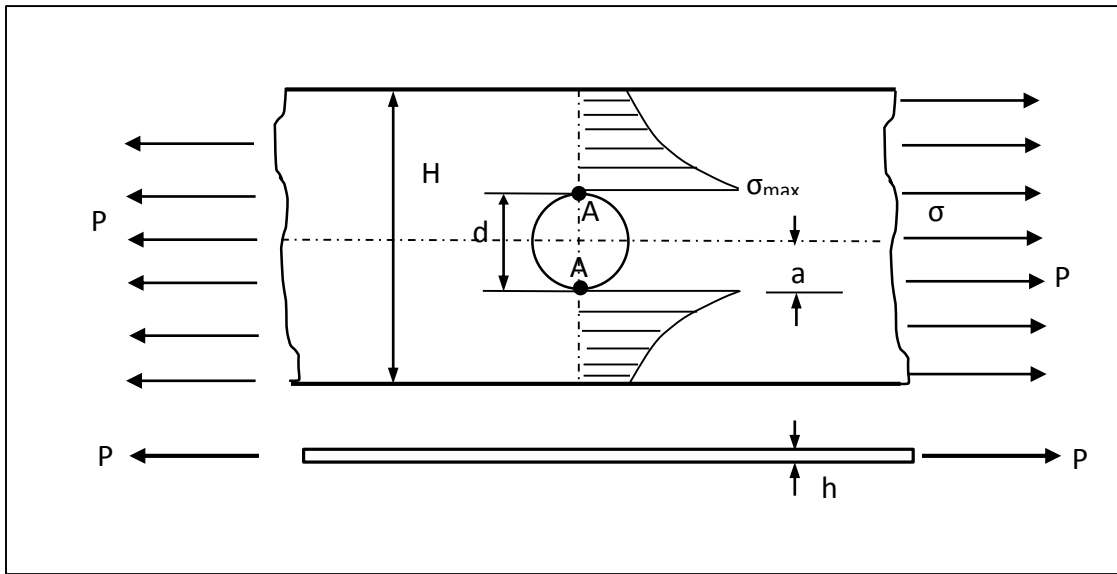


Figure 16 Stress Distribution on a Tension Plate with Hole

The stress concentration factor based on the reference stress $\sigma_n = \sigma_{nom}$ can be obtained using Eq. (22) as:

$$K_{tn} = \frac{\sigma_{max}}{\sigma_n} = \frac{\sigma_{max}(H - d)h}{P} \quad (22)$$

The stress distribution in three dimensional case for a rectangular notched tension bar and round shaft is shown in Figure 17 and Figure 18.

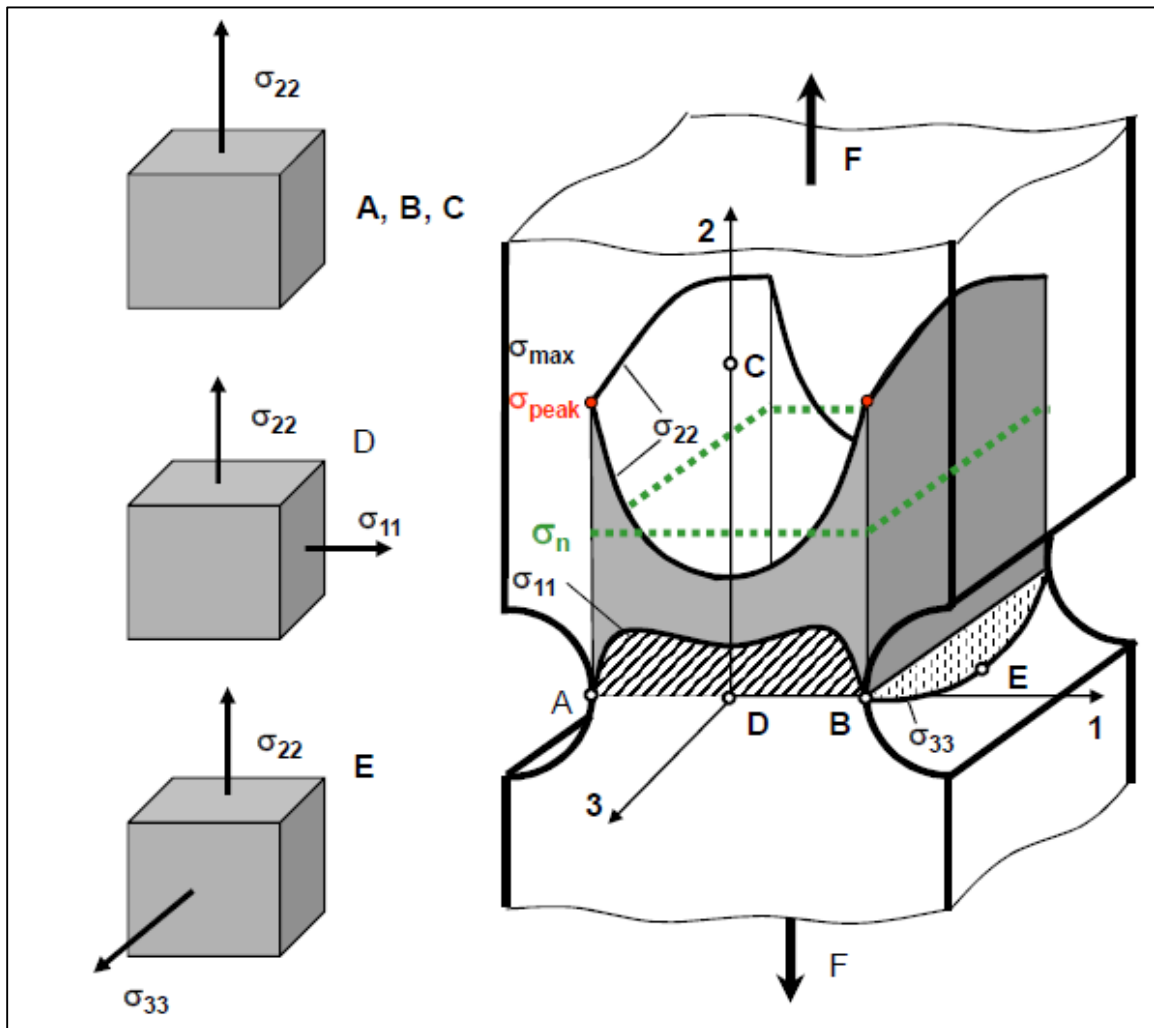


Figure 17 Maximum and minimum stress in rectangular notched bar under axial tension.

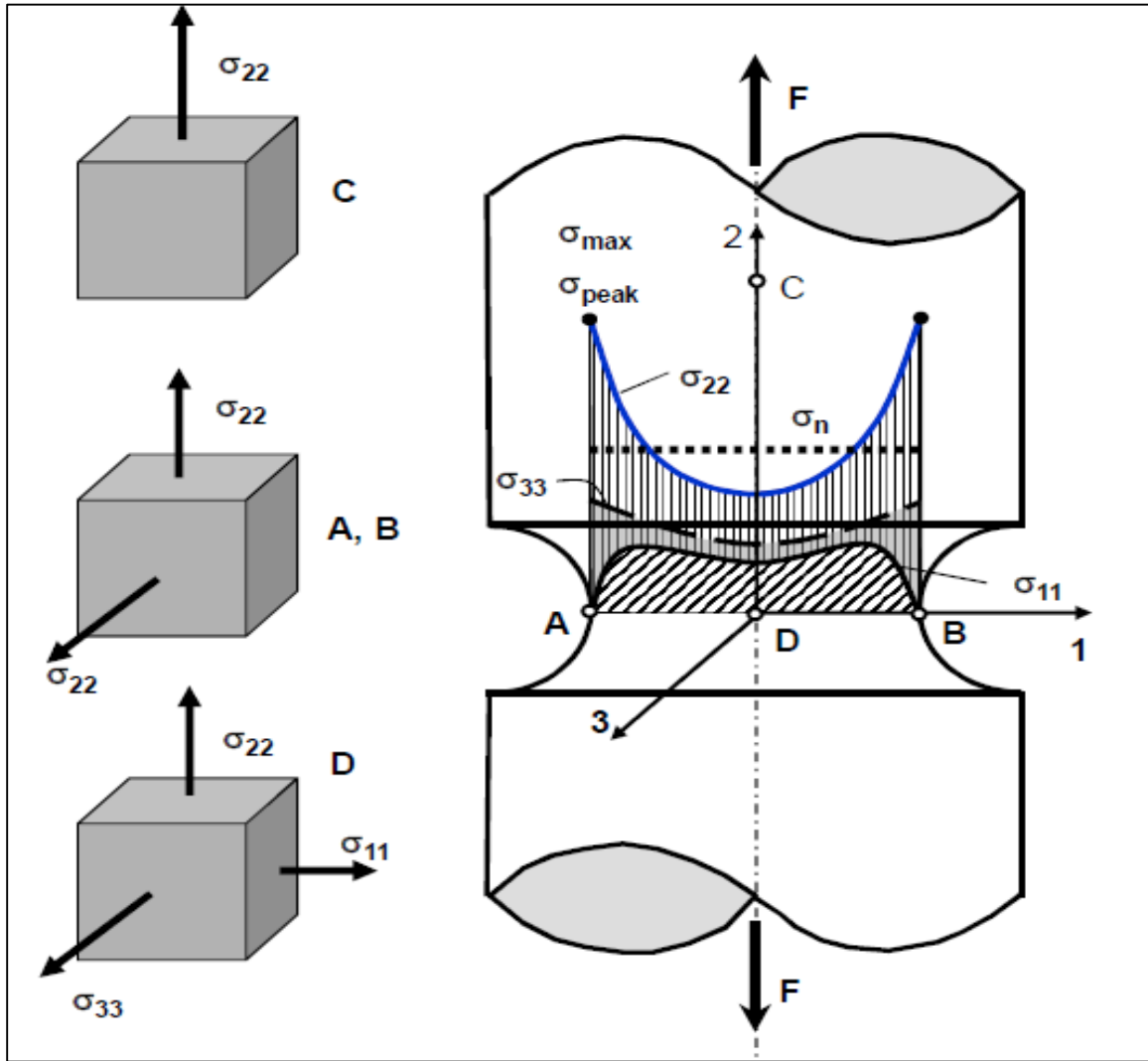


Figure 18 Maximum and minimum stress for a notched shaft under axial tension

The stress concentration factor is affected by the component geometry. Figure 19 shows the variation of K_t with the diameter width ratio for a tension bar with a hole subjected to a tensile load.

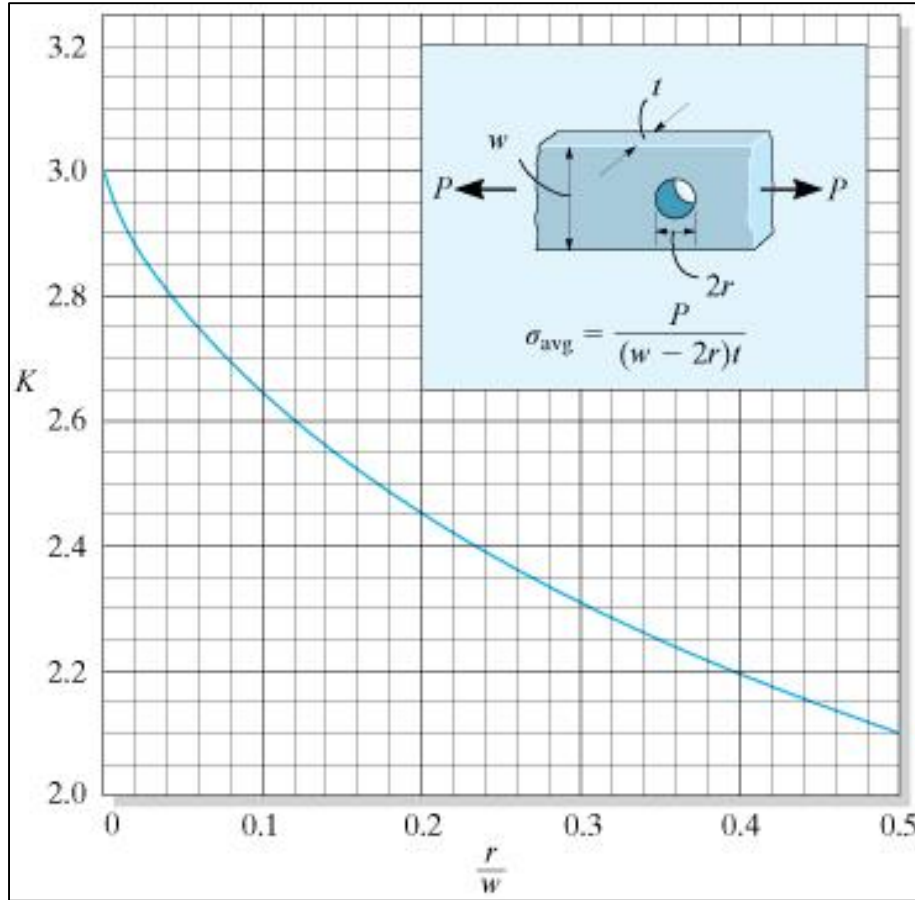


Figure 19 Variation of K_t with r/w Ratio [12]

Different techniques can be used to calculate the stress concentration factor such as, photoelasticity and strain gages, but the most powerful technique used in industry is the finite element analysis. Theory of elasticity is used to calculate the stress concentration factor, this theory is based on formulations that include assumptions that the material is isotropic and homogenous. However, in reality the material may be neither be isotropic nor homogenous or it may have defects such as voids, porosity or microcracks. Accuracy of K values for some materials and applications is still an issue.

The stress concentration factor is used mainly to correlate the nominal stress with the maximum stress generated in some local areas on the component which in most cases exceeds the yield limit of the material. There are different models proposed to obtain the maximum stress with the aid of the elastic stress concentration factor.

1.7.2 Plane Stress and Plane Strain

1.7.2.1 Plane Stress

Plane stress is a state of stress in which the normal stress σ_z , shear stress τ_{xy} and τ_{yz} are assumed to be zero. The plane stress is the simplest form of behavior of continuum structures and is the most used condition in practice.

1.7.2.2 Plane Strain

Plane strain is a state of strain in which the strain normal to the x-y plane, ϵ_z and shear strains are assumed to be zero, in this case the dimension of the structure in z-direction is very large compared with other directions, the surrounding elastic material restrain notch deformation in the thickness direction.

The plane stress and plane strain conditions are schematically shown in Figure 20.

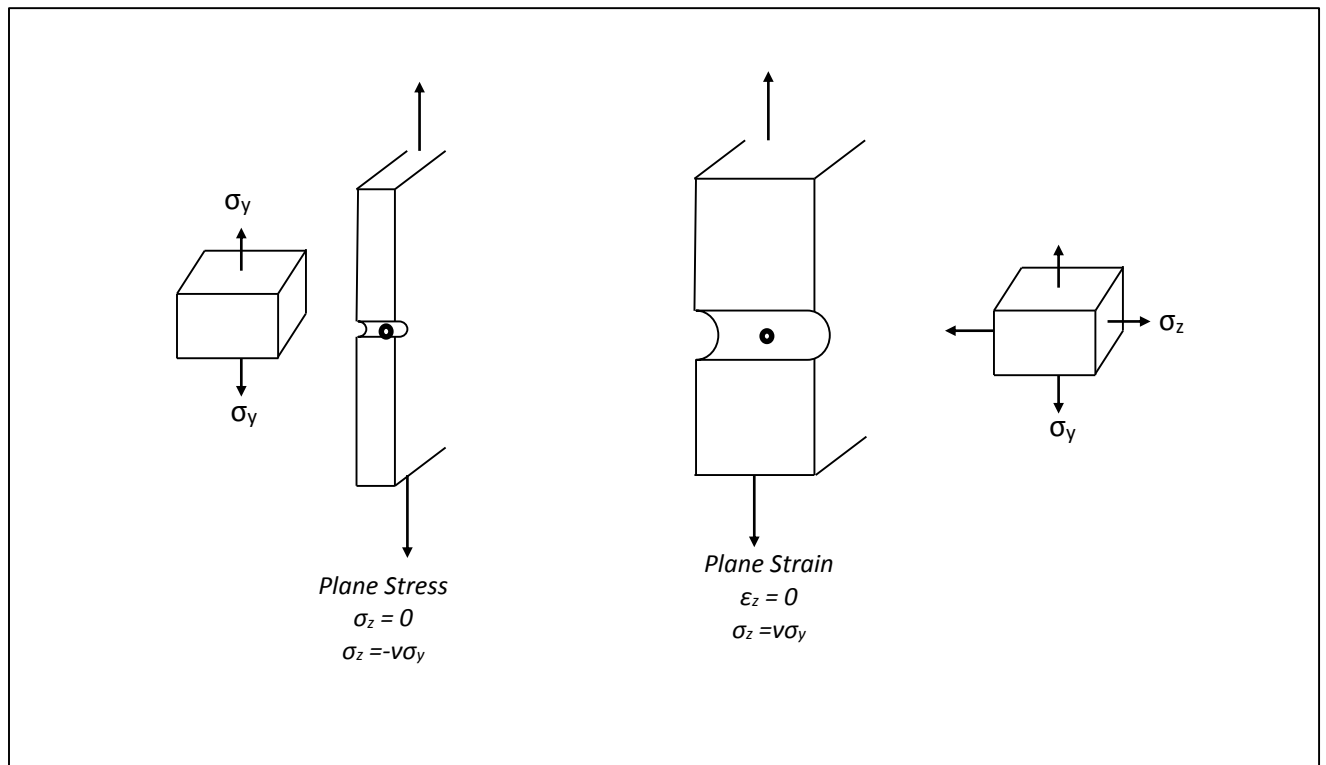


Figure 20 Schematic Representations of Notch Root Plane Stress and Plane Strain

Conditions

1.8 MOTIVATION

Considering the amount of time and effort required to obtain the fatigue parameters from fatigue experiment, many researchers have attempted to develop correlations between monotonic tensile data, so that, prediction of fatigue parameters from simple material properties can be used instead of physically testing the material. One of the aims of this study is to find a good correlation between simple material properties which are easy to obtain, and fatigue parameters.

The best fatigue parameters prediction model for steels is the Modified universal Slopes model Eq.(121), where the prediction of σ_f' and ε_f' is based mainly on the ultimate tensile strength, modulus of elasticity ratio (S_u/E). Ultimate tensile strength is a material property obtained by conducting a tensile test on a material sample until failure, it is a destructive test that needs time to prepare the samples. The aim is to predict the fatigue parameters using a less expensive and easy to obtain material property such as hardness in the Modified Universal Slopes model and replace the ultimate tensile strength.

Prediction of local stress and strain is essential in design, the best way to obtain stresses and strains at notches is to perform elastio-plastic finite element analysis. However, such an analysis is time consuming and has convergence issues when used on complex components. Neuber's rule is the most popular analytical method used in industry overestimates notch stresses and strains hence, a correction factor is needed. Based on the simplicity of applying elastic finite element analysis the second objective of the study is to use elastic finite element analysis in conjunction with a correlation factor to Neuber's rule to estimate local stresses and strains at notch roots. These results can then be compared with the elastic-plastic finite element results.

2 LITERATURE SEARCH:

2.1 Correlations between Cyclic Deformations with Tensile Properties.

In design, proper selection of material for cyclically loaded structures is very important. In order to know the stress-strain response of cyclically loaded structures, fatigue parameters should be available. Without doubt, the best way is to conduct comprehensive test experiments. However, fatigue test experiments are expensive and time consuming, also in most cases fatigue test experiments do not give an accurate results when they are repeated. In order to optimize the test results the least square fit is applied. Therefore, theoretically estimating the cyclic deformation properties from commonly available monotonic tensile properties such as ultimate tensile strength (S_u), hardness, or strain hardening exponent (n) with reasonable accuracy is very useful.

2.1.1 Existing methods that estimate ultimate tensile strength from hardness

2.1.1.1 For Steels

In order to find correlations between monotonic tensile properties and cyclic properties it may be convenient to start with correlations between monotonic properties based on that correlations with the cyclic properties can be created. The well-known approximation of the ultimate tensile strength, S_u from Brinell hardness, HB, for low and medium strength carbon and alloy steel is presented by a linear relationship given by Eq. (23), [14]:

$$S_u = 3.45HB \text{ (MPa)} \quad (23)$$

Eq. (23) agrees well with experimental data for $HB < 350$, [15].

A second order polynomial approach proposed by Roessle and Fatemi, correlates S_u and hardness as, Eq. (24), [15]:

$$S_u = 0.0012(HB)^2 + 3.3(HB) \text{ (MPa)} \quad (24)$$

Figure 21; shows the two relations in Eq. (23),(24).

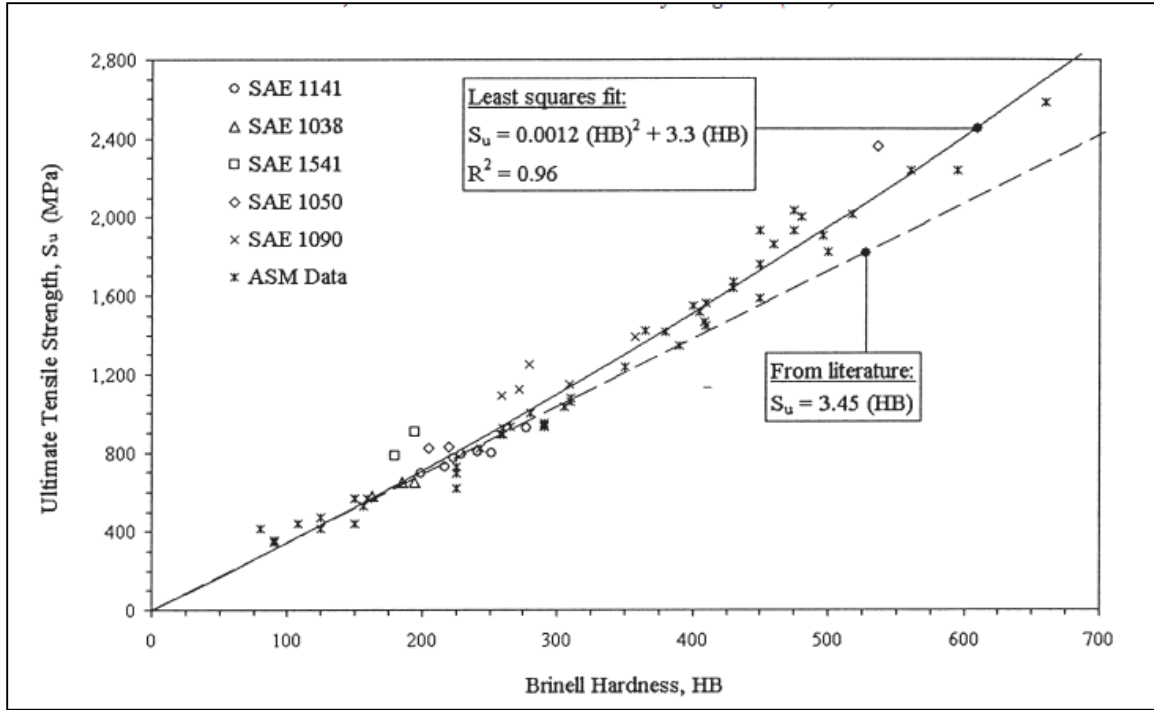


Figure 21 Ultimate Tensile Strength vs. Brinell Hardness [15].

Baumel-Seeger's [16] proposed the following relationship between ultimate tensile strength and Vickers hardness:

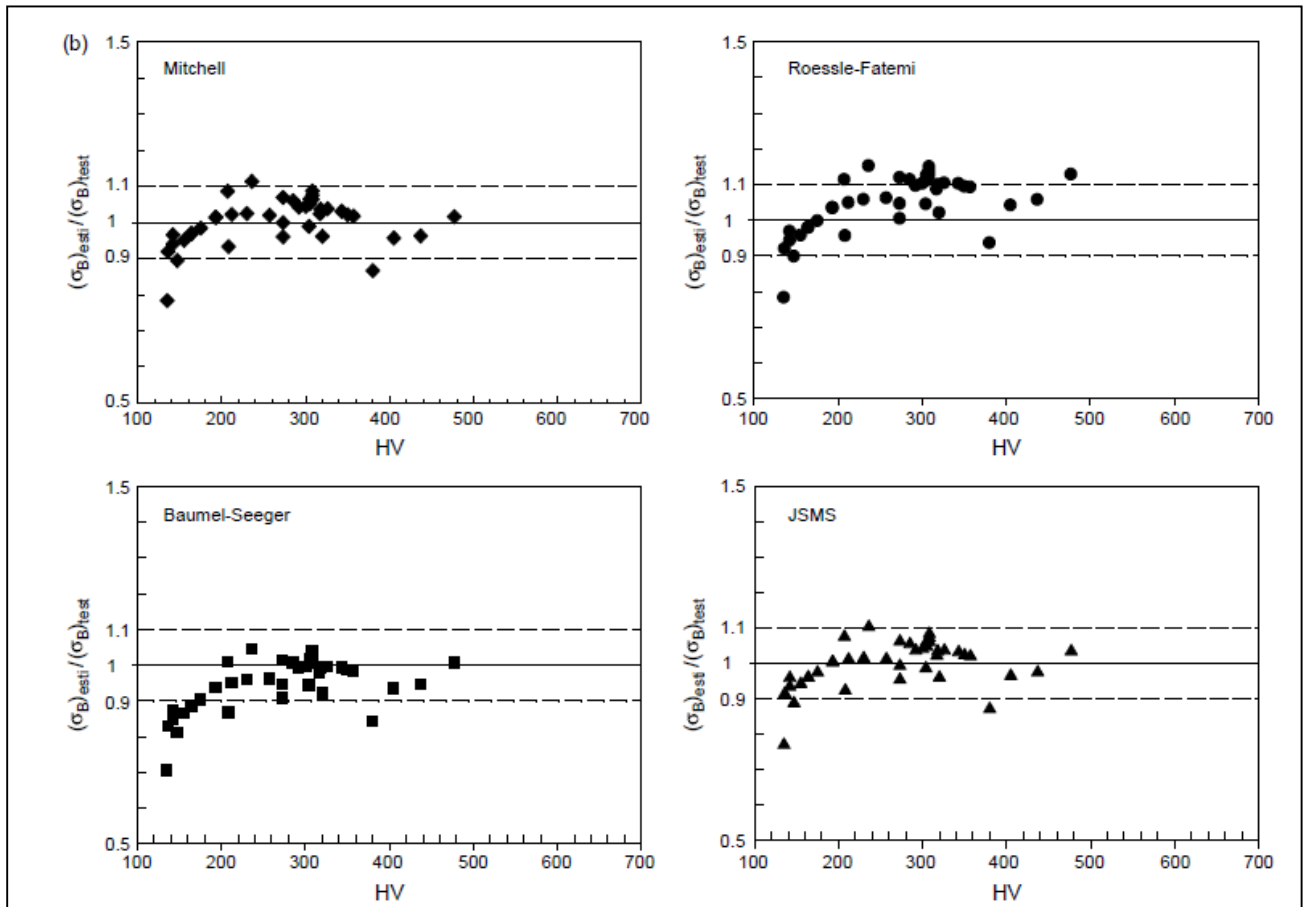
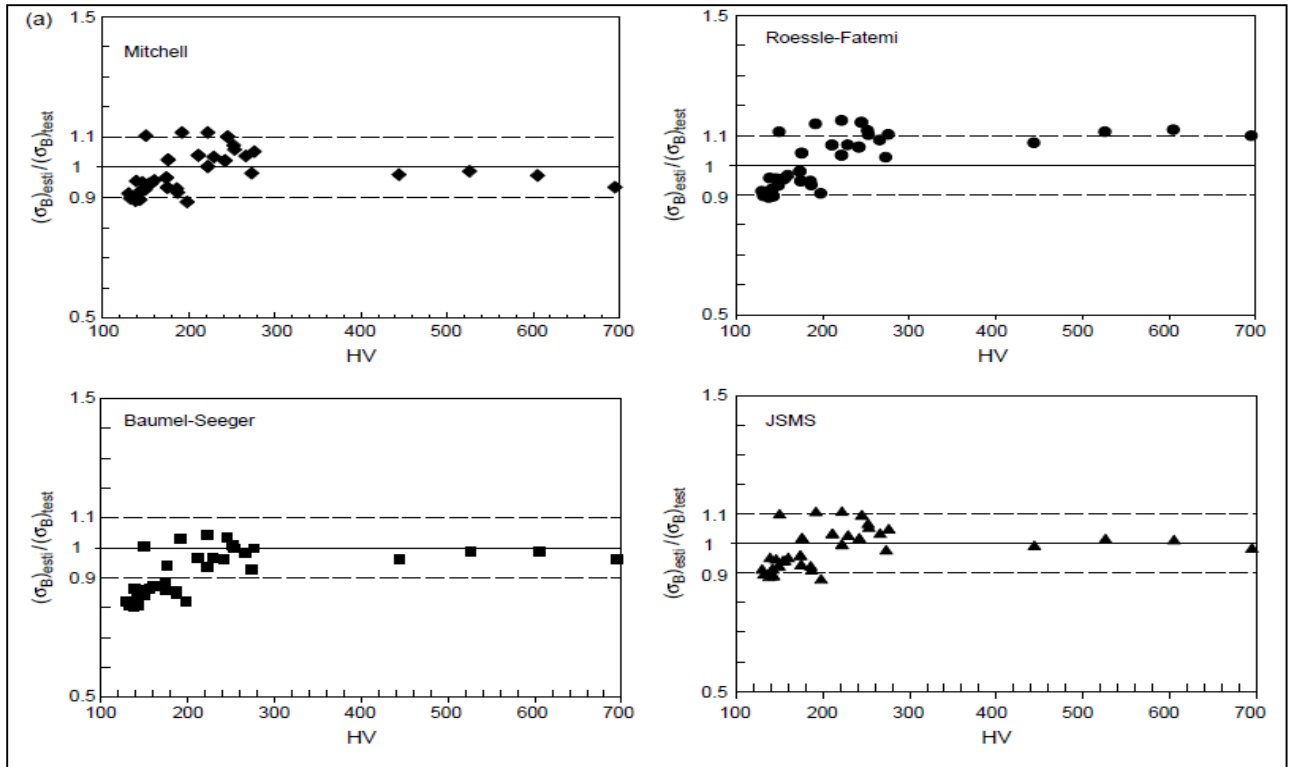
$$\begin{aligned} \sigma_u &= 3.29HV - 47 \text{ (MPa)} \text{ for } HV \leq 445 \\ \sigma_u &= 4.02HV - 374 \text{ (MPa)} \text{ for } HV > 445 \end{aligned} \quad (25)$$

Where, HV is Vickers Hardness.

JSMS (The Society of Materials Science, Japan) [17] proposed the equation below:

$$\sigma_u = \frac{(HV - 1.837)}{0.304} \text{ (MPa)} \quad (26)$$

Kwang-Soo Lee [18], evaluated the four proposed estimation methods using different data sources, (NRIM, Boller-Seeger, JSMS). Figure 22; shows the comparison of these methods for different alloy steels. It concluded that Roessle-Fatemi's ultimate tensile strength-hardness method gives a reasonable results compared with the other methods.



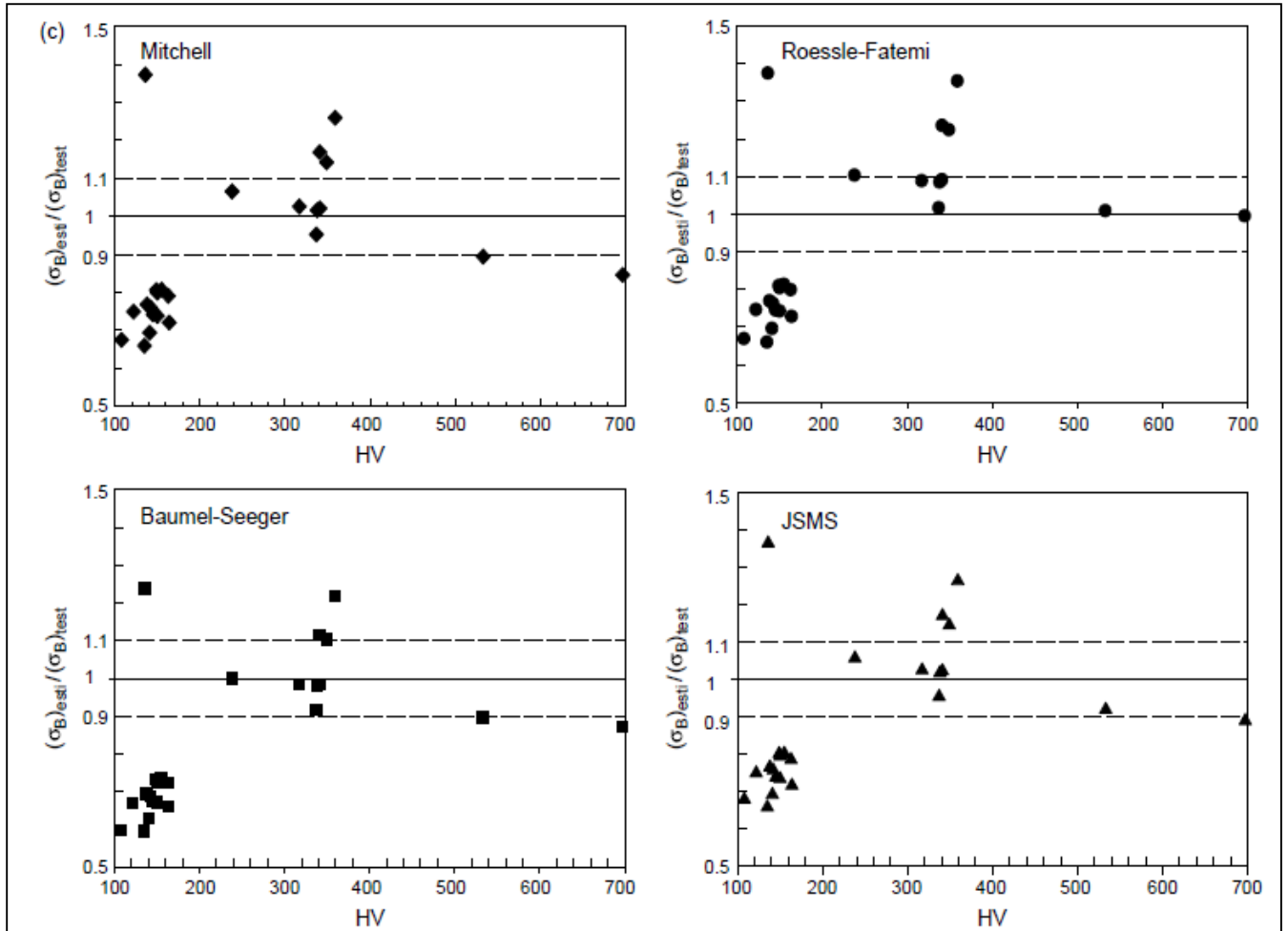


Figure 22 Comparison of the Predicted and Experimental S_u for (a) Unalloyed Steel (b) Low-Alloy Steel (c) High-alloy Steels [18].

2.1.1.2 For Non-Ferrous Materials

JSMS [17], proposed an equation to estimate ultimate tensile strength from hardness for aluminum and copper as:

$$\sigma = \frac{(HV - 21.9)}{0.242} (\text{MPa}) \quad (27)$$

2.1.2 Existing Correlations between Monotonic Tensile Properties and Fatigue Cyclic Deformation Properties.

Many researchers proposed correlation methods to predict the fatigue cyclic deformation behavior of steels from monotonic tensile properties and hardness. The first correlation method was developed by Manson [19], it correlates the hardening or softening behavior with the ultimate tensile strength to yield strength ratio (S_u/S_y) for sixteen different materials including steel, aluminum, and titanium alloys. Different types of steels were used, AISI 4340 (annealed and hard), AISI 52100, AISI 304 ELC (annealed and hard), AISI 310 (annealed) and AM 350 (annealed and hard). Tensile tests to obtain the monotonic tensile properties and strain-controlled fatigue tests to find the cyclic stress-strain curves were performed on each material. The results show that materials that have $S_u/S_y \geq 1.4$, hardened under cyclic strain; materials that have $S_u/S_y \leq 1.2$ soften under cyclic strain; materials that have $1.2 < S_u/S_y < 1.4$ have both behaviors. This is shown in Figure 23.

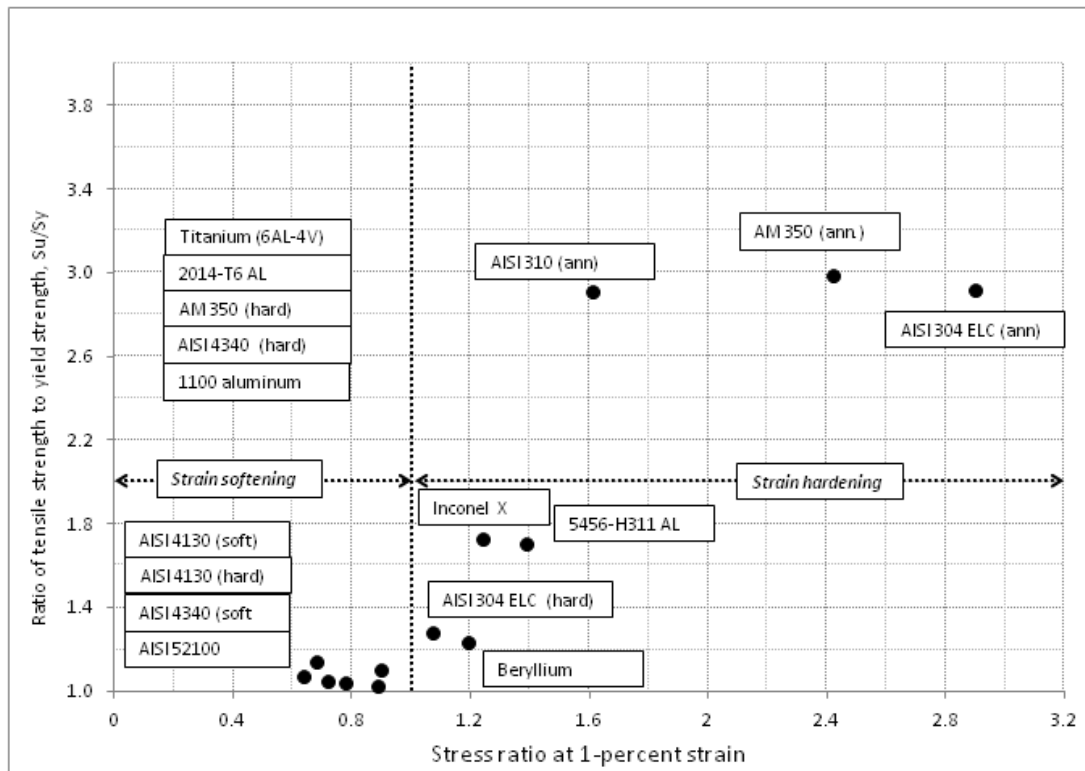


Figure 23 Comparison of Stress Ratio at 1-Percent Strain with Virgin Tensile Properties [19]

Landgraf et al. [5], proposed a correlation between the strain hardening exponent (n) and the cyclic hardening and softening for several materials as shown in Table 1.

Z.P. Zhang [20], proposed a parameter called fracture ductility (α) and defined as:

$$\alpha = \psi \varepsilon_f = -\psi \ln(1 - \psi) \quad (28)$$

Because ψ , a percent reduction in area, it reflects the fracture ductility of materials, α also reflects the fracture ductility of materials.

Zhang et al. [21], conducted a study to relate (α) and cyclic hardening or softening behavior using 40 different alloys including (aluminum, titanium, and steel), according to this study they found that as the fracture ductility parameter is less 2% or between 20% and 65%, the material behavior soften under cyclic loading, for fracture ductility between 2% and 20% the material is cyclically harden.

There are many approaches that relate the cyclic strength coefficient (K') and cyclic strain exponent (n') using monotonic tensile properties and hardness. Zhang et al. [21], proposed a method to estimate the cyclic strain exponent from monotonic tensile properties. In order to estimate the strain hardening exponent (n'), three characteristics are defined based on monotonic tensile properties; these are:

$$n' > n \text{ for } \alpha < 20\% \text{ and for } \sigma_f'/\sigma_{0.2} < 1.6. \quad (29)$$

$$n' < n \text{ for } \alpha < 20\% \text{ and for } \sigma_f'/\sigma_{0.2} > 1.6 \quad (30)$$

$$(\sigma_f - \sigma_u)/\sigma_{0.2} \approx n/n' \text{ for } \alpha > 20\% \quad (31)$$

Where σ_f , σ_u , $\sigma_{0.2}$ are strength coefficient, ultimate tensile strength, and yield strength respectively.

According to the above characteristics the following relationships was proposed:

$$n' = 1.06n \left(1 + \beta \left| 1 - \frac{\sigma_u}{\sigma_{0.2}} \right| \right) \quad (32)$$

For $\alpha < 5\%$ or for $10\% \leq \alpha < 20\%$

$$n' = 1.06n \left(1 + \beta \left| 1 - \frac{\sigma_f}{\sigma_u} \right| \right) \quad (33)$$

For $5\% < \alpha < 10\%$

$$n' = \left[\frac{\sigma_{0.2}}{\sigma_f - \sigma_u} \right] n \quad (34)$$

For $\alpha > 20\%$

In Eq. (32),(33), $\beta = 1$ for $\sigma_f'/\sigma_{0.2} < 1.6$, but $\beta = -1$ for $\sigma_f'/\sigma_{0.2} > 1.6$.

Zhang, Qiao [21], proposed an estimation method to predict cyclic strength coefficient (K') in MPa from monotonic strength coefficient (K) in MPa as:

$$K' = 57K^{0.545} - 1220 \quad (35)$$

Eq. (35), obtained by using a least squares for experimental data of seventeen alloys including (Aluminum, steel, and titanium).

Basan et al. [22], derived an equation that correlate the cyclic strength coefficient (K') and Brinell hardness by investigation of forty 42CrMo4 steels gathered from literature, a least squares fit using second order polynomial results in the following equation with $R^2 = 0.703$.

$$K' = 0.009(HB)^2 + 0.117(HB) + 376.75 \quad (36)$$

Li et al. [23], provided an estimation method to predict cyclic strength (S_y') using ultimate tensile strength (S_u) and percent reduction in area (RA) as:

$$S_y' = (1 + RA)S_u \left[\frac{0.002}{\ln(1 - RA)} \right]^{0.16} \quad (37)$$

The data used to derive the above expression was based on studies performed on twenty-seven alloys from [24, 25].

Table 1 shows that when (n) is greater than 0.2, cyclic hardening is expected. When (n) less than 0.1 cyclic softening is experienced. Mixed behavior experienced in between.

Table 1 Correlation between Strain Hardening Exponent and Material's Behavior [21]

Material	Condition	0.2% S_y S_y/S_y' (ksi)	n/n'	Cyclic behavior
OFHC Copper	annealed	3/20	0.4/0.15	hardens
	partial annealed	37/29	0.13/0.16	stable
	cold worked	50/34	0.1/0.12	soften
2024 aluminum	T4	44/65	0.2/0.11	harden
7075 aluminum	T6	68/75	0.11/0.11	harden
Man-Ten steel	as-received	55/50	0.15/0.16	soften and harden
SAE 4340 steel	Q&T, 350 BHN	170/110	0.066/0.14	soften
Ti-8Al-1Mo-1V	duplex annealed	145/115	0.078/0.14	harden
SAE 1045 steel	Q&T, 595 BHN	270/250	0.071/0.14	stable
SAE 4142 steel	as-quenched, 670 BHN	235/--	0.14/--	hardens

2.1.3 Estimation of Fatigue Parameters using Monotonic Tensile Properties.

Several estimates of Coffin-Manson's parameters have been proposed in the literature.

Table 2 since Morrow [26], who in 1964 correlated the b and c exponents with the cyclic hardening exponent n'. Manson's universal slopes method [27], Manson's four-point correlation method [27], Rask-Morrow method [28], Mitchell method [29], Muralidharan and Manson [30], Baumel and Seeger [16], Ong's modified 4-point correlation method [31], Roessle and Fatemi [15], Median's method [32].

Among the above mentioned methods, Baumel-Seeger's uniform material law [16] and Maggiolaro-Castro's medians method [32] two tensile monotonic properties are needed to predict fatigue parameters this make them easy to apply. Roessle-fatemi method requires only hardness and modulus of elasticity make it the most convenient prediction method.

Park and Song [33], evaluated systematically all the methods proposed until 1995 using published data on 138 different materials. Figure 24 shows the prediction capability for each estimation method, it is clearly shown that the modified universal slopes method provides the best estimates.

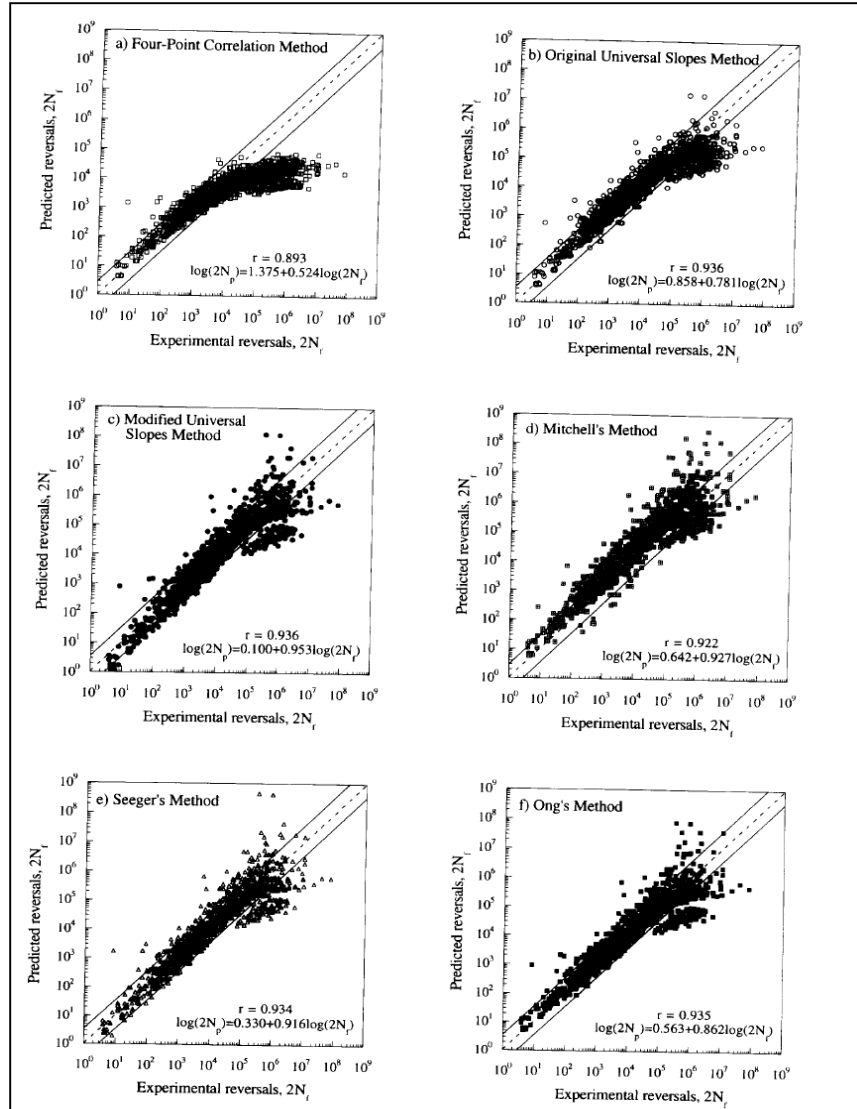


Figure 24 Comparison of Predicted and Experimental Fatigue Lives for low-alloy Steel [18]

Table 2 Estimation Methods for Coffin-Manson's Parameters

Estimation Method	σ'_f	ϵ'_f	b	c
Morrow (1964)	-	-	$\frac{-n'}{1+5n'}$	$\frac{-1}{1+5n'}$
Manson's Universal Slopes (1965)	1.9S _u	$0.76[\ln(\frac{1}{1-RA})]^{0.6}$	-0.12	-0.6
Manson's four-point (1965)	1.25σ _{f(2)} ^b	$\frac{0.125}{20^c} [\ln(\frac{1}{1-RA})]^{3/4}$	$\frac{\log(0.36S_u/\sigma'_f)}{5.6}$	$(.33)\log\frac{[0.0066 - \sigma'_f(2 \times 10^4)^b]}{0.239E [\ln(\frac{1}{1-RA})]^{3/4}}$
Rask-Morrow (1969)	-	$0.002(\sigma'_f/S'_y)^{1/n'}$	-	-
Mitchell (Steel, 1977)	S _u +345 MPa	ϵ_f	$(-1.67)\log(\frac{0.5S_u}{S_u+345})$	-0.6(ductile) or -0.5 (strong)
Muralidharan-Manson (1988)	$0.632E(\frac{S_u}{E})^{.832}$	$0.0196\epsilon'_f(\frac{S_u}{E})^{-.53}$	-0.09	-0.56
Baumel-Seeger (Steels,1990)	$1.5(\frac{S_u}{E})$	0.59 if S _w /E ≤ 0.003 0.812-74S _w /E	-0.087	-0.58
Baumel-Seeger (Al and Ti,1990)	1.67S _u	0.35	-0.95	-0.69
Ong (1993)	S _u (1+ε _f)	ϵ_f	$\frac{1}{6}\log\frac{(S_u/E)^{0.81}}{6.25\sigma'_f/E}$	$\frac{1}{4}\log\frac{0.0074 - \frac{\sigma'_f(10^4)^b}{E}}{2.074\epsilon_f}$
Roessle-Fatemi (2000)	4.25HB+225 MPa	$[0.32HB^2 - 487HB + 191000]/E$	-0.09	-0.56
Medians (Steel,2002)	$1.5(\frac{S_u}{E})$	0.45	-0.09	-0.59
Medians (AL, 2002)	1.9S _u	0.28	-0.11	-0.66
Modified Mitchell (2003)	$\frac{S_u + 335}{E}$	ϵ_f	$-\frac{1}{6}(\frac{S_u + 335}{0.446S_u})$	-0.664

Seven estimation methods, i.e. Manson's original 4- points correlation method, universal slopes method, modified universal slopes method, Mitchell's method, modified 4-point correlation method, modified Mitchell's method and uniform materials law method were evaluated by Jeon and Song [34], this study leads to a conclusion that the modified universal slopes method provides the best results for steels and modified Mitchell's method, for aluminum and titanium alloys. As these two modified methods require both ultimate tensile strength S_u and fracture ductility ε_f data, they also reported that when the fracture ductility ε_f is not available, the uniform material law may be utilized as an alternative to obtain estimation results [18].

Kim et al. [35] used eight steels to evaluate seven different prediction methods, Manson's original 4- points correlation method and universal slopes method, modified universal slopes method, Mitchell's method, modified 4-point correlation method and, uniform materials law method and Roessle-Fatemi's hardness method, concluded that modified universal slopes method, the uniform materials law and Roessle-fatemi's hardness method provide good results.

Maggiolaro and Castro [32] proposed medians method and compared with seven other prediction methods, the evaluation is based on the prediction ratio ($N_{\text{predicted}}/N_{\text{observed}}$), they concluded that the medians method provides better results and reasonable results are obtained from modified universal slopes method and Roessle-Fatemi hardness method, Figure 25, shows the average life prediction ratio for each estimation method with the strain amplitude levels between 1.2% to 5%.

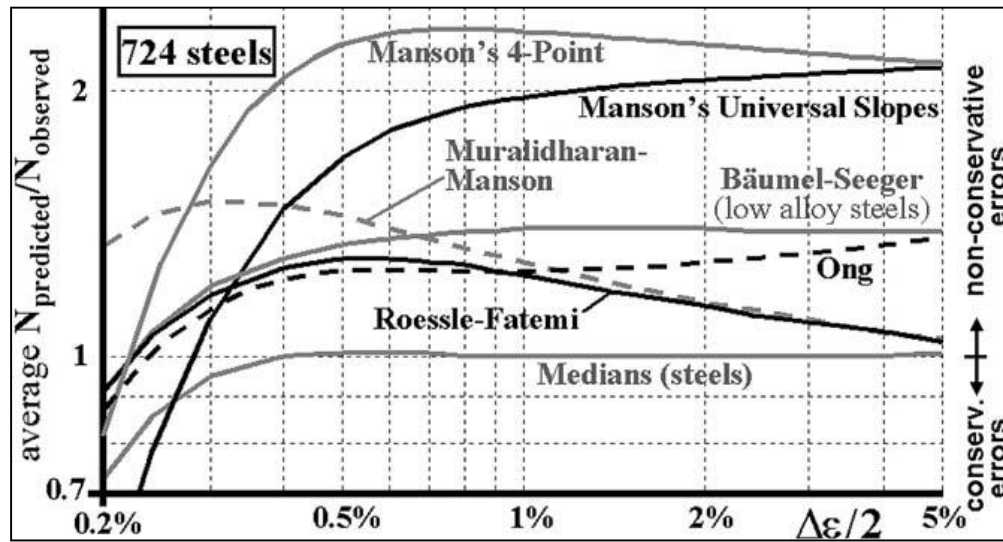


Figure 25, Average Prediction Ratio versus Strain Amplitude [32]

Kwang-Soo Lee and Ji-Ho Song [18] stated in their study that, for steel, it is the best to use the modified universal slopes method with experimentally obtained ultimate tensile strength S_u and fracture ductility ϵ_f , also they ranked the estimated methods as shown in Table 3.

Table 3 Ranking of Estimation Methods in Total Predictability for each Material Group [18]

Material group	Ranking			
	1	2	3	4
Unalloyed steels	Modified universal slopes method	Roessle-Fatemi's direct hardness method	Uniform material law	
Low-alloy steels	Modified universal slopes method	Roessle-Fatemi's direct hardness method	Indirect hardness method of (Mitchell's hardness method + medians method)	Medians method
High alloy steels	Modified universal slopes method	Medians method	Roessle-Fatemi's direct hardness method	
Aluminum alloys	Medians method	Indirect hardness method of (Roessle-Fatemi's hardness + medians method)	Uniform material law	
Titanium alloys	Modified Mitchell's method	Uniform material law	Indirect hardness method of (hardness method proposed + uniform material law	

Based on the above literature search, it can be concluded that for steels, the modified universal slopes method has the best prediction capability among the other prediction methods.

For aluminum and titanium alloys the Medians and Modified Mitchell's method are the most applicable methods.

2.1.4 Commonly Used Notch Stress-Strain Models

The models frequently used for notch stress-strain calculations are linear rule, Neuber's rule, and Glinka's rule. These rules can be used only when the nominal stress is below the elastic limit of the material which is the case for most components and structures designed to resist fatigue failure.

2.1.4.1 Linear rule

This rule is based on the assumption that both stress and strain concentration factors are the same as shown in Eq. (38)

$$\sigma = K_t S \quad , \quad \varepsilon = K_\varepsilon e = K_t e \quad (38)$$

Stephens et al. [1], stated that the linear rule is applicable for plane strain situations.

2.1.4.2 Neuber's Rule

Neuber [36], proposed the theory of notch stress for prismatic body subjected to a pure shear loading as:

$$K_\varepsilon K_\sigma = K_t^2 \quad (39)$$

$$\varepsilon \sigma = K_t^2 e S \quad (40)$$

When the elastic strain e replaced by S/E , and ε replaced by Eq. (2), the Neuber's rule for nominally elastic behavior becomes:

$$\frac{S^2 K_t^2}{E} = \frac{\sigma^2}{E} + \sigma \left(\frac{\sigma}{K} \right)^{\frac{1}{n}} \quad (41)$$

To find the notch stress the above equation can be solved using iterative or numerical schemes.

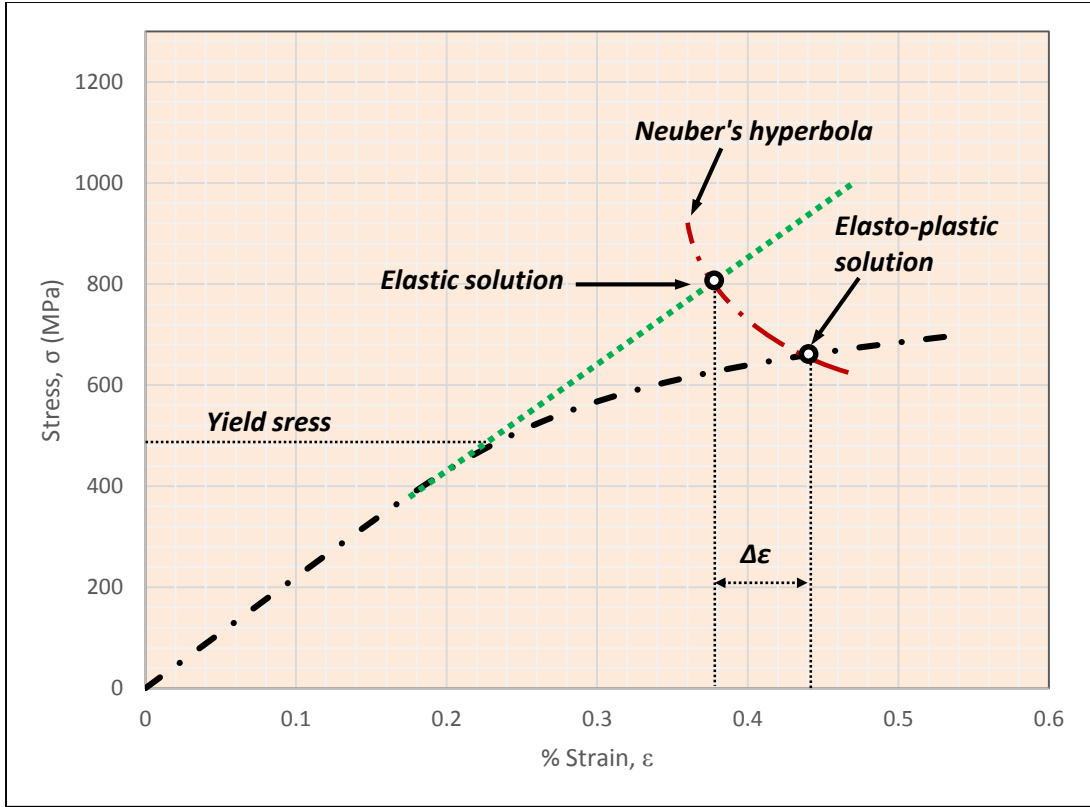


Figure 26 Determination of Monotonic Notch Strain using Neuber's Rule

Topper et al. (1969), [37] extended Neuber's rule to fatigue problems, the monotonic properties are replaced by the equivalent fatigue properties and Eq. (41) is modified as:

$$\frac{\Delta S^2 K_t^2}{E} = \frac{\Delta \sigma^2}{E} + 2\Delta \sigma \left(\frac{\Delta \sigma}{2K'} \right)^{\frac{1}{n'}} \quad (42)$$

Figure 26 shows the determination of notch stress-strain using Neuber's rule. Figure 27 represents the cyclic local stress-strain determination. Based on published studies in the literature, Neuber's rule predicts a conservative estimates of local strain compared to experimental data.

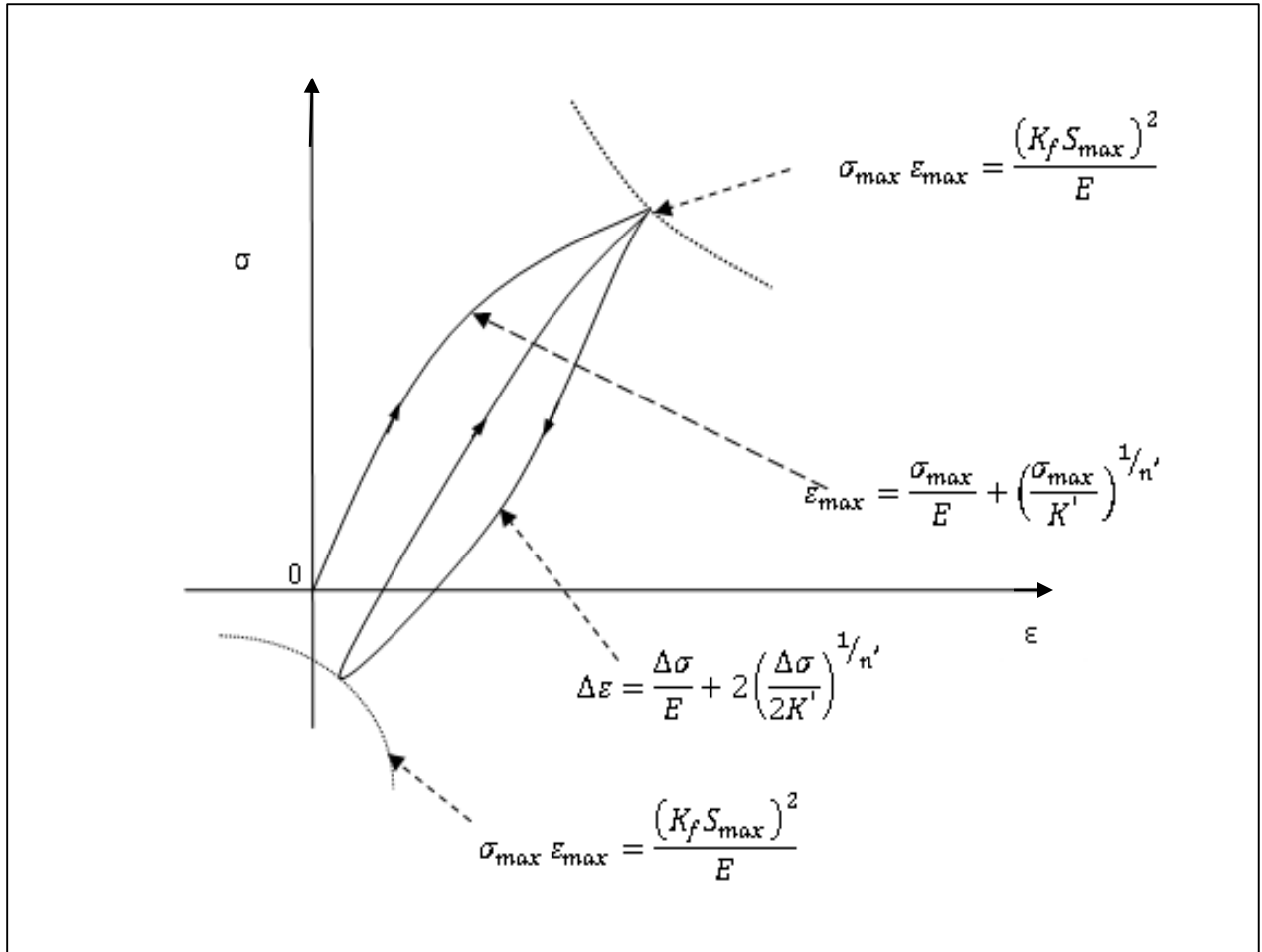


Figure 27 Cyclic Notch Stress-Strain Determination for Constant Amplitude using Neuber's Rule.

Most of studies show that Neuber's rule provides good estimation for thin sheets and plates "plane stress", and gives a conservative results under plane strain conditions [38], [39] and [40], the reason for the conservative nature of Neuber's rule was investigated and partially explained by Tipton [41], according to this study the multiaxial notch stress state constrains plastic flow and thus resists straining along load direction.

Under cyclic loads, the state of stress at the notch is assumed to be uniaxial. This is only true when the specimen thickness is small relative to the notch radius, in this case the notch root material freely contracts in the transverse direction. The opposite is true for the plane

strain condition. In such cases the transverse contractions are restricted. Hence the uniaxial stress-strain curve cannot be used in a biaxial condition at the notch tip.

Dowling et al. [42] (1977), proposed a transformation procedure from uniaxial to a biaxial condition by applying Hooke's law and von Mises's criterion for the elastic and plastic terms in the stress and strain relationship. Dowling, suggested the following simplified transformation equations to translate the uniaxial cyclic stress-strain curve ($\sigma_a - \varepsilon_a$) into a biaxial "plane-strain" relation $\sigma'_{1a} - \varepsilon'_{1a}$, Eq. (43),(44),(45)and (46)

$$\sigma'_{1a} = \frac{\sigma_a}{\sqrt{1 - \mu + \mu^2}} \quad (43)$$

$$\varepsilon'_{1a} = \frac{\varepsilon_a(1 - \mu^2)}{\sqrt{1 - \mu + \mu^2}} \quad (44)$$

$$\mu = \frac{\nu + \frac{E \varepsilon_{pa}}{2\sigma_a}}{1 + \frac{E \varepsilon_{pa}}{\sigma_a}} \quad (45)$$

$$\varepsilon_a = \frac{\sigma_a}{E} + \varepsilon_{pa} \quad (46)$$

2.1.4.3 Glinka's Rule

This method was proposed by Molski and Glinka [43] (1981), using the strain energy approach, it is based on the assumption that when the plastic yielding at the notch tip is small in this case it is controlled by the surrounding elastic stress field and the energy density distribution for the plastic zone is the same for linear elastic materials.

The proposed model has the form:

$$\frac{S^2 K_t^2}{E} = \frac{\sigma^2}{E} + \frac{2\sigma}{n+1} \left(\frac{\sigma}{K}\right)^{1/n} \quad (47)$$

The only difference with Neuber's rule is the term $2/(n+1)$, since this term is greater than unity a lower σ value is needed to satisfy the equation which means that this method gives a lower notch stress value as compared to Neuber's method.

Glinka [44], modified Eq. (47) by introducing a factor, C_p based on the fact that when stress redistribution occurs in the area neighboring the notch tip, the plastic zone expand to reach an equilibrium condition, in this case Eq. (47), should be multiplied by the correction factor C_p and is given by:

$$C_p = 1 + \frac{\Delta r_p}{r_p} \quad (48)$$

Where r_p , is the plastic zone size and Δr_p is the increment of plastic zone growth. The value of C_p ranges from 1 to 2.

The modified Glinka's method is proposed in Eq. (49):

$$C_p \frac{S^2 K_t^2}{E} = \frac{\sigma^2}{E} + \frac{2\sigma}{n+1} \left(\frac{\sigma}{K}\right)^{1/n} \quad (49)$$

Based on a studies conducted on Glinka's local stress-strain prediction, results in a conclusion that, it is a non-conservative method (it gives lower strain than the actual).

Hoffman and Seeger part 1 and 2 (1985), [45], [46] extended the well-known uniaxial notch stresses to multiaxial stress states which requires two steps: First, a relationship between applied load and equivalent stress and strain is established. Neuber's rule is chosen, replacing the uniaxial quantities σ , ε and Kt by equivalent quantities σ_q , ε_q and K_{tq} using von Mises yield criterion. In the second step, the principal stresses and strains at the notch root are correlated to the equivalent quantities σ_q , ε_q obtained from the first step as:

$$\varepsilon_q = \frac{\sigma_a}{E} F \left(\frac{\sigma_{e,q}}{\sigma_q} \right) \quad 1 \leq \frac{\sigma_{e,q}}{\sigma_q} < K_p \quad (50)$$

Where, ε_q and σ_a denote the equivalent notch strain and stress, respectively. K_p is defined as the limit load factor and defined as the ratio of the load producing cross section yielding to the yield initiation load. F , is defined as the geometry correction factor.

The assumption is that the principal stress directions remain unchanged during loading which is satisfied under the condition of symmetry and approximate for other cases of proportional loading. In this case Henky's equation is used by assuming that the strain component in one direction is a function of a strain component in a mutually normal direction. The proposed method is comparable to Dowling's method [42], the difference is in formulating the approximation formulas. In Dowling's method it is written in terms of maximum stress σ_1 and strain ε_1 instead of the equivalent quantities σ_q , ε_q . In the second part of Hofmann and Seeger paper [46], the proposed method is applied on a round bar with a circumferential notch under tensile load and a thick-walled cylinder under internal pressure. A comparison of the results with an elasto-plastic finite element analysis produced a maximum deviation of 30 percent. The method proposed an estimation for stresses and strains under proportional loading condition, they used different steps to estimate multiaxial notch stresses and strains. 1) Definition of material stress-strain curve $\sigma = g(\varepsilon)$ and selection of Von Mises as a yield criterion. 2) Definition of the elastic material constants and principal stresses σ_{e1} , σ_{e2} , and principal stress directions. 3) Estimation of plastic limit stress, S_p for elastic perfectly-plastic material. 4) Calculation of the theoretical elastic equivalent notch stress σ_q based on Von Mises and computation of K_{tq} . 5) Use of Neuber's rule as an approximation formula. 6) Application of notched element boundary conditions, fixed principal stress direction and constant strain ratio. 7) Calculation of stress and strain components. This method is based on isotropic hardening rule which fails to represent the Bauschinger effect.

James et al. [47], (1989) proposed a numerical approximation method for calculating plastic notch stress and strains. The method ignores the compatibility condition and uses the total deformation theory of plasticity. It starts with the analytical elastic stress and strain

distribution for hyperbolic notches and predicts elastic stress and strain distributions for semicircular and U-shaped notches. The results were compared with a plane stress finite element analysis, it showed that the notch root strains were underestimated by (20-30) percent.

The Gowhari-Anaraki and Hardy [48], (1991) prediction method is a modified Neuber's method for multi-axial states. This is accomplished by substituting either the equivalent or meridional stress and strain into the Neuber's equation as:

1. Based on equivalent stress and strain:

$$\Delta\sigma_{eq}\Delta\varepsilon_{eq}^1 = K_{teq}^2\Delta\sigma_a\Delta\varepsilon_a \quad (51)$$

Where: the subscripts, a and eq are nominal and equivalent respectively.

2. Based on the meridional stress and strain:

$$K_{\sigma m}K_{\varepsilon m} = K_{tm}^2 \frac{E}{E_{eff}} \quad (52)$$

Where: E_{eff} and m, are the effective modulus of elasticity of the notch and meridional respectively.

A study was conducted by Sharp et. al. [49], (1992) using finite element analysis and a laser based technique to measure the biaxial strains. The results compared with results obtained using Neuber's and Glink's methods; and led to the conclusion that, Neuber's method gives a reasonable prediction under plane stress condition and Glink's rule works best for plane strain conditions.

Tashkinov and Filatov [50], (1993) proposed an improved energy density method for inelastic notch tip strain calculations using a partial power approximation of the stress-strain curve of the material. The plastic zone correction factor C_p , in Glink's rule could be expressed explicitly. In this approximation, the stress-strain curve is expressed as:

$$S = S_y \left(\frac{\varepsilon}{\varepsilon_y} \right) \text{ for } S \leq S_y \text{ and } S = S_y \left(\frac{\varepsilon}{\varepsilon_y} \right)^m \text{ for } S > S_y \quad (53)$$

Where ε_y the yield strain and m is a material constant. The technique is extended to the generalized strain and axisymmetric conditions for which the energy postulate of the energy density method is modified. A scheme for analysis has been proposed for the case of nominal plastic yield. The results have been compared with the finite element method and experimental data.

Lee et al. [51] (1995), proposed an estimation techniques for multiaxial notch stresses and strains on the bases of elastic stress solutions. This technique utilizes a two-surface model with the Morz hardening equation and the associated flow rule to simulate the local notch stress and strain responses for any geometrical constrains of the specimens under monotonic behavior for in-phase out-of phase loading. The uniaxial material properties associated with the two-surface model are determined by the Neuber's rule, Glink's rule and FEA results. The results obtained were compared with elasto-plastic FEA and experimental results. Reasonable correlation was found between the measured and predicted notch strains for SAE 1045 material. The elastic stress versus strain relation proposed by Lee et al., can be summarized as:

1. Determine the uniaxial elastic stress versus true strain relation by Neuber's rule or Glink's energy density method.
2. Estimation of material parameters K' and n' by fitting the stress strain curve.
3. Calculate deviatoric stress vector by:

$$\bar{ds} = \bar{d}\sigma - \frac{1}{3}(\bar{d}\alpha * \bar{I}) \quad (54)$$

Where, $\bar{d}\sigma$, $\bar{d}\alpha$, and \bar{I} denotes the stress incremental tensor, the change of back stress position center and is the unit tensor respectively.

4. Calculate hardening modulus as:

$$H = \frac{2}{3} K' n' \left[\frac{2(\sigma_{yc}^L - \sigma_{yc})(D - 1) + \sigma_{yc}^L}{K'} \right]^{\frac{n'-1}{n'}} \quad (55)$$

Where, D , σ_{yc}^L , are the normalized distance from has value from 0 to 1 and the limit surfaces.

5. Calculate plastic strain increments as:

$$\bar{d}\varepsilon^p = \frac{3}{2H\sigma_{yc}^2} (\bar{s} - \bar{\alpha}) [(\bar{s} - \bar{\alpha}) * \bar{d}s] \quad (56)$$

6. Calculate elastic strain increments as:

$$\bar{d}\varepsilon^e = \frac{1 + \nu}{E} \left[\bar{d}\sigma - \frac{\nu}{1 + \nu} (\bar{d}\sigma * \bar{l}) \bar{l} \right] \quad (57)$$

7. Calculate total strain increments as:

$$\bar{d}\varepsilon' = \bar{d}\varepsilon^e + \bar{d}\varepsilon^p \quad (58)$$

8. Determine the back stress by

$$\bar{d}\alpha = \frac{(\bar{s} - \bar{\alpha}) * \bar{d}s}{(\bar{s} - \bar{\alpha}) * [\bar{s}(\sigma_{yc}^L - \sigma_{yc}) - \bar{\alpha}\sigma_{yc}^L]} [\bar{s}(\sigma_{yc}^L - \sigma_{yc}) - \bar{\alpha}\sigma_{yc}^L] \quad (59)$$

Buczynski and Glinka [52], (1995) proposed their analytical method to calculate the notch-tip stresses and strains in elastic-plastic bodies subjected to non-proportional loading sequences. It is based on the axis invariant incremental relationship between elastic and elastic-plastic strain energy density at the notch tip. This method appears to be suitable for fatigue life analysis of notch bodies subjected to multiaxial cyclic loading paths.

Z. Zeng and A. Fatemi [53], (2000) investigated the stress and strain behaviour at notch root under monotonic and cyclic loading, the results obtained from Neuber's rule, Glink's rule were compared with elasto-plastic finite element analysis results. The results show that the Glink's rule is suitable for calculating notch root strain and stress amplitudes of a notched components, where the notch is under either a plane stress or plane strain condition. Neuber's rule may only be suitable for calculating notch root strain and stress amplitudes of notched component, where the notch stress state is plane stress.

Stevan Maksimovic [54], (2005) proposed method that combined Neuber's and finite element method with strain-life criterions in order to accurately predict fatigue crack initiation life and then establish an estimated schadual of fatigue life. The local strain obtained using the equivalent stress strain relationship as:

$$\Delta\sigma_{eq}\Delta\varepsilon_{eq} = \frac{K_t^2\Delta S_{eq}^2}{E} \quad (60)$$

Where, $\Delta\sigma_{eq}$ and $\Delta\varepsilon_{eq}$ are equivalent stress and strain ranges respectively.

The fatigue life is calculated as:

$$\frac{\Delta\varepsilon_{eq}}{2} = \frac{\sigma'_f - \sigma_m}{E} (2N_f)^b + \varepsilon'_f (2N_f)^c \quad (61)$$

Where, σ_m is the mean stress.

L. Samuelsson [55], (2008) used titanium alloy "Ti6-4" in a study and proposed a prediction method based on a correlation between linear FEA and Neuber's rule estimation solution with assumption of a linear relationship between the linear and nonlinear notch root stress and strain solutions as:

$$\sigma_{corr} = \sigma_n + (m - 1) * (\sigma_l - \sigma_n) \quad (62)$$

$$\varepsilon_{corr} = \varepsilon_n + (m - 1) * (\varepsilon_l - \varepsilon_n) \quad (63)$$

Where, σ_n , ε_n are Neuber's stress and strain respectively

σ_l , ε_l are the stress and strain obtained using the linear rule.

$m = 1$ represent the Neuber's rule.

$m = 2$ represent the linear rule.

$1 < m < 2$ represent a linear interpolation between the Neuber's rule and the linear rule.

Tanweer et al. [56], (2012) developed a method to predict large elastic-plastic notch stress and strains, for materials with power-hardening law. The proposed method is implemented within simple structures with combination of limit load S_p and elastic stress concentration factor. The method can be summarized as:

$$\sigma_{eq} = \left[(1 - n) \frac{\sigma_y}{S_p} + nK_{tq} \right] S \quad (64)$$

$$\varepsilon_{eq} = \left[\frac{(1 - n) \frac{\sigma_y}{S_p} + nK_{tq}}{K} \right] S^{\frac{1}{n}} \quad (65)$$

Where, σ_y , K_{tq} , are the yield stress and equivalent stress concentration factor respectively.

2.2 PLASTICITY

The adjective “plastic” originally comes from a Greek word means “to shape”. Metals undergoes a permanent shape change when plastically deformed.

To understand plasticity it is convenient to split the stress tensor into two parts, one called a hydrostatic or spherical stress and the other is deviatoric stress tensor. The hydrostatic stress is responsible for material volume change, on the other hand the deviatoric stress causes the shape change. The hydrostatic stress can be expressed by a general form as P_{ij} whose elements are given by $\sigma_m \delta_{ij}$ where σ_m is the mean stress, Eq. (66) and [57]

$$P_{ij} = \sigma_m \delta_{ij} = \begin{bmatrix} \sigma_m & 0 & 0 \\ 0 & \sigma_m & 0 \\ 0 & 0 & \sigma_m \end{bmatrix} \quad (66)$$

$$\sigma_m = \frac{\sigma_1 + \sigma_2 + \sigma_3}{3} \quad (67)$$

Experimental work on metal alloys reveals that the effect of hydrostatic stress is insignificant and can be neglected. In plastic flow considerations only the difference between the stress tensor and hydrostatic stress is important Eq. (68) and [57]:

$$S_{ij} = \sigma_{ij} - P_{ij} = \sigma_{ij} - \sigma_m \delta_{ij} = \begin{bmatrix} \sigma_x - \sigma_m & \tau_{xy} & \tau_{xz} \\ \tau_{yx} & \sigma_y - \sigma_m & \tau_{yz} \\ \tau_{zx} & \tau_{zy} & \sigma_z - \sigma_m \end{bmatrix} \quad (68)$$

Yielding has to be considered as a yield surface, the yield surface is defined in a stress space as a convex surface separate elastic and elastic-plastic regions. Outside this surface the material exhibit a permanent deformation “plastic deformation” where at any stress value within or lower represent a reversal behavior “elastic condition”. When a metal alloy has been loaded beyond the yield surface and plasticity occurred unloaded followed by reload it yields at a higher value, in other word the yield surface grows in a positive

direction, this behavior called material hardening. In general there are two types of hardening, isotropic and kinematic hardening.

Plastic deformation due to cyclic loading is the major factor during fatigue damage process. Therefore, an understanding of multi cyclic plastic deformation is essential specially when there is significant plastic deformation as in notches.

Plastic deformation theory consists of the following basic elements:

1. A yield criteria to define the initiation of plastic flow.
2. A flow rule which relates the applied load increments to the corresponding plastic strain increments after plastic flow has initiated.
3. A hardening rule which describes the change in yield surface with plastic strains.

2.2.1 Failure Theories

2.2.1.1 Von Mises

Failure and fracture of material have two different meanings, for design purposes it is assumed that if the material starts yielding it will not serve the intended purpose. The current terminology is related to yielding rather than failure theories. The most famous yield theory used in finite element packages is Von Mises criteria or distortion energy theory. The Von Mises theory describes the multi-axial stress state at a point in a body in one stress value called equivalent stress " σ_e ", which can be compared with a uniaxial yield stress value.

In order to understand the bases of Von Mises theory it is conventional to define the magnitude of the principal stresses value at a point **P** Figure 28, where the stress vector **T** is normal to a plane passing through point **P**, in other word, a plane or planes where the shear stress is absent. These planes are called principal planes, [57].

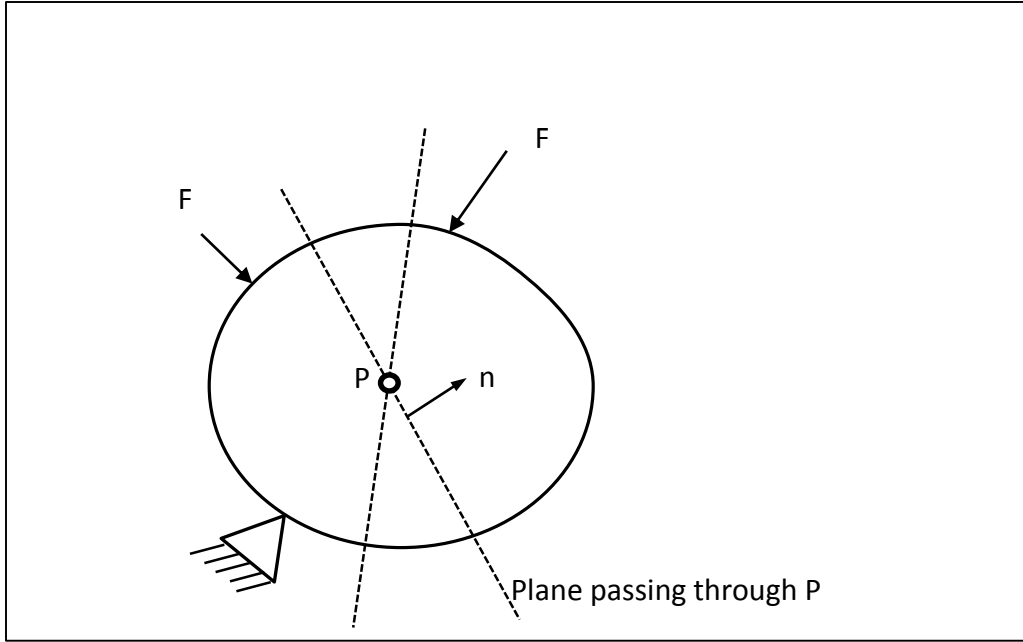


Figure 28 Planes Passing through Point P in a body under Applied Surface Forces.

This can be written mathematically:

$$T_i = \sigma n_i \quad (69)$$

Where, T_i is a stress vector, σ is the magnitude of the stress vector which is totally normal to a plane whose normal is defined by n_i .

Eq. (69) can be expressed in terms of indicial notation as:

$$\sigma_{ji} n_i = \sigma n_i \quad (70)$$

σ , is an eigen value of stress tensor σ_{ji} , and represent the value of principal stresses.

Eq. (70) can be written such as Eq. (71)

$$\sigma_{ji} n_j = \sigma \delta_{ij} n_j \quad (71)$$

Where δ_{ij} , is a mathematical operator called kronecar delta.

Rearranging of Eq. (71) gives the form below:

$$(\sigma_{ij} - \sigma\delta_{ij})n_j = 0 \quad (72)$$

The non-trivial solution of the above equation can be obtained as:

$$\det(\sigma_{ji} - \sigma I) = 0 \quad (73)$$

The result will be a cubic equation such as, Eq. (74):

$$\sigma^3 - I_1\sigma^2 - I_2\sigma - I_3 = 0 \quad (74)$$

Where, I_1 , I_2 and I_3 called invariant which they are independent of planes.

The value of each invariant is expressed mathematically as:

$$I_1 = \sigma_{ii} \quad (75)$$

$$I_2 = 1/2 (\sigma_{ij}\sigma_{ij} - I_1^2) \quad (76)$$

$$I_3 = \det[\sigma] \quad (77)$$

The roots of the Eq. (74), σ_1 , σ_2 and σ_3 represent the values of principal stresses. The eigen vectors are the principal planes which they are orthogonal.

Von Mises stated that the stress tensor can be composed additively into two parts, a hydrostatic stress tensor responsible for volume change and deviatoric stress tensor responsible for distortion as.

$$\sigma_{ij} = \begin{bmatrix} P & 0 & 0 \\ 0 & P & 0 \\ 0 & 0 & P \end{bmatrix} + \begin{bmatrix} (\sigma_{11} - P) & \sigma_{12} & \sigma_{13} \\ \sigma_{21} & (\sigma_{22} - P) & \sigma_{23} \\ \sigma_{31} & \sigma_{32} & (\sigma_{33} - P) \end{bmatrix} \quad (78)$$

$$[\sigma_{ij}] = [P] + [S_{ij}] \quad (79)$$

Where, P and S_{ij} are the hydrostatic and deviatoric stress tensors respectively.

For metals, experimental studies reveals that the hydrostatic part is not significant, and can be neglected. The second part has invariants named $J_1, J_2, \text{ and } J_3$.

These invariants can be obtained using the same analogy of the pervious process as:

$$J_1 = I_1 = 0 \quad (80)$$

$$J_2 = \frac{1}{2}(S_{ij}S_{ij}) \quad (81)$$

$$J_3 = \det[\sigma] \quad (82)$$

Yielding is independent of coordinate system, it is a function of J_2 and J_3 . It has been found experimentally that J_3 is insignificant for metals.

Metals starts yielding when J_2 reaches a critical value k^2 which is related to the uniaxial yield stress σ_y .

For uniaxial load stress can be expressed in Eq. (83) as:

$$[\sigma] = \begin{bmatrix} \sigma & 0 & 0 \\ 0 & 0 & 0 \\ 0 & 0 & 0 \end{bmatrix} \quad (83)$$

The hydrostatic stress part is the mean value:

$$P = \frac{\sigma}{3} \quad (84)$$

The deviatoric stress is defined in Eq. (85) as:

$$[S] = \begin{bmatrix} \sigma - \sigma/3 & 0 & 0 \\ 0 & -\sigma/3 & 0 \\ 0 & 0 & -\sigma/3 \end{bmatrix} \quad (85)$$

$$J_2 = K^2 \quad (86)$$

$$J_2 = \frac{1}{2}(S_{ij}S_{ij}) \quad (87)$$

Substitution and simplification of Eq. (85),(86) and (87) gives:

$$J_2 = \frac{1}{2}(S_{11}^2 + S_{22}^2 + S_{33}^2) \quad (88)$$

$$= \frac{1}{2} \left[\left(\sigma - \frac{\sigma}{3} \right)^2 + \left(-\frac{\sigma}{3} \right)^2 + \left(-\frac{\sigma}{3} \right)^2 \right] = \frac{1}{3} \sigma^2 \quad (89)$$

Yielding occurs in a uniaxial case when stress reaches σ_y , so each stress value σ is substituted by σ_y . In this case the multiaxial condition can be compared with a uniaxial case as in Eq. (90) and (91):

$$J_2 = K^2 = \frac{1}{3} \sigma_y^2 \quad (90)$$

$$K = \frac{1}{\sqrt{3}} \sigma_y \quad (91)$$

The Von Mises stress can be rewritten as:

$$\sqrt{J_2} = \frac{\sigma_y}{\sqrt{3}} \quad (92)$$

$$\sqrt{\frac{3}{2} S_{ij} S_{ij}} = \sigma_y = \sigma_e \quad (93)$$

Where σ_e is called equivalent stress. Yielding occurs when equivalent stress σ_e exceed the uniaxial yield point σ_y . σ_e can be expressed in stress tensor components as [58]:

$$\sigma_e = \sqrt{\frac{1}{2} (\sigma_{11} - \sigma_{22})^2 + (\sigma_{22} - \sigma_{33})^2 + (\sigma_{33} - \sigma_{11})^2 + 6(\sigma_{12}^2 + \sigma_{23}^2 + \sigma_{31}^2)} \quad (94)$$

Von Mises yield criterion is the most commonly used for metals, it is visualized in three dimensional stress space as a circular cylinder. In the case of unyielded material the axis of the cylinder passes through the origin of the coordinates. It lies at equal amounts to the three coordinate axes and represents pure hydrostatic stress (i.e, $\sigma_1 = \sigma_2 = \sigma_3$).

2.2.1.2 Maximum Shear Stress Theory (Tresca)

Tresca theory define yielding as a condition when the maximum shear stress at a point reach the same value of maximum shear stress at yield in a uniaxial tension given by.

$$\tau_{max} = \frac{\sigma_1 - \sigma_3}{2} = \frac{\sigma_{max} - \sigma_{min}}{2} \quad (95)$$

Figure 29 shows graphically the shape of the Von Mises's and Tresca's yield surfaces, Tresca yield theory is considered to be more conservative than Von Mises [59].

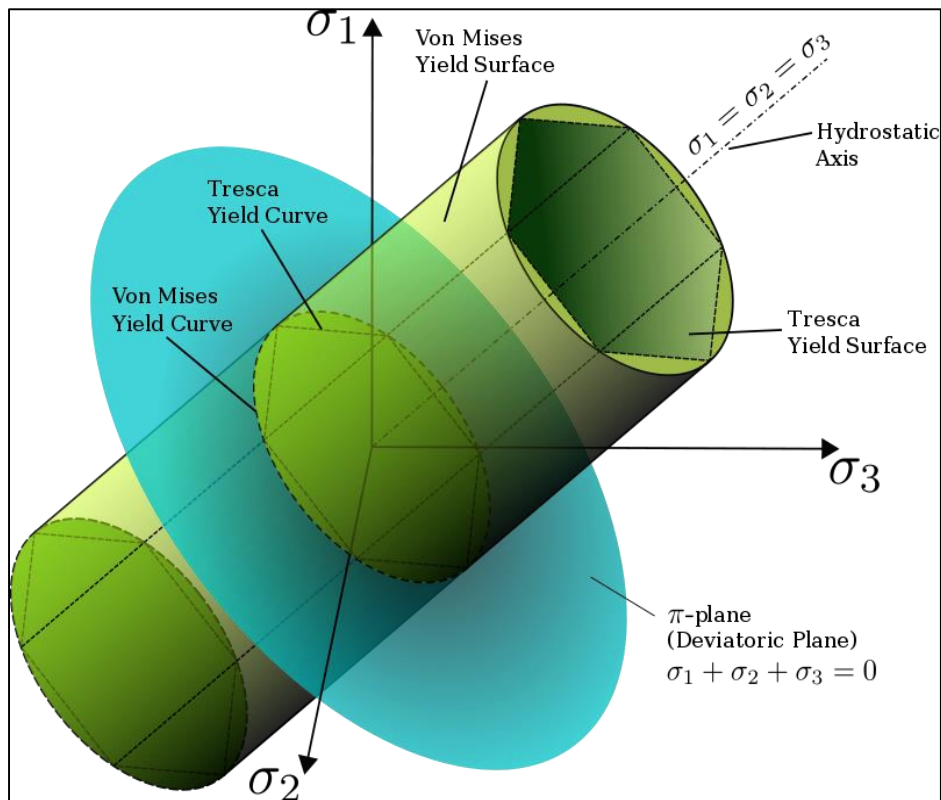


Figure 29 Von Mises/Tresca Yield Surfaces in Principal Stress Coordinates [59].

Eq. (94) is a general form of Von Mises equation, it can be reduced based of the loading condition. In case of uniaxial loading condition, $\sigma_{11} \neq 0$, $\sigma_{22} = \sigma_{33} = 0$, Eq.(62) can be reduced to a simple form to:

$$\sigma_1 = \sigma_e \quad (96)$$

Table 4 summarizes Von Mises equation for different stress conditions

Table 4 Summary of Von Mises Criterion at Different Stress Conditions

Load	Restrictions	Corresponding Von Mises equation
General	No	$\sigma_e = \sqrt{\frac{1}{2}(\sigma_{11} - \sigma_{22})^2 + (\sigma_{22} - \sigma_{33})^2 + (\sigma_{33} - \sigma_{11})^2 + 6(\sigma_{12}^2 + \sigma_{23}^2 + \sigma_{31}^2)}$
Principal stress	$\sigma_{12} = \sigma_{13} = \sigma_{23} = 0$	$\sigma_e = \sqrt{\frac{1}{2}(\sigma_1 - \sigma_2)^2 + (\sigma_1 - \sigma_3)^2 + (\sigma_2 - \sigma_3)^2}$
Plane stress	$\sigma_3 = 0$ $\sigma_{12} = \sigma_{13} = \sigma_{23} = 0$	$\sigma_e = \sqrt{\sigma_1^2 - \sigma_1\sigma_2 + \sigma_2^2 + 3\sigma_{12}^2}$
Principal plane stress	$\sigma_3 = 0$ $\sigma_{12} = \sigma_{13} = \sigma_{23} = 0$	$\sigma_e = \sqrt{\sigma_1^2 - \sigma_1\sigma_2 + \sigma_2^2}$
Pure shear	$\sigma_1 = \sigma_2 = \sigma_3 = 0$ $\sigma_{13} = \sigma_{23} = 0$	$\sigma_e = \sqrt{\sigma_1^2 - \sigma_1\sigma_2 + \sigma_2^2}$
Uniaxial	$\sigma_2 = \sigma_3 = 0$ $\sigma_{12} = \sigma_{13} = \sigma_{23} = 0$	$\sigma_e = \sigma_1$

2.2.2 Isotropic and Kinematic Hardening

When a solid material is plastically deformed by exceeding the elastic limit and then unloaded followed by reloading it does not yield at the same previous load level, since a plastic flow resistance has been induced in the material. This behavior called “strain hardening”

Usually in finite element materials model, two approaches are used; isotropic hardening and kinematic hardening.

2.2.2.1 Isotropic Hardening

Isotropic hardening occurs when a plastic material is loaded in tension past its yield stress which is followed by a compressive load does not yield until it reaches the same load level in tension. In other word, when the yield stress increases due to hardening the compression yield stress grows by the same value.

The yield surface grows in size but the origin does not move. As shown in Figure 30. This type of hardening is unusual in metallic materials.

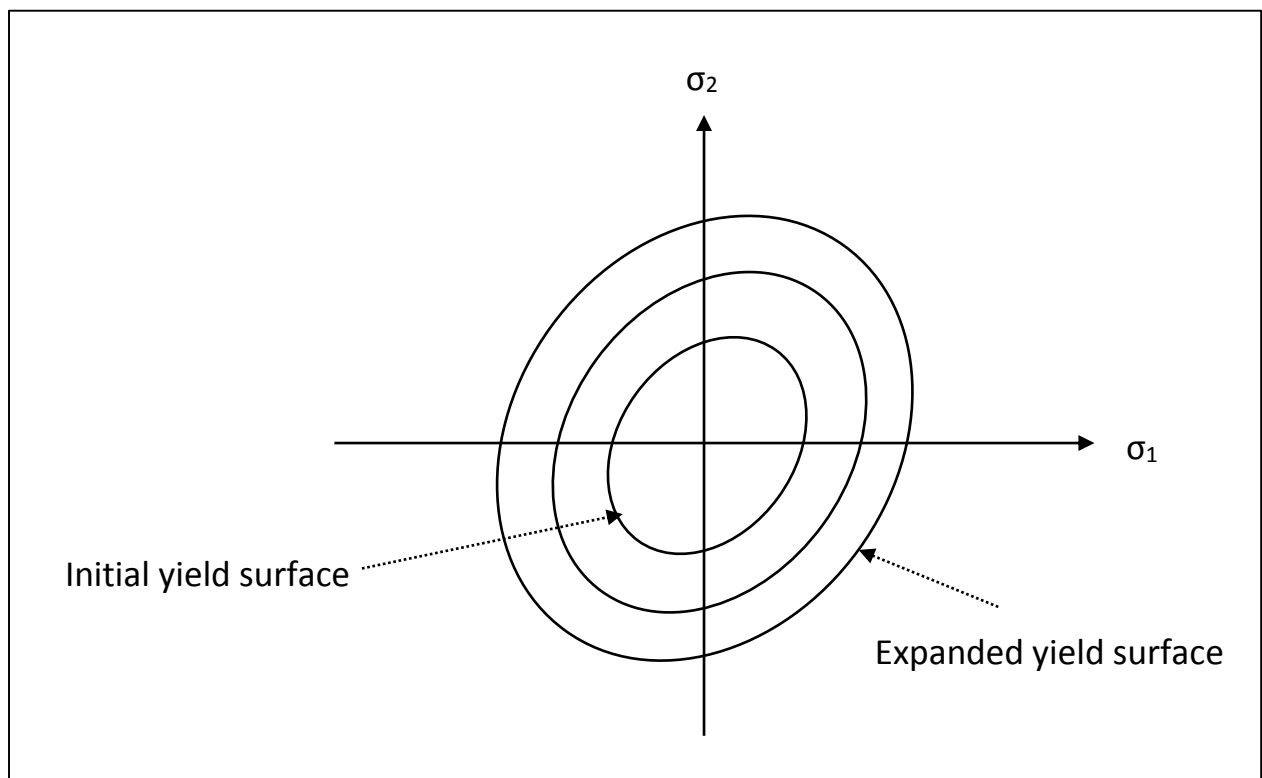


Figure 30 Schematic Representation of Isotropic Hardening “same shape, different size”

2.2.2.2 Kinematic Hardening

In kinematic hardening the material yields in compression at a lower level than the tension yield stress level, (it follows the Bauschinger effect). In reality most metals exhibit kinematic hardening and some isotropic hardening. Figure 31 shows schematically the kinematic hardening behavior. Figure 32 shows the difference between isotropic and kinematic hardening when the material is subjected to cyclic loading condition.

It is convenient to describe some existing hardening models, along with their advantages and drawback.

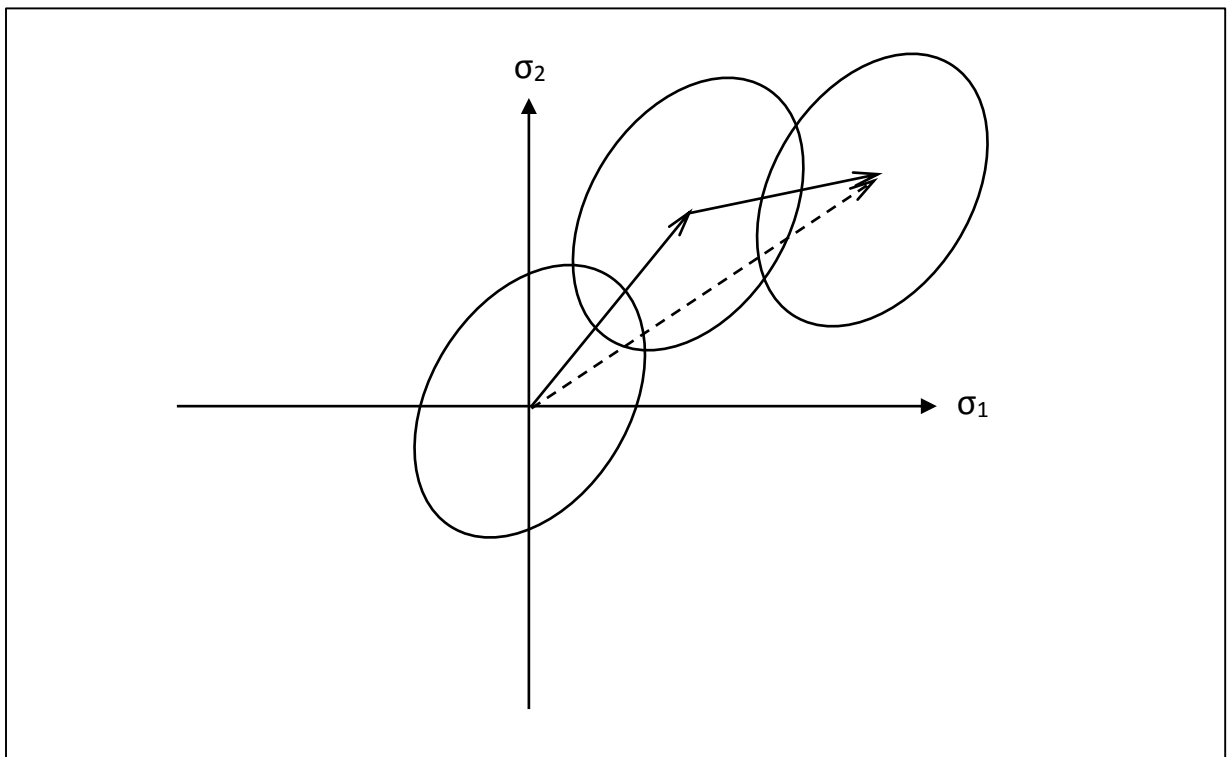


Figure 31 Kinematic Hardening Representation "same shape, same size"

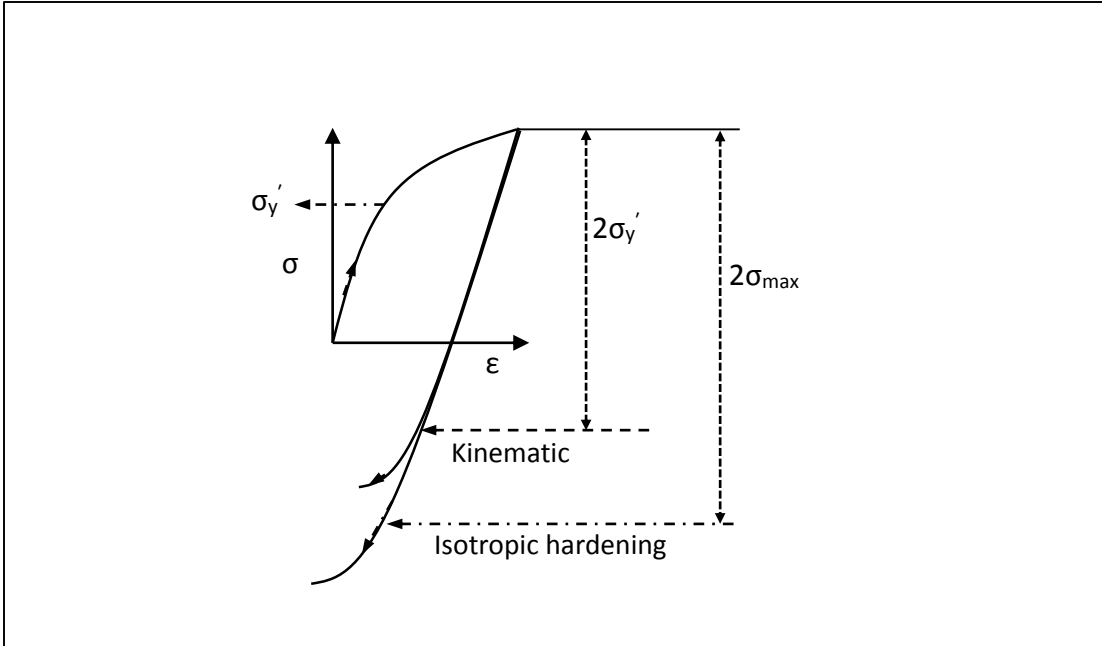


Figure 32 Isotropic and Kinematic Hardening under Cyclic Loading

2.2.2.3 Prager Rule

Prager [60] (1955), introduced the term “kinematic hardening” and proposed the first kinematic hardening model. As described earlier in kinematic hardening the assumption is that during plastic loading the yield surface translate in stress space without a change in shape or size. This behavior predicts the Bauschinger effect in uniaxial tension and compression.

When the initial yield surface described by:

$$F = f(\sigma) - k = 0 \quad (97)$$

So, due to the kinematic hardening the subsequent yield surface takes the form of:

$$f(\sigma - \alpha) - k = 0 \quad (98)$$

Where α , is a hardening parameter that is called back stress. The back stress represent the center of the yield surface in the stress space; k , is a material property that is related to the size of the yield surface. As α , changes due to plastic strain hardening, the yield surface translate in the stress space without a change in initial shape or size. Prager proposed a linear equation for the back stress α , as:

$$d\alpha = C d\varepsilon^p \quad (99)$$

Where C is a material constant derived from the monotonic uniaxial curve. This model states that the yield surface retains its initial shape and size and moves in the direction of strain increment with the direction of normal to the yield surface that is defined by Eq. (100):

$$d\alpha = C \lambda \frac{\partial F}{\partial \sigma} \quad (100)$$

Where λ , is the proportional positive scalar factor, and is determined using the yield criterion.

2.2.2.4 Armstrong and Frederick

Armstrong and Frederick (1966) proposed a model which simulates the multiaxial Bauschinger effect [61]. When compared to experimental results the model exhibits better accuracy than Prager's model. It is based on the assumption that the most recent part of the strain history of material effects the mechanical behavior. Armstrong-Frederick added a memory term to the Prager's rule as in Eq. (101):

$$d\alpha = \frac{2}{3} C d\varepsilon_p - \gamma \alpha dp \quad (101)$$

Where C and γ are material parameters, dp , is an increment of accumulated plastic strain given by Eq. (102):

$$dp = \sqrt{\frac{2d\varepsilon_p : d\varepsilon_p}{3}} \quad (102)$$

2.2.2.5 Mroz Model

The kinematic hardening rule commonly used in fatigue is the Mroz kinematic hardening rule. Mroz [62, 63], (1967, 1969), proposed a multi-surface model by defining a field of different plastic modulus in the stress space in order to obtain a better approximation of the stress-strain curve and generalize the plastic modulus in multiaxial case.

During plastic loading, the stress surfaces are activated subsequently and move until the stress point meets the next stress inactive stress surface. When the stress point meets a stress surface, this surface active. By increasing the load, the active surface and entire, previously activated surface (inner surface) move together until unloading occurs.

To define the movement direction of active stress surface, the steps in the non-proportional loading are as follow:

1. Find a similar point on the next surface that has the same normal vector as the current normal vector.

$$S_{ij}^* = \frac{R_{k+1}}{R_k} (S_{ij} - a_{ij}) + a_{ij}^{k+1} \quad (103)$$

Where:

- a) S_{ij}^* , is the point of the next stress surface.
 - b) R , stress value at the end of i th surface.
 - c) a_{ij} , tensor of yield surface.
 - d) k , plastic tangent modulus.
2. Determine the direction of the center of active surface.

$$da_{ij}^k = d\eta(S_{ij}^* - S_{ij}) \quad (104)$$

Where: η , is normal vector on the active yield surface.

3. Other inner surfaces, $1 < k < k - 1$, need to be in touch with the active surface during plastic loading. In this case, the back stress of the other internal defined as:

$$a_{ij}^r = S_{ij} - \sqrt{\frac{2}{3}} R_r n_{ij}, \quad 1 < r < k - 1 \quad (105)$$

2.2.2.6 Garud

Garud [64], (1981), noticed that there is a possibility of intersection of Mroz model yield surfaces under certain loadings, therefore, Garud proposed a modified Mroz model to prevent such intersection. Movement of the surfaces in Garud's model is dependent on the stress direction. The following steps are needed to determine the Garud model:

1. Find the normal vector on the next surface

$$n_{ij}^B = \sqrt{\frac{3}{2}} \frac{S_{ij}^B - a_{ij}^{k+1}}{R_{k+1}} \quad (106)$$

2. Find the stress point on the next inactive surface.

$$S_{ij}^* = \sqrt{\frac{2}{3}} R_k n_{ij}^* + a_{ij}^k \quad (107)$$

3. Determine the direction of the center of active surface.

$$da_{ij}^k = d\eta(S_{ij}^B - S_{ij}^*) \quad (108)$$

Chu [65], (1984), proposed an infinite surface model that does not require a discrete number of surfaces. Chu's model only requires position and radius for the current active surface.

2.2.2.7 Wang and Ohno

The model proposed by Wang and Ohno (1991), [66] Eq. (109) is based on the nonlinear kinematic hardening rule of Armstrong-Frederick [61], the model demonstrates the effect of two terms, temperature and reliable translation.

$$dp^{(i)} = H(f_i) \langle d\varepsilon_p : \frac{a^{(i)}}{\bar{a}_i} \rangle \quad (109)$$

Where $\bar{a}_i = \sqrt{\frac{3}{2} a^{(i)} : a^{(i)}}$, $f_i = \bar{a}_i^2 - \left(\frac{c_i}{\gamma_i}\right)^2$ and $H(f_i)$ denotes Heavyside step function.

On (1993) Wang and Ohno [67] proposed another model given by Eq. (110):

$$dp^{(i)} = \left(\frac{\bar{a}_i}{c_i/\gamma_i}\right)^{m_i} \langle d\varepsilon_p : \frac{a^{(i)}}{\bar{a}_i} \rangle \quad (110)$$

2.2.2.8 Chaboche

The yield function for nonlinear kinematic hardening model is expressed in Eq. (111) as:

$$F = \sqrt{\frac{3}{2} (S_{ij} - \alpha_{ij}) : (S_{ij} - \alpha_{ij})} - \sigma_y \quad (111)$$

Where S_{ij} is the deviatoric stress, α_{ij} refers to the back stress and σ_y is the yield stress obtained from the yield surface.

According to Chaboche model [68] the back stress α can be calculated using Eq.

(112),(113) as:

$$\{\alpha\} = \sum_{i=1}^n \{\alpha_i\} \quad (112)$$

$$\{\Delta\alpha\}_i = \frac{2}{3} C_i \{\Delta\varepsilon^{pl}\} - \gamma_i \{\alpha_i\} \Delta\varepsilon^{pl} + \frac{1}{C_i} \frac{dC_i}{d\theta} \Delta\theta \{\alpha_i\} \quad (113)$$

Where $\hat{\varepsilon}^{pl}$ is the accumulated plastic strain, θ is temperature, C_i and γ_i are the Chaboche material parameters for n number of pairs, (back stress versus plastic strain).

2.2.2.9 Initial Hardening Modulus

When $n=1$, C_1 represent the initial hardening modulus. If γ_i is set to zero, in this case the parameter C_1 represent the slope of stress versus equivalent plastic strain. This is called linear kinematic hardening model as shown in Figure 33 and Figure 34.

It should be noted that there is a difference between the tangent modulus E_{tan} which is based on the relationship between stress and total strain and C_1 obtained using equivalent plastic strain. There is a relationship between the two expressions given by:

$$E_{tan} = \frac{\sigma - \sigma_y}{\frac{\sigma - \sigma_y}{C_1} + \frac{\sigma}{E_{elastic}} - \frac{\sigma_y}{E_{elastic}}} \quad (114)$$

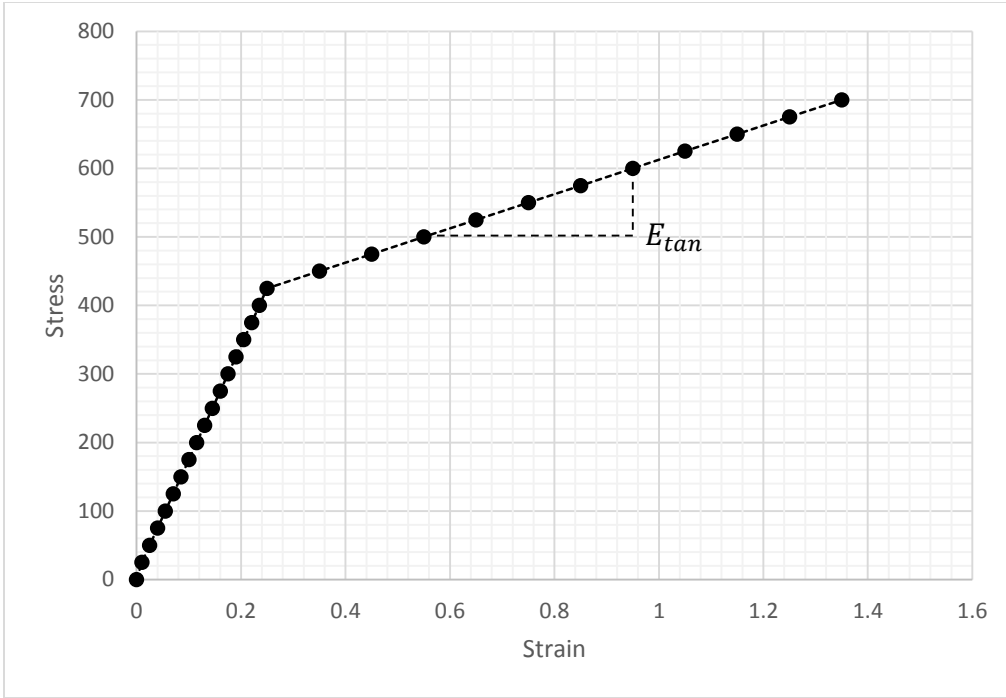


Figure 33 Schematic Representation of Linear Kinematic Hardening

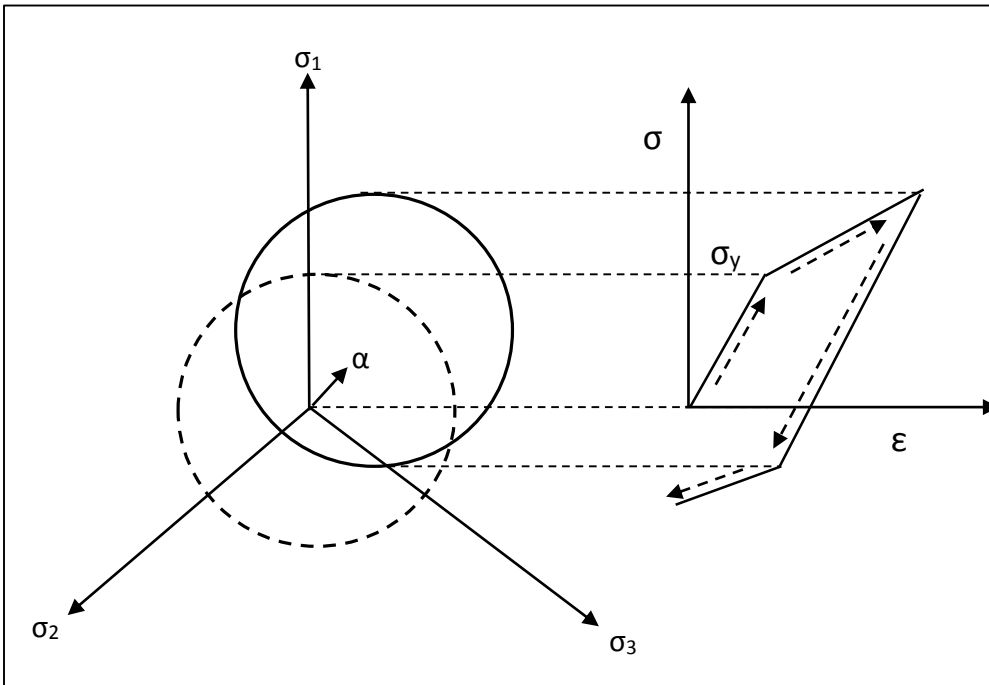


Figure 34 Stress-Strain Behavior of Linear Kinematic Hardening Model.

2.2.2.10 Nonlinear Recall Parameters

The other material parameter in Chaboche model is γ_i , which indicates the rate of hardening decreases with increasing plastic strain. The Chaboche back stress in Eq. (113) indicates that the back stress increment lowers as plastic strain gets higher. C_i/γ_i refers to a limiting value where the yield surface cannot translate anymore.

For a non-zero γ_1 parameter, the hardening modulus starts with same value as the linear kinematic hardening and keep decreasing until it reaches zero value at a high plastic strain value, this is known as the limiting or asymptotic value. This behavior is schematically represented in Figure 35 and Figure 36.

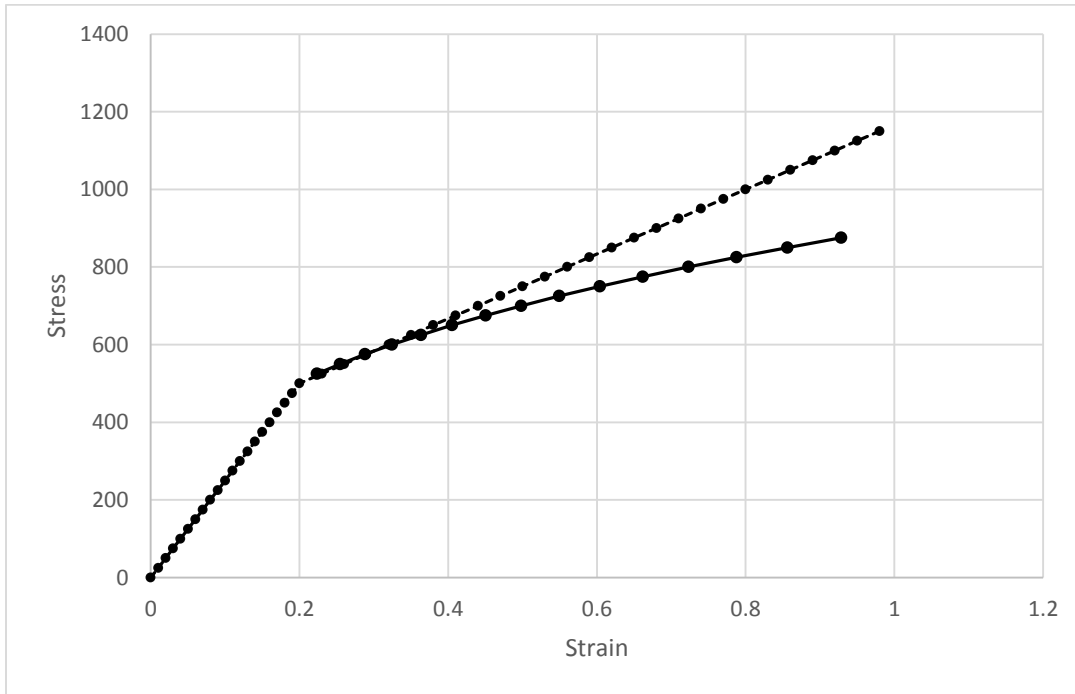


Figure 35 Small Strain

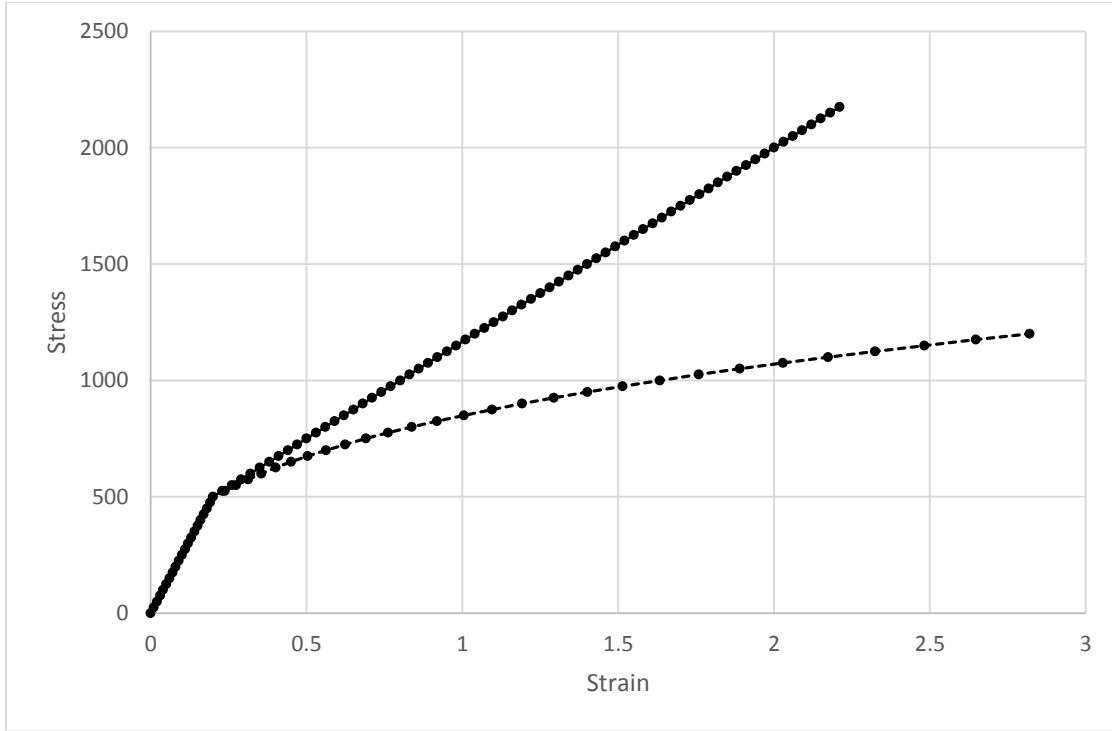


Figure 36 High Strain

2.2.2.11 Multiple Kinematic Hardening Models

In some cases the single nonlinear kinematic hardening model described by two material parameters, C_1 and γ_1 is not sufficient to describe the complex response of a given material. In this situation n can be increased to a higher value, most finite element packages use n values up to 5, which corresponds to $\gamma_1, \gamma_2, \gamma_3, \gamma_4, \gamma_5$ and C_1, C_2, C_3, C_4, C_5 .

Figure 37 shows a comparison of three results of stress versus plastic strain as:

1. Case I, represent linear kinematic hardening.
2. Case II, single nonlinear kinematic.
3. Case III, two material parameters nonlinear kinematic hardening.

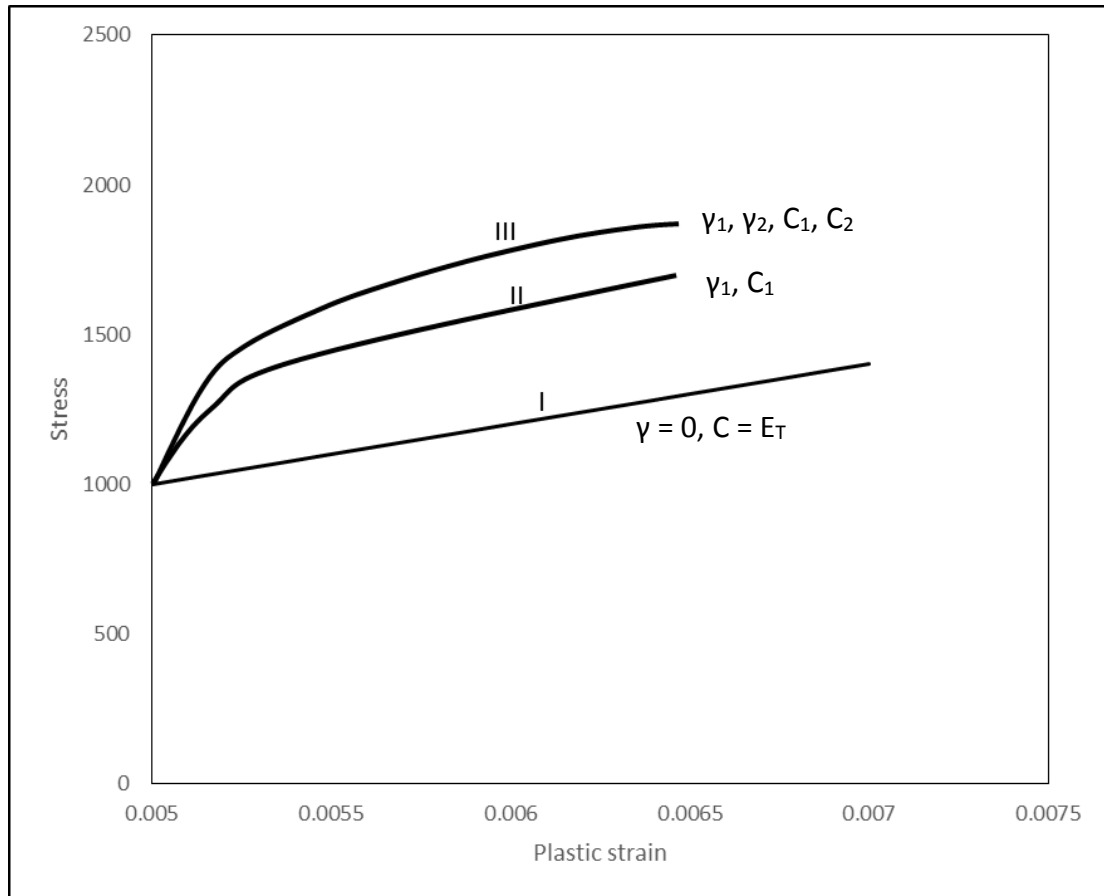


Figure 37 Effect of Kinematic Hardening Parameters Numbers

2.2.3 Identification of Parameter

The most challenging issue for researchers and designers is to identify the constants associated with any proposed material model and obtain better estimation of these parameters. The identification procedure for the material constants that describe the backstress evolution equation is based on experimental data results. Stabilized cycle behaviors is usually used for this purpose. If limited test data are available, C and γ can be estimated from the stress – strain data obtained from half cycle uniaxial tension or compression experiments as shown in Figure 38.

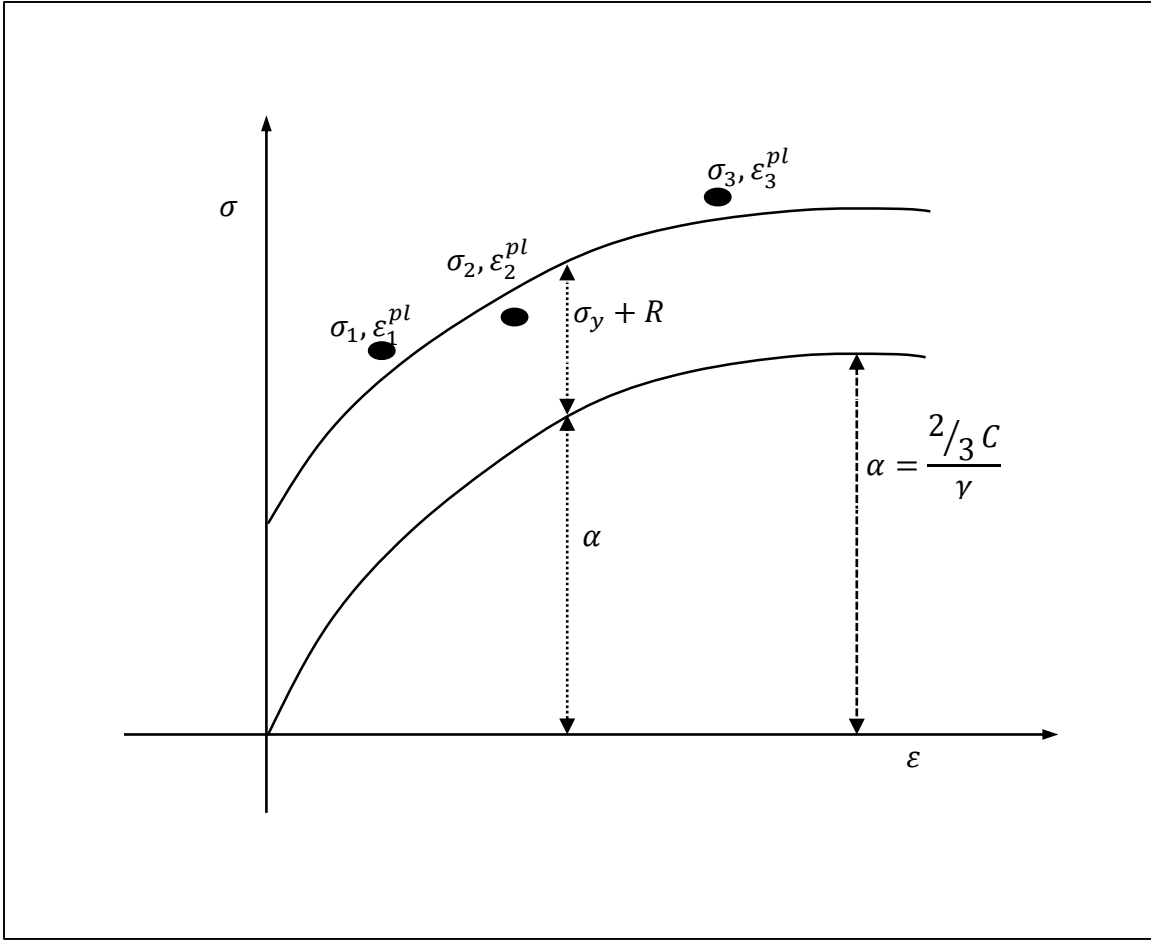


Figure 38 Half Cycle of Stress-Strain Data

For each data point $(\sigma_i, \varepsilon_i^{pl})$ a value of α_i (α_i is the overall backstress obtained by summing all the backstresses at this data point) is obtained from the test data as in Eq.(115):

$$\alpha_i = \sigma_i - \sigma_i^0 \quad (115)$$

Where, σ_i^0 is the yield surface size defined by the user at the corresponding plastic strain for the isotropic hardening component or the initial yield stress if the isotropic hardening component is not defined.

Integration of the backstress evolution laws over a half cycle leads to the expressions given by Eq. (116) :

$$\alpha_i = \frac{C}{\gamma} \left(1 - e^{-\gamma \varepsilon^{pl}}\right) \quad (116)$$

Which is used for calibrating C and γ .

According to Chaboche approach the material parameters C_i and γ_i can be obtained from the tension- compression stabilized hysteresis loops which correspond to different strain amplitudes. A numerical or graphical method can be used in this case.

The method can be summarized in five steps as follow:

1. Determine the yield stress from the elastic domain which is usually the half of elastic domain size.
2. Determine the plastic strain range $\Delta\varepsilon^{pl}$.
3. Determine the stress range $\Delta\sigma$.
4. Estimate the asymptotic value of C_i/γ_i by plotting $(\Delta\sigma/2 - \sigma_y)$ against $(\Delta\varepsilon^{pl}/2)$.
5. Using the expression $\frac{\Delta\sigma}{2} - \sigma_y = \frac{C_i}{\gamma_i} \tanh\left(\gamma_i \frac{\Delta\varepsilon^{pl}}{2}\right)$, using curve fitting to determine C_i and γ_i .

Graphical representation of the above steps are shown in Figure 39.

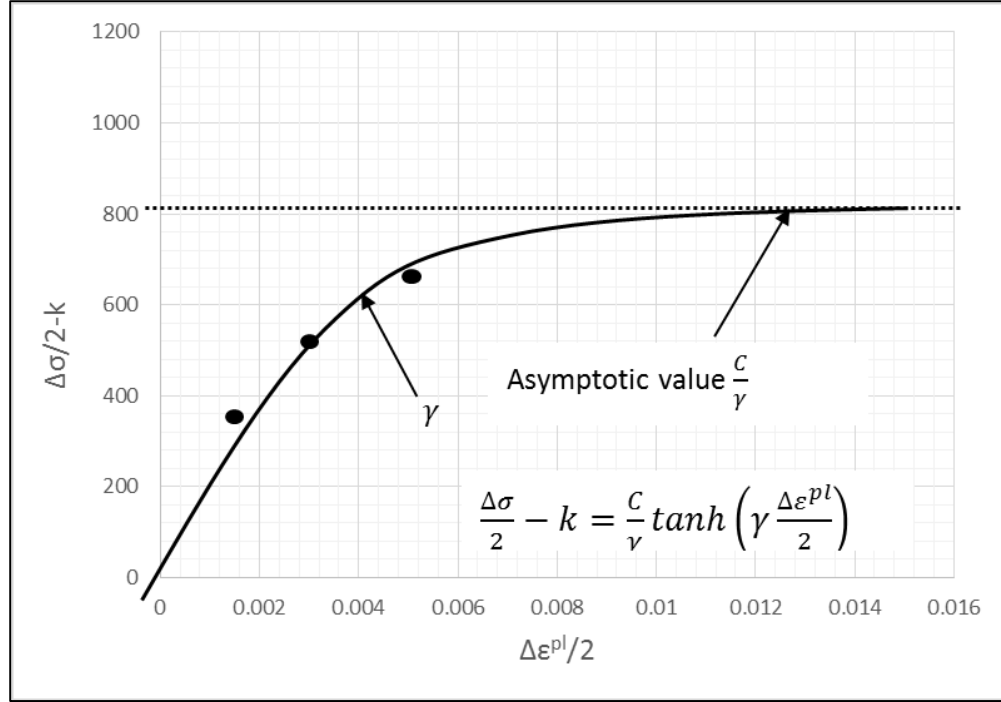


Figure 39 Identification of Coefficients C and γ from Three Tension-Compression Cycles of Different Strain Amplitudes.

2.2.4 Combined Kinematic-Isotropic Hardening Model

In practice the real plastic behavior for metallic materials does not purely follow the nonlinear kinematic hardening model, the yield surface not only translate but has both behaviors translation and expansion, in this case the isotropic behavior should be included. To reach a maximum accuracy a combined model is used which is a combination of nonlinear kinematic and nonlinear isotropic hardening model. The plastic strain increment is decomposed into two components as in Eq. (117):

$$d\varepsilon_{ij}^p = d\varepsilon_{ij}^i + d\varepsilon_{ij}^k \quad (117)$$

Where $d\varepsilon_{ij}^i$ and $d\varepsilon_{ij}^k$ refers to isotropic expansion and kinematic translation of the yield surface respectively. When the temperature term is omitted, the model takes the form for each backstress:

$$\dot{\alpha}_k = C_k \frac{1}{\sigma_0} (\sigma - \alpha) \varepsilon^{pl} - \gamma_k \alpha_k \varepsilon^{pl} \quad (118)$$

Where σ_0 defines the size of the yield surface.

2.2.5 Multiaxial State of Stress

Multiaxial states of stress and strain cannot be avoided in most engineering applications, for example:

1. In a tensile bar the state of strain is triaxial.
2. In most shafts the state of stress is biaxial.
3. For a thin-walled pressure vessel subjected to cyclic pressure the state of stress is biaxial.

Usually the state of stress in notches is multiaxial and it is not the same as the main body. The state of stress-strain at the root of bolt is biaxial but the state at the main body may be uniaxial.

The state of stress and strain at arbitrary point in the body can be described using six stress components ($\sigma_x, \sigma_y, \sigma_z, \tau_{xy}, \tau_{xz}, \tau_{yz}$) and six strain components ($\varepsilon_x, \varepsilon_y, \varepsilon_z, \gamma_{xy}, \gamma_{xz}, \gamma_{yz}$) acting on orthogonal planes x, y, and z. defining stress or strain at any other direction can be done by using transformation equations or in some cases graphically by using Mohr's circle. In fatigue there are important magnitudes and directions where maximum stress and strains developed and failure can be expected:

- Maximum normal principal stress, σ_1 .
- Maximum shear stress, τ_{max} .
- Maximum octahedral shear stress, τ_{oct} .
- Maximum normal principal strain, ε_1 .
- Maximum shear strain, γ_{max} .
- Maximum octahedral shear strain, γ_{oct} .

2.2.6 Finite Element Analysis

Finite element method recently becomes a powerful technique for numerical solution of many engineering problems. With the aid of advanced computer technology and CAD

systems a complex structures can be modeled and analyzed. In automotive industry this technique is used mainly for elastic-plastic analysis of structures. A constitutive model is employed to capture the material response “stress and strain” at each integration point called local integration. Structural response is the product or a combination of all local integration points it is called global integration. Local and global integrations are carried out simultaneously. The level of accuracy for structural solution mainly relies on the accuracy of calculations at the local integration points. In finite element the model body is divided into an equivalent system of many smaller units “finite elements” interconnected to points common to two or more elements “nodes” [69] Figure 40.

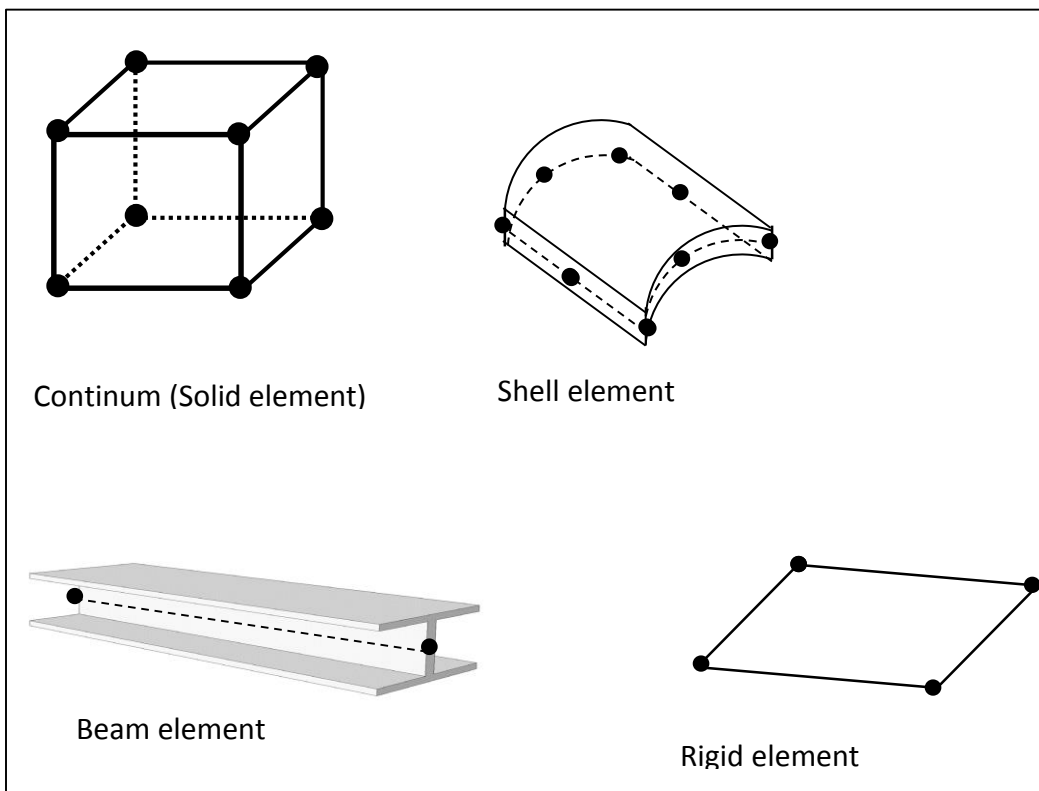


Figure 40 Some Types of Elements in ABAQUS

3 STATEMENT OF PROBLEM AND THEORY

3.1 The Strain-Life Prediction Model

The original form of Universal Slopes Equation was proposed by Manson and Hirschberg in 1965 Eq. (119), [27] as:

$$\Delta\varepsilon = 3.5 \frac{\sigma_u}{E} (N_f)^{-0.12} + \left[\frac{N_f}{D} \right]^{-0.6} \quad (119)$$

Where $\Delta\varepsilon$ = total strain range

N_f = fatigue life

D = ductility

σ_u = ultimate tensile strength

The slopes of elastic and plastic lines were universalized as -0.12 and -0.6 for all materials. U. Muralidharan and Manson [30], modified Eq. (119) and proposed the Modified Universal slopes equation. Their work started with a general form as shown in Eq. (120):

$$\Delta\varepsilon = A_1 D^{\alpha_1} \left[\frac{\sigma_u}{E} \right]^{\beta_1} (N_f)^{\gamma_1} + A_2 D^{\alpha_2} \left[\frac{\sigma_u}{E} \right]^{\beta_2} (N_f)^{\gamma_2} \quad (120)$$

γ_1 and γ_2 exponents are assumed to be constant for all materials. The coefficients are generalized and allowed to be power functions of ductility (D), ultimate tensile strength σ_u and modulus of elasticity (E), for both elastic and plastic components. Optimization for the constants by the least squares method using 47 different materials results in the final form of Modified Universal Slopes method shown in Eq. (121).

$$\frac{\Delta\varepsilon}{2} = 0.623 \left(\frac{\sigma_u}{E} \right)^{0.832} (N_f)^{-0.09} + 0.0196 (\varepsilon_f)^{0.155} \left(\frac{\sigma_u}{E} \right)^{-0.53} (2N_f)^{-0.56} \quad (121)$$

The above study showed that the effect of ductility (D) on the elastic line is negligible, so it is eliminated from the elastic part of Eq. (119). For the plastic component the effect of ductility become less important and the exponent reduced from 0.6 to 0.155. It was found

that the ratio $\left(\frac{\sigma_u}{E}\right)$ has a high effect on both elastic and plastic components. The universal slopes which were -0.6 and -0.12 have become -0.53 and -0.09 respectively.

3.1.1 Objectives

One of the objectives of this thesis is to develop a prediction model that predicts cyclic deformation properties using Brinell hardness HB, the reason being that hardness test is a nondestructive test and hence easy to obtain. Hence it is advantages to use Brinell hardness (HB) instead of ultimate tensile (S_u) strength in Modified Universal Slopes method with optimization of the coefficients. Out of several estimation methods the Modified Universal Slopes method Eq. (121) was selected based on estimation studies made on the existing prediction methods which show that this model is the most recommended for prediction of fatigue life of steels. The Modified Universal Slopes model predicts cyclic properties based on ultimate tensile strength (σ_u), modulus of elasticity (E) and fracture ductility (ϵ_f).

Since ultimate tensile strength strongly correlates to brinell hardness, “Roessel and Fatemi” proposed a correlation model with $R^2 = 0.96$ [15]. Hence, it is possible to use an estimated value of ultimate tensile strength from Brinell hardness in the Modified Universal Slopes method. The first stage in this study was to find a high correlation model similar to Roessel-Fatemi model between Brinell hardness and ultimate tensile strength, and then this value will be substituted in the Modified Universal Slopes method. The constants were then optimized using experimental data. In this case the fatigue parameters were predicted using Brinell hardness (HB), modulus of elasticity (E) and fracture ductility (ϵ_f).

The true fracture ductility (ϵ_f) still undesirable term in the model because it is not always available in the data, however, it was stated in the previous section that the effect of this term has less importance than indicated by the earlier Universal Slopes equation [27].

In general this term ranges from 0.15 to 1.5 for steels; and the value of (ϵ_f^{155}) ranges from 0.75 to 1.02 with an average value of 0.9, this term still needs further investigations, so that it can be replaced by an approximate constant value.

To validate the proposed method it was compared with the original method Eq. (108) and experimental data values, different data sources including low, medium, and high strength

steels were used. Matlab was used to solve for the number of cycles to failure for each strain amplitude value.

3.2 Notch Strain Prediction Models.

Eq. (121) can be used for a smooth specimen where the differences between the nominal and local stresses and strains are negligible, however, in case of notched components which are most common the differences are significant, in this case the local strain amplitude has to be predicted. One of the objectives of this study was to create a notch root stress-strain prediction model based on using a combination of elastic finite element analysis and Neuber's prediction method Eq. (42).

The aim is to simplify the notch root predictions by introducing an alternative method which rely on a linear finite element analysis which is accurate and easy to conduct with the aid of Neuber's analytical method, this saves time and cost compared with an expensive and time consuming elasto-plastic finite element analysis where the definition of materials constants is a challenge. The proposed model was compared with elastic-plastic finite element analysis. The elastic and elasto-plastic was obtained using ABAQUS 6.13 software, and the materials cyclic properties experimental data sources used in ABAQUS elasto-plastic analysis are:

- American Iron and Steel Institute (AISI) [24]
- Metals data for cyclic loading [16]

3.2.1 Notch Geometry

To investigate the cyclic loading behavior two different geometries were used. A double notched plate geometry with a notch depth of 6.35 mm and notch radius of 2.778 mm to create the plane stress condition and a round bar with a groove of radius 1.588 mm notch radius to create the plane strain condition. Figure 41 shows the two geometric configurations used in this study, where (a) represent the plane stress condition and (b) reflect the plane strain condition

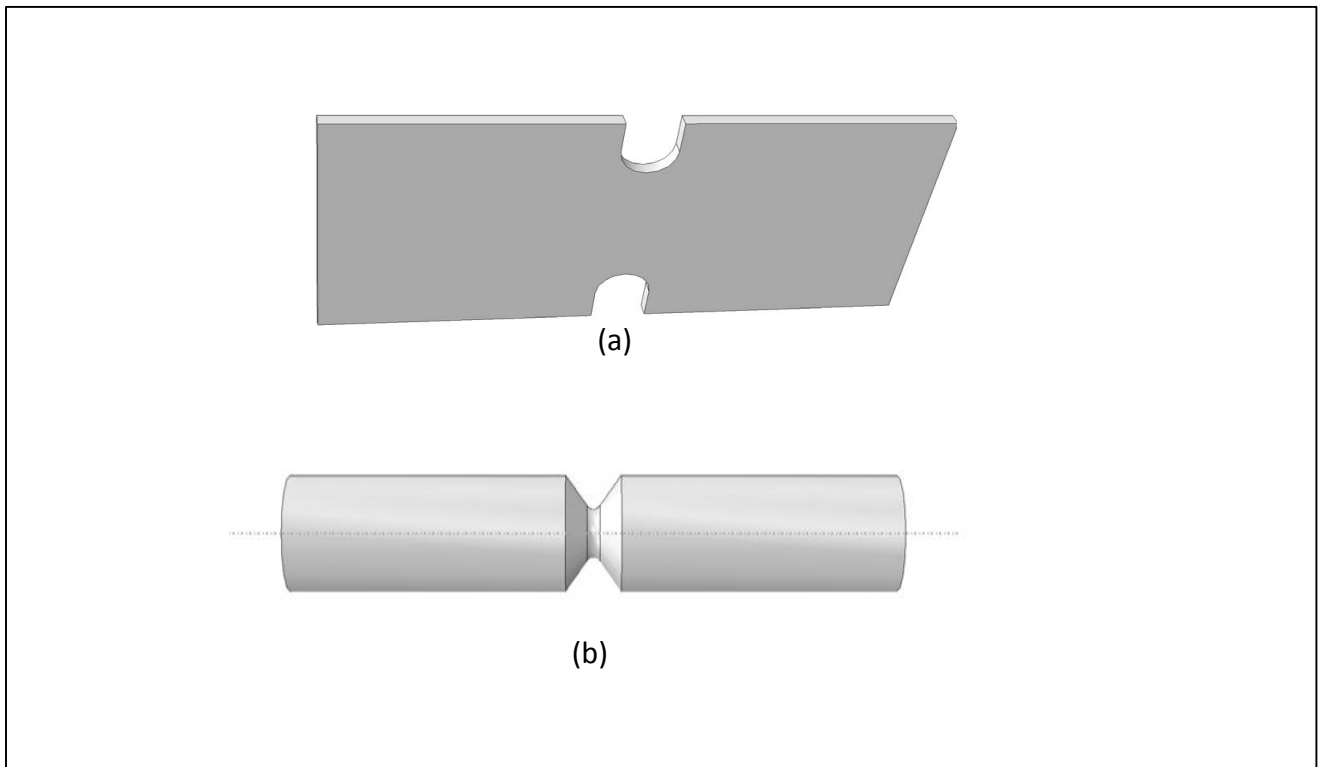


Figure 41 Notched Configurations (a) Notched Plate with 2.77 mm Radius (b) Circumference Notched Round bar with 1.588 mm Radius

4 PERFORMING PREDICTION METHODS

4.1 Perform fatigue properties estimation model

As mentioned earlier, Park and Song [33] compared different approaches of prediction fatigue life using monotonic tensile properties. Three methods have been compared, the Modified Universal Slopes, Seeger's, and Ong's method, the three methods give reasonably good life predictions. Among them, the Modified Universal Slopes method gives the best results. Consequently, the Modified Universal Slopes method can be recommended as one of the best estimation methods that are currently available [70].

The Modified Universal Slopes method proposed by Muraliharan and Manson [30] predicts fatigue properties using ultimate tensile strength (S_u), true fracture ductility (ϵ_f) and modulus of elasticity (E), and is given by Eq. (121)

In this method fatigue strength exponent b and fatigue ductility exponent c, are approximated by a constant of values -0.09 and -0.56 respectively.

4.1.1 Correlations Among Tensile Data

As stated earlier, it is desirable to estimate fatigue properties of materials from material properties that are quick and easy to obtain, with a reasonable degree of accuracy, such as hardness and ultimate tensile strength.

The well-known approximation of the ultimate tensile strength, S_u from Brinell hardness, HB, for low and medium strength carbon and alloy steel is presented by a linear relationship given by Eq. (23)

Eq. (23) agrees well with experimental data for $HB < 350$, [14]. A nonlinear approach proposed by Roessle and Fatemi, correlates S_u and hardness using fatigue properties of 20 steels commonly used in the ground vehicle industry as follow [15]:

$$S_u = 0.0012(HB)^2 + 3.3(HB) \text{ (MPa)} \quad (122)$$

In this study, an extensive data from 246 various steels selected from the American Society for Metals (ASM) reference book [71] was used. The materials used cover the ultimate

tensile strength values range from (386 to 2034) MPa and Brinell hardness range from (111 to 555) MPa, this range covers most of steels used in automotive industry, part of these data is shown in Table 5, the rest is tabulated in appendix A. Different nonlinear functions been used in order to reach the best correlation between Brinell hardness HB and ultimate tensile strength S_u . A least squares fit results in an exponential relationship as:

$$S_u = 320e^{0.0036HB} \quad MPa \quad (123)$$

Where, HB is the Brinell hardness in MPa.

An extensive application of Eq. (123) on each experimental data shows that it is need to be modified to enhance the accuracy. Many modified equations has been produced and the most accurate one has the following form:

$$S_u = \{410(\exp(0.00155HB))^{2.1} - 150\} \quad (MPa) \quad (124)$$

Eq. (124), was applied on 246 different steels to predict the ultimate tensile strength from Brinell hardness HB, the results are compared with Roessle-Fatemi's prediction method. Also the ratios of (predicted/experimental) ultimate tensile strength values are calculated.

The produced data from proposed as well as Roessle-Fatemi's methods are compared with experimental data, part of the produced results were shown in Table 5, the rest of data is shown in appendix A. The closest the (predicted S_u /experimental S_u) ratio to one the better prediction capability, the ratio of one is the optimum value.

Table 5 Ultimate Tensile Strength Values Obtained from Proposed Method and Rossel-Fatemi Compared with Experimental Data

Number	AISI	Treat. Temp. C ⁰	HB	S _u (Exp.)	S _u (Prop.)	S _u (Prop.)/S _u (Exp.)	S _u (R-F)	S _u (R-F)/S _u (Exp.)
1	1015	126	420	468	1.11	435	1.04
2	1015	925	121	424	458	1.08	417	0.98
3	1015	870	111	386	438	1.14	381	0.99
4	1020	143	448	503	1.12	496	1.11
5	1020	870	131	441	478	1.08	453	1.03
6	1020	870	111	394	438	1.11	381	0.97
7	1022	925	143	482	503	1.04	496	1.03
8	1022	870	137	429	490	1.14	475	1.11
9	1030	...	179	551	584	1.06	629	1.14
10	1030	845	126	463	468	1.01	435	0.94
11	1040	...	201	620	639	1.03	712	1.15
12	1040	900	170	589	563	0.96	596	1.01
13	1040	790	149	518	516	1.00	518	1.00
14	1050	229	723	714	0.99	819	1.13
15	1050	900	217	748	681	0.91	773	1.03
16	1050	790	187	636	604	0.95	659	1.04
17	1060	241	813	749	0.92	865	1.06
18	1060	790	179	625	584	0.93	629	1.01
19	1080	...	293	965	914	0.95	1070	1.11
20	1080	900	293	1010	914	0.91	1070	1.06

To validate the proposed relationship a qualitative as well as a quantitative analysis were conducted, the results were compared with the best model in the literature. Evaluation of estimation methods for strain-life fatigue properties from hardness conducted by Kwang-Soo Lee at al., reveals that among 4 existing methods for estimating ultimate tensile strength from hardness, the Roessle-Fatemi's method Eq. (122) provides the most reasonable estimation results. Figure 42 shows a plot of predicted versus experimental ultimate tensile strength values using proposed method in Eq. (124) together with Roessel-Fatemi's correlation Eq. (122). In Figure 43, the ratio of estimated/experimental ultimate tensile strength plotted versus the Brinell hardness HB, where the dashed lines indicate a factor of $\pm 10\%$ scatter band.

Eq. (124) covers a range of hardness from, 150 (HB) to 550 (HB) and with ultimate tensile strength that range from 386 (MPa) to 2034 (MPa).

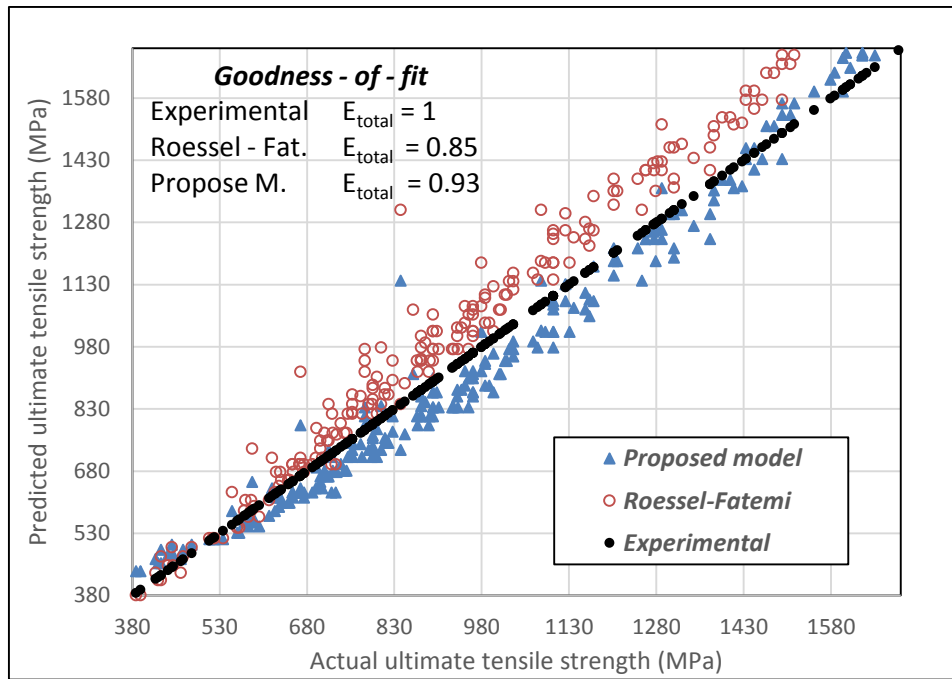


Figure 42 Predicted vs Experimental Ultimate Tensile Strength

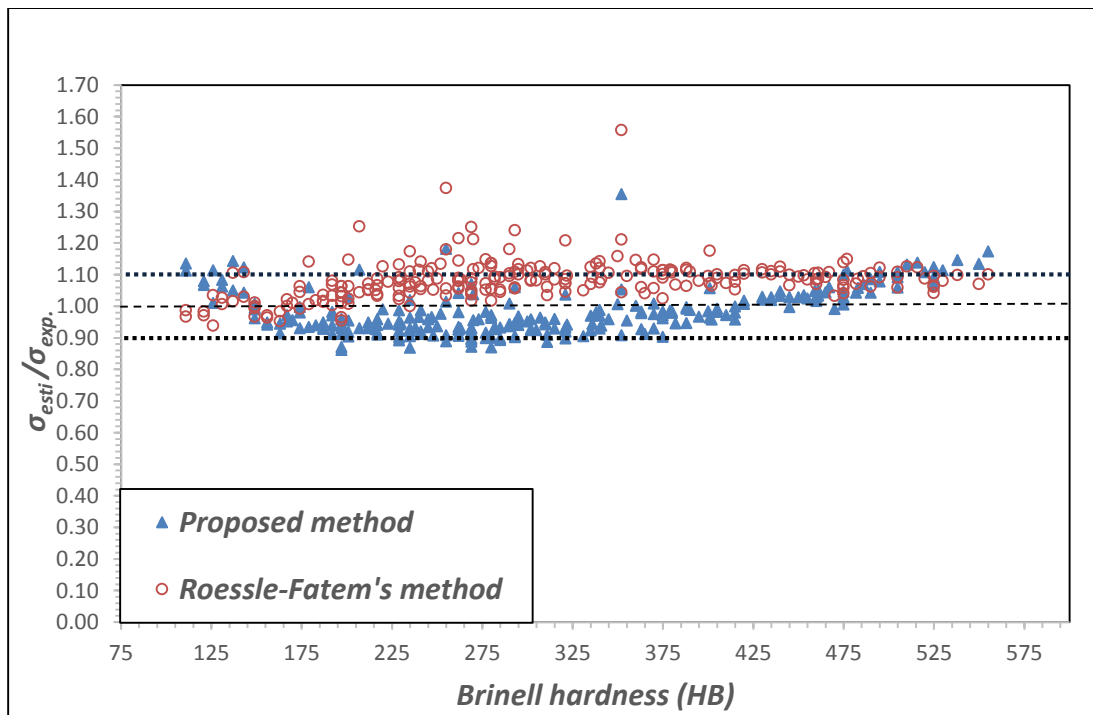


Figure 43 Estimated, Experimental Data Ratio versus Brinell Hardness (HB)

The results obtained in Figure 42 and Figure 43 are useful for evaluating the $S_u - HB$ estimation methods, but give only qualitative information. For quantitative evaluation the following three terms; error criterion, mean value and coefficient of variance were used.

$$E_{f(s=10\%)} = \frac{\text{Number of data falling within } 0.9 \leq \frac{(S_u)_{Pred.}}{(S_u)_{Exp.}} \leq 1.1}{\text{Number of total data}} \quad (125)$$

$$\text{Mean value} = \text{Mean of } \frac{(\sigma_{Prop.})}{(\sigma_{Exp.})} \quad (126)$$

$$CV \text{ (Coefficient of variance)} = \frac{\text{Standard deviation}}{\text{Mean}} \quad (127)$$

E_f is the error criterion which is usually used to evaluate the estimation methods. It is evaluates the accuracy of estimation in terms of fraction of data that falls within a scatter band of a specified factor S . The mean value of data is employed as additional value because the error criterion E_f is not enough to evaluate the deviation of data value from the optimum value of $\frac{(\sigma_{Prop.})}{(\sigma_{Exp.})} = 1$. The coefficient of variance is another measure of normalized scatter. The closer the E_f is to 1, the better the estimation and it is true for the other two items, the mean and coefficient of variance.

$$E_{mean} = 1 - |1 - \text{mean}| \quad (128)$$

$$E_{CV} = 1 - |CV| \quad (129)$$

By assuming that the three evaluation values are equally important, the total evaluation is made using the mean values of E values defined as:

$$\bar{E} = \frac{E_f + E_{mean} + E_{CV}}{3} \quad (130)$$

Table 6 shows the comparisons of estimation methods in terms of evaluation values described.

Table 6 Estimated Ultimate Tensile Strength Quantitative Analysis

E values	Proposed method	Roessle-Fatemi
$E_{f(s=10\%)}$	0.882	0.695
E_{mean}	0.98	0.917
E_{CV}	0.927	0.942
\bar{E}	0.931	0.852

As mentioned in the earlier the fatigue material parameters as predicted in Modified Universal Slopes Method using ultimate tensile strength, modulus of elasticity and true fracture ductility are obtained using the Eq. (131) and (132).

$$\sigma'_{f(M)} = .623E \left(\frac{S_u}{E} \right)^{.832} \quad (131)$$

$$\varepsilon'_{f(M)} = .0196(\varepsilon_f)^{0.155} \left(\frac{S_u}{E} \right)^{-.53} \quad (132)$$

Where $\sigma'_{f(M)}$ and $\varepsilon'_{f(M)}$ are the fatigue strength coefficient and fatigue ductility coefficient respectively.

In this study, Brinell hardness is used instead of ultimate tensile strength based on the correlation proposed in Eq. (124). The optimization of the coefficients after substitution of ultimate tensile strength by Brinell hardness in Eq. (131) and Eq. (132) results in a new prediction model in equations Eq. (133), (134).

$$\sigma'_{f(p)} = 28.74(E) \left(\frac{[4.1(\exp(.00155HB))^{2.1} - 1.5]}{E} \right)^{.832} \quad (133)$$

$$\varepsilon'_{f(p)} = .0017(\varepsilon_f)^{.155} \left[\frac{[4.1(\exp(.00155HB))^{2.1} - 1.5]}{E} \right]^{-.53} \quad (134)$$

Where $\sigma'_{f(p)}$ and $\varepsilon'_{f(p)}$ are the proposed method fatigue strength coefficient and fatigue ductility coefficient respectively.

The final form of the proposed method is provided in Eq. (135)

$$\begin{aligned} \frac{\Delta\varepsilon}{2} = & 28.74 \left(\frac{[4.1(\exp(.00155 * HB))^{2.1} - 1.5]}{E} \right)^{.832} (2N_f)^{-.09} \\ & + .0017(\varepsilon_f)^{.155} \left(\frac{[4.1(\exp(.00155 * HB))^{2.1} - 1.5]}{E} \right)^{-.53} (2N_f)^{-.56} \end{aligned} \quad (135)$$

The new approach eliminates ultimate tensile strength from the original model, where it is replaced by the Brinell hardness. Hardness can be measured nondestructively even for in-service component, but measuring ultimate tensile strength is a destructive testing that needs a prepared specimen. Based on the new model, fatigue parameters can now be predicted by knowing the hardness, the modulus of elasticity, and the true fracture ductility.

The true fracture ductility (ε_f) is still an undesirable term in this method because it is not always available in the data. According to (Meggiolaro, Castro) comprehensive study on the evaluation of the strain-life prediction methods, it is concluded that the correlation of (ε_f) with monotonic cyclic properties is poor, it is recommended that this term is replaced with a constant value. In general this term ranges from 0.15 to 1.3 for steels; and the value of (ε_f)^{0.155} ranges from 0.75 to 1.02 with an average value of 0.9.

4.1.2 Evaluation of the Proposed Strain-Life Estimation Method.

4.1.2.1 Qualitative Evaluation

To evaluate the prediction capabilities of the proposed method given by Eq. (135), it is compared with the Modified Universal slopes method given by Eq. (121) and a real experimental fatigue data. 52 different steels including low, medium and high strength steels from different data sources including J1099, ASM, AISI and material data for cyclic

loading, were used, the constant amplitude fatigue tests were performed according to the ASTM Standard E606 [72]. These steels cover the cyclic hardening/softening characteristics, Brinell hardness ranges from 150 (HB) to 660 (HB), and the ultimate tensile strength is ranges from 300 to 2500 (MPa).

Strain amplitudes data obtained from strain-life curve for each material at fatigue lives that range from 10^3 to 10^6 reversals. Log strain amplitude of $(\Delta\varepsilon/2)$ is plotted versus log life to failure ($2N_f$) which results in strain-life curves for each material; this approach gives better results when compared to the original Modified Universal slopes method and real experimental fatigue data form literature, as observed in Figure 44 - Figure 47 the rest of graphs are shown in appendix A.

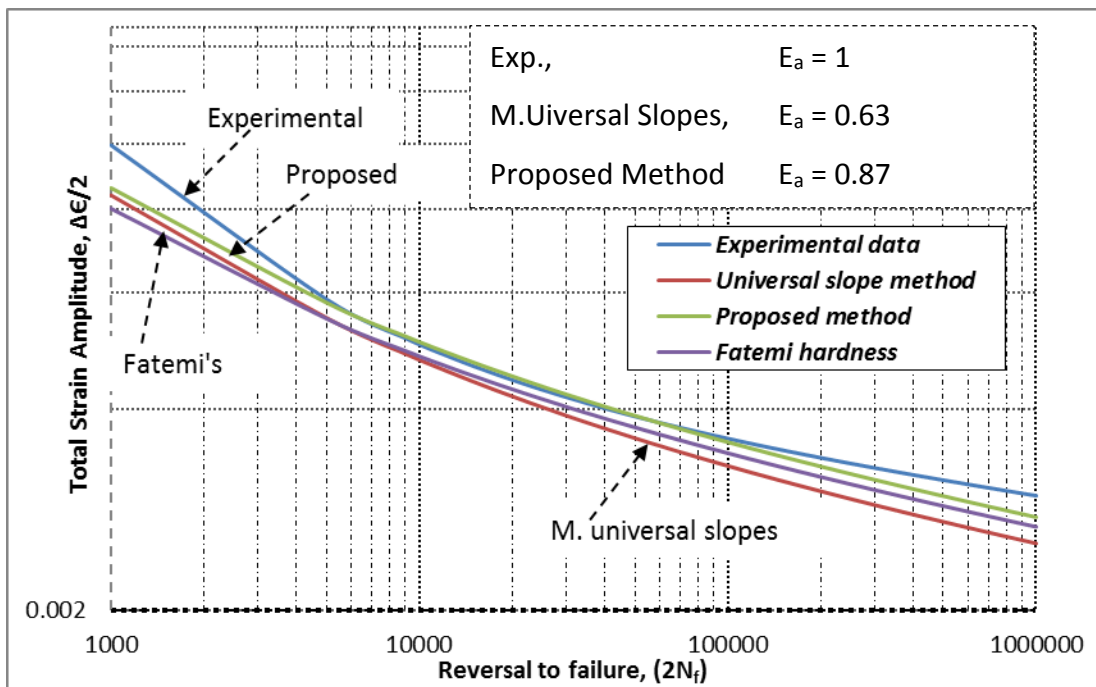


Figure 44 Comparison between Four Prediction Approaches for SAE 4140, HB409 Steel

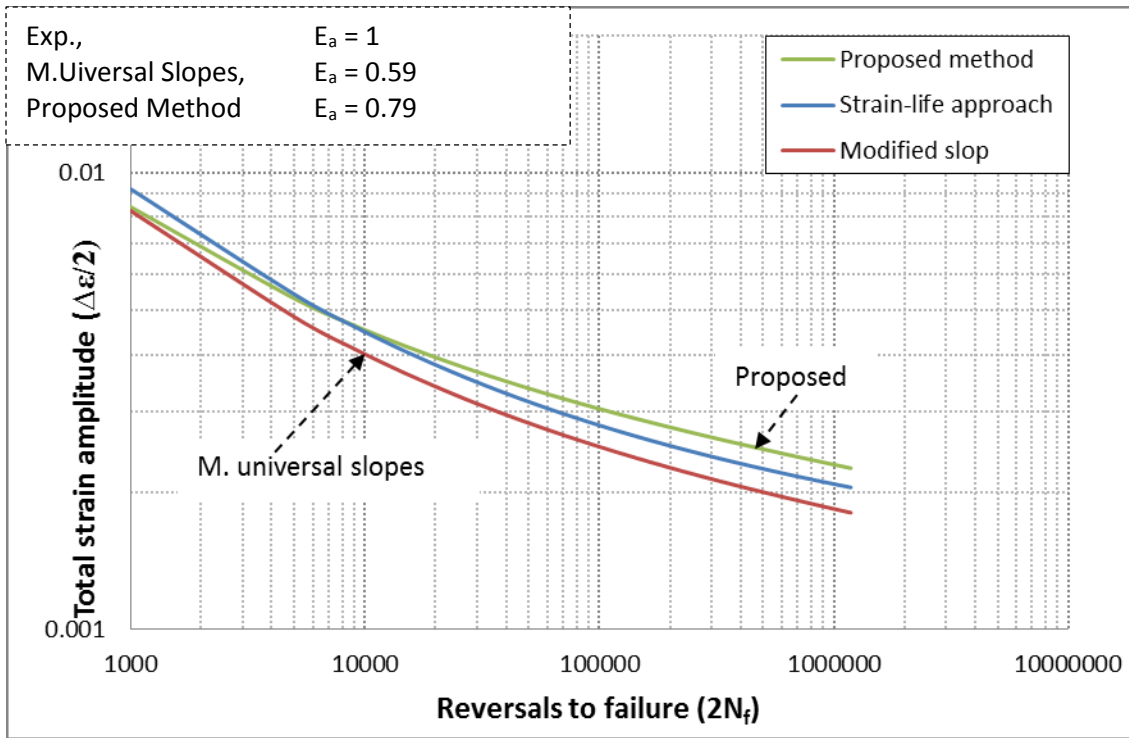


Figure 45 Comparison between Four Prediction Approaches for SAE 1141, HB277 Steel

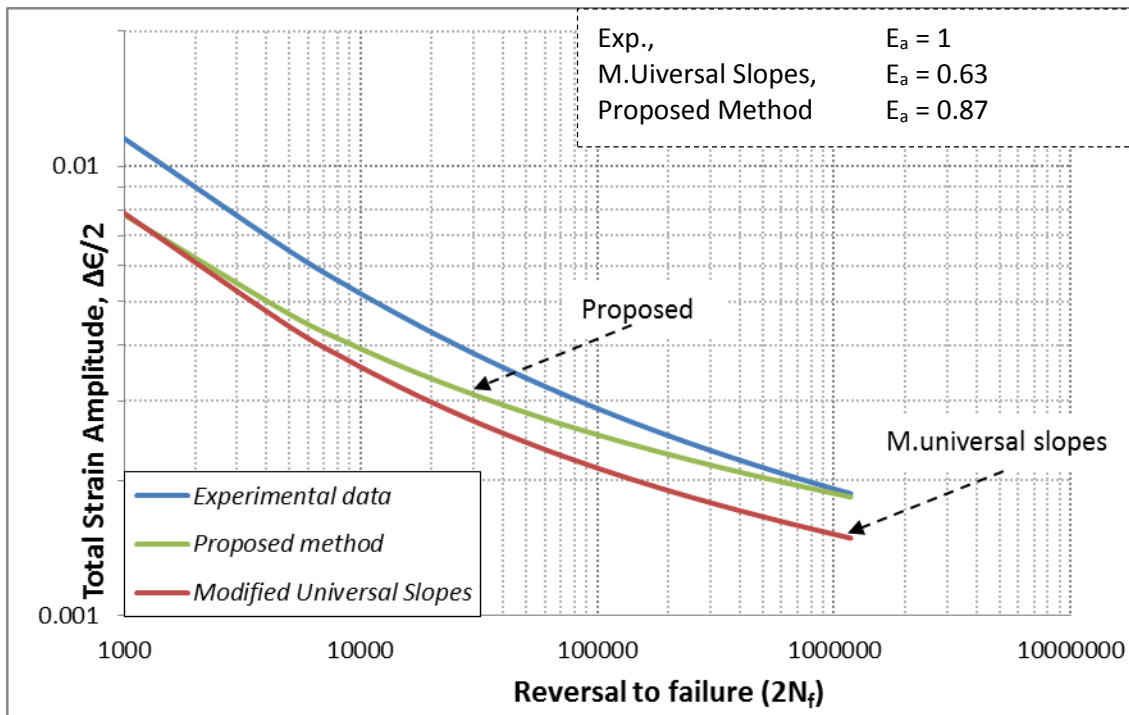


Figure 46 Comparison between Four Prediction Approaches for SAE 1070, HB280 Steel

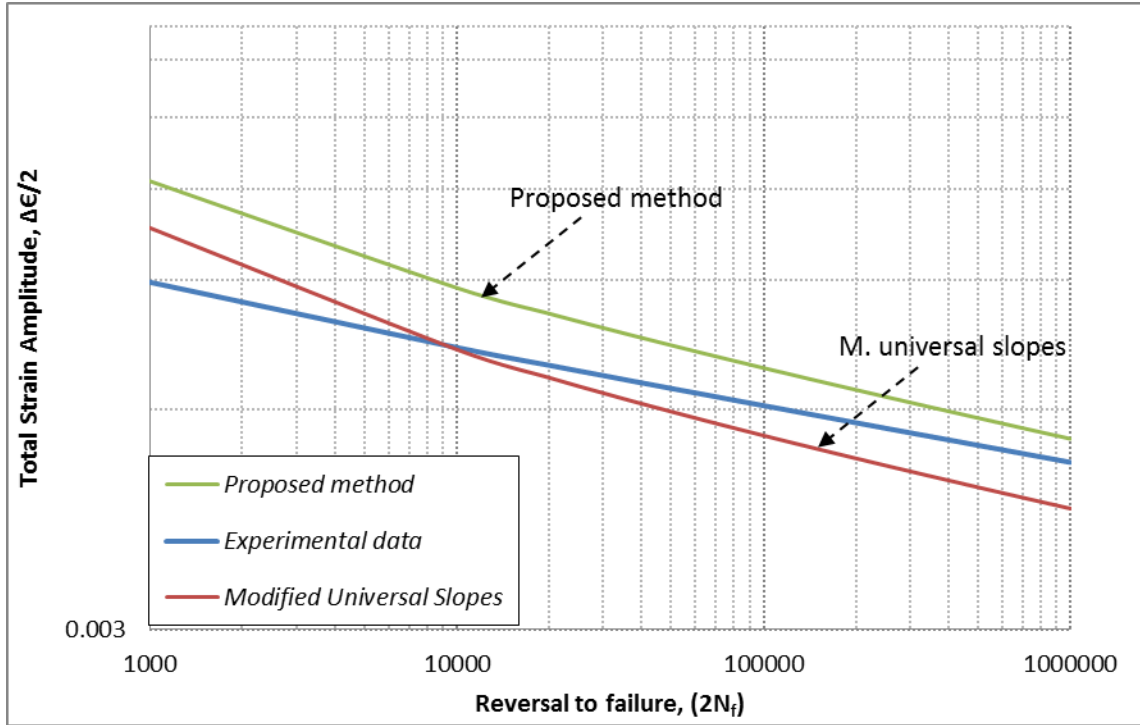


Figure 47 Comparison Between four Prediction Approaches for SAE H-11, HB660 Steel

Figure 48 shows the predicted lives obtained using the proposed method and Universal slopes method compared with the experimental lives for a group of steels within a scatter band value of three, the same method was used in the literatures to validate the existing models. The nearest to the center line at value of 1, is the best prediction, all the evaluation measures to be here employed will be formulated to be unity for ideally good prediction. A group of steels were used in Figure 48 with different ultimate tensile strength values.

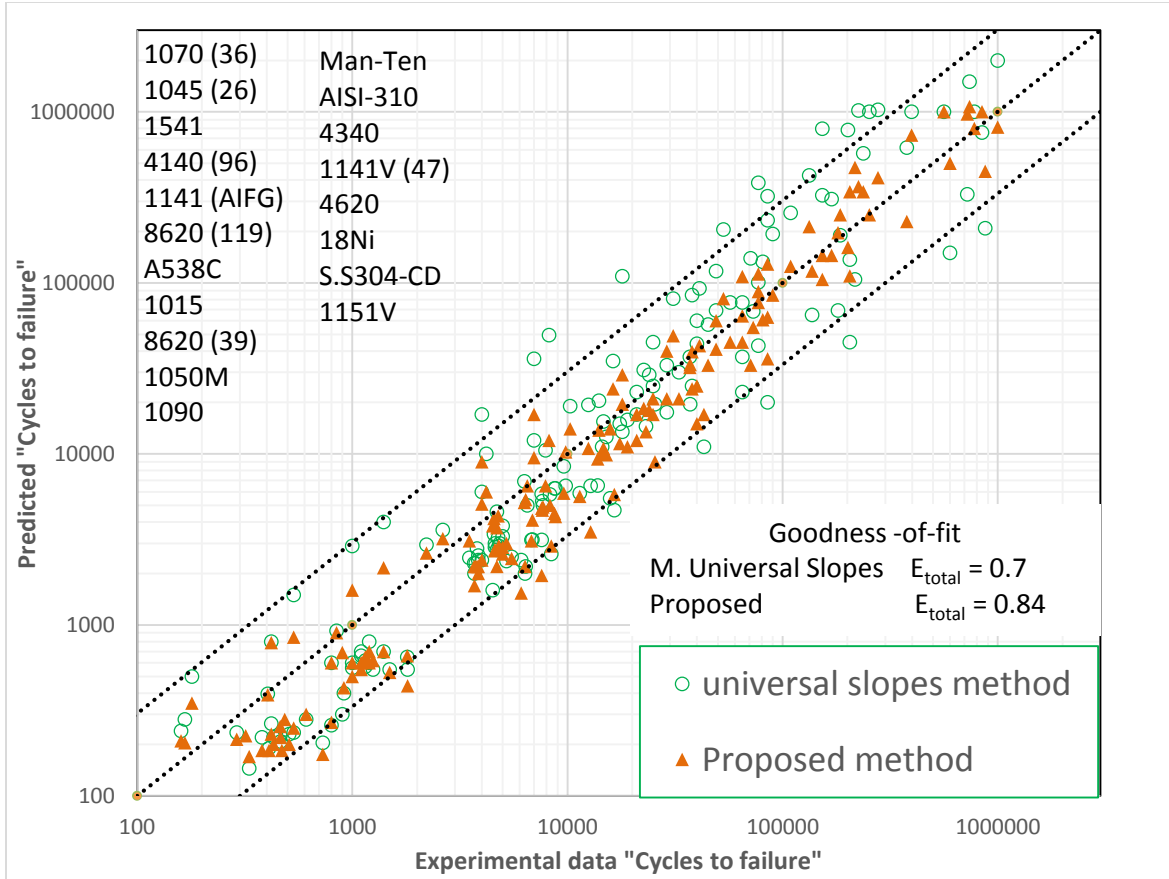


Figure 48 Comparison of the Predicted and Experimental Fatigue Lives for Different Alloys

4.1.2.2 Quantitative Evaluation

To evaluate the proposed estimation method on a quantitative basis, the most popular evaluation criteria proposed by Park and Song [33] were employed. This method is based on introducing three evaluation error criterion, E_f expressed in Eq. (136):

$$E_f(s) = \left[\frac{\text{Number of data falling within } \frac{1}{S} \leq \left(\frac{N_p}{N_f} \right) \leq S}{\text{Number of total data}} \right] \quad (136)$$

Where the value of $S = 3$ is employed for fatigue life prediction.

The second criteria used is the goodness-of-fit between the predicted and experimental values applying a least squares analysis. The goodness-of-fit-evaluation criteria is defined for both combined of all (ϵ -N) data sets and for individual (ϵ -N) data sets, separately as follow:

$$(E_a)_{total} = \frac{(1 - |\alpha_{total}|) + (1 - |1 - \beta_{total}|) + (1 - |1 - \alpha_{total} - \beta_{total}|) + (1 - |1 - r_{total}|)}{4} \quad (137)$$

$$(E_a)_{Dest} = \frac{1}{N} \sum_{i=1}^N (E_a)_i = \frac{1}{N} \sum_{i=1}^N \frac{(1 - |\alpha_i|) + (1 - |1 - \beta_i|) + (1 - |1 - \alpha_i - \beta_i|) + (1 - |1 - r_i|)}{4} \quad (138)$$

Where α and β are the values of the intercept and slope of a least-squares line,

$$\text{Log}(2N_p) = \alpha + \beta \text{Log}(2N_f) \quad (139)$$

and r is the correlation coefficient between the predicted and experimental lives, the subscripts, total and i , refers to the combined data of all (ϵ -N) data sets and i th (ϵ -N) data sets, respectively.

By assuming the above estimates are of equal importance, the final estimates is made by taking the average of the E values given by:

$$\bar{E} = \frac{E_f(S = 3) + (E_a)_{total} + (E_a)_{Dest}}{3} \quad (140)$$

Table 7, shows the values obtained using the above estimation criteria, closer to one is the, better is the prediction model.

Table 7 Strain-Life Quantitative Analysis

E values	Proposed method	Modified universal slopes method
$E_{f(s=3)}$	0.96	0.85
$(E_a)_{Dest}$	0.82	0.73
$(E_a)_{total}$	0.75	0.72
\bar{E}	0.84	0.77

4.2 The Notch Root Strain Prediction Model Technique

The finite element software used in this study was ABAQUS. Due to symmetry one-fourth of the plate was modelled using 2D- solid plane stress elements with input thickness Figure 49. The notched bar axisymmetric two dimensional model was used, Figure 51. To insure an optimum mesh size, the number of elements was increased until there was no significant change in strain at the notch root nodes see (Figure 50 and Figure 52). A far-field uniform tensile load was applied at the end of both notched plate and bar perpendicular to the notch surface. The elastic stress concentration factors, K_t , were obtained using FEA nonlinear analysis based on the net cross-sectional area. Elastic-plastic finite element analyses was conducted using the combined-hardening model. The combined hardening model is a combination of a non-linear kinematic and isotropic hardening model. This option is suitable for cyclic loading analysis taking into account the Bauschinger effect, the von Mises yield criterion with the associated flow rule in addition to kinematic hardening to compute the plastic strain increment. The input material cyclic properties for each material were taken from published experimental tests by AISI Bar Steel Fatigue Database and SAE J1099. K_t values are obtained by taking the ratio of stress amplitude at notch root to the nominal stress amplitude. Application of nominal stress amplitude smaller than $0.8S_y$ results in stress concentration factor of 2.73 and 1.78 for a notched plate and round bar respectively. Variable amplitude cyclic loadings used in this study to investigate the behavior of each material under tension-compression conditions: a maximum nominal stress of 350 MPa and minimum stress amplitude of -240 MPa was applied to a notched plate. In case of round bar the maximum and minimum nominal stress amplitudes were 500 MPa and -240 MPa respectively. These values were selected to ensure that sufficient plastic strain was generated at the notch root.

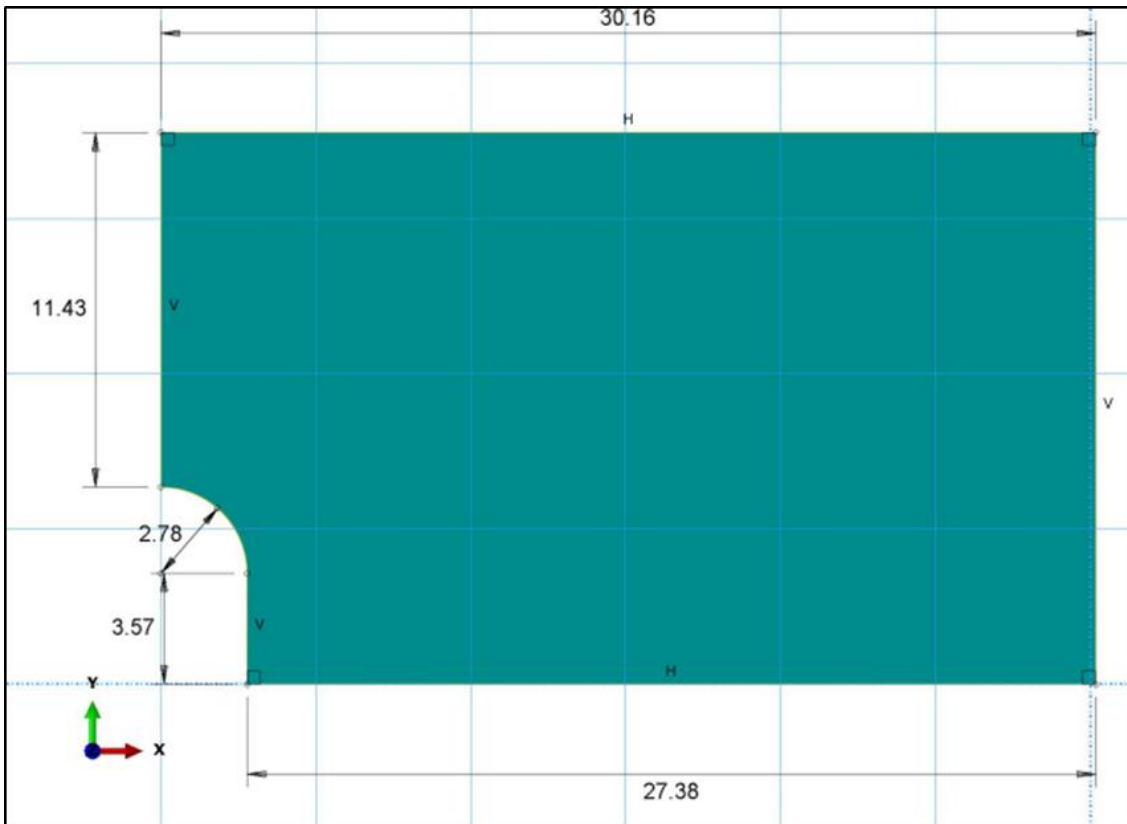


Figure 49 One-Fourth of Flat Plate Finite Element Model.

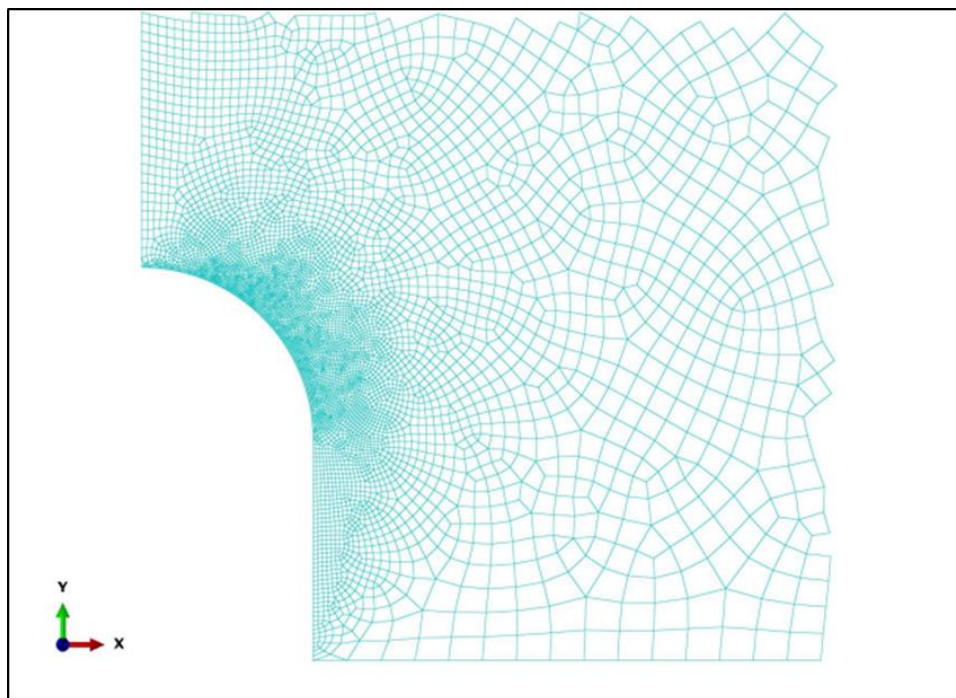


Figure 50 Mesh Configuration for the Area around Notched Plate.

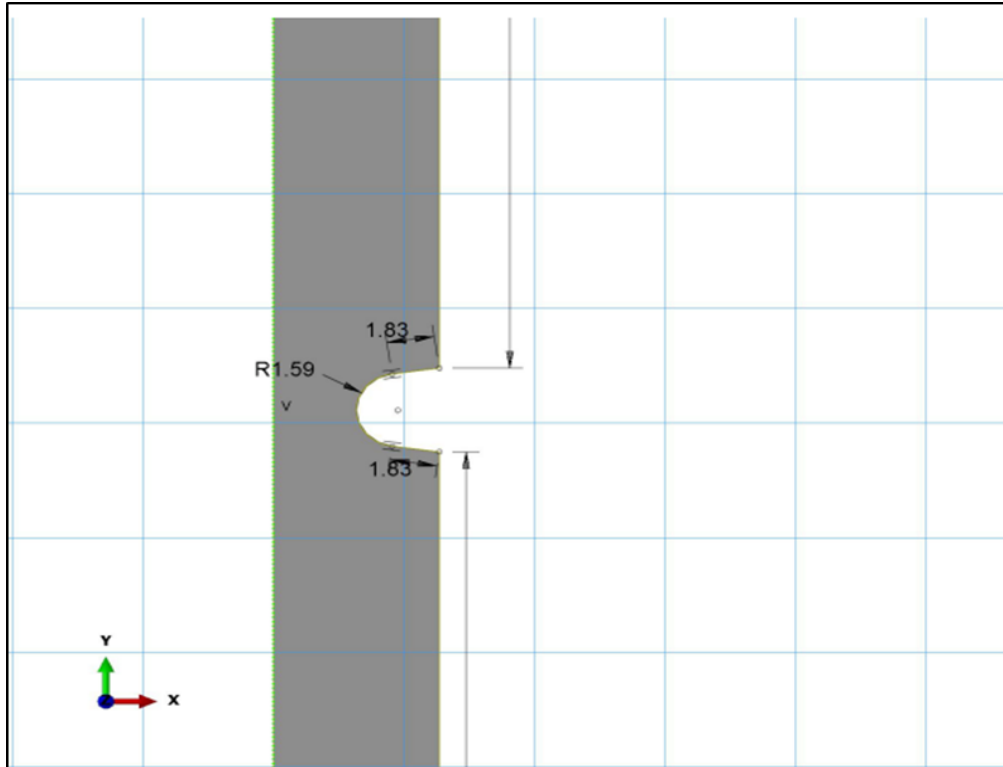


Figure 51 Axisymmetric two Dimensional Model for Round Bar.

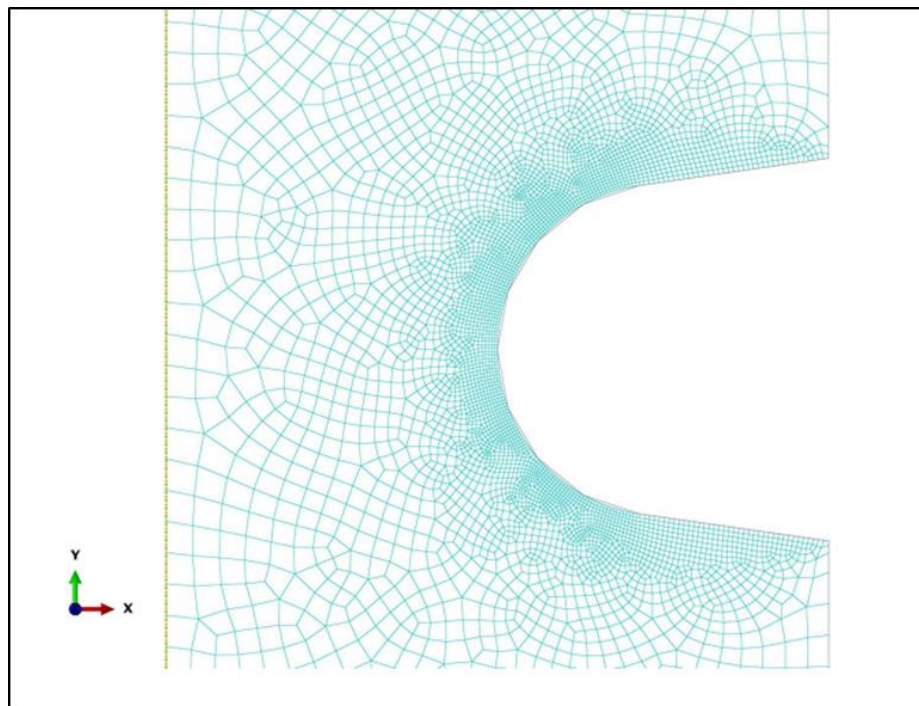


Figure 52 Mesh Distribution around the Round Bar Notch

4.2.1 Methodology

As mentioned earlier Neuber's rule is the most commonly used analytical method for notch root stress and strain predictions. However, studies conducted reveal that Neuber's rule overestimates these values compared to elasto-plastic finite element cyclic analysis. Neuber's rule is based on nonlinear equations (40),(41), a study of these two equations reveals that there are two material cyclic properties that contribute to the difference between the elasto-plastic finite element results and Neuber's predictions especially when the type of material is changed. It becomes to determine, which of these properties has the larger effect on this difference and how this difference changes by changing the type of material. So, does the change behaves in a linear, or nonlinear manner?

Based on Eq. (41), if the geometry factor K_t and nominal stress S are fixed then this equation can be written as in Eq. (141):

$$\Delta\sigma^2 + 2\Delta\sigma E \left(\frac{\Delta\sigma}{2K'} \right)^m = (K_t \Delta S)^2 = \text{Constant} \quad (141)$$

Where $m=1/n'$

The two materials properties that change by changing the type of steel are K' and m . Each type of steel has a unique value of K' and m . the Young's modulus E stays almost constant for all steel types. Figure 53 shows the change of material stiffness with increasing the value of m , each curve expresses a cyclic stress-strain curve for a different steel, where $m= 0$, and $m= \infty$ define the perfectly plastic and perfectly elastic conditions respectively. The difference in result determined by using Neuber's and elasto-plastic finite element analysis notch root strain prediction method should be controlled by selection of K' and m values.

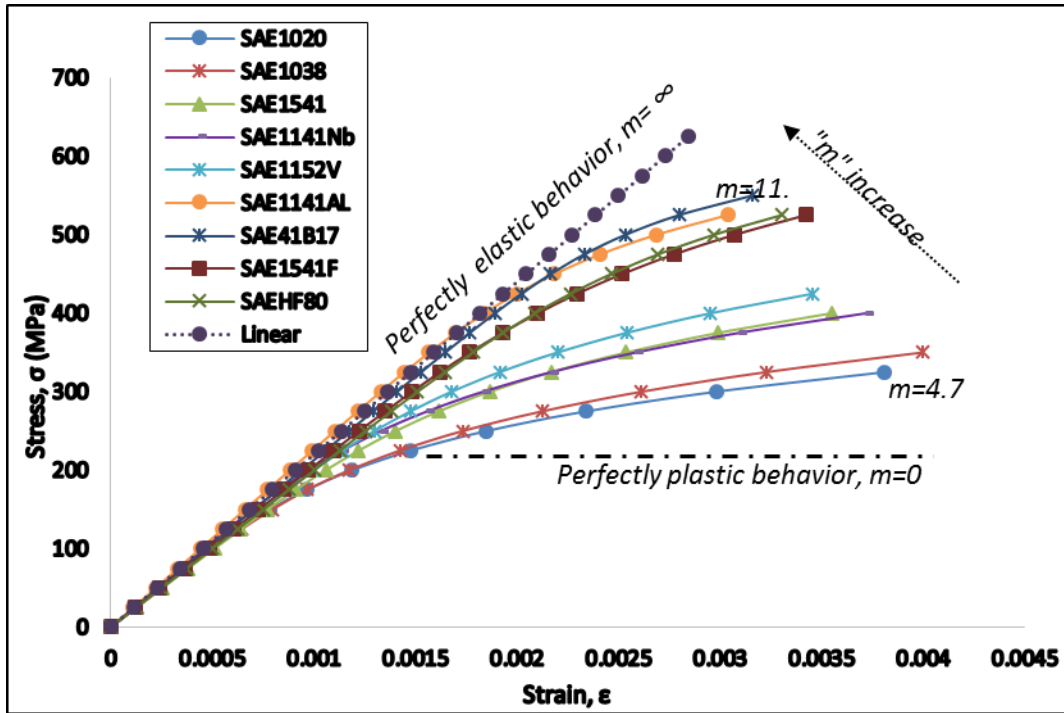


Figure 53 Cyclic Stress-Strain Curves for Different Steels

To know the effect of the two variables m & K' on the stress and strain estimates one of these variables has to be fixed while the other is varied.

For most steels K' can have a value between 900 – 2000 (MPa). In order to investigate the effect of m on the estimation of local strain values, the value of K' was fixed at 1500 (MPa) which corresponds to an average value for most steels. The exponent m was incrementally changed from 11.1 - 4.3 which corresponds to n' value range of 0.09 - 0.23, this range covers a majority of steels used in the industry. E , K_t , and S have values of 200 (GPa), 2.73 and 300 (MPa) respectively.

$\delta\varepsilon$ was defined as the notch strain amplitude difference between Neuber's and FEA elasto-plastic solutions and $\delta\varepsilon$ can be expressed as:

$$\delta\varepsilon = \varepsilon_N - \varepsilon_{FEA} \quad (142)$$

Where, ε_N and ε_{FEA} are the Neuber's and elasto-plastic FEA notch root strain amplitude results respectively. Based on Eq. (142) if $\delta\varepsilon$ can be predicted and the cyclic properties for

the material are known, it is easy to find ϵ_{FEA} which corresponds to the optimum notch root strain amplitude value, thus elasto-plastic finite elements analysis can be avoided. This is desired due to the complexity of the plastic deformation behavior, and the difficulty of defining materials parameters in the FEA software.

Eq. (142) can be written in the form:

$$\epsilon_N - \delta_\epsilon = \epsilon_{FEA} \quad (143)$$

To predict δ_ϵ an elasto-plastic finite element analysis was conducted for n' values that range between 0.09 - 0.23 with an incremental increase of 0.1, and fixed values of E, K_t , and S.

This trial is conducted in order to know the effect of the n' values on the difference between Neuber's and FEA elasto-plastic estimates, the proposed prediction model will be based on this behavior.

To investigate the effect of increasing nominal applied stress, three different nominal stress amplitude levels were used, 250, 300, 350 (MPa) at the same n' range specified above.

In the final step the effect of K' was investigated at three different values 900, 1400, 1500 (MPa) with a value of m equal 6.02 which represent a mean value for most steels. Maximum nominal stress amplitude used is 350 MPa which corresponds to nearly 1000 MPa notch stress, since most of the targeted steels have ultimate tensile strength below 1000 MPa ($K_t * S_{max} = 2.73 * 350 = 955$ (MPa)).

4.2.2 Developing a Prediction Method.

The change of δ_ϵ with reciprocal cyclic hardening exponent m is shown in Figure 54, the values of δ_ϵ in y-axis are multiplied to 10^6 just to make them visible. It is clear that the relationship of the equation that describes the change in the prediction error δ_ϵ , and m is a power relationship. Based on curve fitting, different power law equations were obtained. The curve that has the optimal power relation for different nominal stress values is presented in Eq. (144). The equation obtained from Figure 54, has the form:

$$y = A(m)^\beta \quad (144)$$

Eq. (144) was applied on a range of steels, and a the correction error was calculated for each steel using elasto-plastic finite element analysis and calculated strains using Neuber's rule, the prediction error data was used to optimize the values of A and β . The optimal value was 0.015 for A and -2.019 and β , as shown in Eq. (145).

$$\delta_\varepsilon = 0.015(m)^{-2.019} \quad (145)$$

Eq. (145) is a correction factor that depends on ($m = 1/n'$), which can be subtracted from Neuber's notch strain to get the optimum strain value that corresponds to the elasto-plastic finite element analysis given by Eq. (146).

$$\varepsilon_N - 0.015(m)^{-2.019} = \varepsilon_{FEA} \quad (146)$$

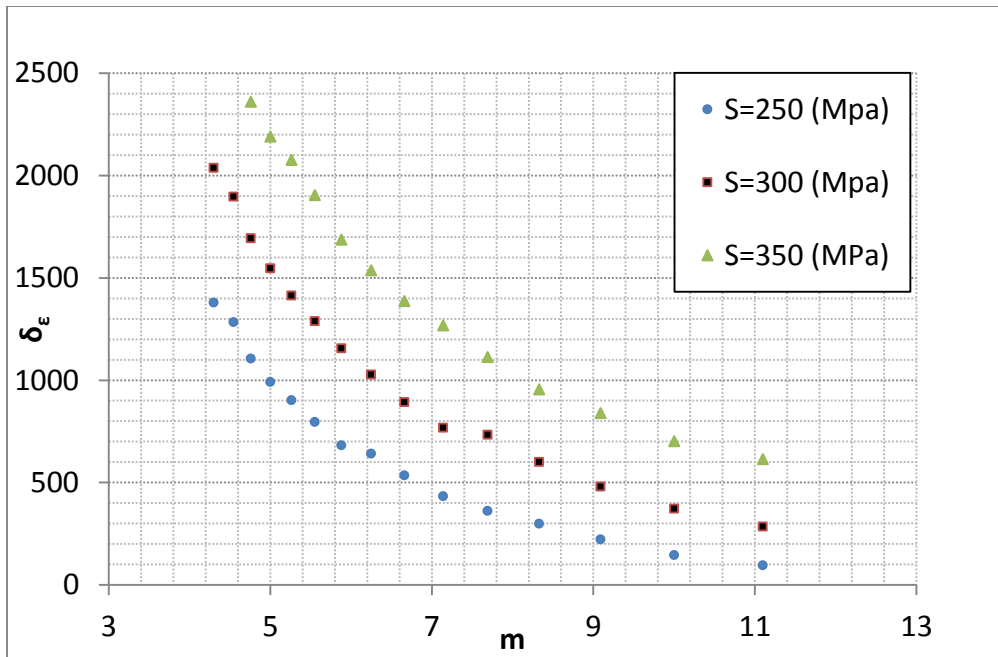


Figure 54 Variation of δ_ε with Different m Values

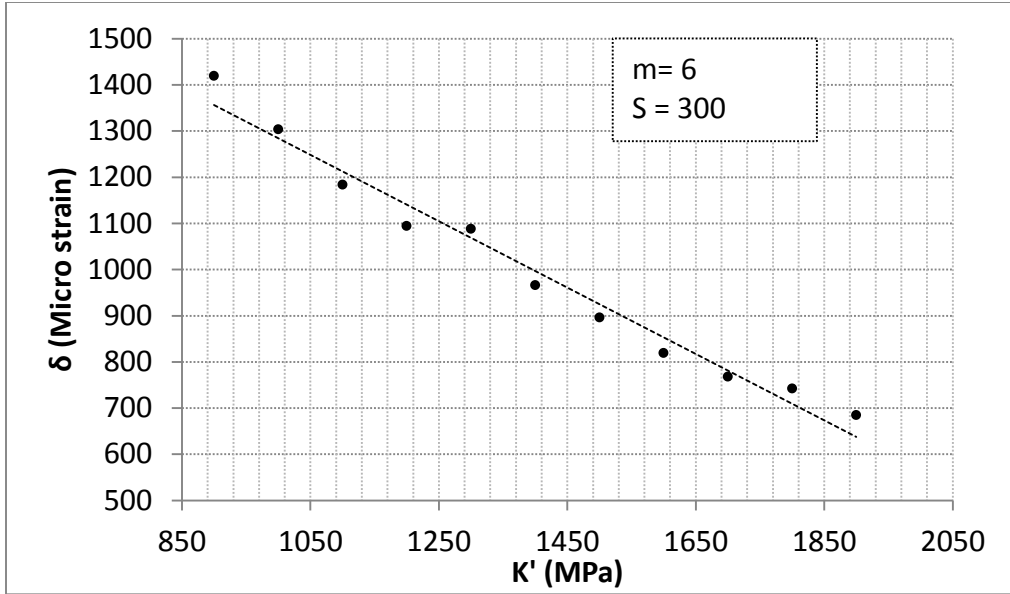


Figure 55 Variation of δ with K' at Fixed Value of m & S

The same elasto-plastic FEA analysis is conducted by fixing m and changing K' with values specified earlier. Figure 55 shows the change of δ_ε with K' for a fixed value of $S_a = 300$ (MPa) and $m = 6$, in this case a linear trend is observed. Based on this behavior the value of K' is not included in Eq. (146) at this point it is assumed that the effect of K' is not significant and the proposed model is optimized to compensate for the effect of K' .

To increase the prediction capability of Eq. (146) the interpolation technique proposed by Calladine [73], was used Eq. (147); shown in Figure 56. Where; equation (12) in Figure 56 represents the best linear interpolation equation, and the curved dashed line represents the experimental or exact curve. F_m relies on the maximum stress developed at each corresponding m value. This scheme is employed for strain rate-independent prediction, and described by Eq.(147).

$$\varepsilon = \varepsilon_N + x(\varepsilon_{el} - \varepsilon_N) \quad (147)$$

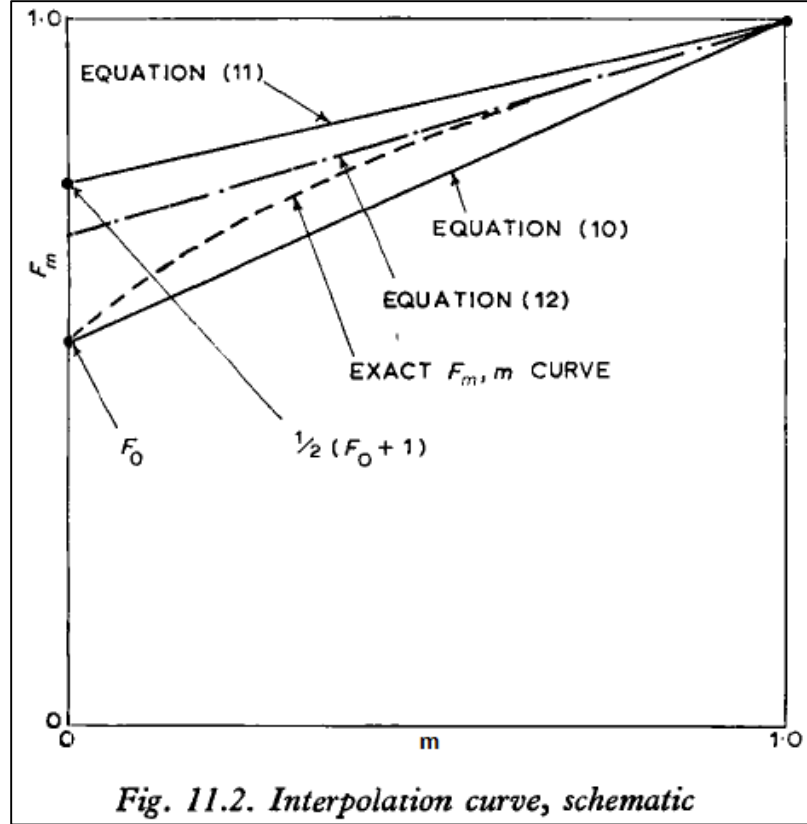


Figure 56 Interpolation Assumption by Calladine [73]

Eq. (147) assumes that the variation of notch root strain and m is perfectly linear; however the relationship is not linear as shown in Figure 56. Combining Eq. (146) and Eq. (147) results in a model given by Eq. (148) which takes into account the nonlinear behavior.

$$\varepsilon = (\varepsilon_N - \delta_\varepsilon) + x[\varepsilon_{el} - (\varepsilon_N - \delta_\varepsilon)] \quad (148)$$

Eq. (148) can be rearranged to give:

$$\varepsilon = (1 - x)(\varepsilon_N - \delta_\varepsilon) + x\varepsilon_{el} \quad (149)$$

Studies show that the optimum value for x is 0.35. The main advantage of Eq. (149) is that, the elasto-plastic finite element analysis can be avoided. Since linear finite element analysis using the proposed method provides closer results as elasto-plastic finite element analysis.

Local stress σ can be predicted using a direct linear interpolation between linear finite element and Neuber's rule solution using Eq. (150) where the values of strains are replaced with stresses and the value of x is replaced by 0.1 as:

$$\sigma = \sigma_N + x(\sigma_{el} - \sigma_N) \quad (150)$$

Where, σ_N and σ_{el} are the local stress obtained using Neuber's and the linear finite element analysis method respectively.

4.2.3 Evaluation of the Proposed Method

To validate the proposed model in Eq. (149) and (150) different steels were tested using two geometries, double notched flat plate and a circumference notched round bar. Elastic, elastic-plastic finite element and Neuber's rule prediction were used at two loading conditions. The results were compared with the proposed notch root prediction method. Applied conditions for different steels:

- I. Completely reversed applied loads, 2 nominal stress amplitudes are applied, 250 MPa, and 300 MPa on the following steels, 1020, 1541, 1551V, 1022, 1141AL, 1141Nb, 1141V, 1045, 5150, 9310, 41B17, C-70 and 9262
- II. Completely reversed load from zero to 0.8 cyclic yield strength (MPa) applied on the following steels, RQC-100, SAE1045, SAE1050, and SAE1141MA.
- III. Variable amplitude where, a time history segment is used for each geometry, as shown in Figure 57. To investigate the behavior of each material under variable tension-compression conditions: a maximum nominal stress of 350 MPa and minimum stress amplitude of -240 MPa was applied to a notched plate. In case of the round bar the maximum and minimum nominal stress amplitudes were 500 MPa and -240 MPa. These values were selected to insure that sufficient plastic strain was generated at notch root.

The types of materials used in the evaluation are SAE1141V, RQC-100, SAE1038, SAE1050M, SAE1117, SAE15V24, SAE1141Nb, SAE1045, SAE1141, Al-2024-T350 including low strength, medium strength steels. Elastic and elasto-plastic finite element

analysis were carried out for each type of steel, maximum stresses and strains are recorded for the nodes at the notch root location.

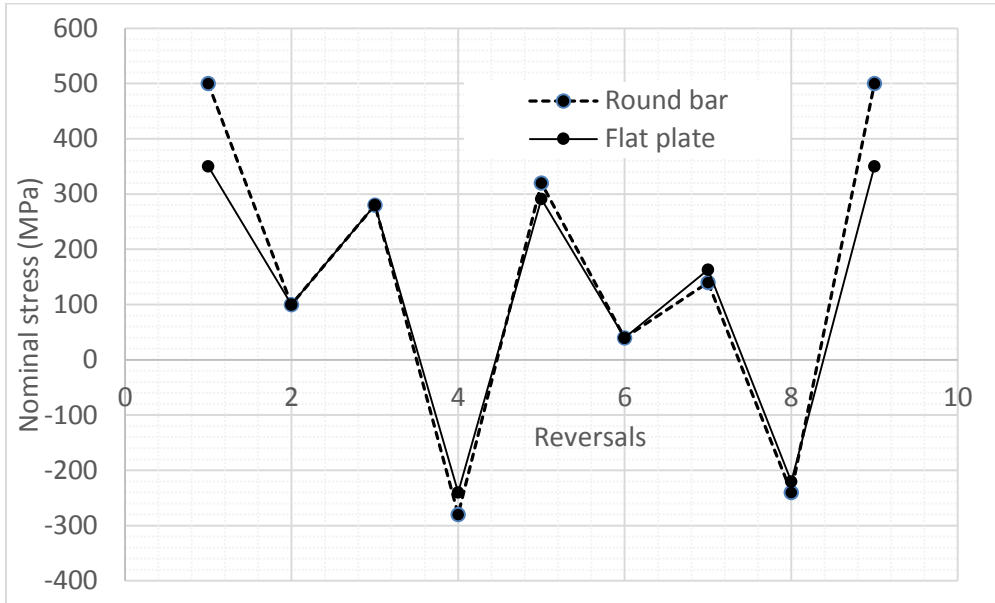


Figure 57 Applied Nominal Stress for Different Geometries

5 RESULTS AND DISCUSSIONS

5.1 Ultimate Tensile Strength HB Correlation Model

Brinell hardness HB and ultimate tensile strength S_u correlation model was created using data on 246 different steels to create a fatigue life prediction model. The model was evaluated using qualitative as well as a quantitative criteria. Figure 42, Figure 43 show the prediction capability qualitatively, in Figure 42 the predicted ultimate tensile strength S_u is plotted versus the actual values. The other qualitative analysis is done comparing the most utilized method in industry, Roessel Fatemi's method, where the ratio of predicted and actual tensile strength is plotted versus the Brinell hardness HB. A count of the points falling in the scatter band of $\pm 10\%$ indicates that more points fall within the scatter band for the proposed model than for the Fatemi-Roessel model, as shown in Figure 43.

The other criteria used to evaluate the proposed model are; error criterion, mean value and coefficient of variance, which is a quantitative statistical analysis described earlier, the average of the three \bar{E} values represent the goodness of the prediction model where the value of 1 represent the optimum value, the nearest to one is the best prediction, table 8 shows the \bar{E} value for proposed method is 0.931 compared with the value of 0.852 for the Roessel-Fatemi's model.

5.2 Strain-Life Prediction Proposed Method

The data proposed in Table 8 provides the fatigue parameters obtained from the proposed and Modified Universal Slopes prediction methods for 52 different materials; these values were compared with the experimental data from the sources mentioned above. Reference to the experimental data for each steel, proposed method provides better estimation for more than 92% of the proposed steels for fatigue strength coefficient (σ_f') values, which represent the elastic coefficient in strain-life prediction model. The proposed method is not only based mainly on hardness of the material which is easy to obtain, but it also provides a better results compared with the modified universal slopes estimation method.

Table 8 Fatigue Parameters Obtained from the Proposed and Modified Universal Slopes Methods.

SAE Specification	Brinell Hardness (HB)	Tensile strength (MPa)	Exp. ϵ_f	Exp. σ'_f (MPa)	$\sigma'_{f(p)}$ (MPa)	$\sigma'_{f(M)}$ (MPa)	Exp. ϵ'_f	$\epsilon'_{f(p)}$	$\epsilon'_{f(M)}$	
A538A(b)	405	1515	1.1	1655	1960	2116	0.3	0.27	0.25	
A538B(b)	460	1860	0.82	2135	2309	2510	0.8	0.22	0.22	
A538C(b)	480	2000	0.81	2240	2437	2654	0.6	0.21	0.21	
AM-350(c)	496	1905	0.23	2690	2554	2548	0.1	0.17	0.17	
RQC-100	290	940	0.56	1240	1401	1447	0.66	0.31	0.31	
1005-1009	125	470	1.09	515	807	813	0.3	0.5	0.51	
1045	410	1450	0.72	1860	2016	2067	0.6	0.25	0.25	
1541F	290	950	0.68	1275	1401	1460	0.68	0.32	0.32	
1541F	260	890	0.93	1275	1273	1383	0.93	0.35	0.35	
4130	258	895	1.12	1275	1280	1406	0.92	0.38	0.37	
4142	310	1060	0.35	1450	1485	1593	0.22	0.27	0.27	
4142	380	1415	0.66	1825	1850	2034	0.45	0.26	0.26	
4142	450	1760	0.54	2000	2281	2439	0.4	0.22	0.22	
4140	310	1075	0.69	1825	1485	1611	1.2	0.31	0.29	
4340	243	825	0.57	1200	1195	1287	0.45	0.33	0.33	
4340	409	1470	0.48	2000	2010	2091	0.48	0.24	0.24	
4340	350	1240	0.84	1655	1674	1807	0.73	0.28	0.28	
5160	430	1670	0.87	1930	2131	2314	0.4	0.24	0.24	
9262	410	1565	0.38	1855	2016	2202	0.38	0.23	0.23	
H-11	660	2585	0.4	3170	4180	3357	0.08	0.15	0.17	
950X(g)	156	530	1.24	1005	900	898	0.85	0.46	0.48	
1141	223	771	0.85	1168	1139	1238	0.257	0.4	0.38	
1141	241	802	0.77	1080	1209	1280	0.36	0.38	0.37	
1141	277	925	0.88	1127	1367	1453	0.31	0.37	0.36	
1141	252	797	0.88	1162	1251	1272	0.53	0.38	0.37	
1038	185	652	0.76	1004	1005	1079	0.2	0.43	0.41	
1038	195	649	1.1	1009	1040	1075	0.23	0.44	0.44	
1541	195	906	0.54	1044	1028	1403	0.51	0.38	0.32	
1050(M)	205	821	0.68	989	1069	1299	0.43	0.4	0.35	
1050(M)	220	829	0.42	1094	1116	1301	0.3	0.35	0.32	
1090	259	1090	0.15	1310	1267	1634	0.25	0.27	0.23	
SAE	Iter. #	Brinell Hardness (HB)	Tensile strength (MPa)	Exp. ϵ_f	Exp. σ'_f (MPa)	$\sigma'_{f(p)}$ (MPa)	$\sigma'_{f(M)}$ (MPa)	Exp. ϵ'_f	$\epsilon'_{f(p)}$	$\epsilon'_{f(M)}$
1070	36	280	659	0.5	1289	1359	1079	0.361	0.32	0.37
10B21	24	322	1105	1.22	1284	1557	1664	0.69	0.34	0.33
1538	131	285	973	3.33	1355	1365	1474	0.8	0.29	0.27
15B35	45	286	940	0.1	1127	1398	1463	0.96	0.25	0.25
4130AL	29	442	1482	0.6	2294	2242	2128	1.44	0.24	0.25
41B17	72	277	872	1.13	1023	1353	1368	1.48	0.37	0.37
8620	119	326	991	0.76	1639	1576	1521	0.47	0.32	0.32
9254V	34	536	2050	0.4	2914	2935	2771	4.17	0.19	0.2
41B17M	79	627	1877	0.056	4712	3807	2572	0.34	0.12	0.15
4320	49	188	994	0.99	909	1002	1512	0.86	0.43	0.33
Man-Ten	-	150	972	1.17	972	885	960	0.85	0.46	0.4
AISI304	-	327	951	1.1	2275	1526	1430	0.89	0.3	0.28
18Ni	-	460	1862	0.82	2137	2310	2550	0.8	0.23	0.21
AISI-310	-	145	641	0.73	1655	860	1056	0.6	0.44	0.38
VAN-80	-	225	696	1.13	1055	1125	1132	0.21	0.38	0.39
15B27 HT	-	264	916	1.09	1062	1284	1430	1.68	0.36	0.34
S.S 304	-	327	951	1.16	2047	1526	1439	0.554	0.29	0.19

Figure 58 represent a plot between the experimental/predicted fatigue strength (σ_f') ratios for the proposed and Modified Universal Slopes model.

The scattering of the proposed method was around 1 which is slightly lower than the results obtained using the Modified Universal Slopes method this means that the proposed method provides better prediction of the fatigue strength coefficient parameter as compared to the original method (Modified Universal Slopes Method)

Figure 59 shows the scattering of fatigue ductility coefficient (ϵ_f') which represent the second fatigue parameter or the plastic coefficient in the model, it is clear that the predictability of this parameter is relatively poor for both models with slightly less scattering for the proposed method. This conclusion agrees with the results in the literatures. The literature also mentioned that the correlation between the fatigue ductility coefficient (ϵ_f') and the monotonic tensile properties is poor for all currently existing prediction models

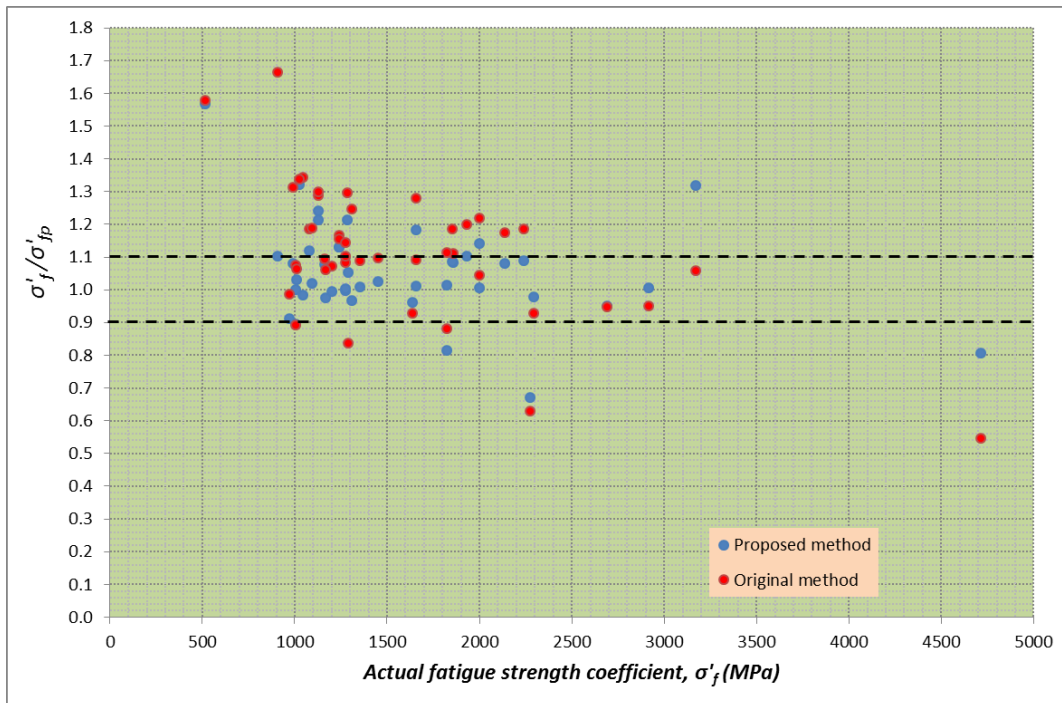


Figure 58 Actual/ Predicted Fatigue Strength Ratio vs Actual Values

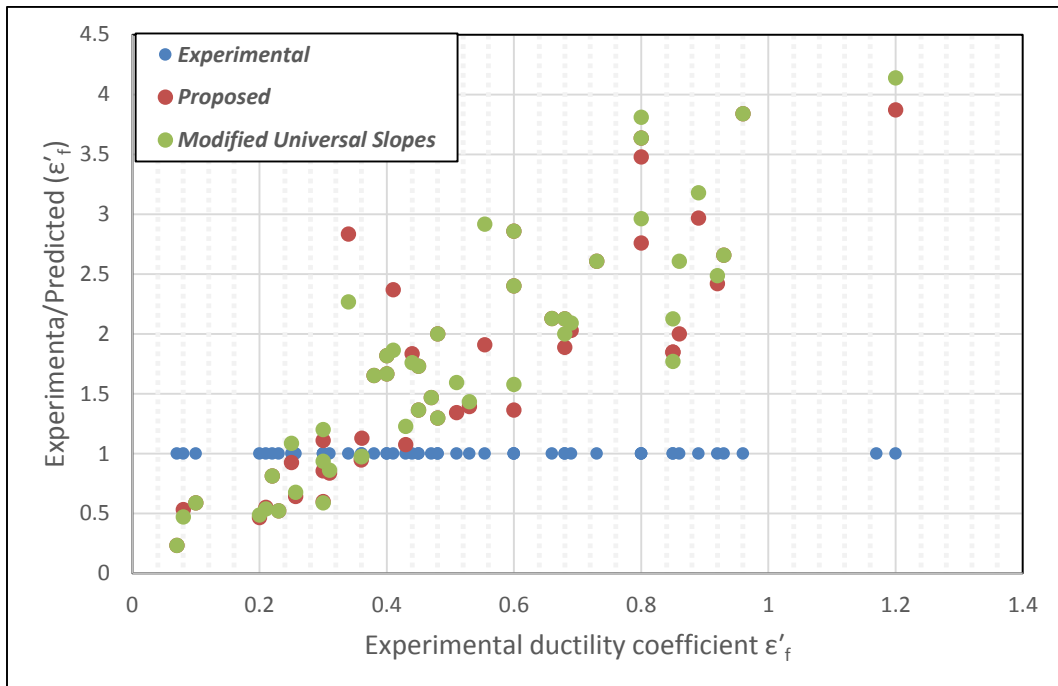


Figure 59 Comparison of Predicted Fatigue Ductility Coefficient with Experimental Data

Figure 44 - Figure 47 show the strain –life curve for each prediction method for different steels, the proposed method curve appears to be closer to the experimental data curves, which means it gives better prediction values than the Modified Universal Slopes Method. The performance of proposed method tends to get closer to the experimental results at low cycle fatigue rather than a high cycle fatigue conditions, which is shown in Figure72 - Figure 97, Appendix A.

For high strength material SAE H-11, with $S_u=2585$ (MPa), the proposed method shows comparable prediction results, as shown in Figure 47.

Figure 48 shows a comparison between the experimental results and predicted lives obtained by the proposed method and Modified Universal slopes method within a scatter band of three, both methods give a good prediction capability by considering the number of points falling in the scatter band at relatively lower number of cycles below approximately 16000 cycles, at higher number of cycles above 20000 cycles the proposed method exhibit a lower scattering with a higher number of points falling within the range

of 3 scatter band. In design 20000 cycles is not a significant number, in most cases in design the objective is 10 times more than this number, this gives the proposed a significant advantage over the Modified Universal Slopes method.

The quantitative analysis criteria used for strain-life prediction is more complex than the criteria used for ultimate tensile strength Brinell hardness prediction, as described earlier.

Table 7 shows the comparison between the two methods, 20 different steels are employed, the \bar{E} values are 0.84 and 0.77 for proposed and Modified Universal Slopes method respectively, where closer to one is the best prediction.

5.3 Notch Root Prediction Model

Notch root strain amplitudes were calculated for each material under the specified loading condition with the aid of linear finite element analysis using Eq. (88), the results were compared with the elasto-plastic finite element analysis and Neuber's prediction.

- Case I where the applied nominal stresses are 250, 300 MPa:

The results are shown in Table 9 for each material used within the test, the maximum strain values for proposed method has an advantage over the Neuber's prediction when the two methods were compared with the elasto-plastic maximum strain and stress results.

Table 9 Notch Root Stress-Strain for Flate Plate under Completely Reversed Cyclic Loading

Notched flat plate under $S_a=250$ (MPa)								
SAE designation	Neuber's		Linear FEA		Elasto-plastic FEA		Proposed Method	
	σ_{max}	% (ϵ_a)	σ_{max}	% (ϵ_a)	σ_{max}	% (ϵ_a)	σ_{max}	% (ϵ_a)
1020	373	0.61	671	0.30	426	0.43	404	0.46
1541	455	0.52	672	0.34	571	0.38	542	0.42
1151V	475	0.48	672	0.32	632	0.35	505	0.38
1022	397	0.59	670	0.33	479	0.42	431	0.46
1141AL	452	0.48	671	0.31	572	0.35	515	0.37
1141Nb	437	0.49	671	0.3	530	0.35	502	0.38
1038	396	0.59	672	0.33	469	0.42	440	0.48
Notched flat plate under $S_a=300$ (MPa)								
SAE designation	Neuber's		Linear FEA		Elasto-plastic FEA		Proposed Method	
	σ_{max}	% (ϵ_a)	σ_{max}	% (ϵ_a)	σ_{max}	% (ϵ_a)	σ_{max}	% (ϵ_a)
1020	403	0.8	805	0.4	467	0.6	420	0.57
1038	430	0.78	805	0.4	514	0.56	482	0.53
1541	493	0.7	805	0.41	635	0.49	592	0.51
1141Nb	470	0.63	806	0.37	577	0.47	525	0.43
1151V	515	0.64	805	0.39	637	0.46	597	0.46
1141V	508	0.62	805	0.37	625	0.45	580	0.447
1045	500	0.65	805	0.38	626	0.47	577	0.48
1022	428	0.79	805	0.4	522	0.57	503	0.56
1141AL	491	0.64	805	0.37	634	0.44	595	0.44
5150	545	0.59	806	0.38	692	0.43	625	0.44
9310	625	0.55	805	0.37	749	0.47	691	0.48
41B17	617	0.52	805	0.38	703	0.43	682	0.45
C-70	599	0.56	805	0.4	754	0.43	700	0.45
9262	575	0.57	804	0.38	732	0.43	670	0.45

- Case II, completely reversed load from zero to 0.8 cyclic yield strength (MPa), the maximum stress-strain results were listed in Table 10 to Table 13, and the plot of nominal stress versus the local maximum principal strain obtained from each prediction method shown in Figure 60 to Figure 67. All figures show that the gap between the proposed method and elasto-plastic finite element is very small compared with Neuber's - FEA gap. For SAE1045 the proposed method exhibits principal strains below the estimated values for the flat plate geometry compared with FEA results as shown in Figure 62. In general the proposed method provide a reasonable estimation especially in the case of round bar geometry.

- Case III, variable amplitude ,this is the extreme condition where the mean stress become a factor, same analogues used by G. Glinka [44] where the notch strains plotted versus the number of reversals in order to show the difference between the prediction methods instead of using hysteresis loops. Figure 68 to Figure 71 show some snapshots obtained from ABAQUS viewer for strain amplitudes and the corresponding number of cycles to failure contours for each geometry, fe-safe [70] software was used to obtain the number of cycles to failure.

Morrow's mean stress method was used to predict the number of cycles to failure under each condition also shown in Table 15 to Table 23 appendix B. Figure 98 to Figure 133, appendix B show the maximum local strain at each reversal with the corresponding number of cycles to failure for each material, As shown in the Figures, the values of notch strains as well as the number of cycles obtained by the proposed method are closer to the elasto-plastic finite element values especially under tensile nominal cyclic stress, under compression cycles all three methods are close. Notch strain amplitude values are generally lower in case of plane strain condition where the stress is in a multi-axial state.

Some hysteresis loops obtained by elasto-plastic finite element analysis show the local strain amplitudes with the corresponding notch root stress, for each reversal shown in Figure 134 to Figure 136.

Table 10 Results Obtained from RQC-100 under Completely Reversed Nominal Stress.

Notch root stress-strain for RQC-100 Steel flat plate								
S _a (MPa)	Neuber's		Linear FEA		E- Plastic FEA		Proposed	
	σ _{max}	% (ε _a)	σ _{max}	%(ε _a)	σ _{max}	%(ε _a)	σ _{max}	%(ε _a)
0	0	0	0	0	0	0	0	0
50	137	0.066	133	0.064	133	0.064	137	0.047
100	273	0.133	267	0.128	269	0.128	272	0.113
150	409	0.21	404	0.195	404	0.195	409	0.186
200	496	0.29	538	0.259	538	0.259	500	0.261
250	564	0.398	671	0.323	612	0.349	575	0.353
300	613	0.52	809	0.39	638	0.456	633	0.456
350	653	0.67	942	0.454	661	0.565	682	0.576
400	685	0.836	1076	0.518	707	0.701	724	0.706
450	713	0.102	1210	0.583	735	0.847	763	0.849
500	737	1.21	1343	0.647	761	1.000	798	0.995

Notch root stress-strain for RQC-100 Steel round bar								
S _a (MPa)	Neuber's		Linear FEA		E- Plastic FEA		Proposed	
	σ _{max}	% (ε _a)	σ _{max}	%(ε _a)	σ _{max}	%(ε _a)	σ _{max}	%(ε _a)
0	0	0	0	0	0	0	0	0
50	90	0.0396	90	0.037	90	0.037	90	0.018
100	179	0.0789	180	0.073	180	0.073	179	0.056
150	268	0.118	271	0.110	271	0.110	268	0.095
200	355	0.158	358	0.145	358	0.145	355	0.133
250	438	0.201	444	0.180	444	0.180	439	0.173
300	511	0.248	538	0.218	538	0.218	514	0.217
350	572	0.302	625	0.254	624	0.253	577	0.265
400	621	0.362	715	0.29	715	0.290	630	0.316
450	663	0.43	805	0.327	785	0.329	677	0.373
500	697	0.502	896	0.364	815	0.378	717	0.433

Table 11 Results Obtained from SAE1045 under Completely Reversed Nominal Stress.

Notch root stress-strain for SAE1045 Steel flat plate								
S _a (MPa)	Neuber's		Elastic FEA		E- Plastic FEA		Proposed	
	σ _{max}	% (ε _a)	σ _{max}	% (ε _a)	σ _{max}	% (ε _a)	σ _{max}	% (ε _a)
0	0	0	0	0	0	0	0	0
50	136	0.065	137	0.0637	133	0.063	136	0.06
100	263	0.136	273	0.126	267	0.127	264	0.103
150	354	0.226	410	0.193	404	0.193	360	0.185
200	415	0.341	546	0.256	457	0.288	428	0.282
250	461	0.4814	683	0.32	481	0.406	483	0.396
300	498	0.644	819	0.386	507	0.530	530	0.524
350	528	0.82	956	0.448	534	0.689	571	0.661
400	555	1.02	1092	0.513	556	0.868	609	0.813

Notch root stress-strain for SAE1045 Steel round bar								
S _a (MPa)	Neuber's		Elastic FEA		E- Plastic FEA		Proposed	
	σ _{max}	% (ε _a)	σ _{max}	% (ε _a)	σ _{max}	% (ε _a)	σ _{max}	% (ε _a)
0	0	0	0	0	0	0	0	0
50	90	0.0393	90	0.0363	90	0.0363	90	0.037
100	180	0.079	180	0.0727	180	0.0727	180	0.0458
150	260	0.116	271	0.109	270	0.109	261	0.0825
200	335	0.16	354	0.142	359	0.142	337	0.122
250	395	0.209	444	0.179	444	0.179	400	0.167
300	443	0.264	538	0.217	480	0.216	453	0.216
350	481	0.323	625	0.252	521	0.258	495	0.267
400	514	0.39	715	0.288	550	0.310	534	0.323
450	543	0.465	805	0.324	575	0.371	569	0.384

Table 12 Results Obtained from SAE1050M under Completely Reversed Nominal Stress.

Notch root stress-strain for SAE1050M Steel flat plate								
S_a (MPa)	Neuber's		Elastic FEA		E- Plastic FEA		Proposed	
	σ_{max}	% (ϵ_a)	σ_{max}	% (ϵ_a)	σ_{max}	% (ϵ_a)	σ_{max}	% (ϵ_a)
0	0	0	0	0	0	0	0	0
50	137	0.0678	133	0.0459	133	0.046	137	0.0441
100	271	0.135	267	0.132	267	0.132	271	0.117
150	388	0.213	404	0.2	404	0.200	390	0.192
200	465	0.316	538	0.265	530	0.275	472	0.282
250	516	0.447	671	0.331	548	0.383	532	0.390
300	553	0.599	805	0.397	571	0.506	578	0.512
350	583	0.769	938	0.463	593	0.645	619	0.645
400	606	0.956	1076	0.531	620	0.804	653	0.791
450	629	1.18	1210	0.597	643	0.986	687	0.959

Notch root stress-strain for SAE1050M Steel round bar								
S_a (MPa)	Neuber's		Elastic FEA		E- Plastic FEA		Proposed	
	σ_{max}	% (ϵ_a)	σ_{max}	% (ϵ_a)	σ_{max}	% (ϵ_a)	σ_{max}	% (ϵ_a)
0	0	0	0	0	0	0	0	0
50	87	0.0431	90	0.0412	90	0.041	87	0.0264
100	179	0.0892	180	0.0824	180	0.082	179	0.0708
150	257	0.128	270	0.123	270	0.123	258	0.110
200	340	0.176	359	0.164	359	0.164	342	0.155
250	406	0.231	444	0.203	444	0.203	410	0.205
300	455	0.298	538	0.245	485	0.245	463	0.263
350	491	0.374	625	0.285	521	0.290	504	0.326
400	520	0.46	715	0.326	555	0.349	540	0.397
450	545	0.00561	805	0.00368	588	0.00416	571	0.477
500	565	0.0066	896	0.00409	602	0.0049	598	0.556

Table 13 Results Obtained from SAE1050M under Completely Reversed Nominal Stress.

Notch root stress-strain for SAE1141MA Steel flat plate								
S _a (MPa)	Neuber's		Elastic FEA		E- Plastic FEA		Proposed	
	σ _{max}	% (ε _a)	σ _{max}	% (ε _a)	σ _{max}	% (ε _a)	σ _{max}	% (ε _a)
0	0	0	0	0	0	0	0	0
50	137	0.0685	137	0.0685	137	0.066	137	0.04
100	273	0.137	273	0.137	273	0.133	273	0.09
150	400	0.212	404	0.201	400	0.201	400	0.194
200	485	0.3	538	0.268	485	0.268	490	0.274
250	545	0.423	671	0.334	545	0.370	558	0.377
300	585	0.561	805	0.401	585	0.490	607	0.491
350	618	0.73	942	0.47	642	0.607	650	0.625
400	645	0.92	1076	0.536	675	0.755	688	0.771
450	667	1.12	1210	0.603	693	0.92	721	0.925
500	687	1.3	1343	0.669	710	1.09	753	1.065

Notch root stress-strain for SAE1141MA Steel round bar								
S _a (MPa)	Neuber's		Elastic FEA		E- Plastic FEA		Proposed	
	σ _{max}	% (ε _a)	σ _{max}	% (ε _a)	σ _{max}	% (ε _a)	σ _{max}	% (ε _a)
0	0	0	0	0	0	0	0	0
50	90	0.045	90	0.0416	90	0.0416	90	0.0307
100	179	0.0895	180	0.0833	180	0.0833	179	0.0742
150	270	0.135	271	0.125	271	0.125	270	0.118
200	354	0.18	358	0.165	358	0.165	354	0.161
250	427	0.233	444	0.205	444	0.205	429	0.210
300	483	0.299	538	0.248	500	0.248	489	0.268
350	525	0.373	625	0.288	553	0.288	535	0.330
400	557	0.458	715	0.33	590	0.329	573	0.400
450	584	0.00553	805	0.00371	623	0.0038	606	0.476
500	606	0.00662	896	0.00413	665	0.0044	635	0.561

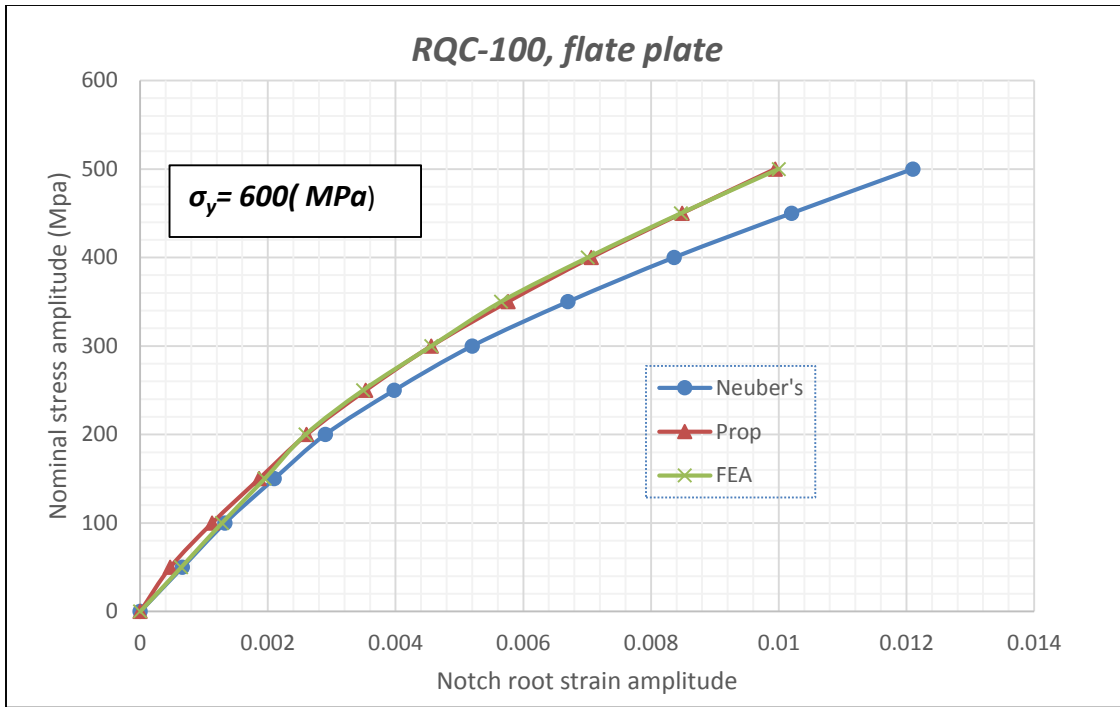


Figure 60 Local Strain Obtained from Elasto-Plastic FEA, Neuber Rule and Proposed Method

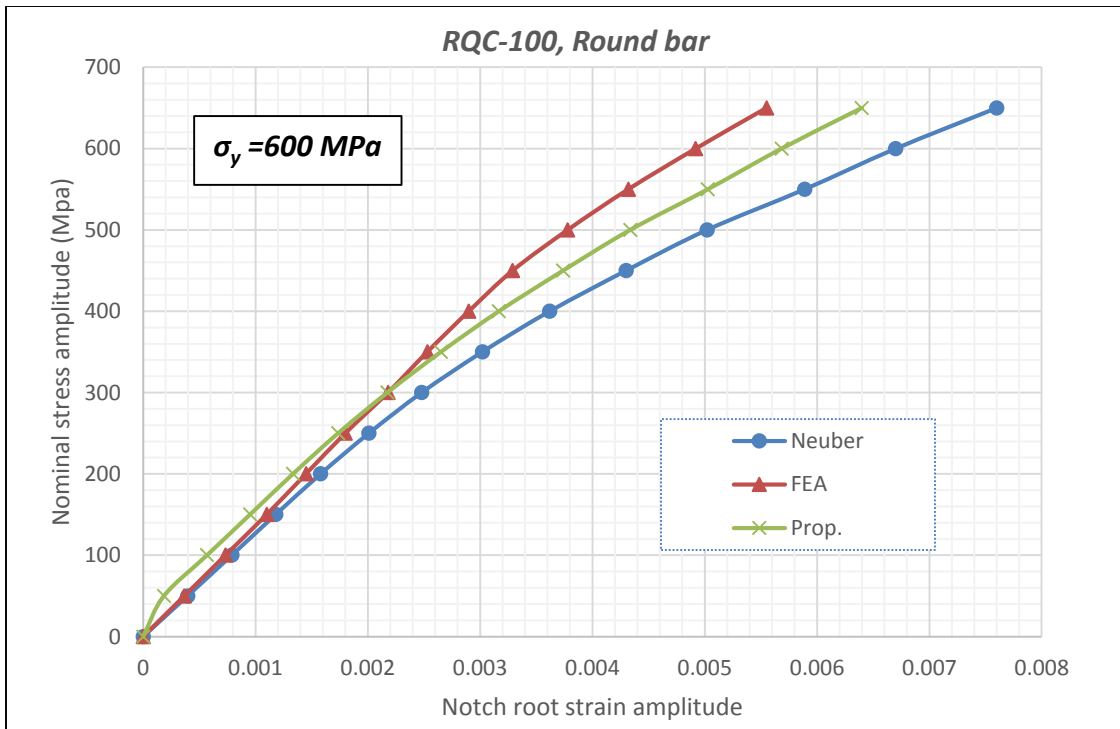


Figure 61 Local Strain Obtained from Elasto-Plastic FEA, Neuber Rule and Proposed Method

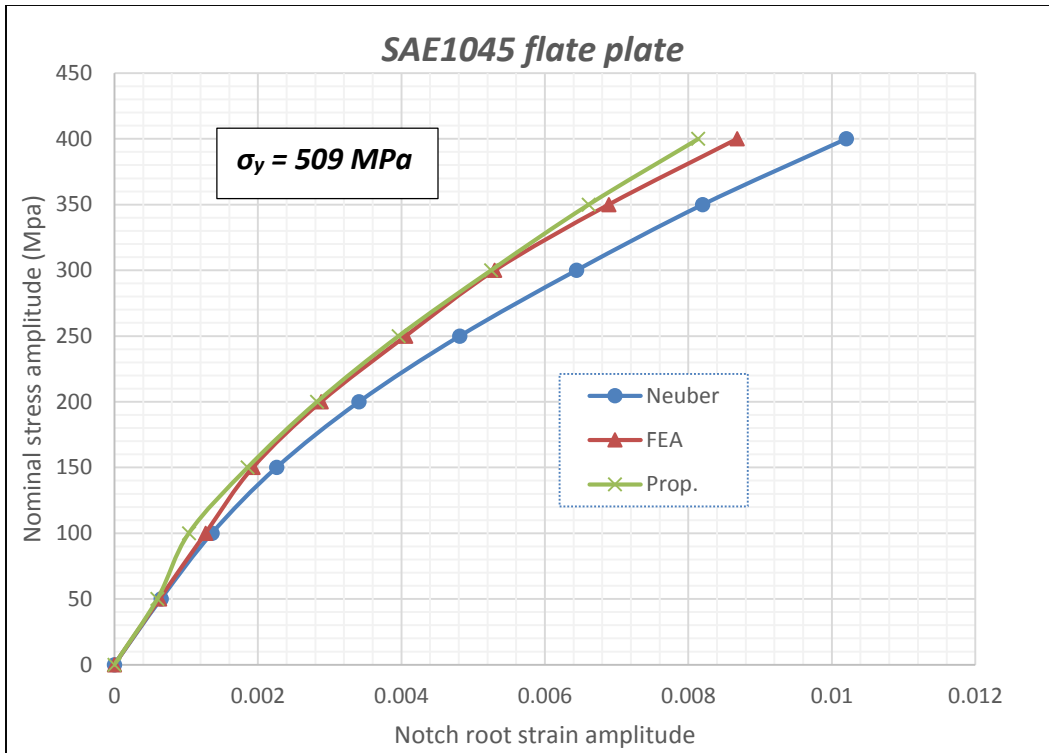


Figure 62 Local Strain Obtained from Elasto-Plastic FEA, Neuber Rule and Proposed Method

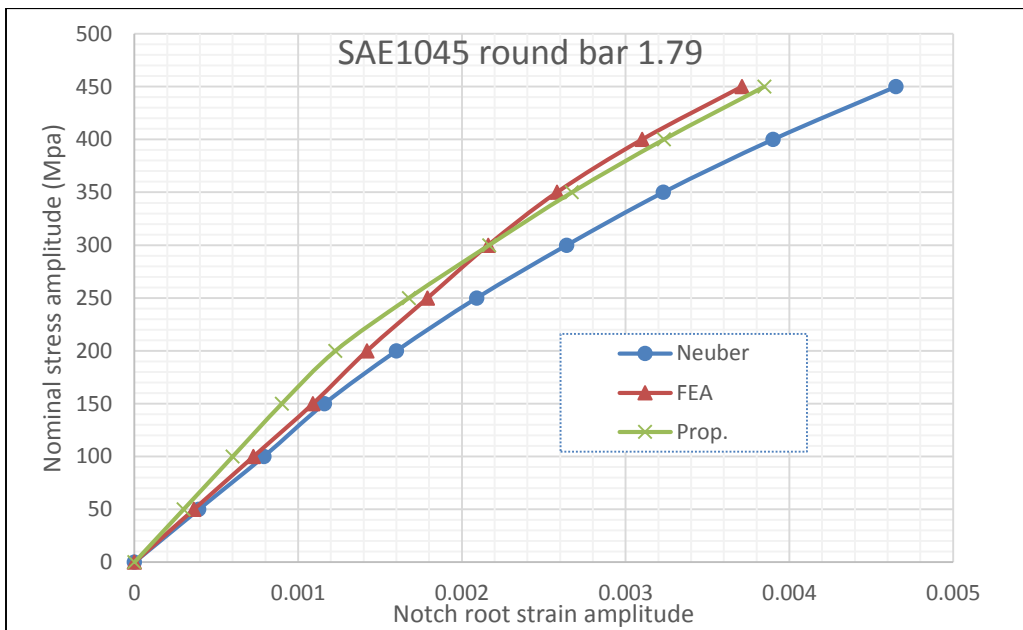


Figure 63 Local Strain Obtained from Elasto-Plastic FEA, Neuber Rule and Proposed Method

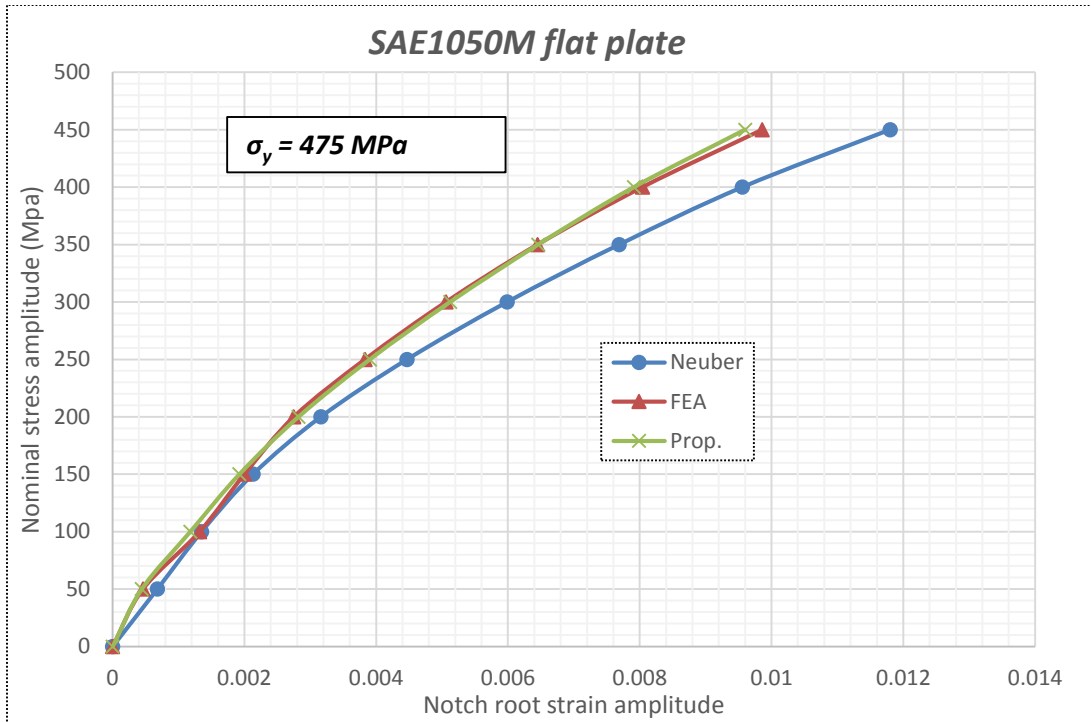


Figure 64 Local Strain Obtained from Elasto-Plastic FEA, Neuber Rule and Proposed Method

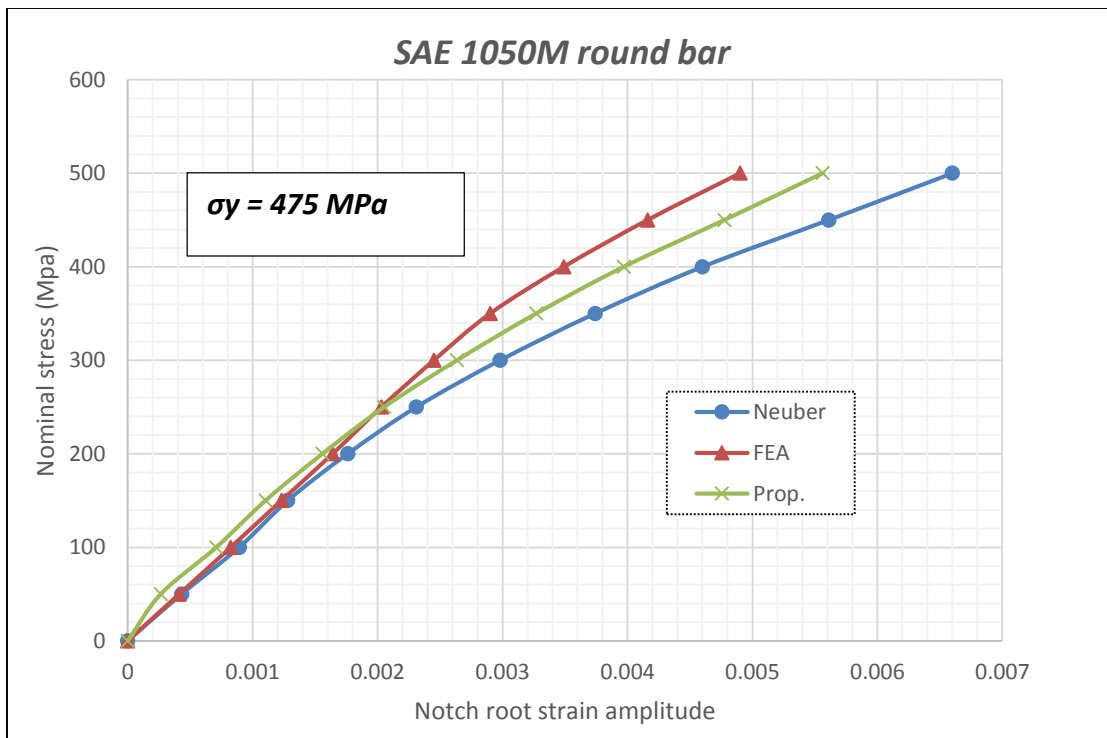


Figure 65 Local Strain Obtained from Elasto-Plastic FEA, Neuber Rule and Proposed Method

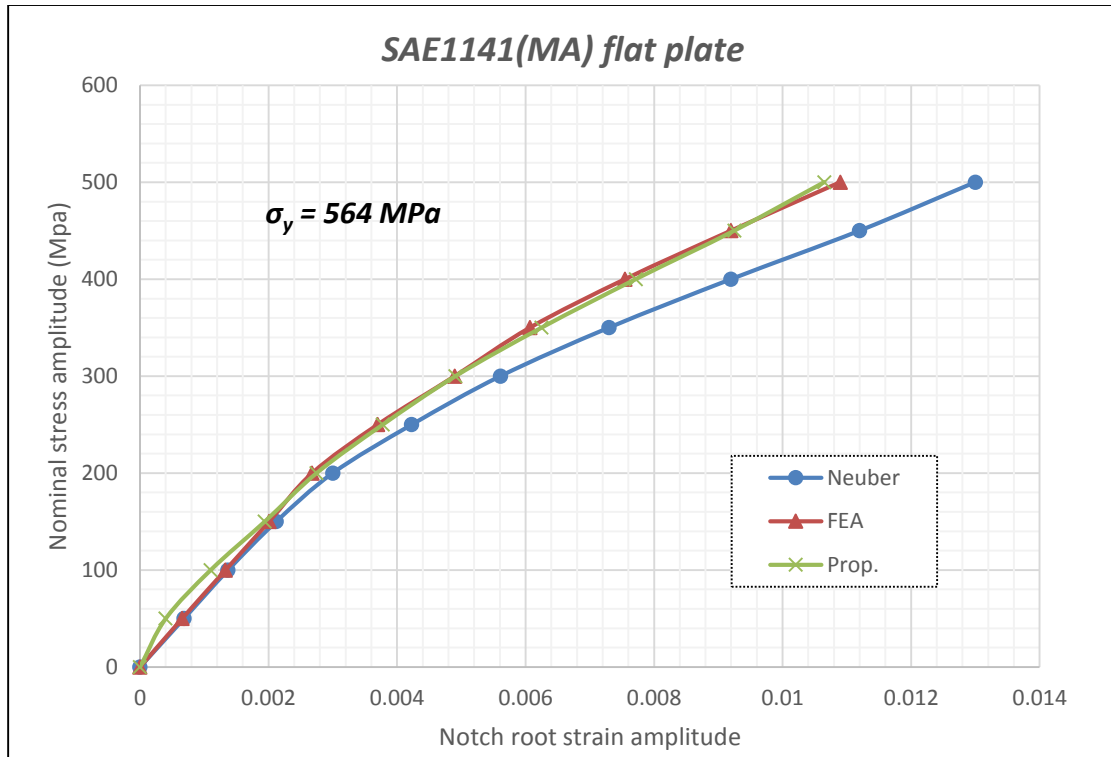


Figure 66 Local Strain Obtained from Elasto-plastic FEA, Neuber Rule and Proposed Method

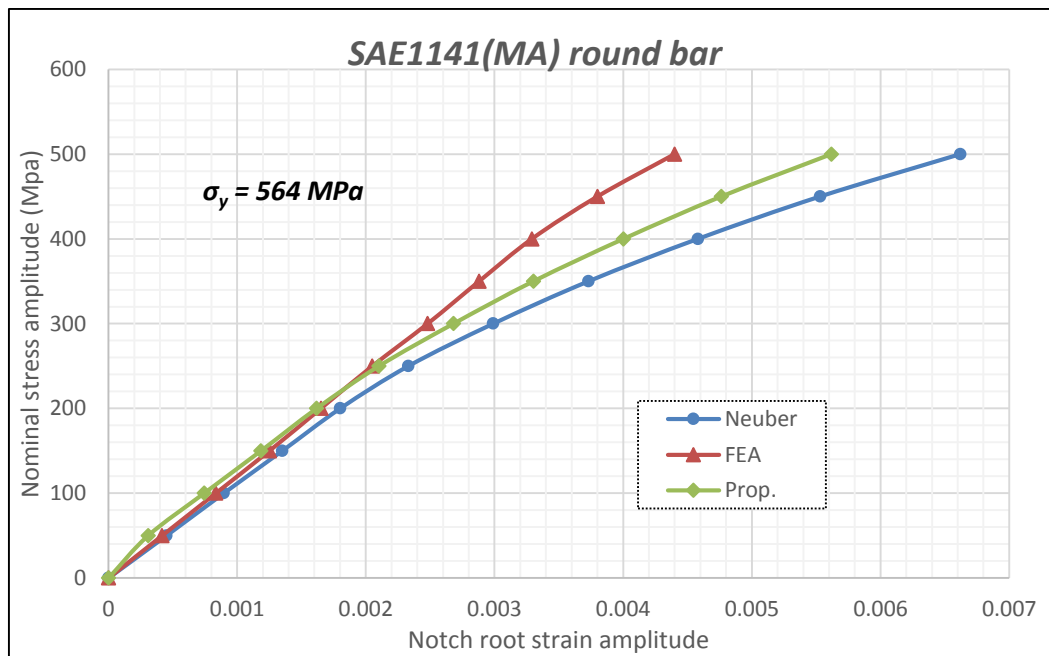


Figure 67 Local Strain Obtained from Elasto-Plastic FEA, Neuber Rule and Proposed Method

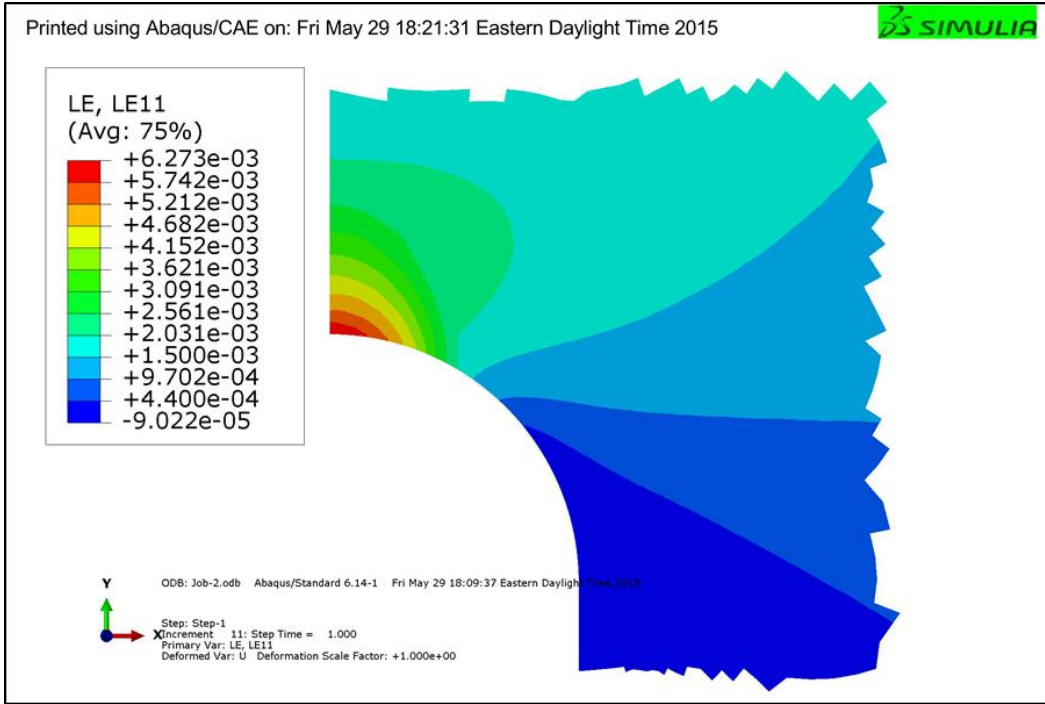


Figure 68 Snapshot from ABAQUS Viewer for Strain Contours of Flat Plate under Tensile Cyclic Load.

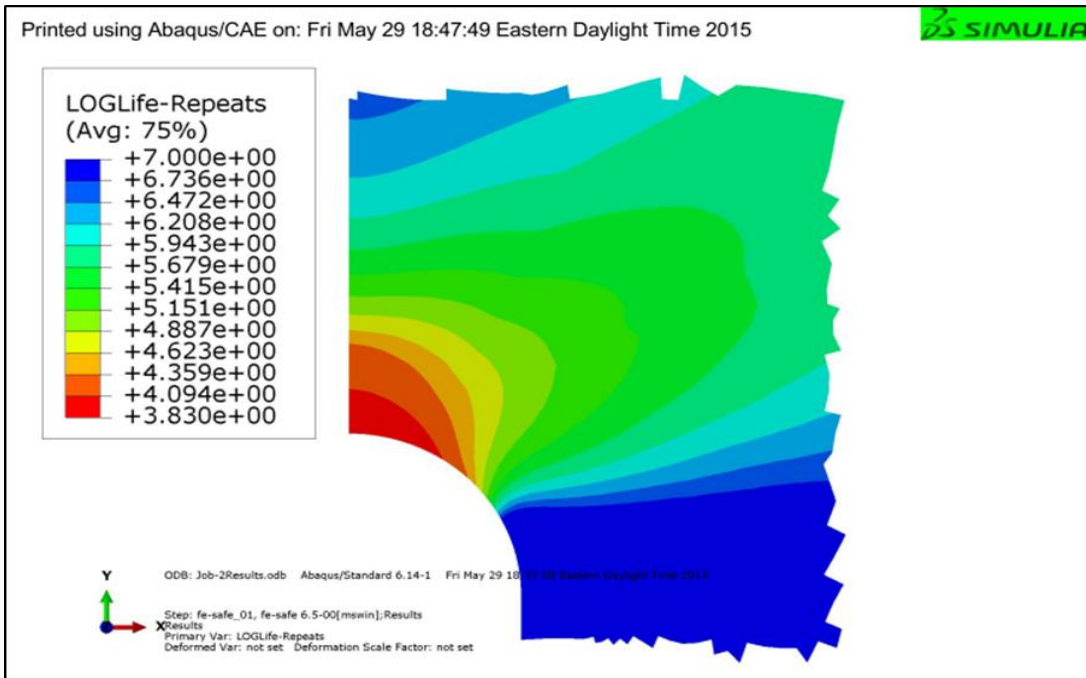


Figure 69 Snapshot using fe-safe/ABAQUS Viewer for Fatigue Life Contours of Flat Plate under Tensile Cyclic Load.

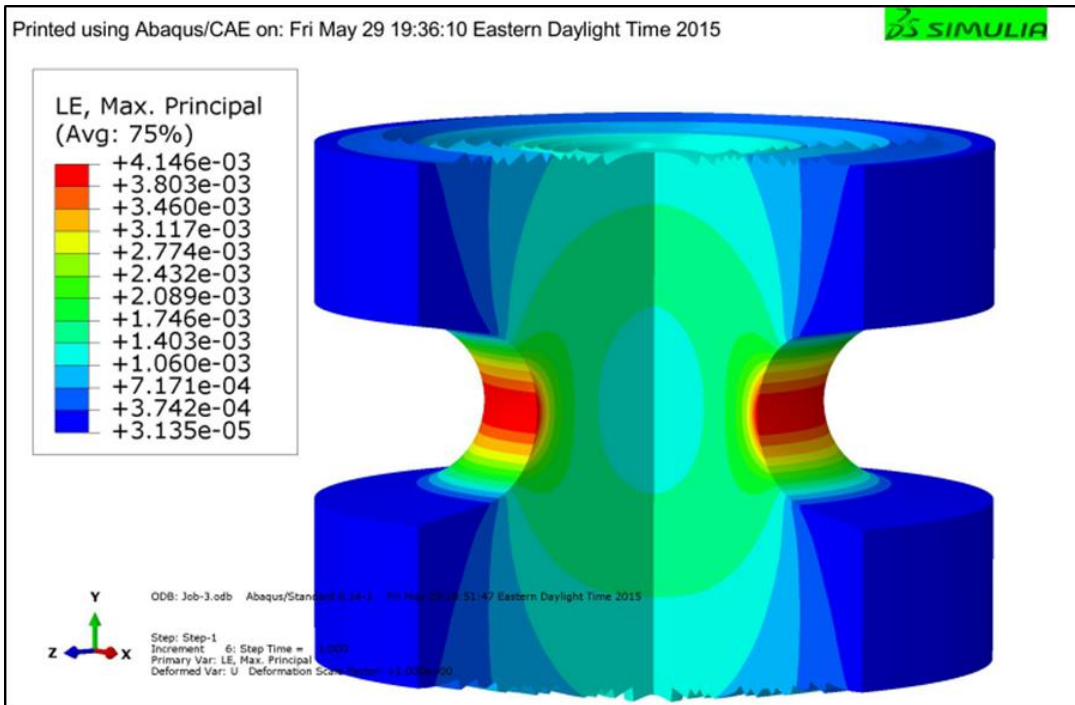


Figure 70 Snapshot from ABAQUS Viewer for Strain Contours of Round Bar under Tensile Cyclic Load.

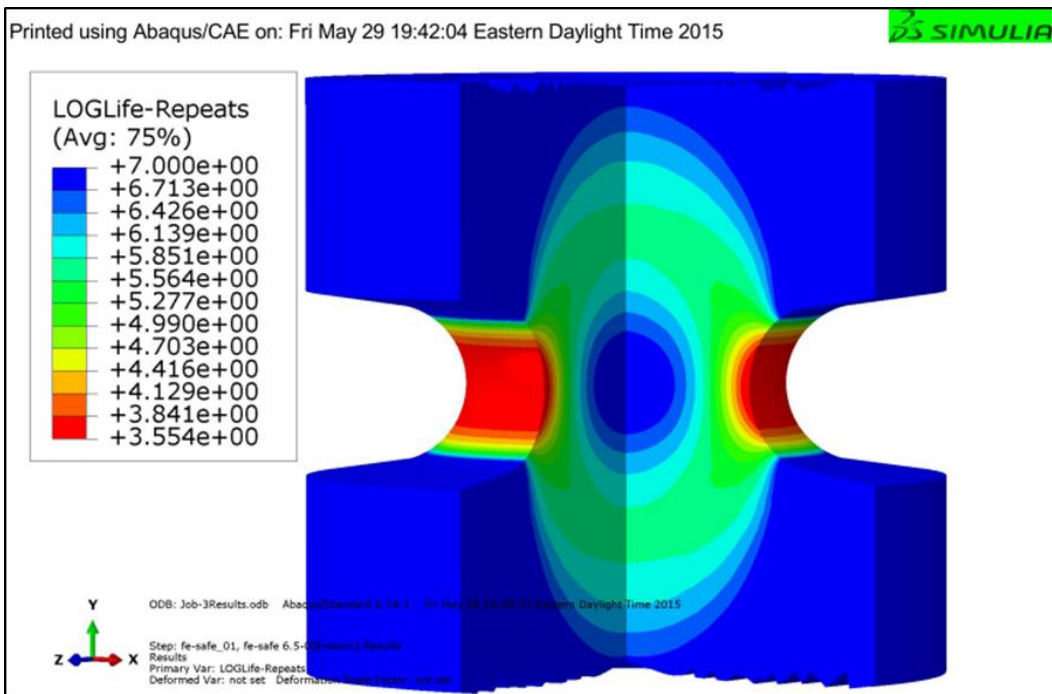


Figure 71 Snapshot using fe-safe/ABAQUS Viewer Fatigue Life Contours of Round Bar under Tensile Cyclic Load

6 CONCLUSIONS

Material data that ranged from low, medium and high strength alloy steels were used in this study, correlations among monotonic tensile data and fatigue properties were investigated, the predicted data was compared with the data predicted using commonly used methods and with experimental data. In the second part of this study, a notch root strain prediction model was developed by creating a notch strain correction expression based on the cyclic material property n' , subtracted from Neuber's rule predicted strain. In the second stage a linear interpolation scheme was applied between the notch strain value obtained from the first stage and elastic finite element analysis notch root strain value. The effect of K' on the notch strain is not included in the model it needs more investigation to combine the two effects (n' and K') into one mathematical model which is out of the scope of this work.

Based on the discussions from the previous sections, the following can be concluded:

1. A strong correlation is found between ultimate tensile strength and hardness, in the proposed method as in Eq. (124), a nonlinear relationship provides a better fit to the existing methods with $R^2=0.98$.
 2. The results obtained by using correlation method proposed in Eq. (124), are closer to experimental data compared with Roessle-Fatemi's ultimate tensile strength-Brinell hardness correlation method.
 3. Ultimate tensile strength obtained from Eq. (124) is substituted with a corresponding Brinell-hardness HB in the Modified Universal Slopes method; that results in a new method Eq. (135), in which fatigue properties can be predicted using Brinell-hardness, true fracture ductility, and modulus of elasticity.
 4. Fatigue parameters obtained by the proposed method are closer to experimental data when they are compared with the results obtained from the Modified Universal Slopes model for most of the tested steels.
- 1) A two-step new prediction method is developed based on the cyclic materials property n' and linear interpolation of Neuber's rule and linear finite element analysis.

- 2) The proposed method notch strain values are in good agreement with the nonlinear finite element analysis compared with the use of Neuber's method.
- 3) Nonlinear finite element analysis can be replaced by linear finite element analysis.
- 4) Prediction capability is slightly better in case of plane strain condition

Appendices

7 APPENDIX A

Table 14 Ultimate Tensile Strength Obtained from Proposed, Roessle-Fatemi S_u – HB Correlation Models Compared with Experimental Data.

Number	AISI	Treatment temperature C^0	HB	S_u (Exp.)	S_u (Prop.)	S_u (Prop.)/ S_u (Exp.)	S_u (R-F)	S_u (R-F)/ S_u (Exp.)
1	1015	126	420	468	1.11	435	1.04
2	1015	925	121	424	458	1.08	417	0.98
3	1015	870	111	386	438	1.14	381	0.99
4	1020	143	448	503	1.12	496	1.11
5	1020	870	131	441	478	1.08	453	1.03
6	1020	870	111	394	438	1.11	381	0.97
7	1022	925	143	482	503	1.04	496	1.03
8	1022	870	137	429	490	1.14	475	1.11
9	1030	...	179	551	584	1.06	629	1.14
10	1030	845	126	463	468	1.01	435	0.94
11	1040	...	201	620	639	1.03	712	1.15
12	1040	900	170	589	563	0.96	596	1.01
13	1040	790	149	518	516	1.00	518	1.00
14	1050	229	723	714	0.99	819	1.13
15	1050	900	217	748	681	0.91	773	1.03
16	1050	790	187	636	604	0.95	659	1.04
17	1060	241	813	749	0.92	865	1.06
18	1060	790	179	625	584	0.93	629	1.01
19	1080	...	293	965	914	0.95	1070	1.11
20	1080	900	293	1010	914	0.91	1070	1.06
21	1080	790	174	615	572	0.93	611	0.99
22	1095	900	293	1013	914	0.90	1070	1.06
23	1095	790	192	656	616	0.94	678	1.03
24	1117	900	137	467	490	1.05	475	1.02
25	1117	855	121	429	458	1.07	417	0.97
26	1118	...	149	521	516	0.99	518	0.99
27	1118	790	131	450	478	1.06	453	1.01
28	1137	...	192	627	616	0.98	678	1.08
29	1137	790	174	584	572	0.98	611	1.05
30	1141	...	192	675	616	0.91	678	1.00
31	1141	900	201	706	639	0.90	712	1.01
32	1141	815	163	598	547	0.91	570	0.95
33	1144	...	212	703	668	0.95	754	1.07
34	1144	900	197	667	629	0.94	697	1.04
35	1144	790	167	584	556	0.95	585	1.00
36	1340	800	207	703	654	0.93	735	1.04

Number	AISI	Treatment temperature C ⁰	HB	S _u (Exp.)	S _u (Prop.)	S _u (Prop.)/S _u (Exp.)	S _u (R-F)	S _u (R-F)/S _u (Exp.)
37	3140	870	262	891	812	0.91	947	1.06
38	3140	815	197	689	629	0.91	697	1.01
39	4130	870	197	668	629	0.94	697	1.04
40	4130	865	156	560	531	0.95	544	0.97
41	4140	870	302	1020	946	0.93	1106	1.08
42	4140	815	197	655	629	0.96	697	1.06
43	4150	815	197	729	629	0.86	697	0.96
44	4320	895	235	792	731	0.92	842	1.06
45	4320	850	163	579	547	0.94	570	0.98
46	4340	870	363	1279	1187	0.93	1356	1.06
47	4340	810	217	744	681	0.92	773	1.04
48	4620	900	174	574	572	1.00	611	1.06
49	4620	855	149	512	516	1.01	518	1.01
50	4820	860	229	750	714	0.95	819	1.09
51	5140	870	229	792	714	0.90	819	1.03
52	5140	830	167	572	556	0.97	585	1.02
53	5150	870	255	870	790	0.91	920	1.06
54	5150	825	197	675	629	0.93	697	1.03
55	5160	855	269	957	834	0.87	975	1.02
56	5160	815	197	722	629	0.87	697	0.96
57	6150	870	269	939	834	0.89	975	1.04
58	6150	815	197	667	629	0.94	697	1.04
59	8620	915	183	632	594	0.94	644	1.02
60	8620	870	149	536	516	0.96	518	0.97
61	8630	870	187	650	604	0.93	659	1.01
62	8630	845	156	564	531	0.94	544	0.96
63	8650	870	302	1023	946	0.92	1106	1.08
64	8650	795	212	715	668	0.93	754	1.05
65	8740	870	269	929	834	0.90	975	1.05
66	8740	815	201	695	639	0.92	712	1.02
67	9255	900	269	932	834	0.90	975	1.05
68	9255	845	229	774	714	0.92	819	1.06
69	9310	890	269	906	834	0.92	975	1.08
70	9310	845	241	820	749	0.91	865	1.05
71	1030b	540	255	669	790	1.18	920	1.37
72	1030b	650	207	586	654	1.12	735	1.25
73	1040b	425	352	841	1140	1.36	1310	1.56
74	1040b	540	269	779	834	1.07	975	1.25

Number	AISI	Treatment temperature C ⁰	HB	S _u (Exp.)	S _u (Prop.)	S _u (Prop.)/S _u (Exp.)	S _u (R-F)	S _u (R-F)/S _u (Exp.)
75	1040b	650	201	669	639	0.95	712	1.06
76	1040	205	262	779	812	1.04	947	1.22
77	1040	315	255	779	790	1.01	920	1.18
78	1040	425	241	758	749	0.99	865	1.14
79	1040	540	212	717	668	0.93	754	1.05
80	1040	650	192	634	616	0.97	678	1.07
81	1050b	540	293	862	914	1.06	1070	1.24
82	1050b	650	235	717	731	1.02	842	1.17
83	1050	315	321	979	1016	1.04	1183	1.21
84	1050	425	277	938	860	0.92	1006	1.07
85	1050	540	262	876	812	0.93	947	1.08
86	1050	650	223	738	697	0.95	796	1.08
87	1060	205	321	1103	1016	0.92	1183	1.07
88	1060	315	321	1103	1016	0.92	1183	1.07
89	1060	425	311	1076	979	0.91	1142	1.06
90	1060	540	277	965	860	0.89	1006	1.04
91	1060	650	229	800	714	0.89	819	1.02
92	1080	205	388	1310	1300	0.99	1461	1.12
93	1080	315	388	1303	1300	1.00	1461	1.12
94	1080	425	375	1289	1240	0.96	1406	1.09
95	1080	540	321	1131	1016	0.90	1183	1.05
96	1080	650	255	889	790	0.89	920	1.03
97	1095b	425	388	1372	1300	0.95	1461	1.06
98	1095b	650	235	841	731	0.87	842	1.00
99	1095	205	401	1289	1363	1.06	1516	1.18
100	1095	315	375	1262	1240	0.98	1406	1.11
101	1095	425	363	1213	1187	0.98	1356	1.12
102	1095	540	321	1089	1016	0.93	1183	1.09
103	1095	650	269	896	834	0.93	975	1.09
104	1137	205	352	1082	1140	1.05	1310	1.21
105	1137	315	285	986	887	0.90	1038	1.05
106	1137	425	262	876	812	0.93	947	1.08
107	1137	540	229	758	714	0.94	819	1.08
108	1137	650	197	655	629	0.96	697	1.06
109	1137b	205	415	1496	1433	0.96	1576	1.05
110	1137b	315	375	1372	1240	0.90	1406	1.02
111	1137b	425	311	1103	979	0.89	1142	1.04

Number	AISI	Treatment temperature C ⁰	HB	S _u (Exp.)	S _u (Prop.)	S _u (Prop.)/S _u (Exp.)	S _u (R-F)	S _u (R-F)/S _u (Exp.)
112	1137b	540	262	827	812	0.98	947	1.15
113	1137b	650	187	648	604	0.93	659	1.02
114	1141	205	461	1634	1689	1.03	1776	1.09
115	1141	315	415	1462	1433	0.98	1576	1.08
116	1141	425	331	1165	1055	0.91	1224	1.05
117	1141	540	262	896	812	0.91	947	1.06
118	1141	650	217	710	681	0.96	773	1.09
119	1144	205	277	876	860	0.98	1006	1.15
120	1144	315	262	869	812	0.93	947	1.09
121	1144	425	248	848	769	0.91	892	1.05
122	1144	540	235	807	731	0.91	842	1.04
123	1144	650	217	724	681	0.94	773	1.07
124	1330b	205	459	1600	1677	1.05	1768	1.10
125	1330b	315	402	1427	1368	0.96	1521	1.07
126	1330b	425	335	1158	1070	0.92	1240	1.07
127	1330b	540	263	876	815	0.93	951	1.09
128	1330b	650	216	731	678	0.93	769	1.05
129	1340	205	505	1806	1972	1.09	1973	1.09
130	1340	315	453	1586	1642	1.04	1741	1.10
131	1340	425	375	1262	1240	0.98	1406	1.11
132	1340	540	295	965	921	0.95	1078	1.12
133	1340	650	252	800	781	0.98	908	1.13
134	4037	205	310	1027	975	0.95	1138	1.11
135	4037	315	295	951	921	0.97	1078	1.13
136	4037	425	270	876	838	0.96	978	1.12
137	4037	540	247	793	766	0.97	888	1.12
138	4037	650	220	696	689	0.99	784	1.13
139	4042	205	516	1800	2050	1.14	2022	1.12
140	4042	315	455	1613	1654	1.03	1750	1.08
141	4042	425	380	1289	1263	0.98	1427	1.11
142	4042	540	300	986	939	0.95	1098	1.11
143	4042	650	238	793	740	0.93	853	1.08
144	4130b	205	467	1627	1725	1.06	1803	1.11
145	4130b	315	435	1496	1540	1.03	1663	1.11
146	4130b	425	380	1282	1263	0.99	1427	1.11
147	4130b	540	315	1034	993	0.96	1159	1.12
148	4130	650	245	814	760	0.93	881	1.08

Number	AISI	Treatment temperature C ⁰	HB	S _u (Exp.)	S _u (Prop.)	S _u (Prop.)/S _u (Exp.)	S _u (R-F)	S _u (R-F)/S _u (Exp.)
149	4140	205	510	1772	2007	1.13	1995	1.13
150	4140	315	445	1551	1596	1.03	1706	1.10
151	4140	425	370	1248	1218	0.98	1385	1.11
152	4140	540	285	951	887	0.93	1038	1.09
153	4140	650	230	758	717	0.95	822	1.09
154	4150	205	530	1931	2152	1.11	2086	1.08
155	4150	315	495	1765	1904	1.08	1928	1.09
156	4150	425	440	1517	1568	1.03	1684	1.11
157	4150	540	370	1207	1218	1.01	1385	1.15
158	4150	650	290	958	904	0.94	1058	1.10
159	4340	205	520	1875	2079	1.11	2040	1.09
160	4340	315	486	1724	1845	1.07	1887	1.09
161	4340	425	430	1469	1513	1.03	1641	1.12
162	4340	540	360	1172	1174	1.00	1344	1.15
163	4340	650	280	965	870	0.90	1018	1.06
164	5046	205	482	1744	1819	1.04	1869	1.07
165	5046	315	401	1413	1363	0.96	1516	1.07
166	5046	425	336	1138	1074	0.94	1244	1.09
167	5046	540	282	938	877	0.93	1026	1.09
168	5046	650	235	786	731	0.93	842	1.07
169	50B46	315	505	1779	1972	1.11	1973	1.11
170	50B46	425	405	1393	1383	0.99	1533	1.10
171	50B46	540	322	1082	1020	0.94	1187	1.10
172	50B46	650	273	883	847	0.96	990	1.12
173	50B60	315	525	1882	2115	1.12	2063	1.10
174	50B60	425	435	1510	1540	1.02	1663	1.10
175	50B60	540	350	1124	1131	1.01	1302	1.16
176	50B60	650	290	896	904	1.01	1058	1.18
177	5130	205	475	1613	1775	1.10	1838	1.14
178	5130	315	440	1496	1568	1.05	1684	1.13
179	5130	425	379	1275	1258	0.99	1423	1.12
180	5130	540	305	1034	957	0.93	1118	1.08
181	5130	650	245	793	760	0.96	881	1.11
182	5140	205	490	1793	1871	1.04	1905	1.06
183	5140	315	450	1579	1624	1.03	1728	1.09
184	5140	425	365	1310	1196	0.91	1364	1.04
185	5140	540	280	1000	870	0.87	1018	1.02

Number	AISI	Treatment temperature C ⁰	HB	S _u (Exp.)	S _u (Prop.)	S _u (Prop.)/S _u (Exp.)	S _u (R-F)	S _u (R-F)/S _u (Exp.)
186	5140	650	235	758	731	0.96	842	1.11
187	5150	205	525	1944	2115	1.09	2063	1.06
188	5150	315	475	1737	1775	1.02	1838	1.06
189	5150	425	410	1448	1408	0.97	1555	1.07
190	5150	540	340	1124	1090	0.97	1261	1.12
191	5150	650	270	807	838	1.04	978	1.21
192	5160	315	555	1999	2348	1.17	2201	1.10
193	5160	425	461	1606	1689	1.05	1776	1.11
194	5160	540	341	1165	1094	0.94	1265	1.09
195	5160	650	269	896	834	0.93	975	1.09
196	51B60	425	460	1634	1683	1.03	1772	1.08
197	51B60	540	355	1207	1152	0.95	1323	1.10
198	51B60	650	290	965	904	0.94	1058	1.10
199	6150	205	538	1931	2213	1.15	2123	1.10
200	6150	315	483	1724	1826	1.06	1874	1.09
201	6150	425	420	1434	1459	1.02	1598	1.11
202	6150	540	345	1158	1111	0.96	1281	1.11
203	6150	650	282	945	877	0.93	1026	1.09
204	81B45	205	550	2034	2307	1.13	2178	1.07
205	81B45	315	475	1765	1775	1.01	1838	1.04
206	81B45	425	405	1407	1383	0.98	1533	1.09
207	81B45	540	338	1103	1082	0.98	1252	1.14
208	81B45	650	280	896	870	0.97	1018	1.14
209	8630	205	465	1641	1713	1.04	1794	1.09
210	8630	315	430	1482	1513	1.02	1641	1.11
211	8630	425	375	1276	1240	0.97	1406	1.10
212	8630	540	310	1034	975	0.94	1138	1.10
213	8630	650	240	772	746	0.97	861	1.12
214	8640	205	505	1862	1972	1.06	1973	1.06
215	8640	315	460	1655	1683	1.02	1772	1.07
216	8640	425	400	1379	1358	0.98	1512	1.10
217	8640	540	340	1103	1090	0.99	1261	1.14
218	8640	650	280	896	870	0.97	1018	1.14
219	86B45	205	525	1979	2115	1.07	2063	1.04
220	86B45	315	475	1696	1775	1.05	1838	1.08
221	86B45	425	395	1379	1334	0.97	1491	1.08
222	86B45	540	335	1103	1070	0.97	1240	1.12

Number	AISI	Treatment temperature C°	HB	S _u (Exp.)	S _u (Prop.)	S _u (Prop.)/S _u (Exp.)	S _u (R-F)	S _u (R-F)/S _u (Exp.)
223	86B45	650	280	903	870	0.96	1018	1.13
224	8650	205	525	1937	2115	1.09	2063	1.07
225	8650	315	490	1724	1871	1.09	1905	1.11
226	8650	425	420	1448	1459	1.01	1598	1.10
227	8650	540	340	1172	1090	0.93	1261	1.08
228	8650	650	280	965	870	0.90	1018	1.06
229	8660	425	460	1634	1683	1.03	1772	1.08
230	8660	540	370	1310	1218	0.93	1385	1.06
231	8660	650	315	1068	993	0.93	1159	1.08
232	8740	315	495	1717	1904	1.11	1928	1.12
233	8740	425	415	1434	1433	1.00	1576	1.10
234	8740	540	363	1207	1187	0.98	1356	1.12
235	8740	650	302	986	946	0.96	1106	1.12
236	9255	425	477	1606	1788	1.11	1847	1.15
237	9255	540	352	1255	1140	0.91	1310	1.04
238	9255	650	285	993	887	0.89	1038	1.05
239	9260	425	470	1758	1744	0.99	1816	1.03
240	9260	540	390	1324	1310	0.99	1470	1.11
241	9260	650	295	979	921	0.94	1078	1.10
242	94B30	205	475	1724	1775	1.03	1838	1.07
243	94B30	315	445	1600	1596	1.00	1706	1.07
244	94B30	425	382	1344	1272	0.95	1436	1.07
245	94B30	540	307	1000	964	0.96	1126	1.13
246	94B30	650	250	827	775	0.94	900	1.09

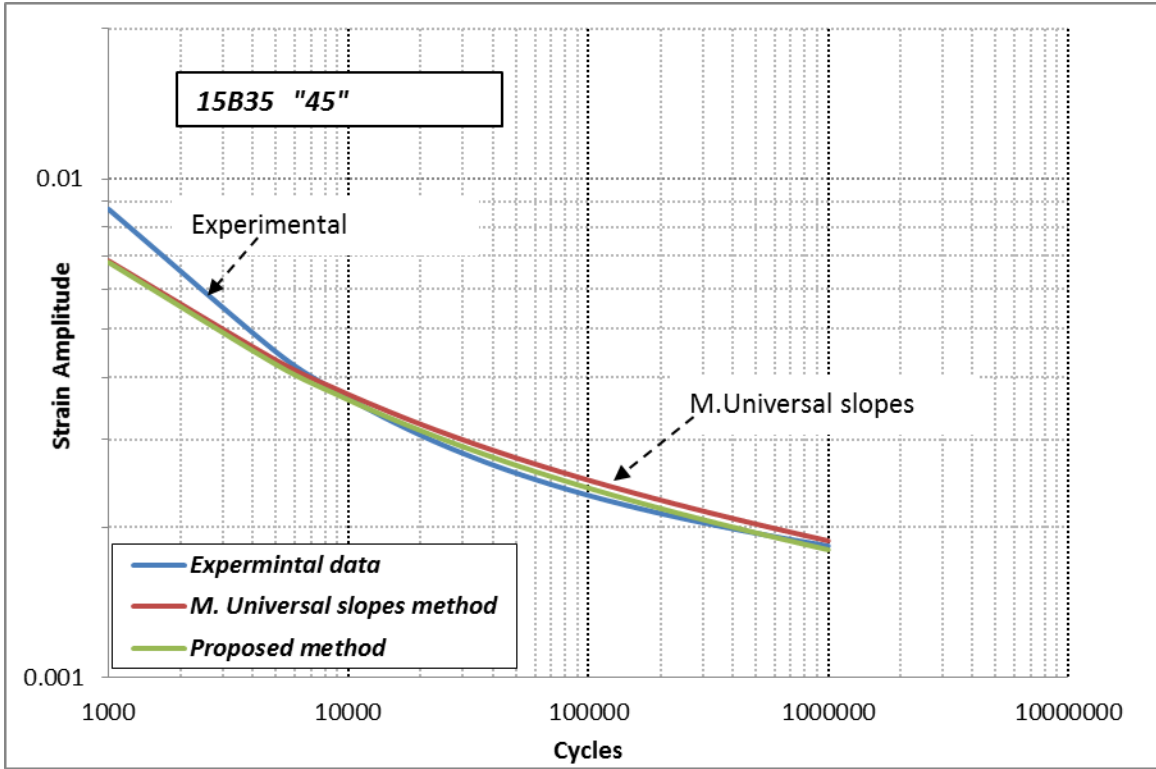


Figure72 Comparison between Three Prediction Approaches for SAE 15B35, HB286 Steel

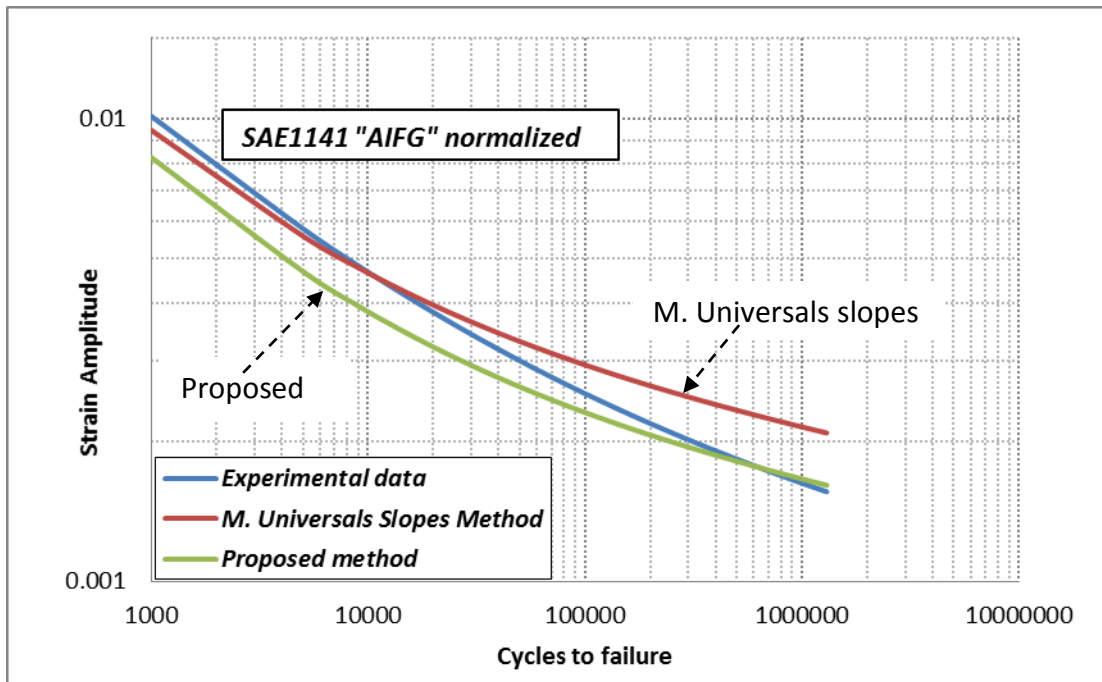


Figure 73 Comparison between Three Prediction Approaches for SAE 1141, HB223 Steel

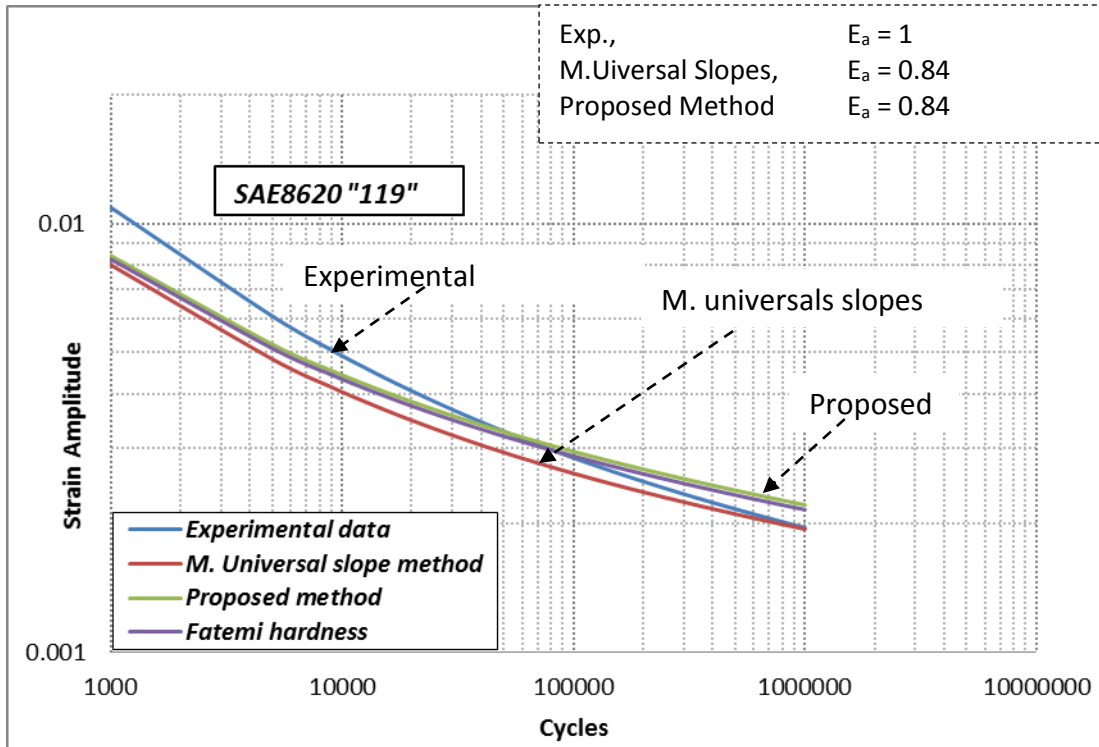


Figure 74 Comparison between Three Prediction Approaches for SAE 8620,HB326 Steel

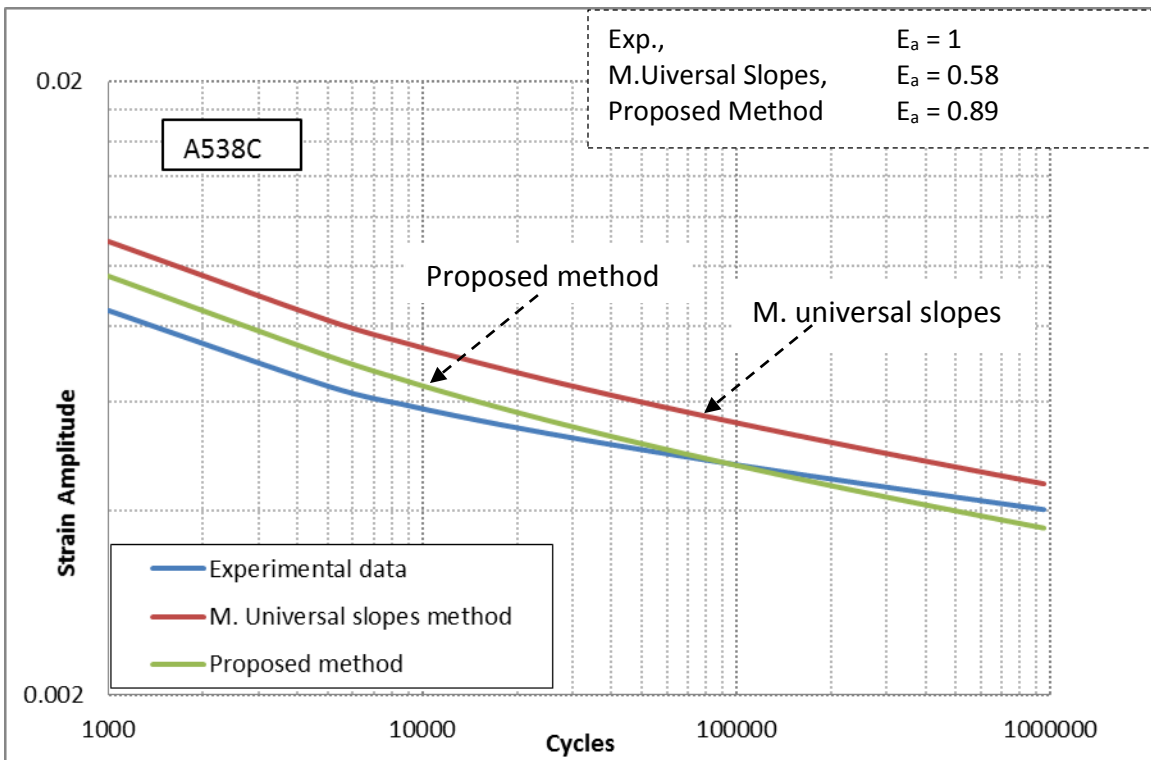


Figure75 Comparison between Three Prediction Approaches for SAE A538C,HB480 Steel

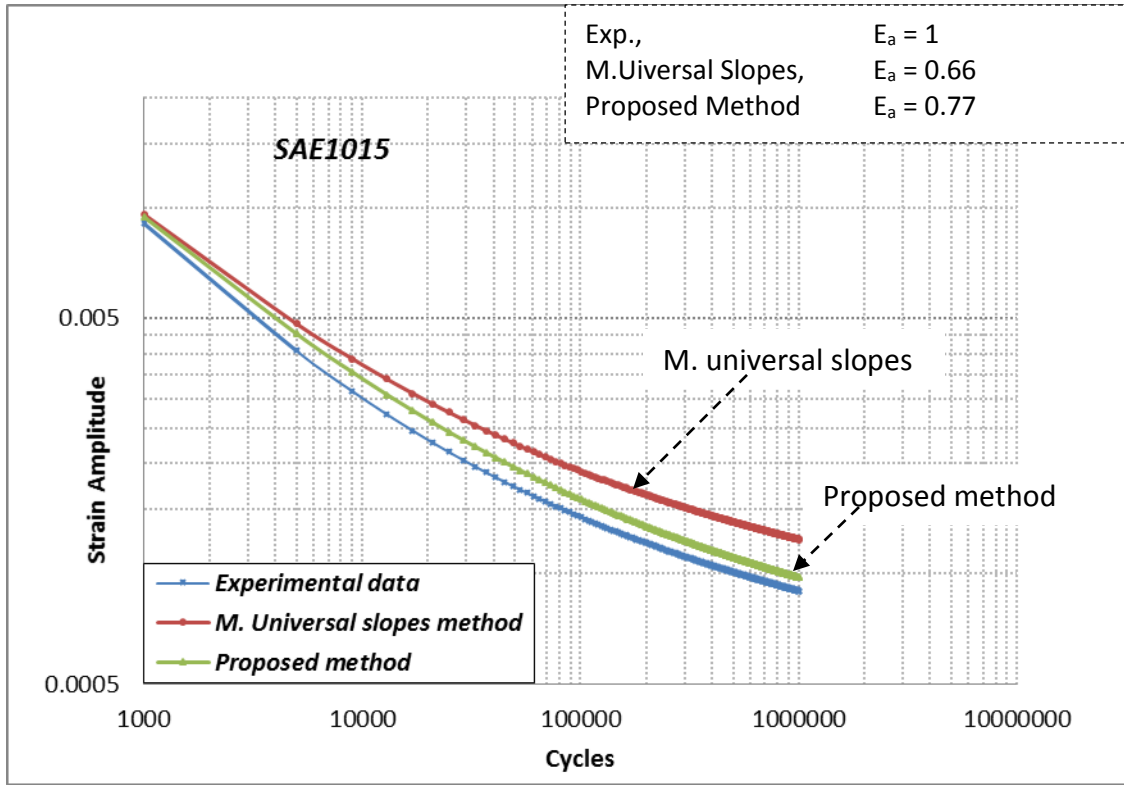


Figure 76 Comparison between Three Prediction Approaches for SAE1015,HB130 Steel

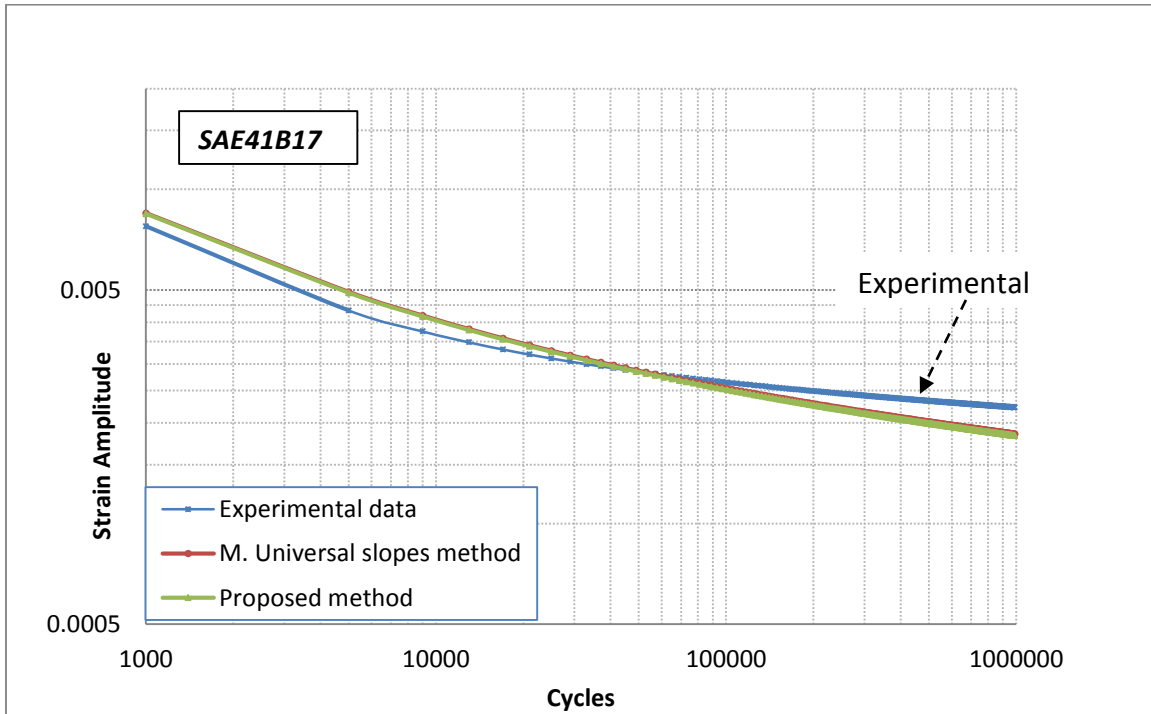


Figure77, Comparison between Three Prediction Approaches for SAE41B17, HB277 Steel

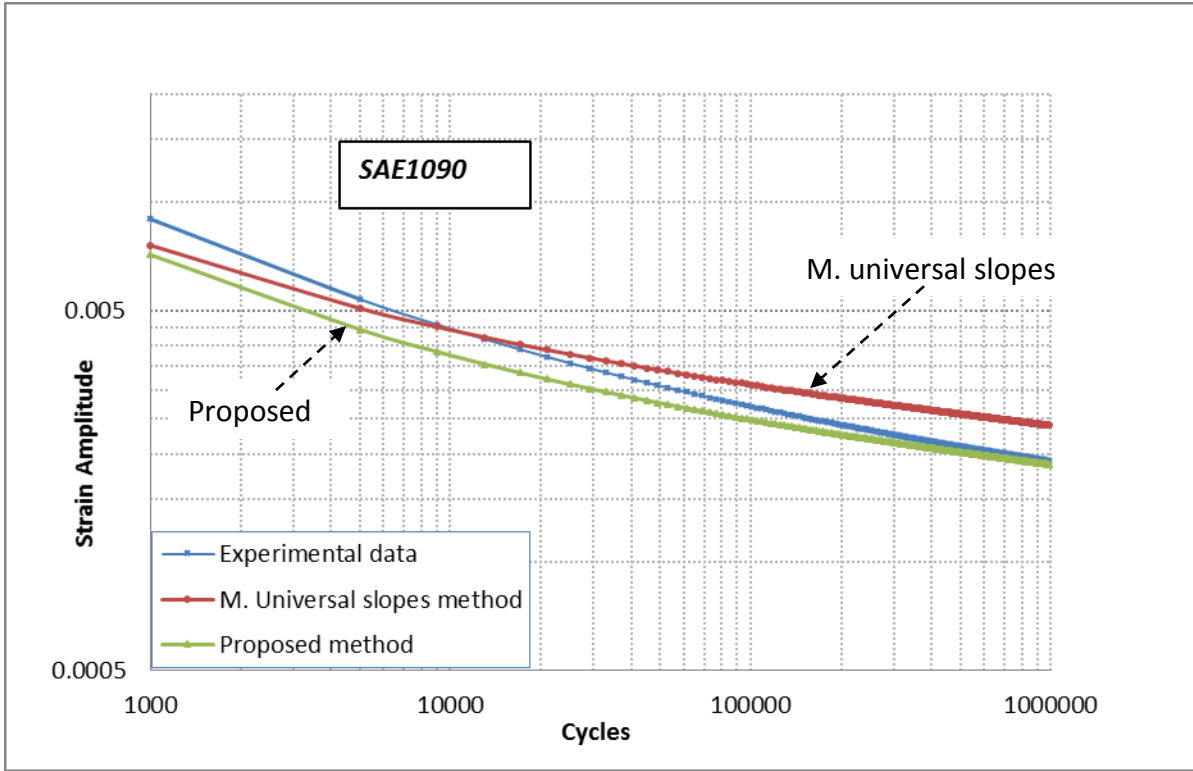


Figure 78 Comparison between Three Prediction Approaches for SAE 1090, HB309 Steel

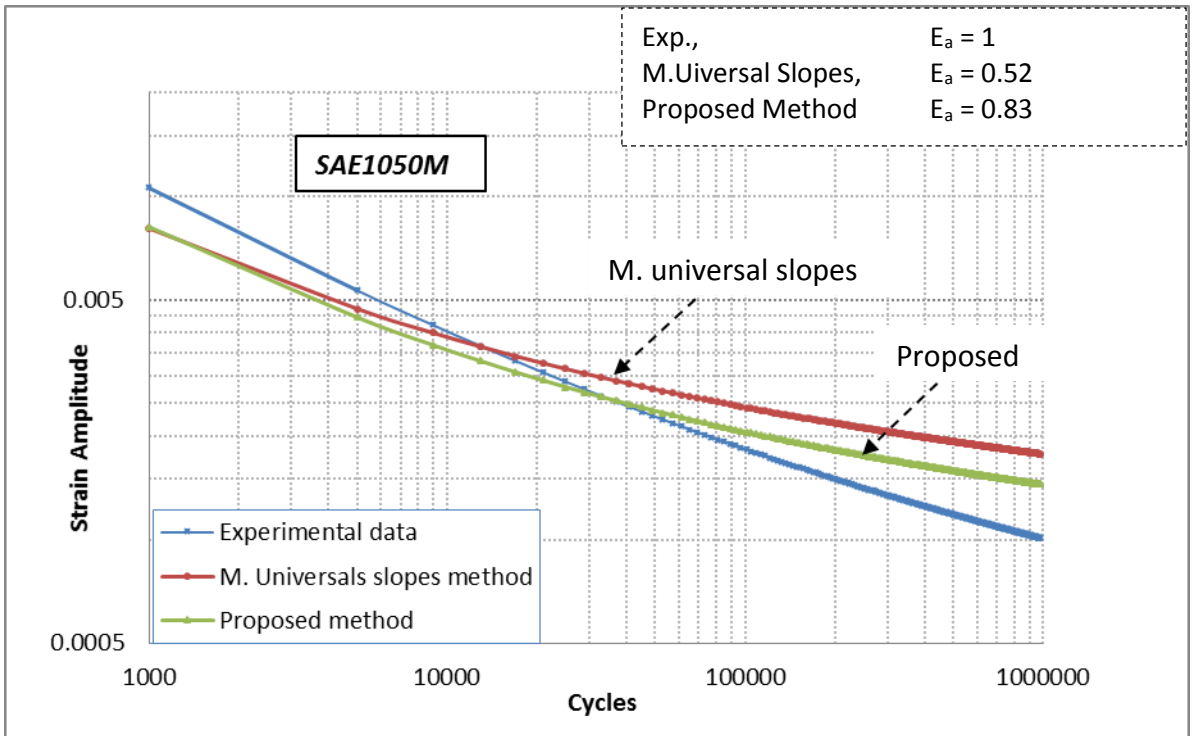


Figure79 Comparison between Three Prediction Approaches for SAE1050M,HB220 Steel

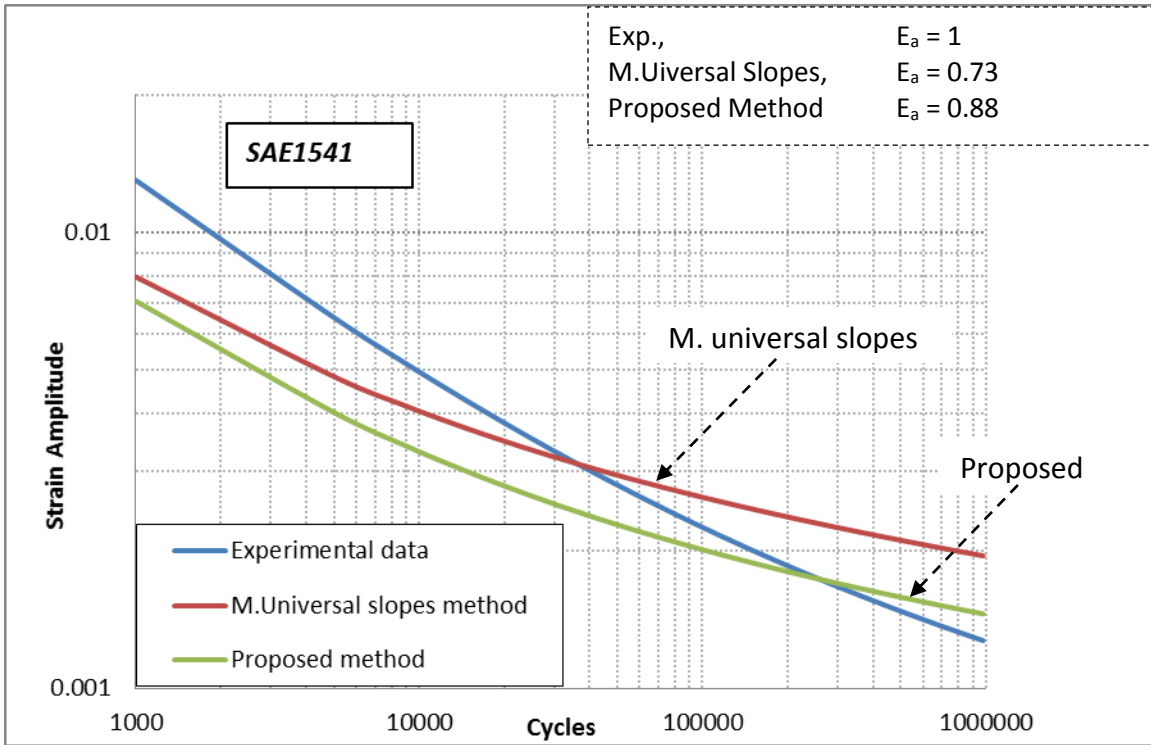


Figure 80 Comparison between Three Prediction Approaches for SAE 1541, HB195 Steel

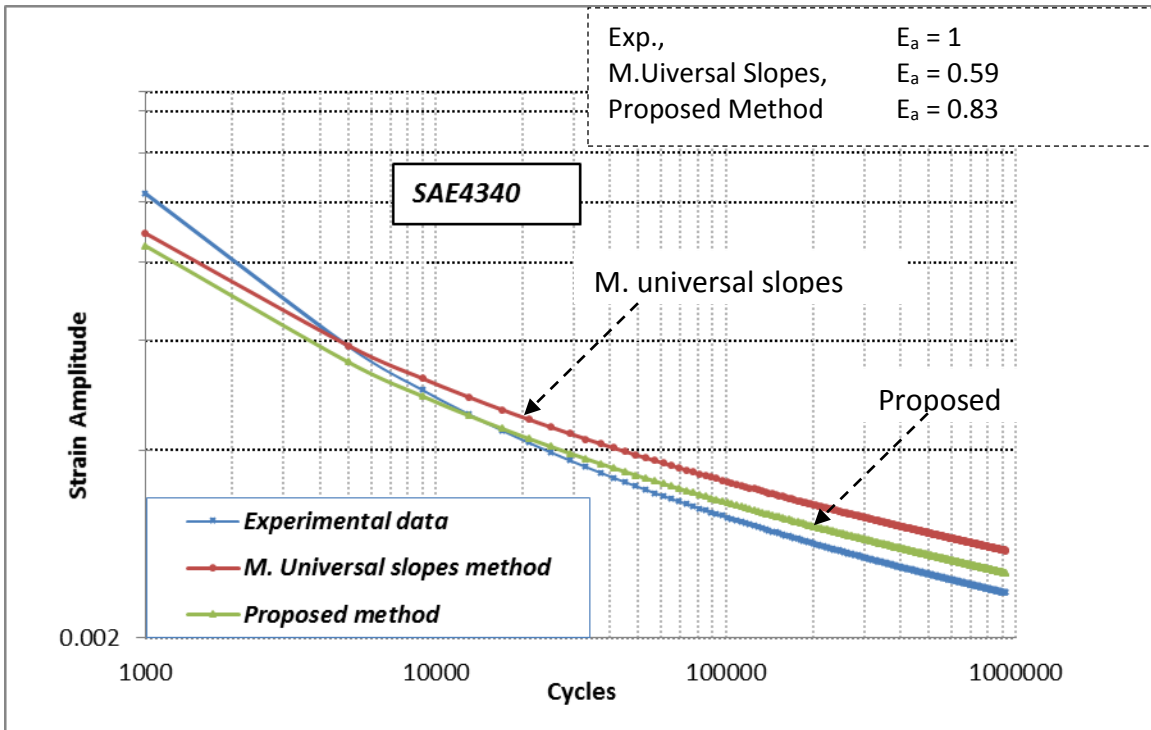


Figure 81 Comparison between Three Prediction Approaches for SAE4340, HB350 Steel

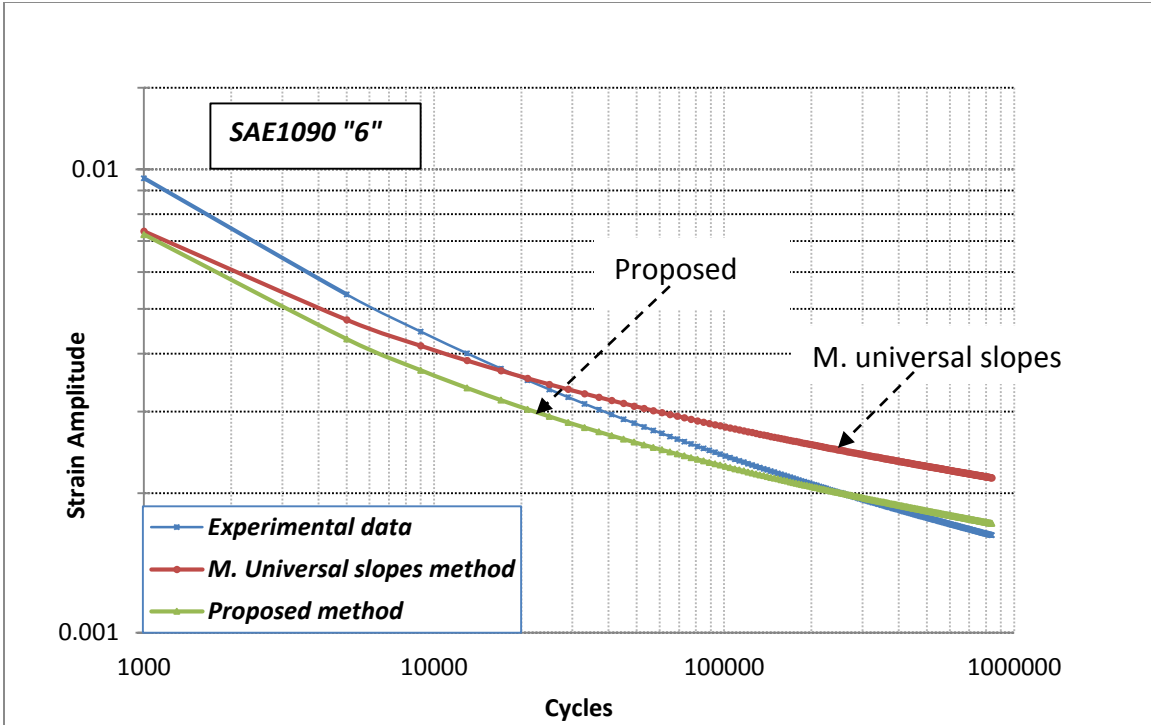


Figure 82 Comparison between Three Prediction Approaches for SAE1090,HB259 Steel

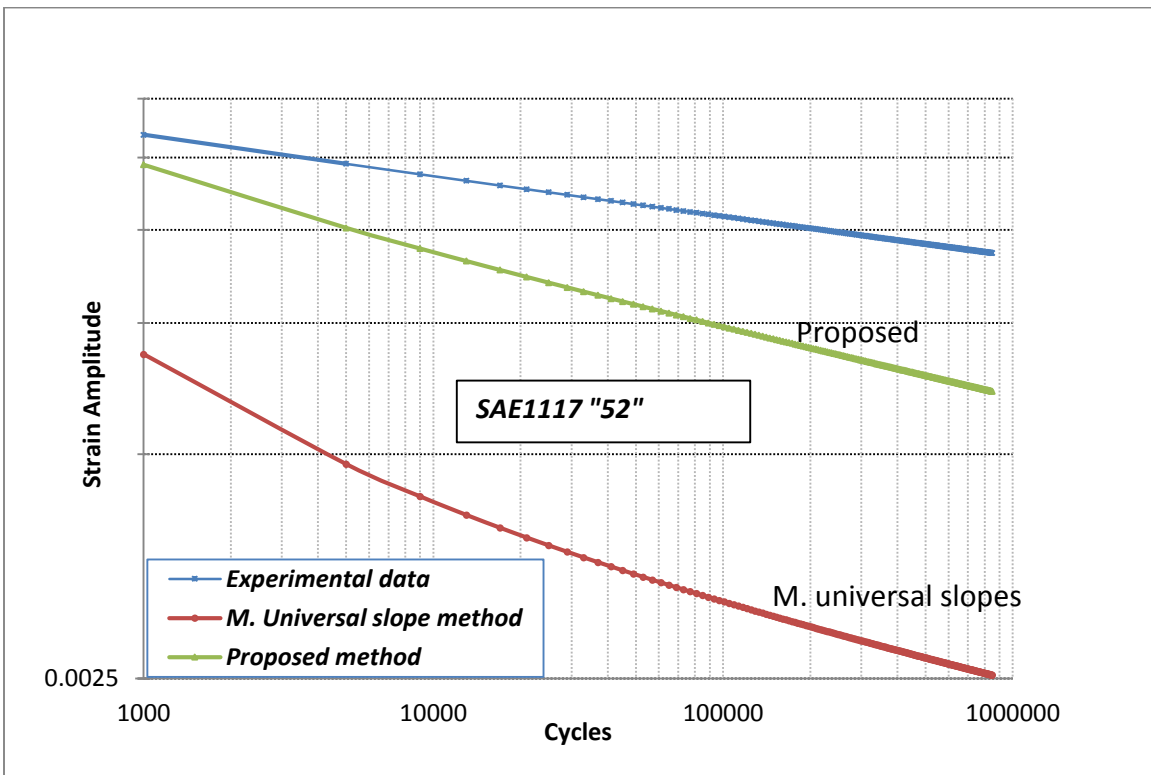


Figure 83 Comparison between Three Prediction Approaches for SAE1117,HB193 Steel

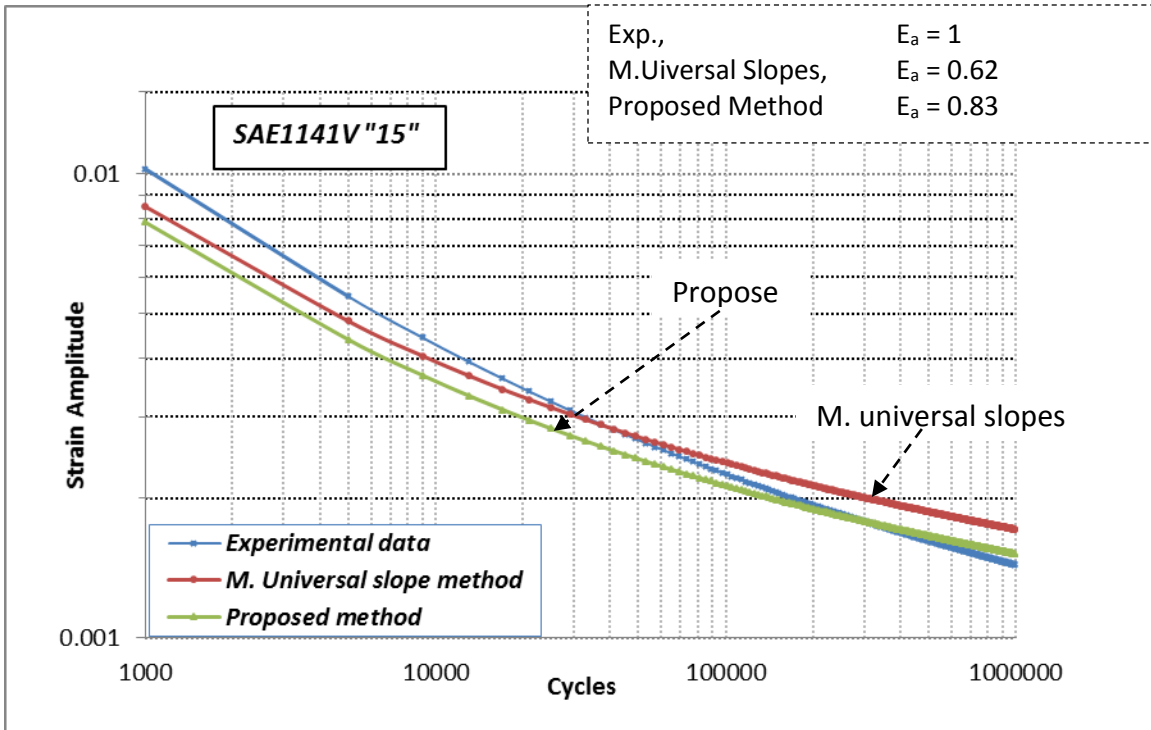


Figure 84 Comparison between Three Prediction Approaches for SAE1141V,HB217 Steel

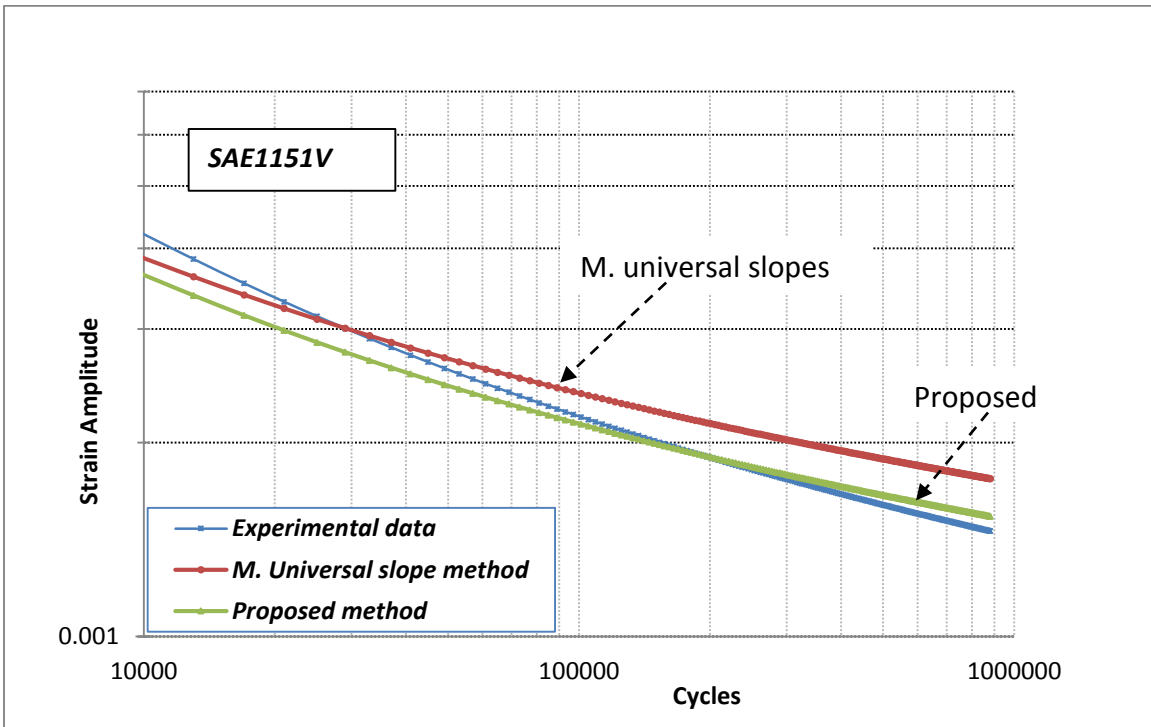


Figure 85 Comparison between Three Prediction Approaches for SAE1151V,HB251 Steel

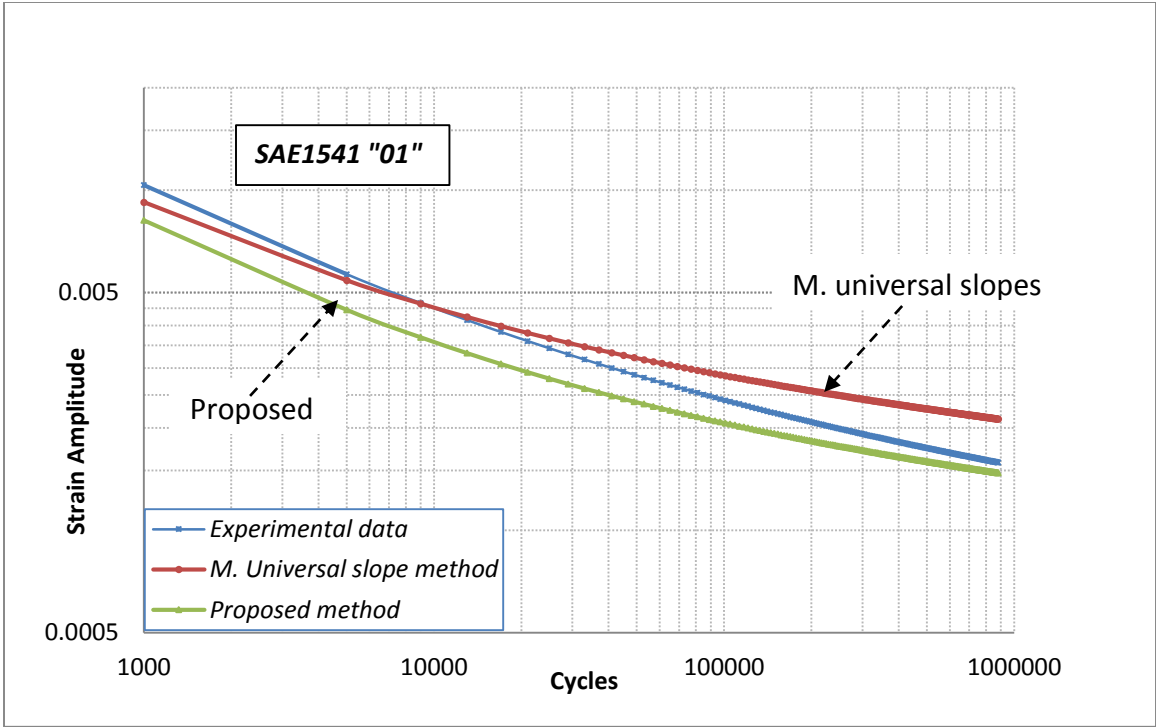


Figure 86 Comparison between Three Prediction Approaches for SAE1541,HB180 Steel

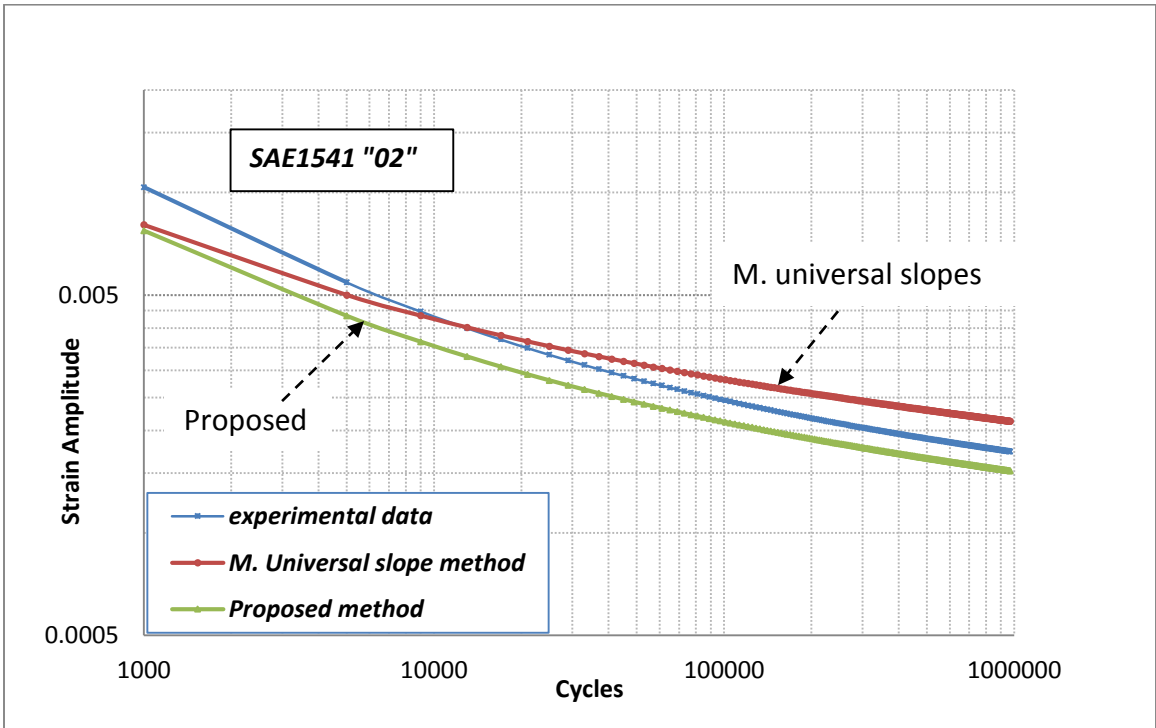


Figure 87 Comparison between Three Prediction Approaches for SAE1541,HB250 Steel

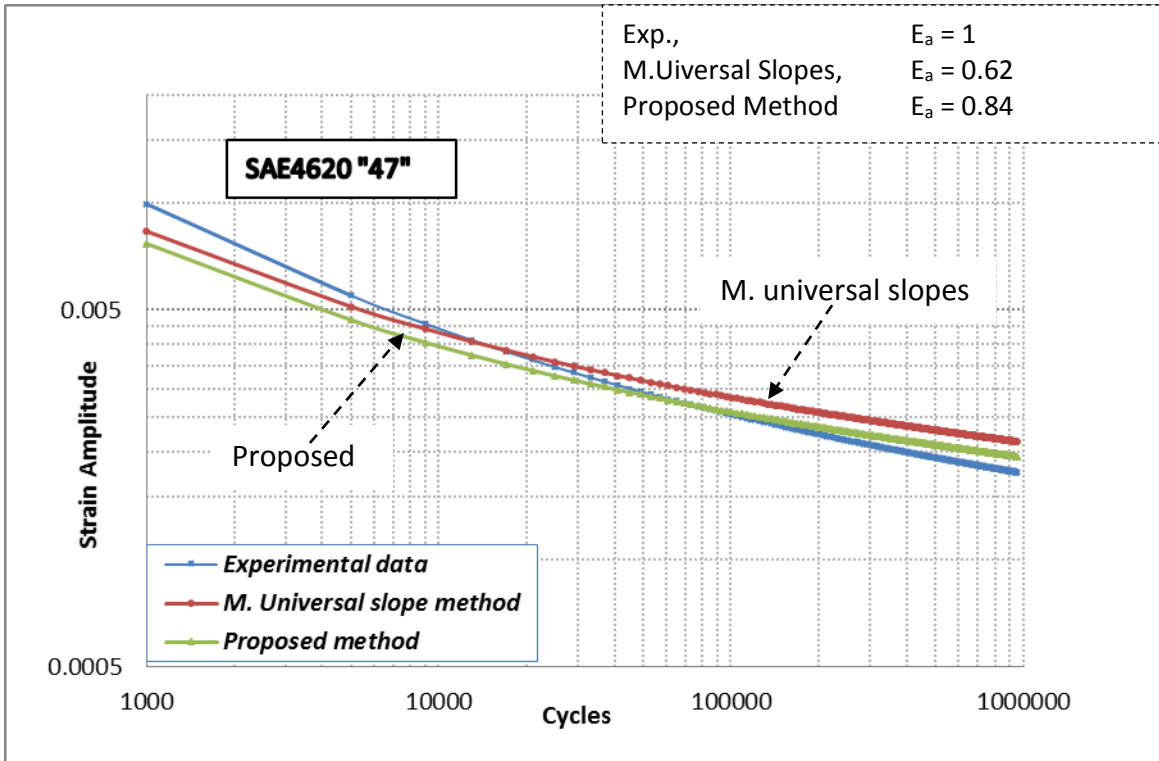


Figure 88 Comparison between Three Prediction Approaches for SAE4620,HB289 Steel

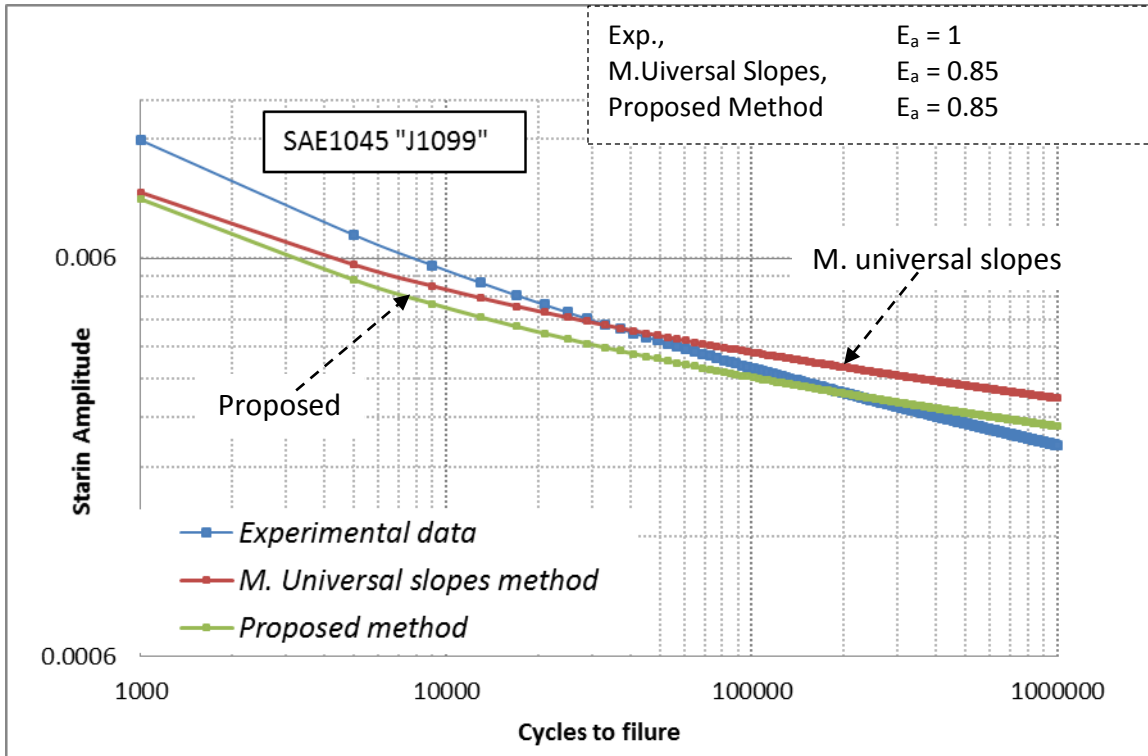


Figure 89 Comparison between Three Prediction Approaches for SAE1045,HB222 Steel

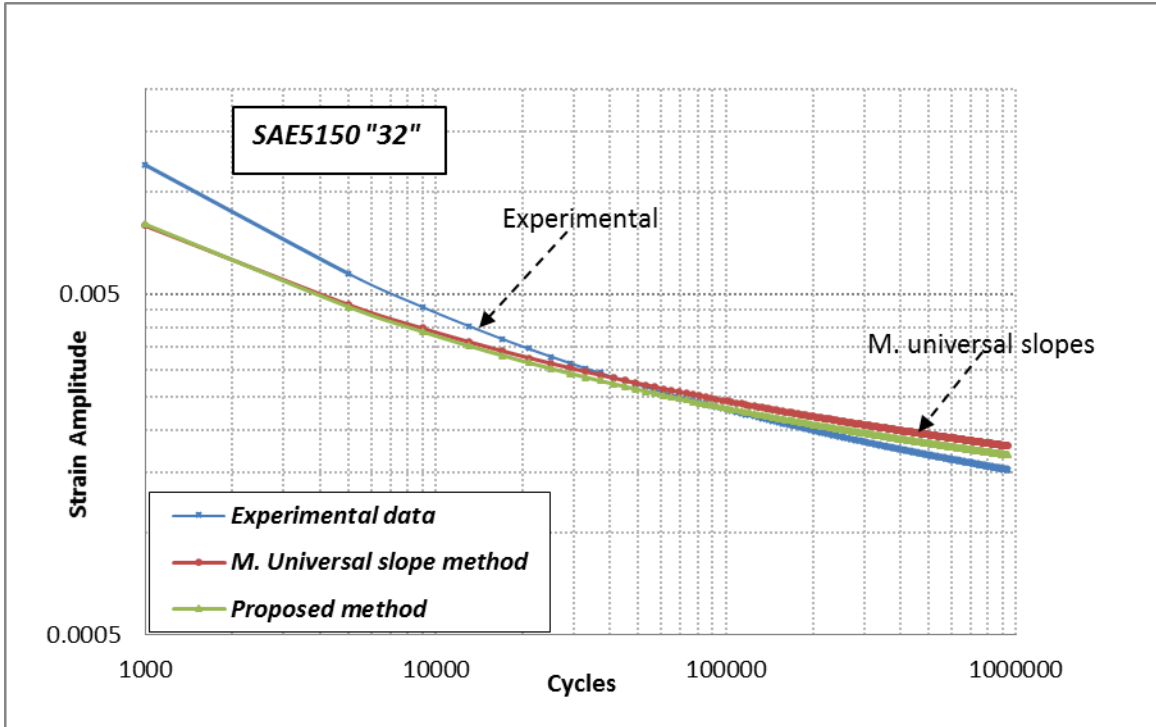


Figure 90 Comparison between Three Prediction Approaches for SAE5150,HB245 Steel

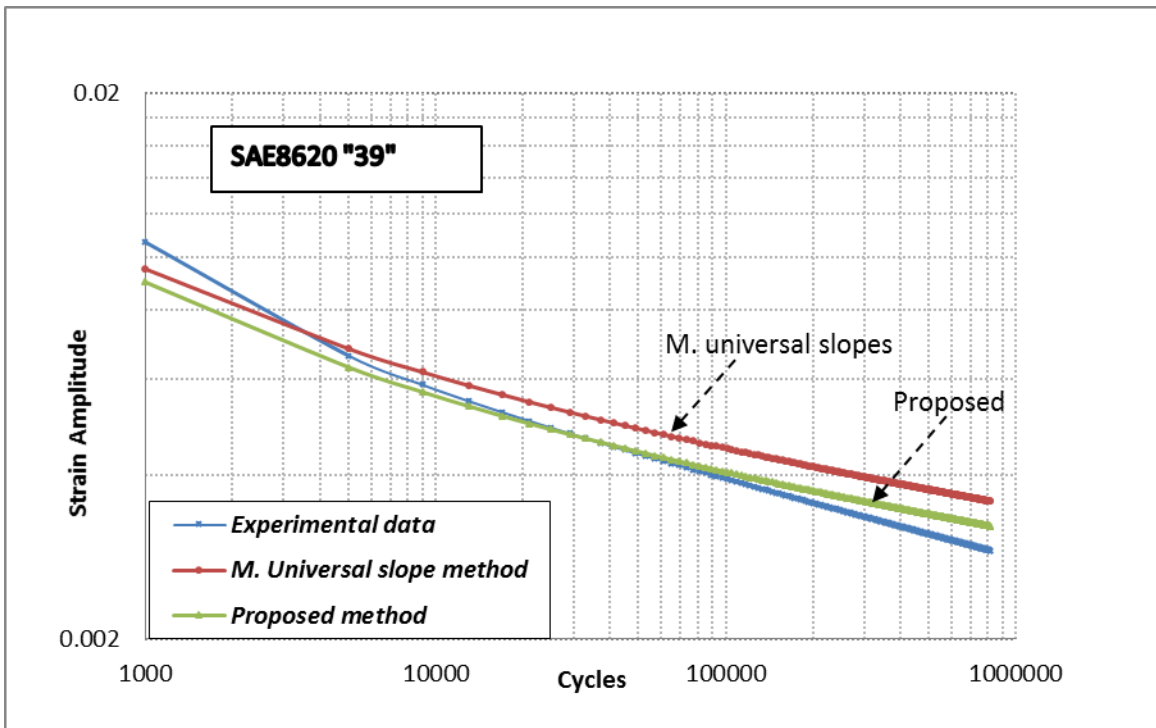


Figure 91 Comparison between Three Prediction Approaches for SAE8620,HB430 Steel

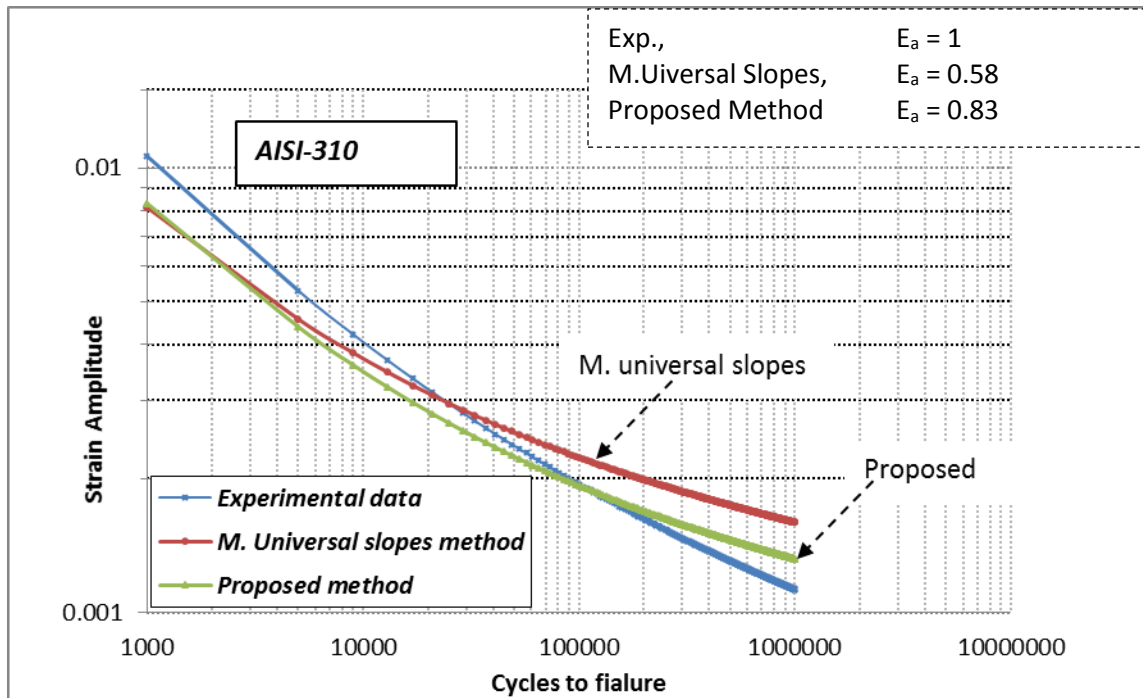


Figure 92 Comparison between Three Prediction Approaches for AISI-310,HB145 Steel

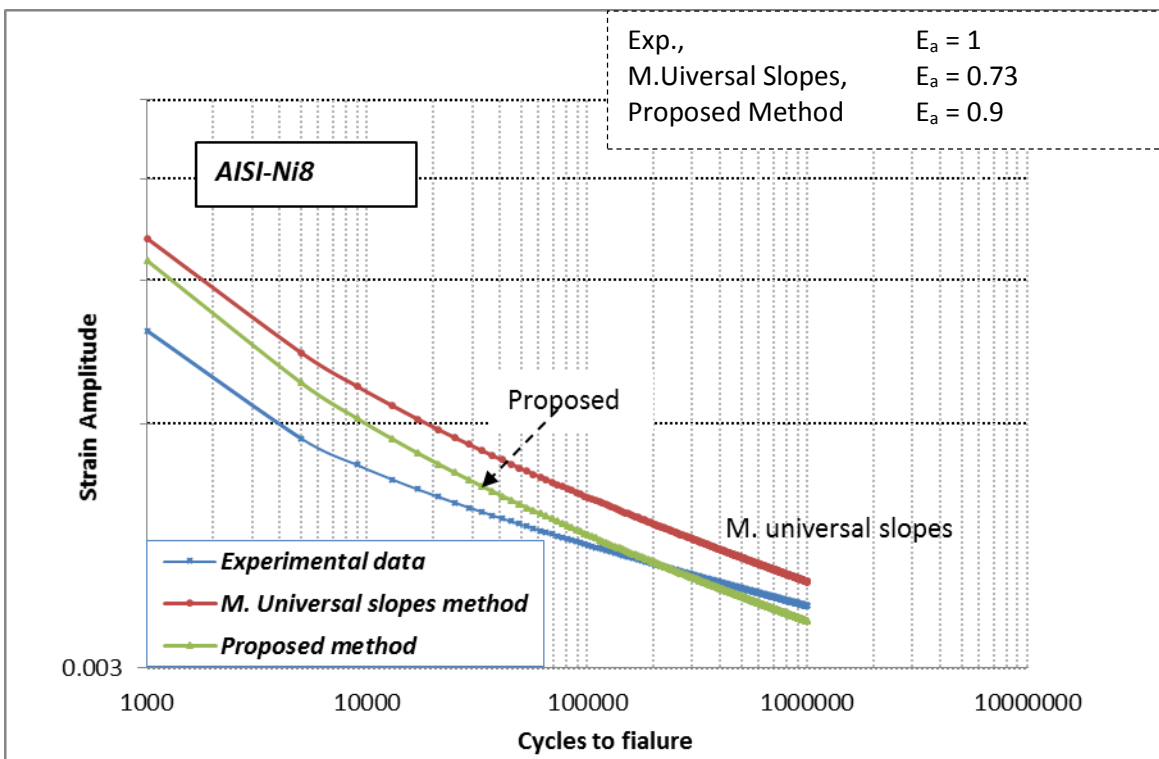


Figure 93 Comparison between Three Prediction Approaches for AISI-Ni8,HB170 Steel

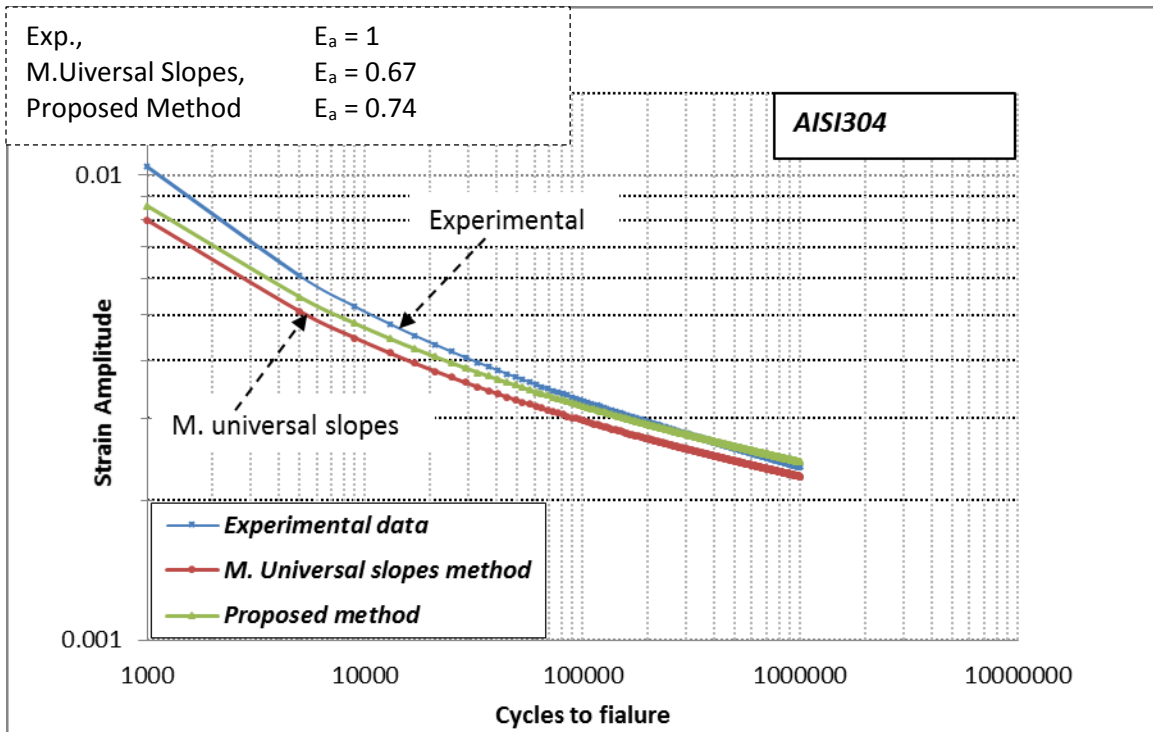


Figure 94 Comparison between Three Prediction Approaches for AISI304,HB327 Steel

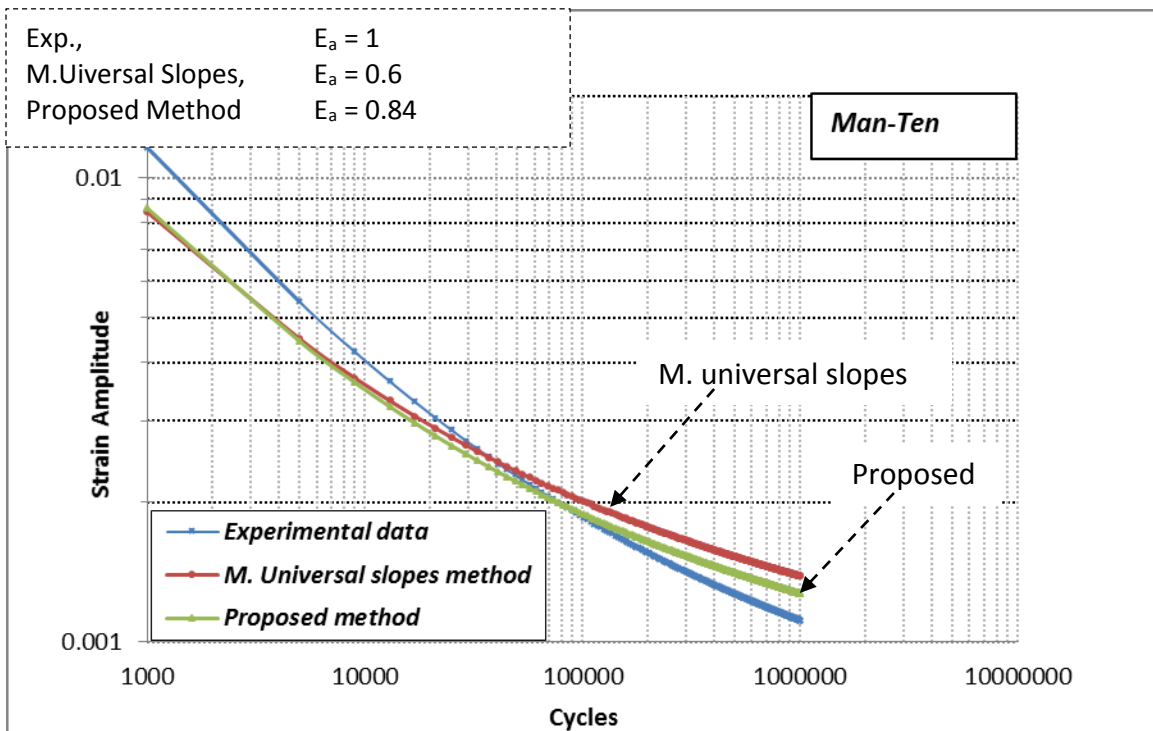


Figure 95 Comparison between Three Prediction Approaches for Man-Ten,HB150 Steel

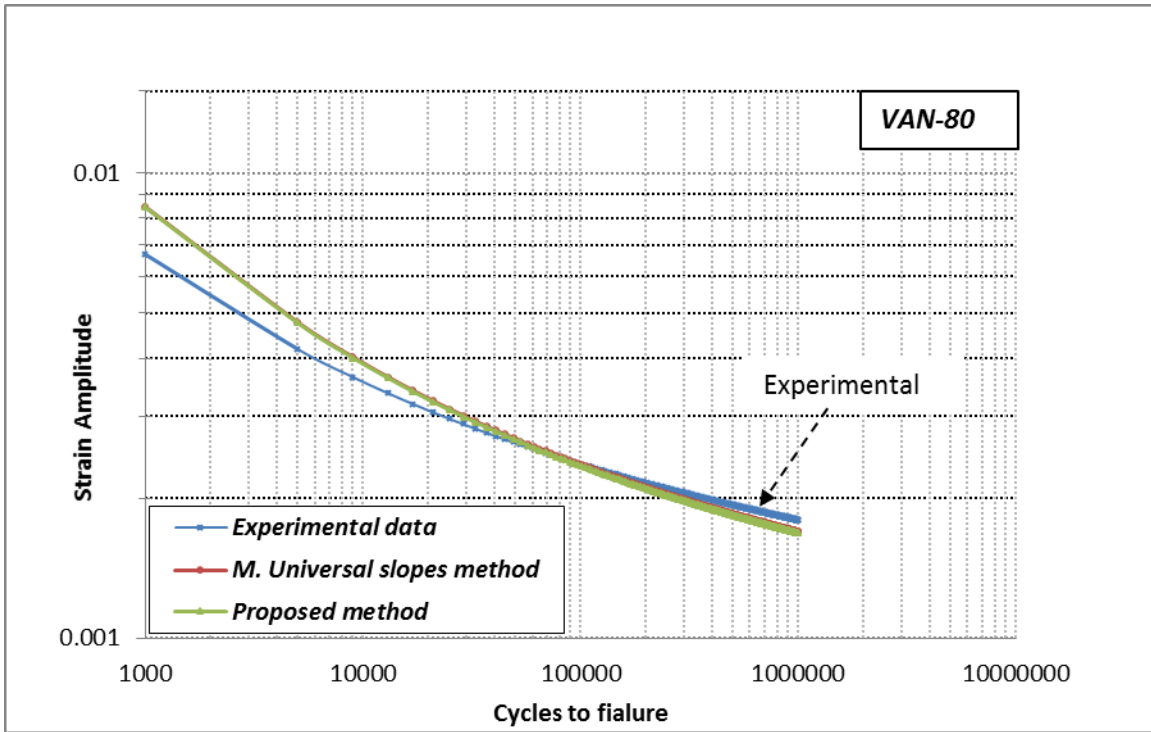


Figure 96 Comparison between Three Prediction Approaches for VAN-80,HB225 Steel

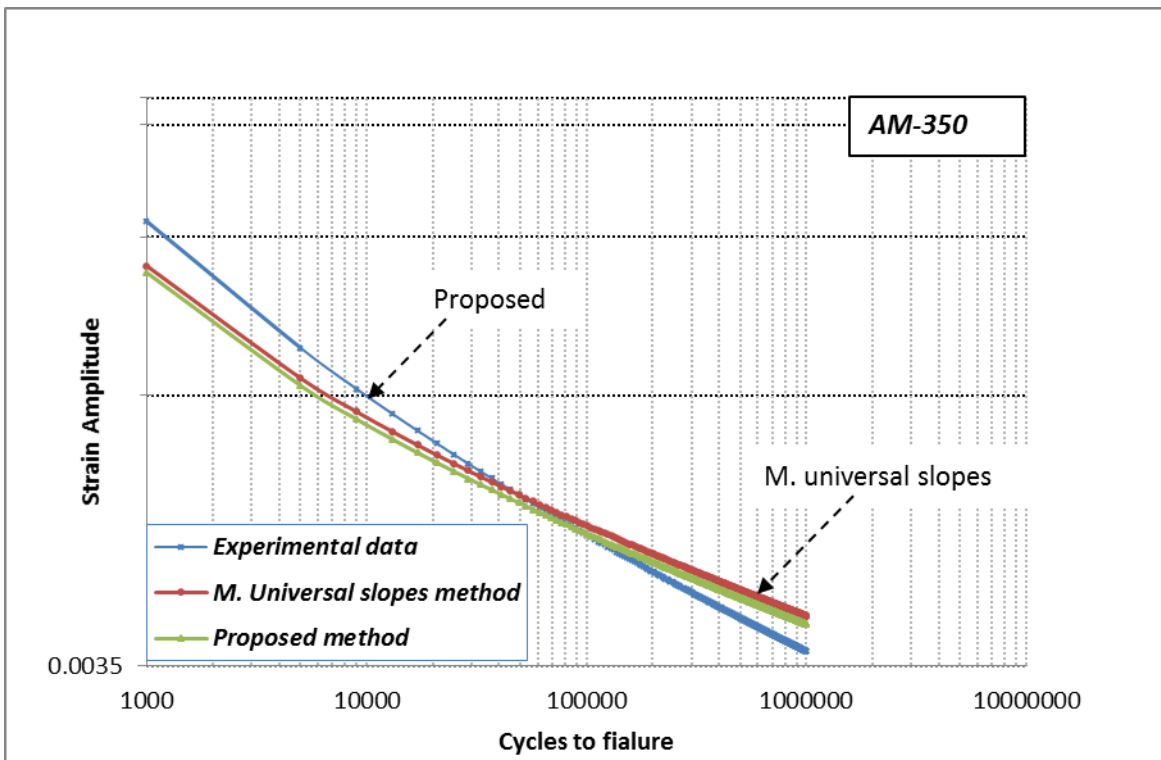


Figure 97 Comparison between Three Prediction Approaches for AM-350,HB325 Steel

8 APPENDIX B

Table 15 Results Obtained from SAE1141V under Variable Amplitudes

Notch root stress-strain for SAE1141V Steel flat plate							
Reversal	S _a (MPa)	Neuber's		E-Plastic (FEA)		Proposed	
		σ_{\max}	% (ϵ_a)	σ_{\max}	% (ϵ_a)	σ_{\max}	% (ϵ_a)
1	350	562	0.74	567	0.607	597	0.612
2	100	-78	0.41	-108	0.303	-44	0.29
3	280	405	0.637	442	0.522	440	0.515
4	-240	-485	-0.38	-528	-0.313	-501	-0.349
5	291	515	0.574	551	0.468	542	0.486
6	40	-127	0.242	-136	0.163	-104	0.157
7	163	208	0.395	222	0.312	231	0.312
8	-220	-468	-0.326	-521	-0.273	-480	-0.329
9	350	564	0.737	571	0.6	599	0.608

Rainflow cycles	Neuber's		E-Plastic (FEA)		Pro. Method		Cycles to failure (N _f)		
	σ_m (MPa)	% (ϵ_a)	σ_m (MPa)	% (ϵ_a)	σ_m (MPa)	% (ϵ_a)	Neuber	FEA	Pro. M
1	39	0.56	20	0.46	40	0.48	3890	6600	5850
2	164	0.113	167	0.11	167	0.112	∞	∞	∞
3	-131	0.539	15	0.37	-132	0.46	4300	12500	7000
4	41	0.153	43	0.0745	42	0.0775	600000	∞	∞

Notch root stress-strain for SAE1141V Steel round bar							
Reversal	S _a (MPa)	Neuber's		E-Plastic (FEA)		Proposed	
		σ_{\max}	% (ϵ_a)	σ_{\max}	% (ϵ_a)	σ_{\max}	% (ϵ_a)
1	500	600	0.555	650	0.439	630	0.451
2	100	-83	0.244	-58	0.14	-57	0.151
3	280	239	0.378	281	0.273	265	0.281
4	-280	-465	-0.205	-524	-0.162	-469	-0.231
5	320	453	0.316	470	0.289	465	0.253
6	40	-42	0.106	-83	0.077	-31	0.063
7	140	137	0.18	158	0.152	148	0.123
8	-240	-425	-0.158	-450	-0.133	-426	-0.191
9	500	611	0.543	655	0.436	640	0.442

Rainflow cycles	Neuber's		E-Plastic (FEA)		Pro. Method		Cycles to failure (N _f)		
	σ_m	% (ϵ_a)	σ_m	% (ϵ_a)	σ_m	% (ϵ_a)	Neuber	FEA	Pro.
1	68	0.38	42	0.3	69	0.341	10000	21000	16000
2	78	0.067	112	.066	80	0.065	∞	∞	∞
3	14	0.237	-38	0.211	14	0.222	55000	100000	80000
4	48	0.074	38	0.0375	49	0.03	∞	∞	∞

Table 16 Results Obtained from RQC-100 under Variable Amplitudes

Notch root stress-strain for RQC-100 Steel flat plate							
Reversal	S _a (MPa)	Neuber's		E-Plastic (FEA)		Proposed	
		σ _{max}	% (ε _a)	σ _{max}	% (ε _a)	σ _{max}	% (ε _a)
1	350	650	0.66	660	0.580	676	0.569
2	100	-19	0.331	-24	0.264	10	0.242
3	280	468	0.566	470	0.497	494	0.476
4	-240	-562	-0.352	-617	-0.311	-596	-0.317
5	291	593	0.508	628	0.457	612	0.443
6	40	-78	0.178	-38	0.134	-59	0.116
7	163	254	0.338	273	0.292	272	0.275
8	-220	-541	-0.305	-580	-0.277	-546	-0.426
9	350	652	0.652	657	0.580	677	0.564

Rainflow cycles	Neuber's		E-Plastic (FEA)		Pro. Method		Cycles to failure (N _f)		
	σ _m (MPa)	% (ε _a)	σ _m (MPa)	% (ε _a)	σ _m (MPa)	% (ε _a)	Neuber	FEA	Pro. M
1	44	0.50	22	0.445	40	0.443	2450	4200	4300
2	244	0.12	217	0.116	242	0.117	∞	∞	∞
3	26	0.49	10	0.367	33	0.41	2800	10100	6000
4	84	0.08	126	0.079	107	0.079	∞	∞	∞

Notch root stress-strain for RQC-100 Steel round bar							
Reversal	S _a (MPa)	Neuber's		E-Plastic (FEA)		Proposed	
		σ _{max}	% (ε _a)	σ _{max}	% (ε _a)	σ _{max}	% (ε _a)
1	500	698	0.504	710	0.416	709	0.435
2	100	-13	0.187	178	0.098	6	0.127
3	280	308	0.328	340	0.240	327	0.264
4	-280	-527	-0.196	-605	-0.205	-524	-0.218
5	320	493	0.3	435	0.274	501	0.257
6	40	-7	0.079	-33	0.050	1	0.042
7	140	173	0.158	178	0.129	181	0.118
8	-240	-474	-0.157	-536	-0.174	-470	-0.183
9	500	711	0.493	707	0.416	721	0.428

Rainflow cycles	Neuber's		E-Plastic (FEA)		Pro. Method		Cycles to failure (N _f)		
	σ _m	% (ε _a)	σ _m	% (ε _a)	σ _m	% (ε _a)	Neuber	FEA	Pro.
1	86	0.35	53	0.283	90	0.315	9500	34000	20000
2	161	0.071	81	0.07	165	.0685	∞	∞	∞
3	10	0.3	-51	0.224	16	0.26	30000	250000	130000
4	83	0.04	73	0.039	91	0.038	∞	∞	∞

Table 17 Results Obtained from SAE1038 under Variable Amplitudes

Notch root stress-strain for SAE1038 Steel flat plate								
Reversal	S _a (MPa)	Neuber's		E-Plastic (FEA)		Proposed		
		σ _{max}	% (ε _a)	σ _{max}	%(ε _a)	σ _{max}	%(ε _a)	
1	350	530	0.788	532	0.665	565	0.637	
2	100	-105	0.45	-149	0.353	-68	0.310	
3	280	377	0.68	392	0.573	414	0.536	
4	-240	-465	-0.402	-514	-0.328	-483	-0.424	
5	291	490	0.598	529	0.503	519	0.489	
6	40	-145	0.259	-169	0.195	-120	0.161	
7	163	190	0.413	214	0.345	215	0.313	
8	-220	-450	-0.352	-506	-0.286	-464	-0.349	
9	350	532	0.748	544	0.651	568	0.611	

Rainflow cycles	Neuber's		E-Plastic (FEA)		Pro. Method		Cycles to failure (N _f)		
	σ _m (MPa)	% (ε _a)	σ _m (MPa)	% (ε _a)	σ _m (MPa)	% (ε _a)	Neuber	FEA	Pro. M
1	33	0.595	9	0.496	40	0.53	6900	12000	9400
2	136	0.114	122	0.11	160	0.113	∞	∞	∞
3	20	0.475	12	0.394	25	0.419	13100	23400	20000
4	23	0.077	23	0.075	45	0.076	∞	∞	∞

Notch root stress-strain for SAE1038 Steel round bar								
Reversal	S _a (MPa)	Neuber's		Nonlinear FEA		Proposed		
		σ _{max}	% (ε _a)	σ _{max}	%(ε _a)	σ _{max}	%(ε _a)	
1	500	582	0.575	600	0.456	609	0.493	
2	100	-106	0.263	-76	0.153	-77	0.184	
3	280	216	0.398	275	0.288	244	0.319	
4	-280	-465	-0.203	-500	-0.159	-469	-0.219	
5	320	450	0.327	465	0.296	463	0.284	
6	40	-50	0.117	-54	0.083	-38	0.073	
7	140	129	0.245	158	0.158	141	0.183	
8	-240	-428	-0.151	-545	-0.130	-428	-0.175	
9	500	593	0.567	602	0.448	618	0.488	

Rainflow cycles	Neuber's		E-Plastic (FEA)		Pro. Method		Cycles to failure (N _f)		
	σ _m	% (ε _a)	σ _m	% (ε _a)	σ _m	% (ε _a)	Neuber	FEA	Pro.
1	59	0.389	35	0.307	60	0.35	19000	45000	28000
2	55	0.0675	100	0.068	56	0.067	∞	∞	∞
3	11	0.239	-40	0.213	12	0.225	120000	200000	155000
4	40	0.064	52	0.038	41	0.0545	∞	∞	∞

Table 18 Results Obtained from SAE1050M under Variable Amplitudes

Notch root stress-strain for SAE1050M Steel flat plate								
Reversal	S _a (MPa)	Neuber's		E-Plastic (FEA)		Proposed		
		σ _{max}	% (ε _a)	σ _{max}	%(ε _a)	σ _{max}	%(ε _a)	
1	350	583	0.776	591	0.639	610	0.648	
2	100	-87	0.431	-84	0.308	-51	0.308	
3	280	404	0.674	440	0.546	439	0.55	
4	-240	-517	-0.324	-564	-0.332	-530	-0.340	
5	291	540	0.656	581	0.490	564	0.544	
6	40	-130	0.31	-108	0.158	-106	0.202	
7	163	205	0.475	253	0.320	228	0.366	
8	-220	-500	-0.265	-556	-0.290	-509	-0.292	
9	350	584	0.825	601	0.626	615	0.68	

Rainflow cycles	Neuber's		E-Plastic (FEA)		Pro. Method		Cycles to failure (N _f)		
	σ _m (MPa)	% (ε _a)	σ _m (MPa)	% (ε _a)	σ _m (MPa)	% (ε _a)	Neuber	FEA	Pro. M
1	33	0.55	14	0.48	34	0.49	5500	9000	8100
2	159	0.121	178	0.119	162	0.121	∞	∞	∞
3	20	0.46	13	0.39	20	0.41	10500	20000	16000
4	38	0.0825	73	0.081	39	0.082	∞	∞	∞

Notch root stress-strain for SAE1050M Steel round bar								
Reversal	S _a (MPa)	Neuber's		Nonlinear FEA		Proposed		
		σ _{max}	% (ε _a)	σ _{max}	%(ε _a)	σ _{max}	%(ε _a)	
1	500	640	0.565	660	0.420	565	0.483	
2	100	-70	0.239	-15	0.112	-45	0.167	
3	280	252	0.384	324	0.253	277	0.308	
4	-280	-515	-0.195	-547	-0.17	-514	-0.214	
5	320	480	0.329	490	0.279	490	0.283	
6	40	-20	0.103	-88	0.068	51	0.062	
7	140	159	0.184	160	0.143	168	0.141	
8	-240	-470	-0.152	-500	-0.141	-466	-0.177	
9	500	655	0.554	665	0.414	678	0.476	

Rainflow cycles	Neuber's		E-Plastic (FEA)		Pro. Method		Cycles to failure (N _f)		
	σ _m	% (ε _a)	σ _m	% (ε _a)	σ _m	% (ε _a)	Neuber	FEA	Pro.
1	63	0.38	47	0.295	64	0.34	16300	40000	25000
2	91	0.0725	155	0.0705	93	0.0705	∞	∞	∞
3	5	0.24	-45	0.21	6	0.23	160000	450000	200000
4	70	0.0405	36	0.0375	71	0.0395	∞	∞	∞

Table 19 Results Obtained from SAE1117 under Variable Amplitudes

Notch root stress-strain for SAE1117 Steel flat plate								
Reversal	S _a (MPa)	Neuber's		E-Plastic (FEA)		Proposed		
		σ _{max}	% (ε _a)	σ _{max}	%(ε _a)	σ _{max}	%(ε _a)	
1	350	573	0.79	578	0.648	599	0.649	
2	100	-75	0.435	-98	0.317	-41	0.302	
3	280	410	0.681	421	0.555	444	0.546	
4	-240	-496	-0.41	-536	-0.341	-511	-404	
5	291	525	0.59	560	0.496	551	0.492	
6	40	-130	0.229	-127	0.163	-106	0.141	
7	163	205	0.395	223	0.325	228	0.306	
8	-220	-480	-0.37	-525	-0.302	-491	-0.369	
9	350	573	0.76	581	0.638	596	0.629	

Rainflow cycles	Neuber's		E-Plastic (FEA)		Pro. Method		Cycles to failure (N _f)		
	σ _m (MPa)	% (ε _a)	σ _m (MPa)	% (ε _a)	σ _m (MPa)	% (ε _a)	Neuber	FEA	Pro. M
1	39	0.6	21	0.49	42	0.526	4800	11000	8500
2	168	0.123	162	0.119	200	0.122	∞	∞	∞
3	23	0.48	17	0.39	30	0.43	11700	25000	18000
4	38	0.083	48	0.081	61	0.0825	∞	∞	∞

Notch root stress-strain for SAE1117 Steel round bar								
Reversal	S _a (MPa)	Neuber's		Nonlinear FEA		Proposed		
		σ _{max}	% (ε _a)	σ _{max}	%(ε _a)	σ _{max}	%(ε _a)	
1	500	627	0.57	660	0.427	654	0.477	
2	100	-73	0.24	-65	0.128	-48	0.158	
3	280	247	0.385	317	0.261	272	0.299	
4	-280	-488	-0.21	-500	-0.167	-489	-0.234	
5	320	472	0.336	474	0.281	482	0.278	
6	40	-28	0.108	-79	0.074	44	0.056	
7	140	151	0.189	100	0.145	161	0.135	
8	-240	-442	-0.161	-463	-0.139	-441	-0.192	
9	500	634	0.57	665	0.422	660	0.477	

Rainflow cycles	Neuber's		E-Plastic (FEA)		Pro. Method		Cycles to failure (N _f)		
	σ _m	% (ε _a)	σ _m	% (ε _a)	σ _m	% (ε _a)	Neuber	FEA	Pro.
1	70	0.39	80	0.297	83	0.355	22000	50000	37000
2	87	0.0725	126	0.0665	112	0.0705	∞	∞	∞
3	15	0.248	6	0.21	21	0.235	180000	500000	400000
4	62	0.0405	33	0.0355	59	0.0395	∞	∞	∞

Table 20 Results Obtained from SAE15V24 under Variable Amplitudes

Notch root stress-strain for SAE15V24 Steel flat plate								
Reversal	S _a (MPa)	Neuber's		E-Plastic (FEA)		Proposed		
		σ _{max}	% (ε _a)	σ _{max}	% (ε _a)	σ _{max}	% (ε _a)	
1	350	663	0.666	671	0.56	685	0.573	
2	100	-14	0.344	-60	0.235	14	0.244	
3	280	476	0.571	490	0.467	503	0.480	
4	-240	-572	-0.334	-585	-0.298	-579	-0.343	
5	291	606	0.52	625	0.477	624	0.452	
6	40	-74	0.18	-135	0.122	-56	0.117	
7	163	261	0.341	293	0.28	279	0.277	
8	-220	-550	-0.295	-565	-0.259	-554	-0.310	
9	350	667	0.665	686	0.553	688	0.572	

Rainflow cycles	Neuber's		E-Plastic (FEA)		Pro. Method		Cycles to failure (N _f)		
	σ _m (MPa)	% (ε _a)	σ _m (MPa)	% (ε _a)	σ _m (MPa)	% (ε _a)	Neuber	FEA	Pro. M
1	46	0.5	11	0.429	47	0.458	5900	10300	8000
2	231	0.118	188	0.116	236	0.12	∞	∞	∞
3	28	0.407	13	0.353	29	0.381	12000	21500	17000
4	94	0.0805	47	0.08	96	0.0765	∞	∞	∞

Notch root stress-strain for SAE15V24 Steel round bar								
Reversal	S _a (MPa)	Neuber's		E-Plastic (FEA)		Proposed		
		σ _{max}	% (ε _a)	σ _{max}	% (ε _a)	σ _{max}	% (ε _a)	
1	500	640	0.55	655	0.415	663	0.465	
2	100	-69	0.231	-80	0.098	-44	0.158	
3	280	254	0.373	290	0.238	279	0.295	
4	-280	-506	-0.196	525	-208	-505	-0.216	
5	320	479	0.318	489	0.271	489	0.271	
6	40	-21	0.098	-27	0.047	-12	0.056	
7	140	158	0.176	157	0.126	167	0.132	
8	-240	-461	-0.153	-482	-0.177	-458	-0.179	
9	500	654	0.536	657	0.413	676	0.457	

Rainflow cycles	Neuber's		E-Plastic (FEA)		Pro. Method		Cycles to failure (N _f)		
	σ _m	% (ε _a)	σ _m	% (ε _a)	σ _m	% (ε _a)	Neuber	FEA	Pro.
1	67	0.373	65	0.31	79	0.34	12500	23000	17300
2	93	0.071	105	0.07	115	0.0685	∞	∞	∞
3	9	0.235	4	0.224	5	0.225	86000	155000	150000
4	69	0.078	65	0.0395	76	0.038	∞	∞	∞

Table 21 Results Obtained from SAE1141Nb under Variable Amplitudes

Notch root stress-strain for SAE1141Nb Steel flat plate								
Reversal	S _a (MPa)	Neuber's		E-Plastic (FEA)		Proposed		
		σ _{max}	% (ε _a)	σ _{max}	% (ε _a)	σ _{max}	% (ε _a)	
1	350	554	0.75	552	0.64	581	0.61	
2	100	-95	0.42	-131	0.33	-59	0.287	
3	280	391	0.648	377	0.55	412	0.513	
4	-240	-486	-0.39	-500	-0.320	-502	-0.385	
5	291	514	0.57	544	0.490	541	0.468	
6	40	-137	0.238	-151	0.181	-113	0.143	
7	163	198	0.392	204	0.332	222	0.296	
8	-220	-468	-0.34	-483	-0.280	-480	-0.345	
9	350	559	0.74	562	0.63	585	0.603	

Rainflow cycles	Neuber's		E-Plastic (FEA)		Pro. Method		Cycles to failure (N _f)		
	σ _m (MPa)	% (ε _a)	σ _m (MPa)	% (ε _a)	σ _m (MPa)	% (ε _a)	Neuber	FEA	Pro. M
1	34	0.57	26	0.48	39	0.49	5000	9000	8200
2	148	0.11	123	0.11	166	0.113	∞	∞	∞
3	23	0.455	31	0.38	30	0.4	10000	19600	16000
4	31	0.077	27	0.0755	52	0.0765	∞	∞	∞

Notch root stress-strain for SAE1141Nb Steel round bar								
Reversal	S _a (MPa)	Neuber's		E-Plastic (FEA)		Proposed		
		σ _{max}	% (ε _a)	σ _{max}	% (ε _a)	σ _{max}	% (ε _a)	
1	500	602	0.563	625	0.426	627	0.464	
2	100	-93	0.253	-60	0.129	-66	0.165	
3	280	229	0.388	281	0.260	256	0.296	
4	-280	-476	-0.197	-495	-0.151	-478	-0.219	
5	320	459	0.321	471	0.266	471	0.263	
6	40	-41	0.111	-53	0.07	-30	0.058	
7	140	138	0.186	73	0.139	149	0.131	
8	-240	-436	-0.149	-452	-0.124	-435	-0.179	
9	500	615	0.551	635	0.402	639	0.455	

Rainflow cycles	Neuber's		E-Plastic (FEA)		Pro. Method		Cycles to failure (N _f)		
	σ _m	% (ε _a)	σ _m	% (ε _a)	σ _m	% (ε _a)	Neuber	FEA	Pro.
1	63	0.38	44	0.29	75	0.341	15000	40000	25000
2	68	0.0675	111	0.0655	95	0.0655	∞	∞	∞
3	12	0.235	-41	0.195	18	0.22	1.15x10 ⁵	4x10 ⁵	2.3x10 ⁵
4	49	0.0375	13	0.0345	58	0.0365	∞	∞	∞

Table 22 Results Obtained from SAE1045 under Variable Amplitudes

Notch root stress-strain for SAE1045 Steel flat plate								
Reversal	S _a (MPa)	Neuber's		E-Plastic (FEA)		Proposed		
		σ _{max}	% (ε _a)	σ _{max}	% (ε _a)	σ _{max}	% (ε _a)	
1	350	529	0.826	530	0.692	570	0.665	
2	100	-96	0.471	-115	0.372	-60	0.322	
3	280	384	0.713	403	0.602	421	0.56	
4	-240	-461	-0.424	-479	-0.338	-479	-411	
5	291	486	0.636	502	0.535	516	0.516	
6	40	-141	0.279	-164	0.214	-116	0.171	
7	163	194	0.44	192	0.370	218	0.330	
8	-220	-446	-0.364	-469	-0.289	-461	-0.364	
9	350	529	0.816	538	0.690	570	0.658	

Rainflow cycles	Neuber's		E-Plastic (FEA)		Pro. Method		Cycles to failure (N _f)		
	σ _m (MPa)	% (ε _a)	σ _m (MPa)	% (ε _a)	σ _m (MPa)	% (ε _a)	Neuber	FEA	Pro. M
1	34	0.625	25	0.515	46	0.538	4900	8000	7000
2	144	0.121	144	0.115	160	0.119	∞	∞	∞
3	20	0.5	17	0.412	27	0.44	2800	14500	12000
4	27	0.0805	14	0.078	45	0.0795	∞	∞	∞

Notch root stress-strain for SAE1045 Steel round bar								
Reversal	S _a (MPa)	Neuber's		E-Plastic (FEA)		Proposed		
		σ _{max}	% (ε _a)	σ _{max}	% (ε _a)	σ _{max}	% (ε _a)	
1	500	569	0.617	600	0.482	602	0.508	
2	100	-103	0.284	-88	0.166	-74	0.182	
3	280	219	0.425	250	0.306	247	0.322	
4	-280	-447	-0.221	-490	-0.169	-452	-0.252	
5	320	438	0.349	460	0.306	452	0.285	
6	40	-52	0.129	-69	0.085	-40	0.064	
7	140	127	0.207	155	0.162	139	0.142	
8	-240	-412	-0.169	-475	-0.139	-414	-0.207	
9	500	576	0.6	603	0.475	608	0.497	

Rainflow cycles	Neuber's		E-Plastic (FEA)		Pro. Method		Cycles to failure (N _f)		
	σ _m	% (ε _a)	σ _m	% (ε _a)	σ _m	% (ε _a)	Neuber	FEA	Pro.
1	61	0.419	55	0.326	75	0.38	10000	21000	15000
2	58	0.0705	81	0.073	87	0.07	∞	∞	∞
3	13	0.259	-8	0.222	19	0.246	41000	80000	60000
4	38	0.039	43	0.039	49	0.039	∞	∞	∞

Table 23 Results Obtained from SAE1141”A₂” under Variable Amplitudes

Notch root stress-strain for SAE1141 Steel flat plate								
Reversal	S _a (MPa)	Neuber's		E-Plastic (FEA)		Proposed		
		σ _{max}	% (ε _a)	σ _{max}	%(ε _a)	σ _{max}	%(ε _a)	
1	350	634	0.63	649	0.527	656	0.539	
2	100	-44	0.33	-40	0.233	-13	0.241	
3	280	451	0.55	475	0.445	481	0.459	
4	-240	-559	-0.33	-581	-0.288	-567	-0.380	
5	291	586	0.49	600	0.414	606	0.372	
6	40	-87	0.19	-52	0.118	-68	0.074	
7	163	253	0.34	271	0.262	272	0.222	
8	-220	-538	-0.27	-553	-0.254	-543	-0.333	
9	350	637	0.64	648	0.530	658	0.494	

Rainflow cycles	Neuber's		E-Plastic (FEA)		Pro. Method		Cycles to failure (N _f)		
	σ _m (MPa)	% (ε _a)	σ _m (MPa)	% (ε _a)	σ _m (MPa)	% (ε _a)	Neuber	FEA	Pro. M
1	38	0.48	34	0.404	45	0.45	7200	14800	9500
2	204	0.11	218	0.106	227	0.109	∞	∞	∞
3	24	0.38	26	0.334	31	0.35	18500	35500	27000
4	83	0.075	110	0.072	103	0.074	∞	∞	∞

Notch root stress-strain for SAE1141A2 Steel round bar								
Reversal	S _a (MPa)	Neuber's		E-Plastic (FEA)		Proposed		
		σ _{max}	% (ε _a)	σ _{max}	%(ε _a)	σ _{max}	%(ε _a)	
1	500	696	0.506	740	0.384	716	0.443	
2	100	-17	0.218	18	0.093	3	0.154	
3	280	303	0.346	363	0.223	323	0.282	
4	-280	-522	-0.138	-550	-0.183	-520	-0.174	
5	320	503	0.312	520	0.254	510	0.271	
6	40	3	0.112	-55	0.048	10	0.069	
7	140	182	0.184	159	0.121	189	0.141	
8	-240	-469	-0.103	-492	-0.156	-465	-0.142	
9	500	714	0.487	743	0.383	732	0.430	

Rainflow cycles	Neuber's		E-Plastic (FEA)		Pro. Method		Cycles to failure (N _f)		
	σ _m	% (ε _a)	σ _m	% (ε _a)	σ _m	% (ε _a)	Neuber	FEA	Pro.
1	87	0.322	124	0.283	98	0.3	25300	47000	35000
2	143	0.064	172	0.065	160	0.064	∞	∞	∞
3	17	0.207	14	0.205	23	0.206	450000	620000	440000
4	90	0.036	52	0.037	90	0.036	∞	∞	∞

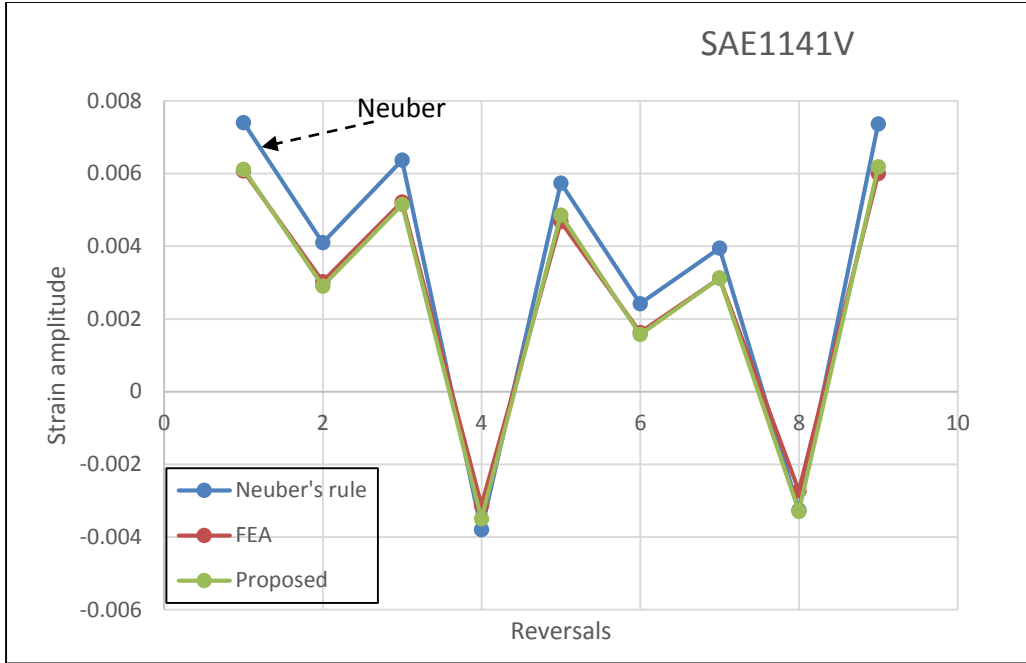


Figure 98 Notch Root Strain Amplitude vs Reversals for Flat Plate of SAE1141V

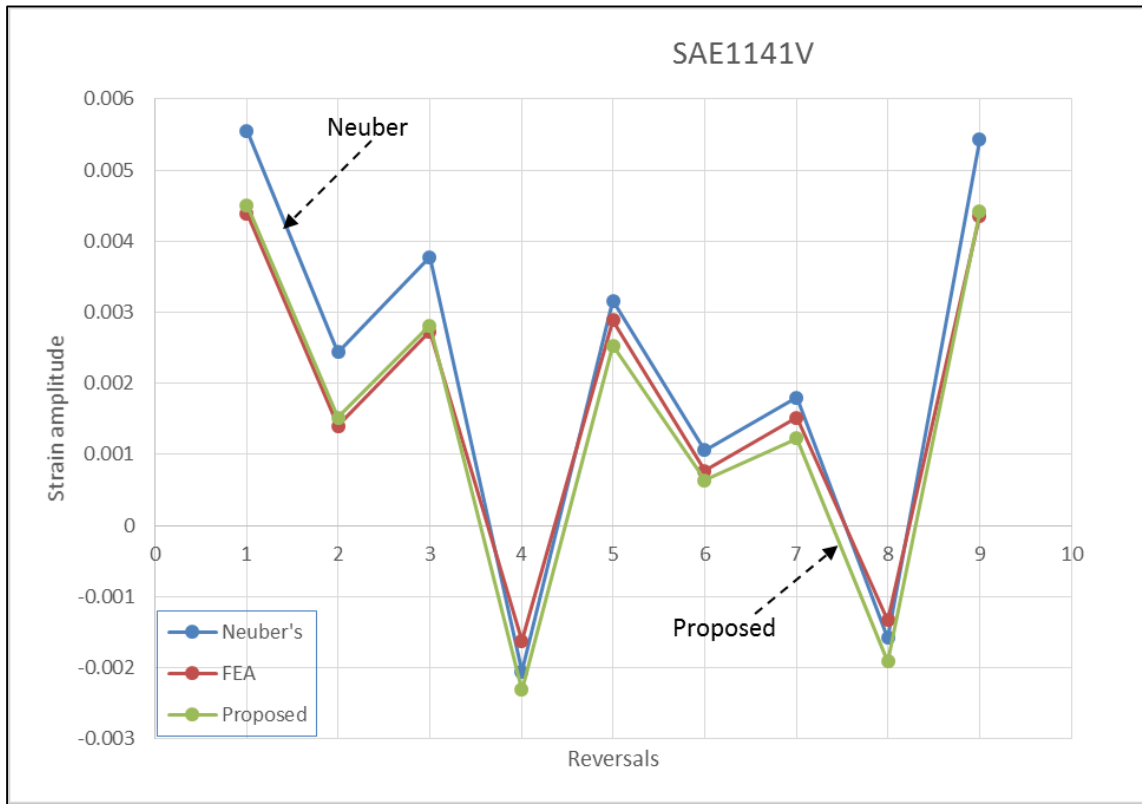


Figure 99 Notch Root Strain Amplitude vs Reversals for Round Bar of SAE1141V

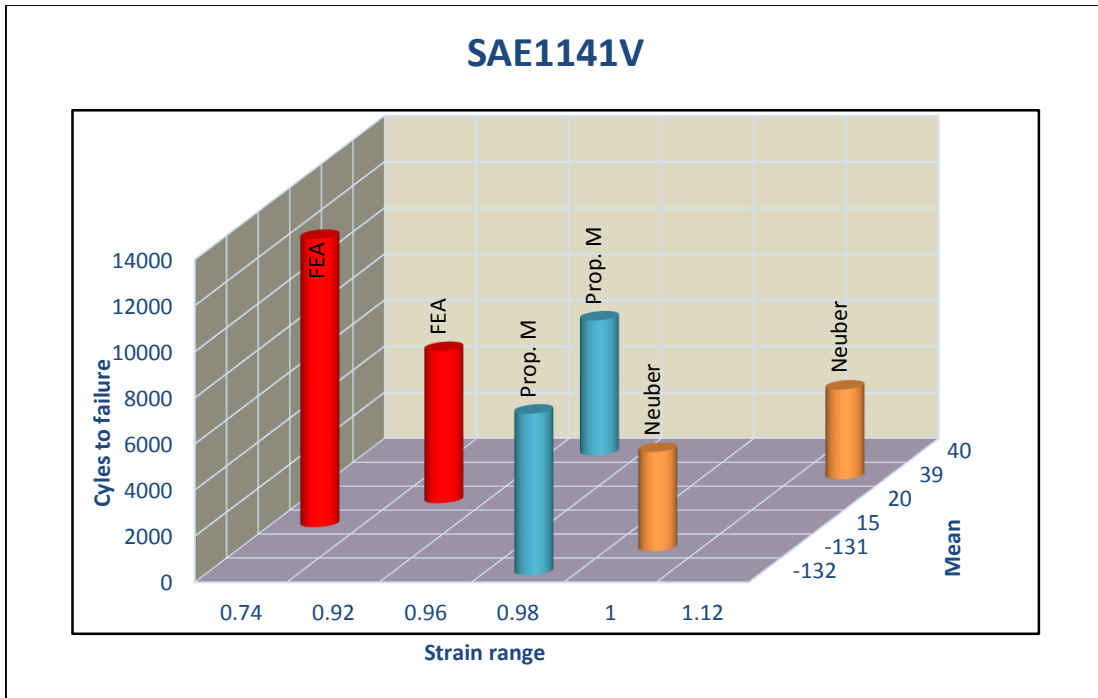


Figure 100 Cycles to Failure vs Strain Range and Mean Stress for SAE1141V

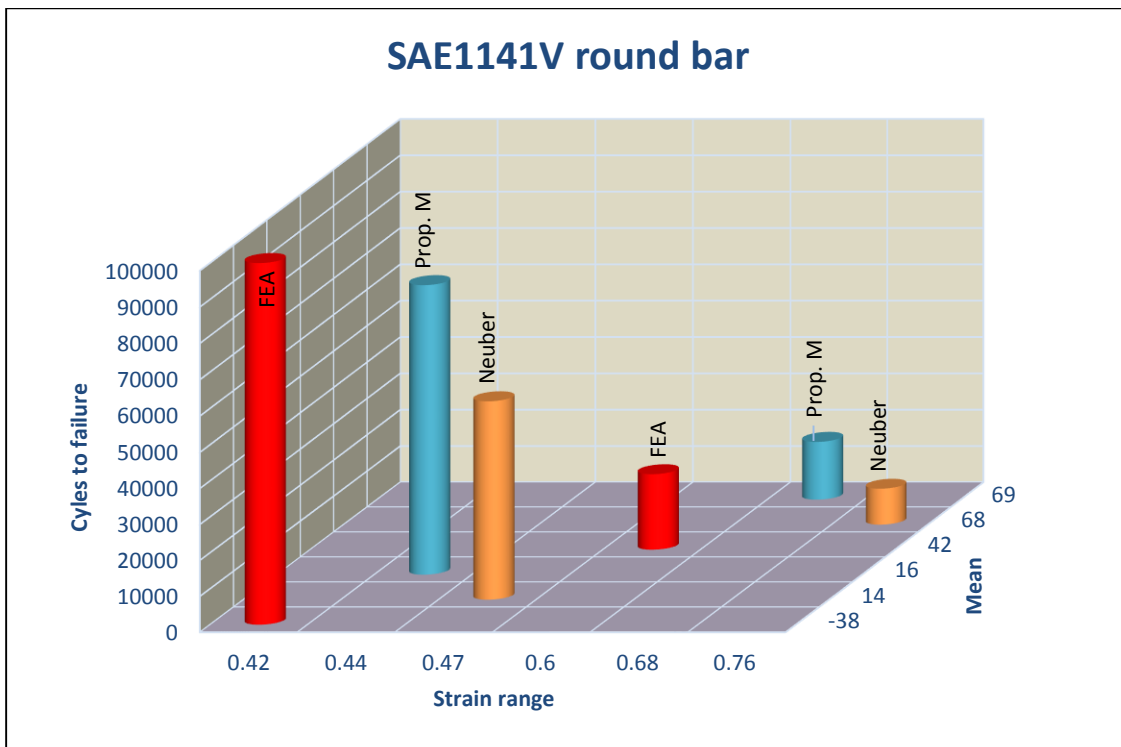


Figure 101 Cycles to Failure vs Strain Range and Mean Stress for SAE1141V

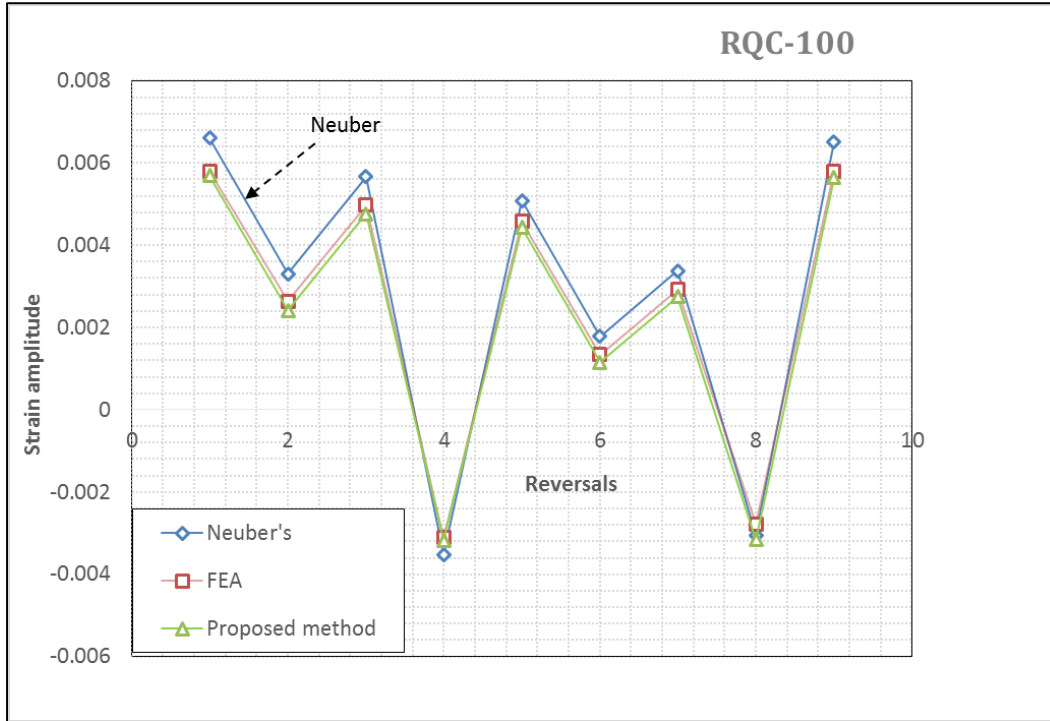


Figure 102 Notch Root Strain Amplitude vs Reversals for Flat Plate of RQC-100

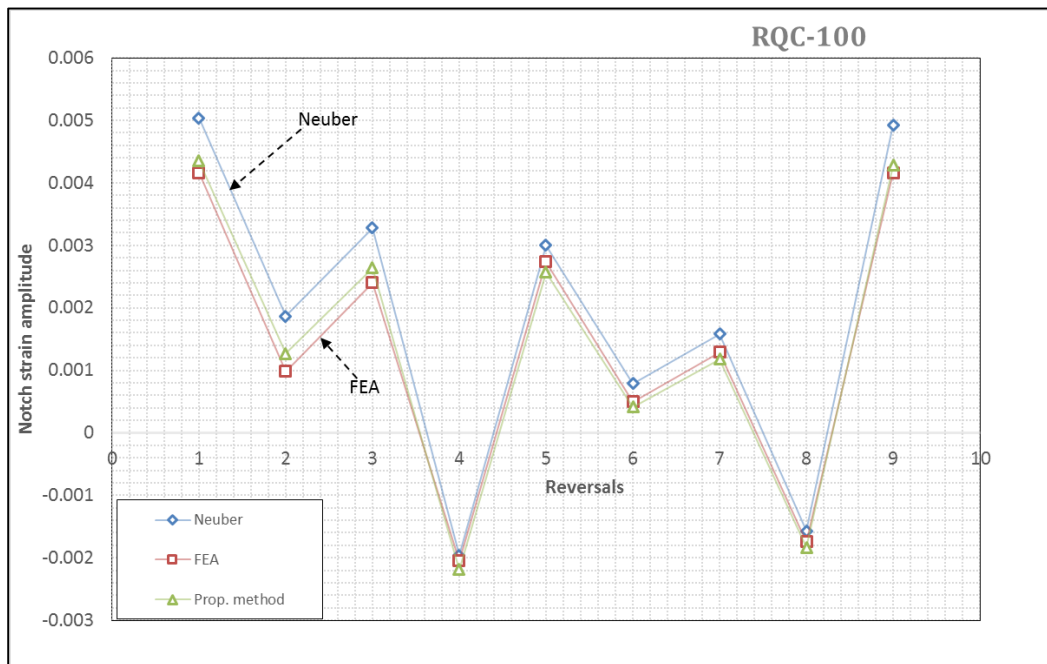


Figure 103 Notch Root Strain Amplitude vs Reversals for Round Bar of RQC-100

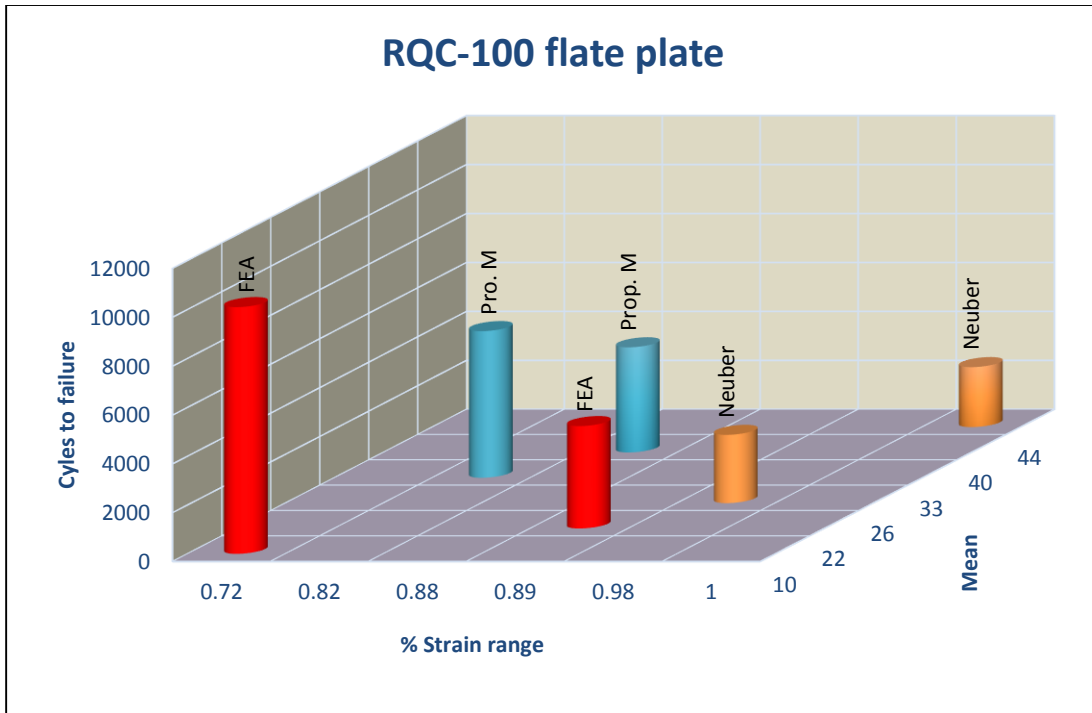


Figure 104 Cycles to Failure vs Strain Range and Mean Stress for RQC-100 Flat Plate

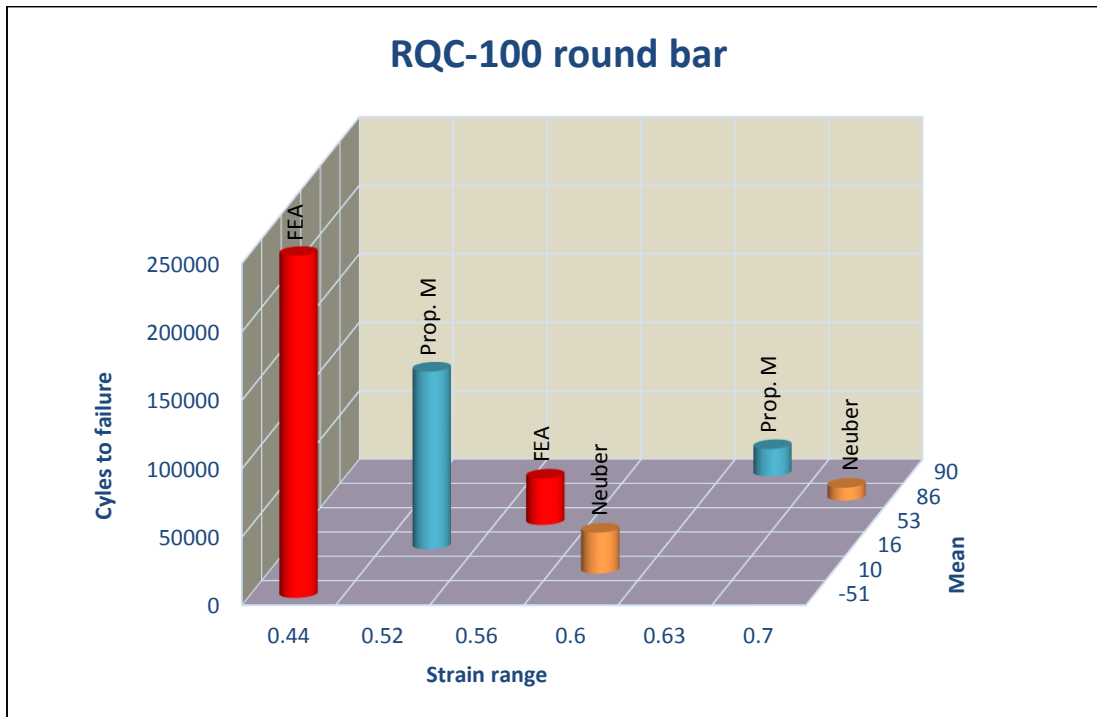


Figure 105 Cycles to Failure vs Strain Range and Mean Stress for RQC-100 Round Bar

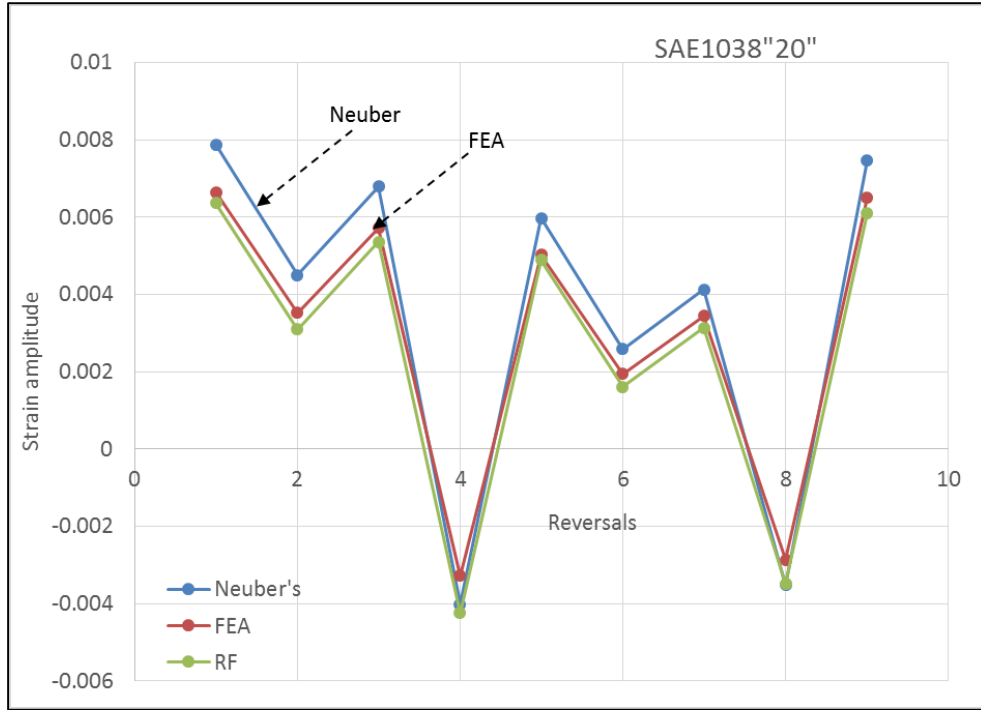


Figure 106 Notch Root Strain Amplitude vs Reversals for Flat Plate of SAE1038

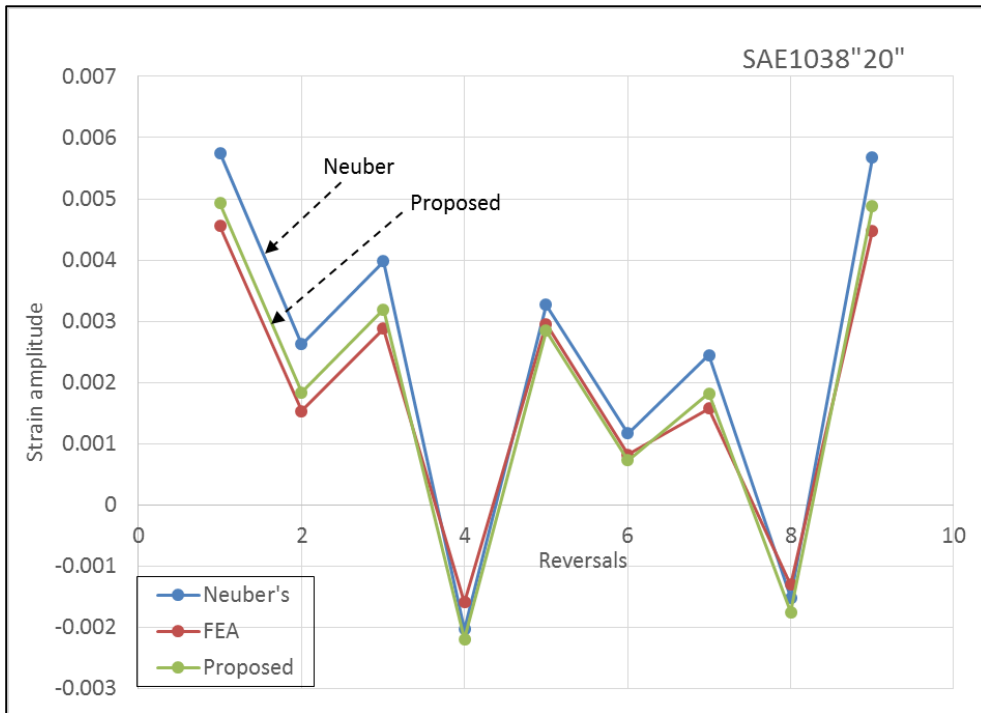


Figure 107 Notch Root Strain Amplitude vs Reversals for Round Bar of SAE1038

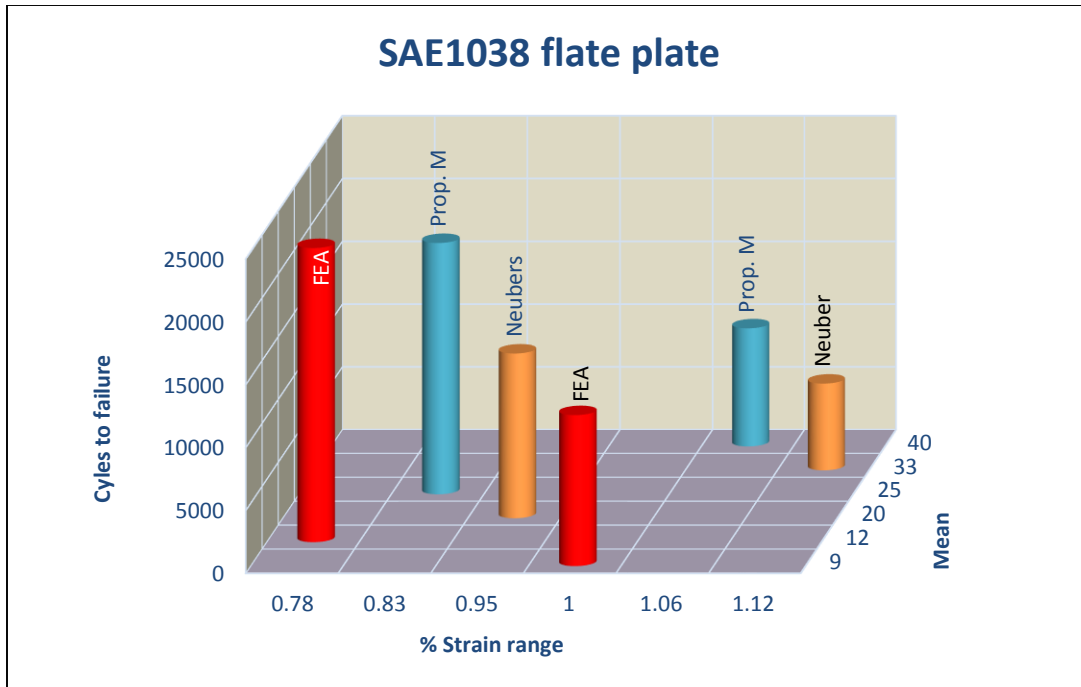


Figure 108 Cycles to Failure vs Strain Range and Mean Stress for SAE1038 Flat Plate

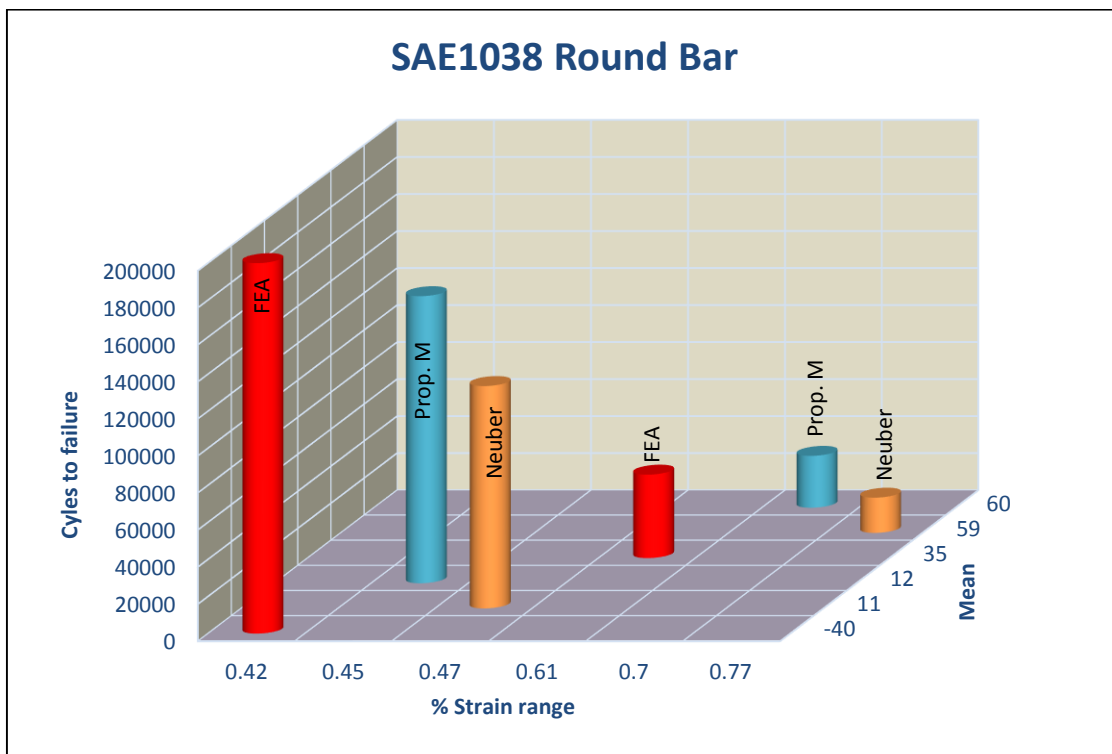


Figure 109 Cycles to Failure vs Strain Range and Mean Stress for SAE1038 Round Bar

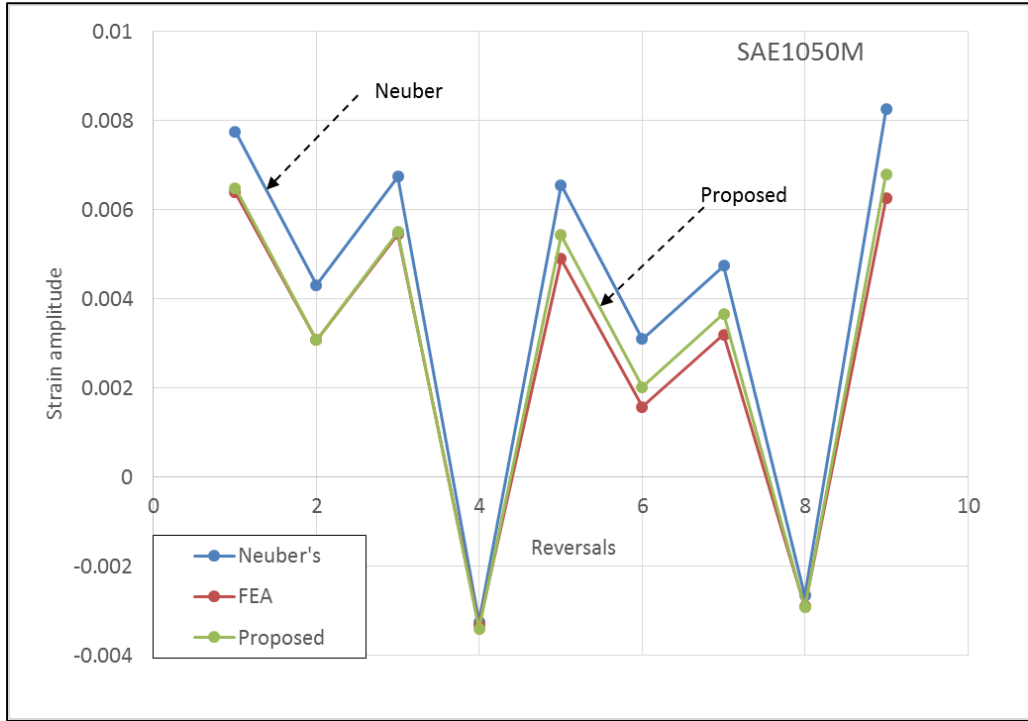


Figure 110 Notch Root Strain Amplitude vs Reversals for Flat Plate of SAE1050M

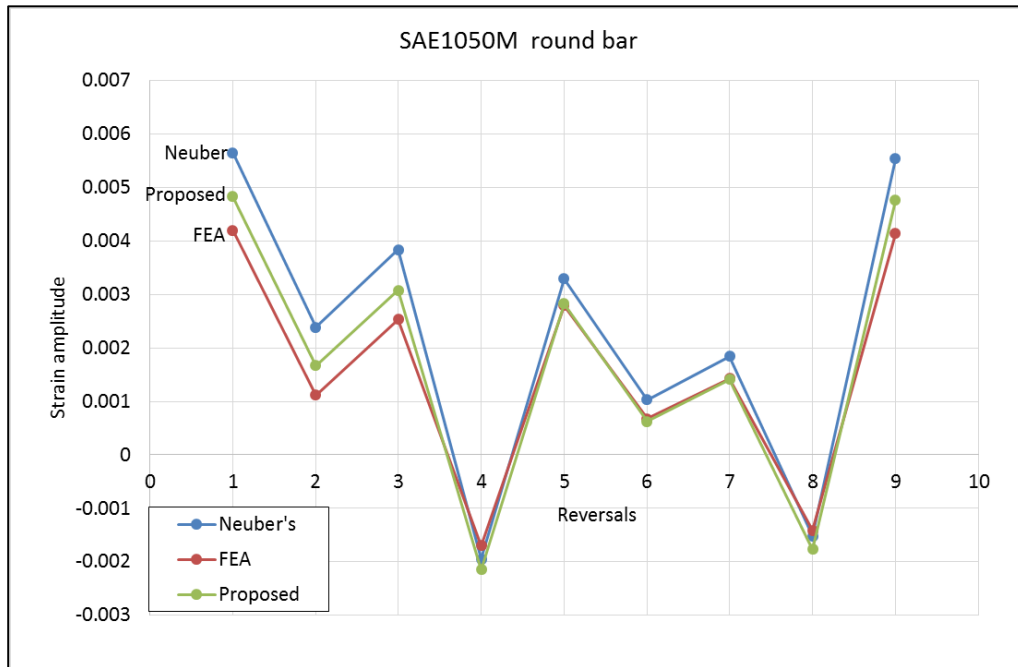


Figure 111 Notch Root Strain Amplitude vs Reversals for Round Bar of SAE1050M

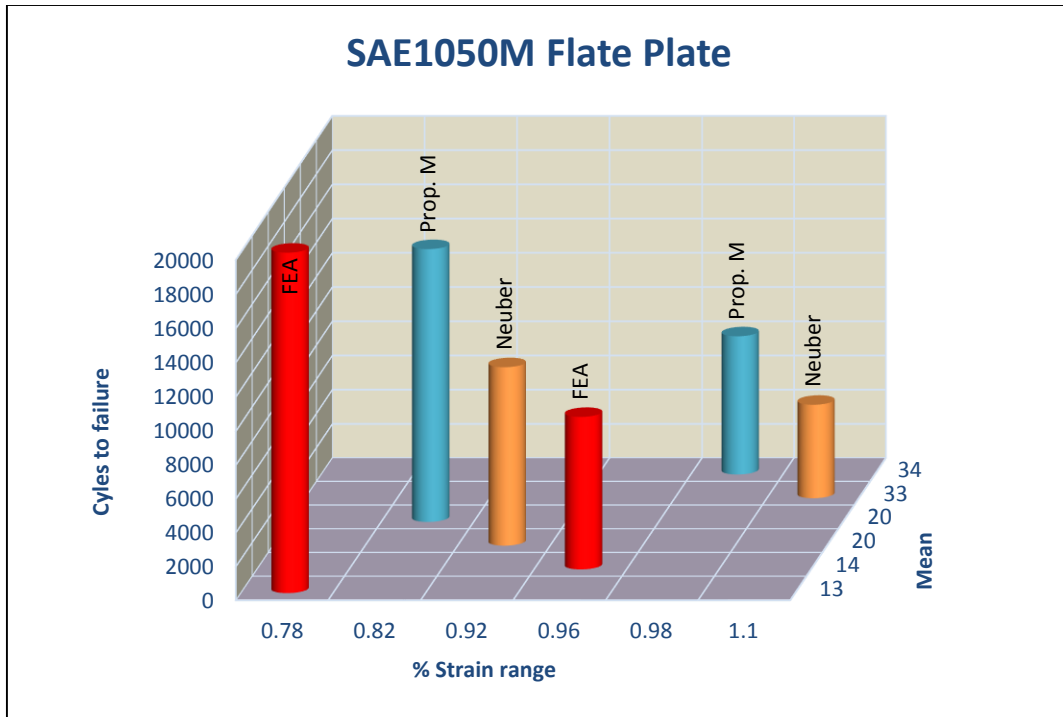


Figure 112 Cycles to Failure vs Strain Range and Mean Stress for SAE1050M Flat Plate

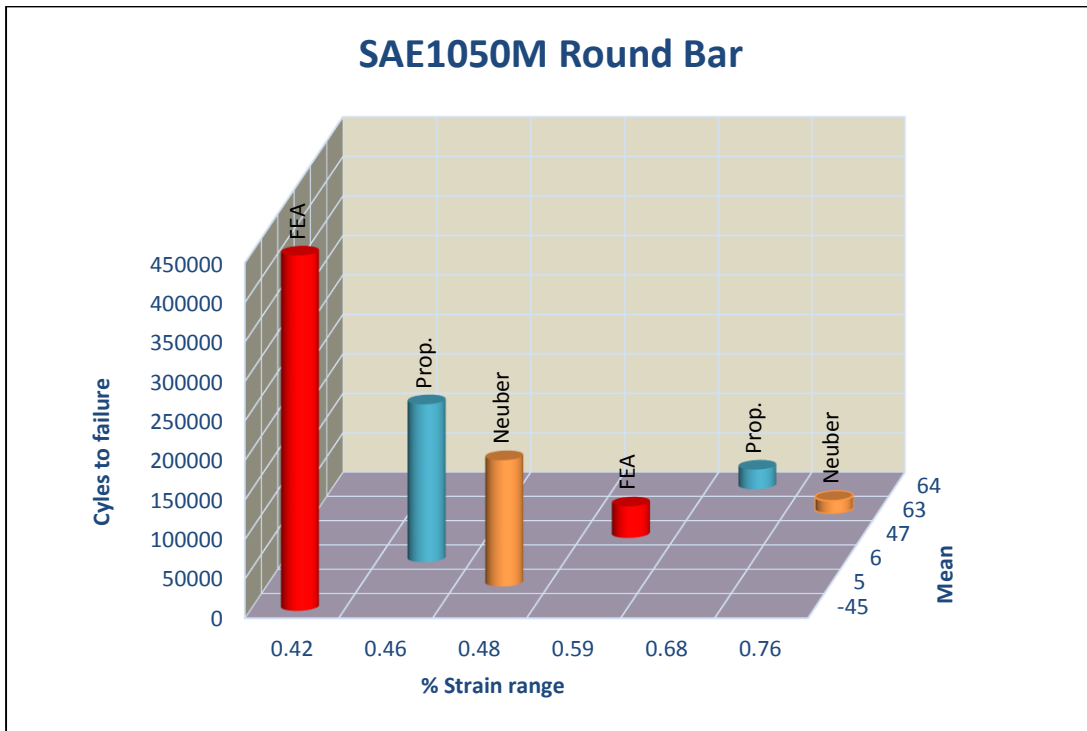


Figure 113 Cycles to Failure vs Strain Range and Mean Stress for SAE1050M Round Bar

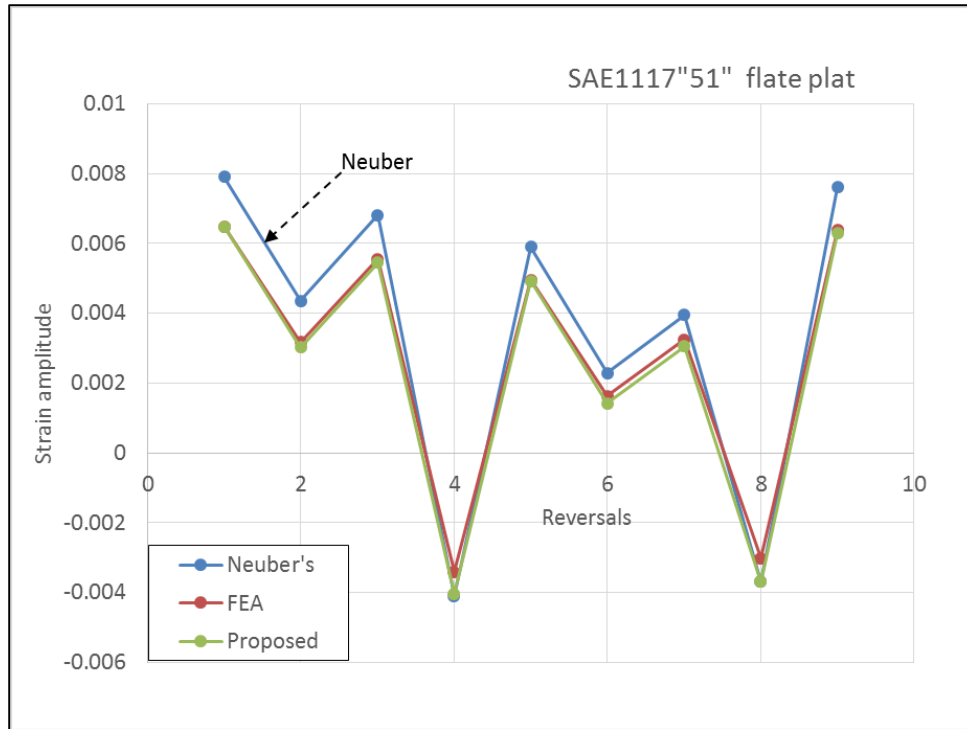


Figure 114 Notch Root Strain Amplitude vs Reversals for Flat Plate of SAE1117

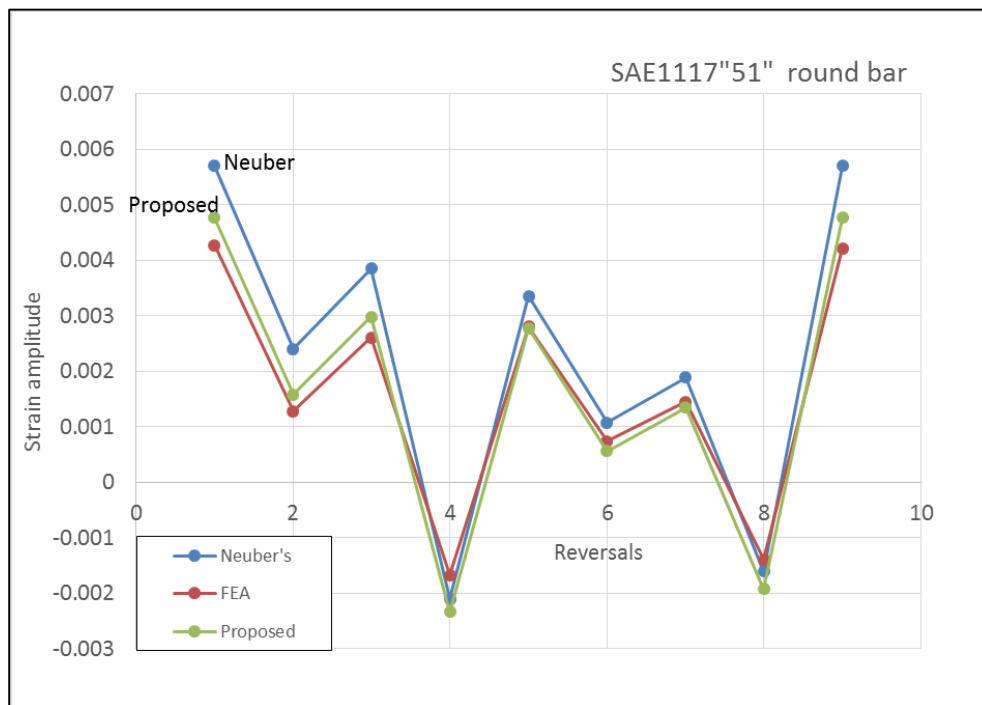


Figure 115 Notch Root Strain Amplitude vs Reversals for Round Bar of SAE1117

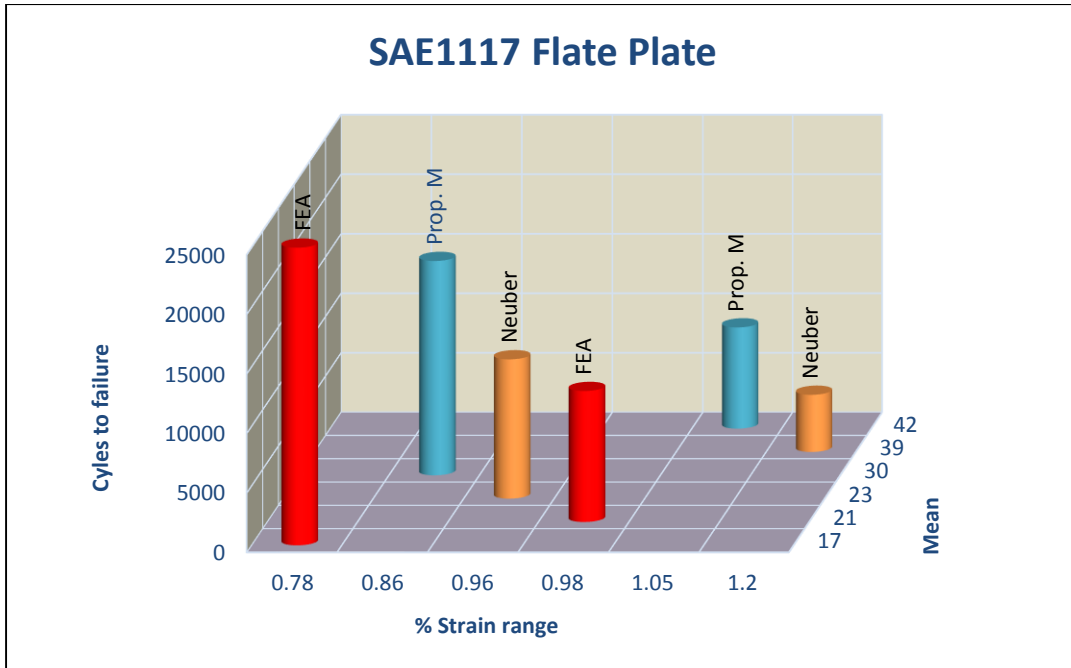


Figure 116 Cycles to Failure vs Strain Range and Mean Stress for SAE1117 Flat Plate

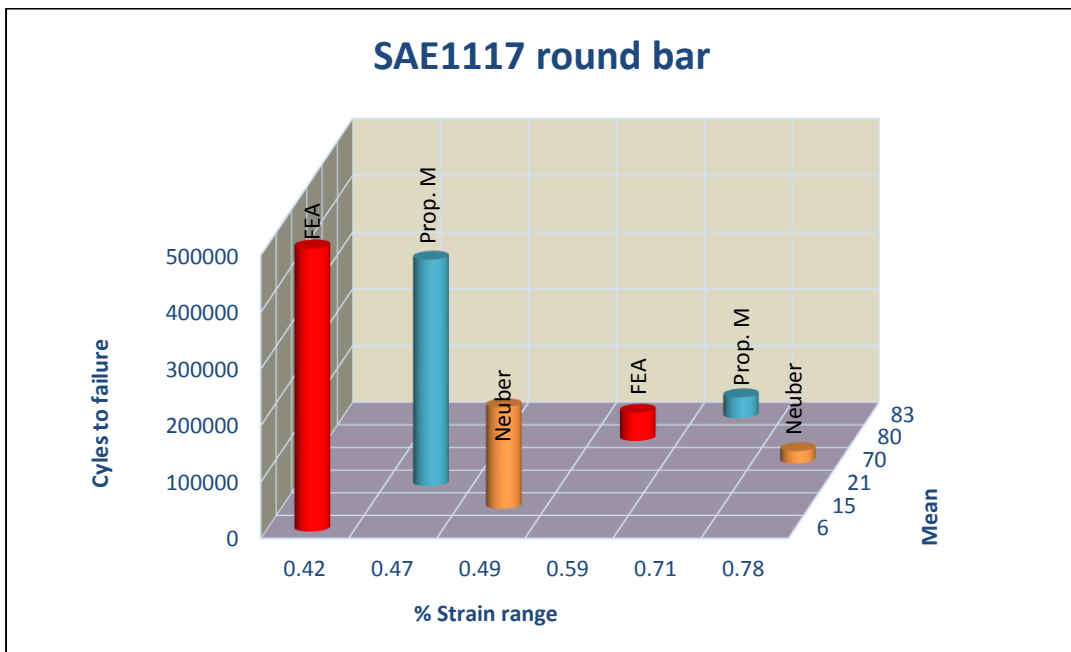


Figure 117 Cycles to Failure vs Strain Range and Mean Stress for SAE1117 Round Bar

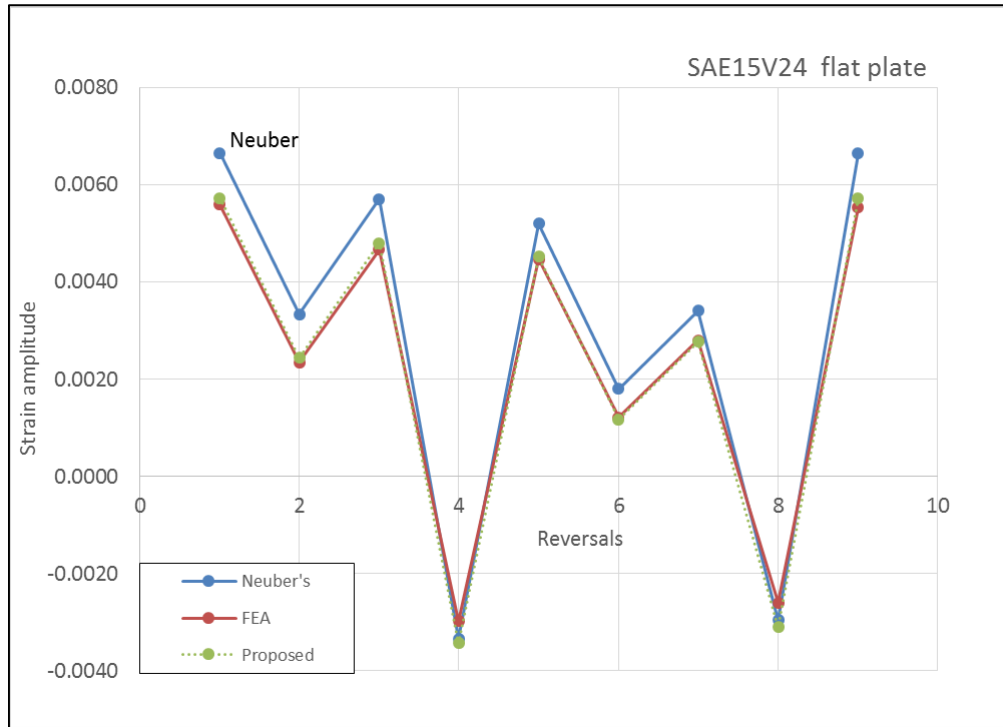


Figure 118 Notch Root Strain Amplitude vs Reversals for Flat Plate of SAE15V24

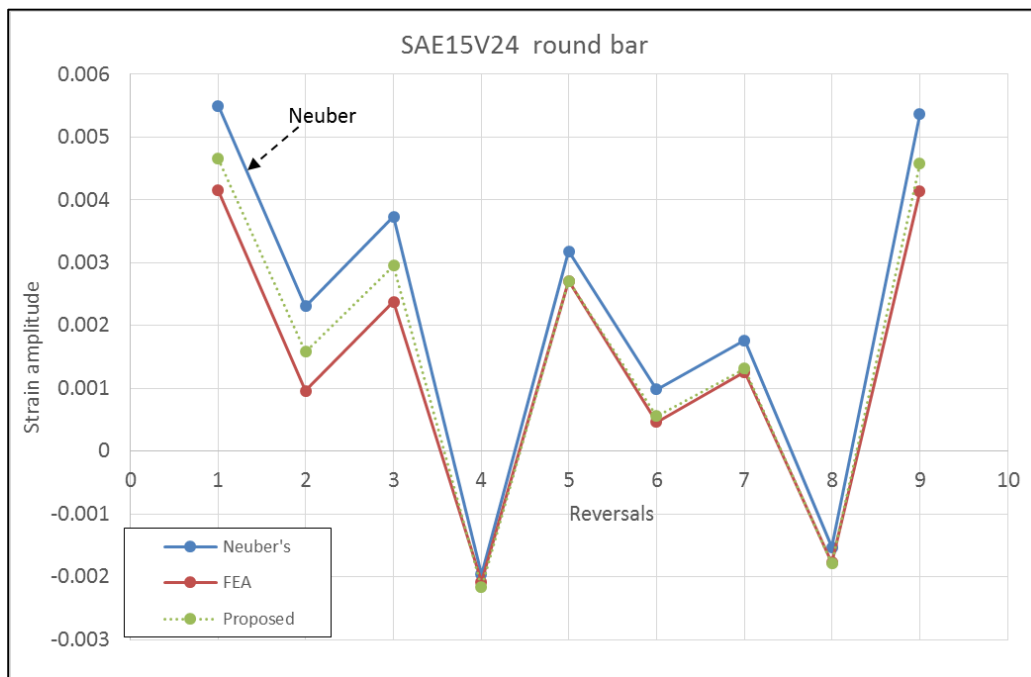


Figure 119 Notch Root Strain Amplitude vs Reversals for Round Bar of SAE15V24

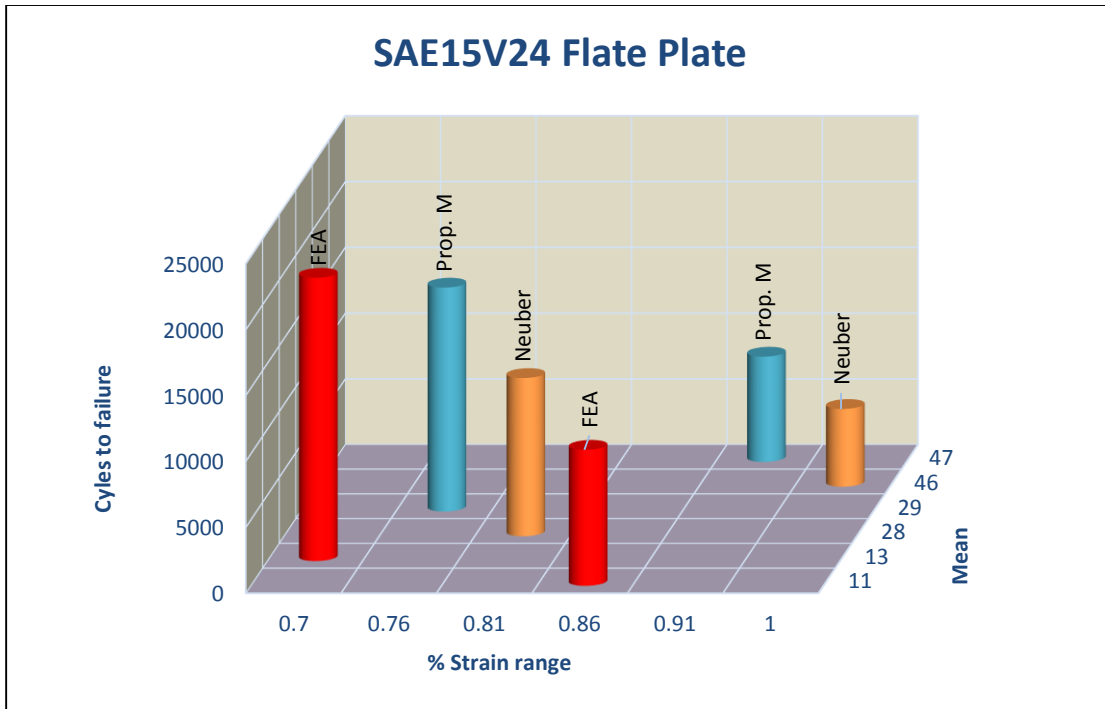


Figure 120 Cycles to Failure vs Strain Range and Mean Stress for SAE15V24 Flat Plate

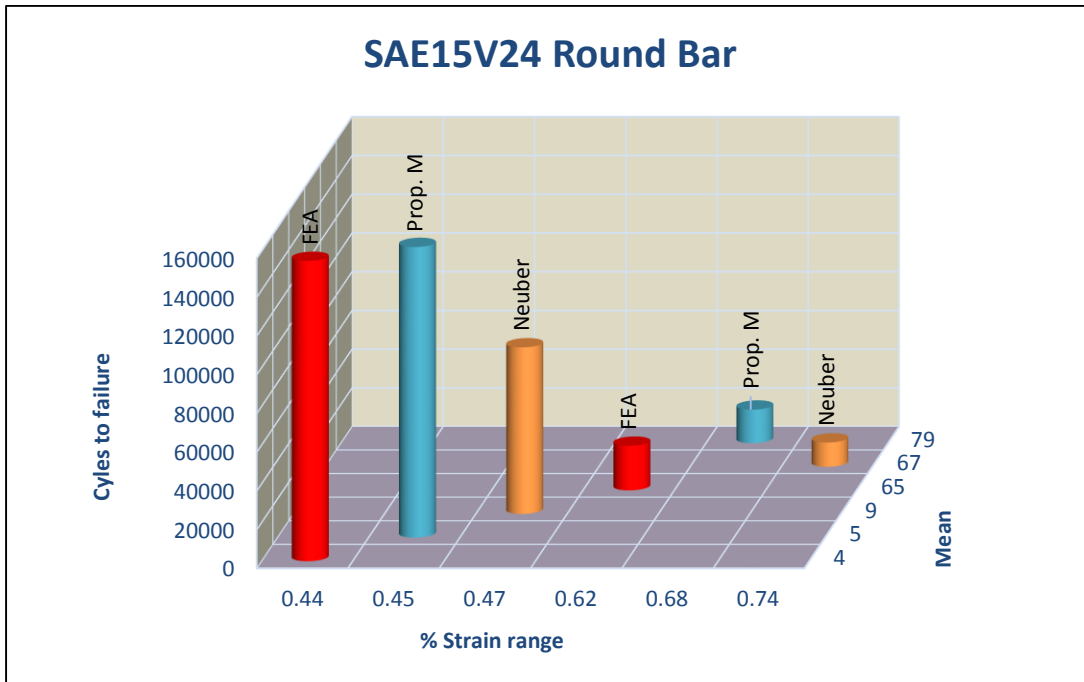


Figure 121 Cycles to Failure vs Strain Range and Mean Stress for SAE15V24 Round Bar

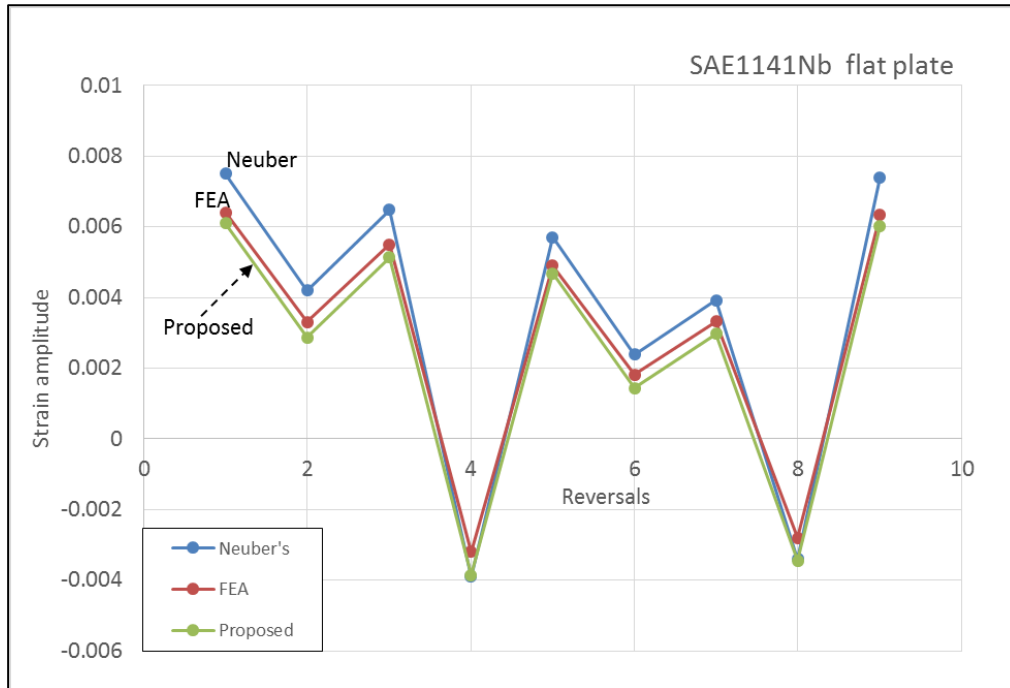


Figure 122 Notch Root Strain Amplitude vs Reversals for Flat Plate of SAE1141Nb

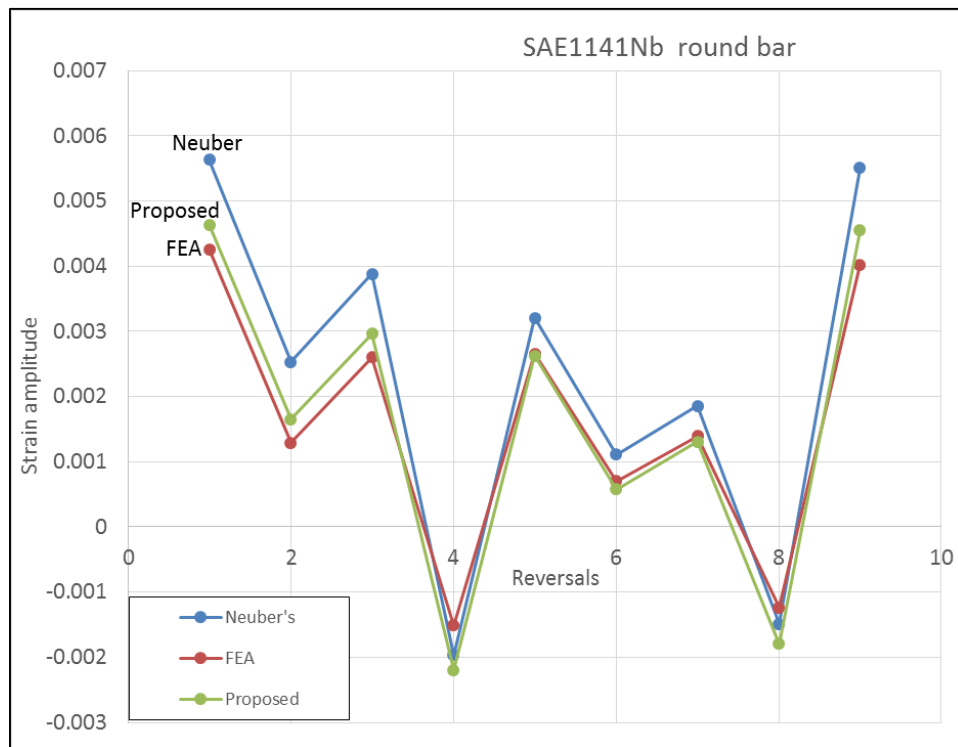


Figure 123 Notch Root Strain Amplitude vs Reversals for Round Bar of SAE1141Nb

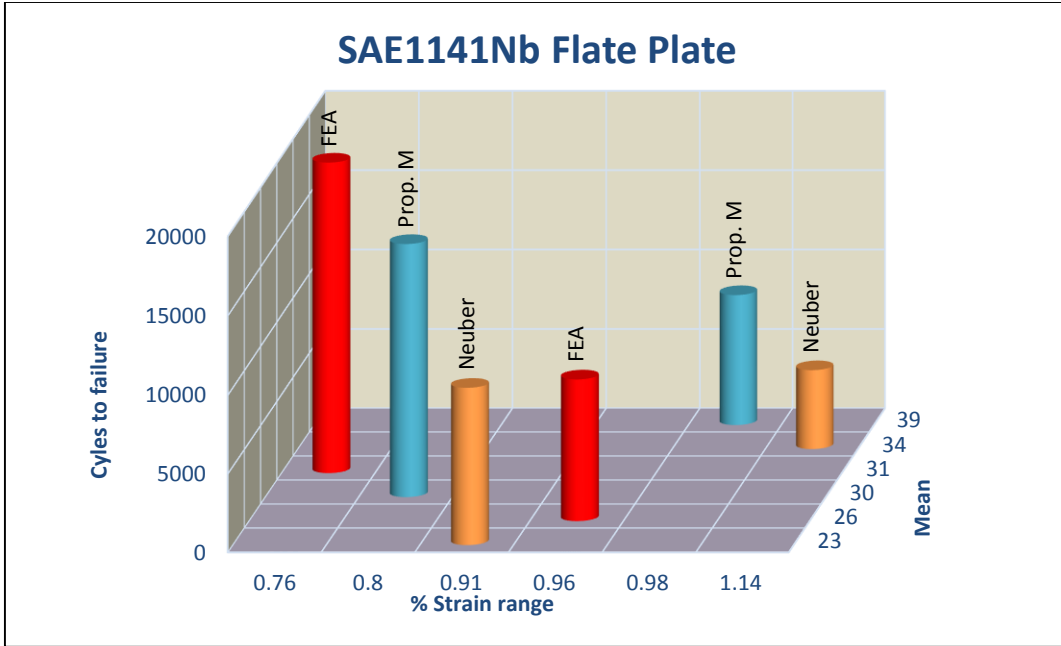


Figure 124 Cycles to Failure vs Strain Range and Mean Stress for SAE1141Nb Flat Plate

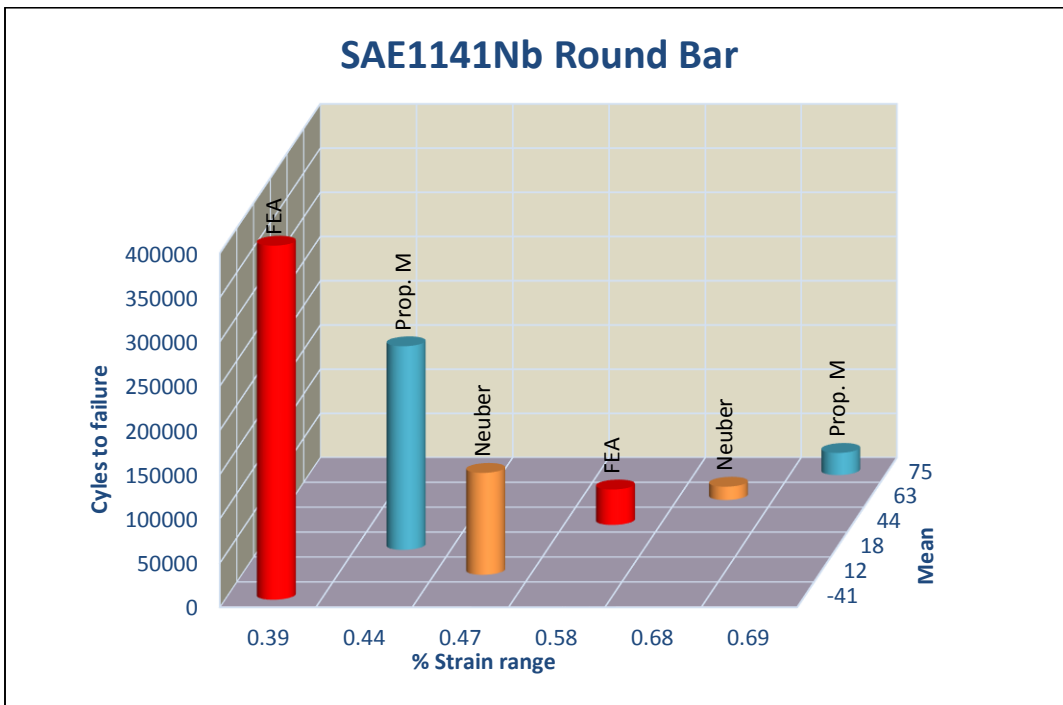


Figure 125 Cycles to Failure vs Strain Range and Mean Stress for SAE1141Nb Round Bar

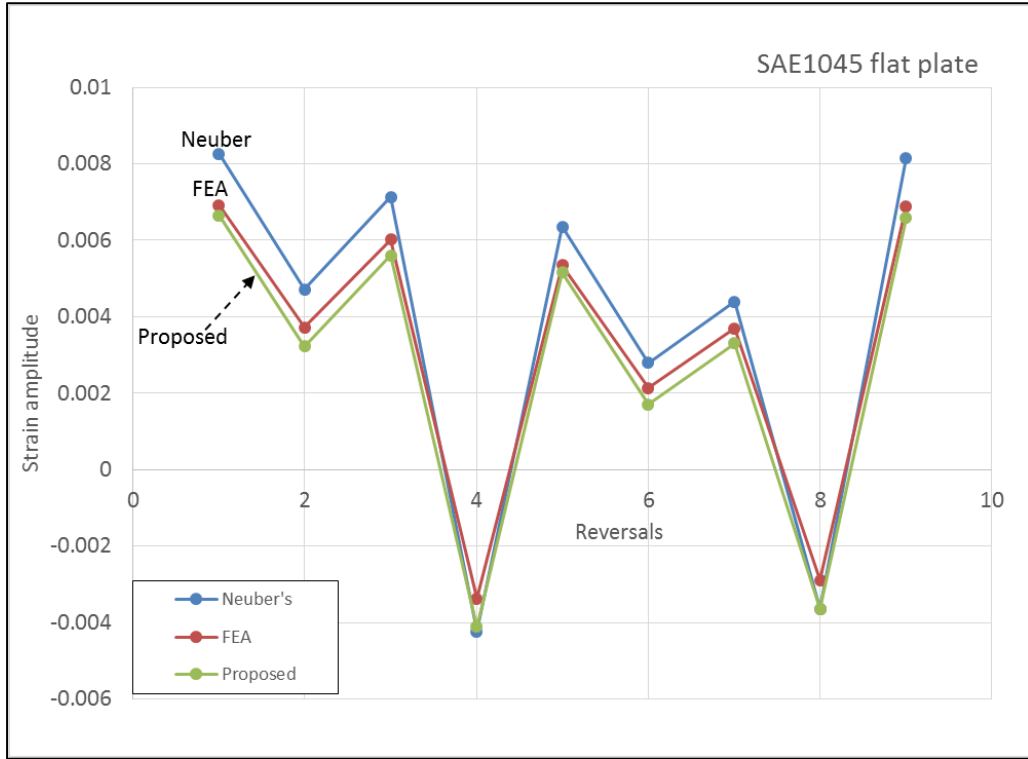


Figure 126 Notch Root Strain Amplitude vs Reversals for Flat Plate of SAE1045

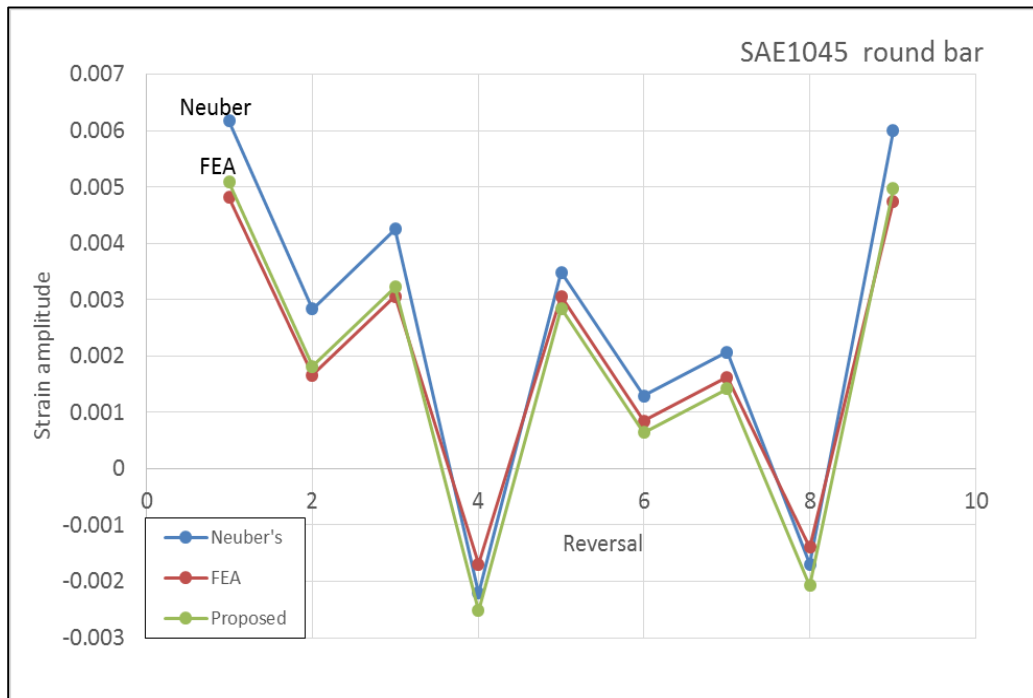


Figure 127 Notch Root Strain Amplitude vs Reversals for Round Bar of SAE1045

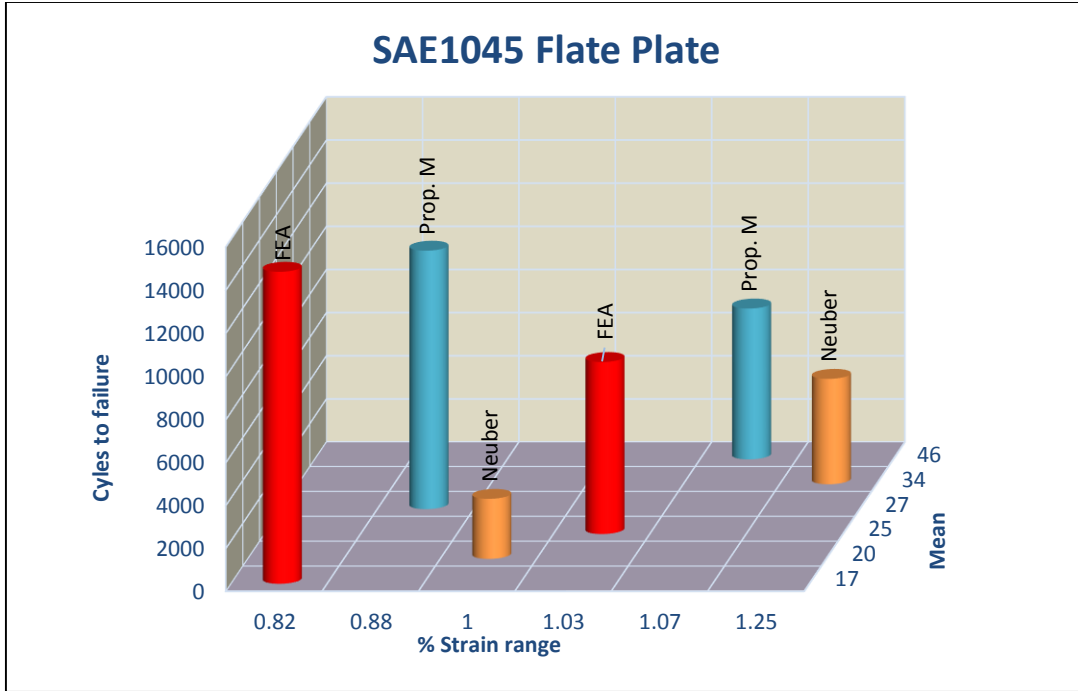


Figure 128 Cycles to Failure vs Strain Range and Mean Stress for SAE1045 Flat Plate

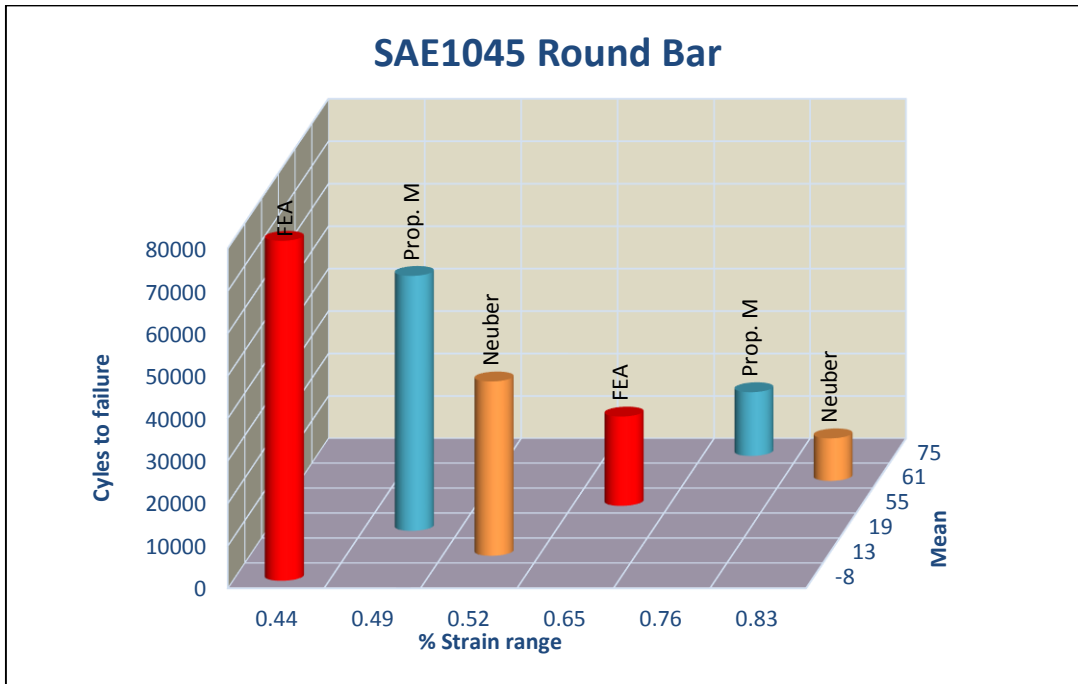


Figure 129 Cycles to Failure vs Strain Range and Mean Stress for SAE1045 Round Bar

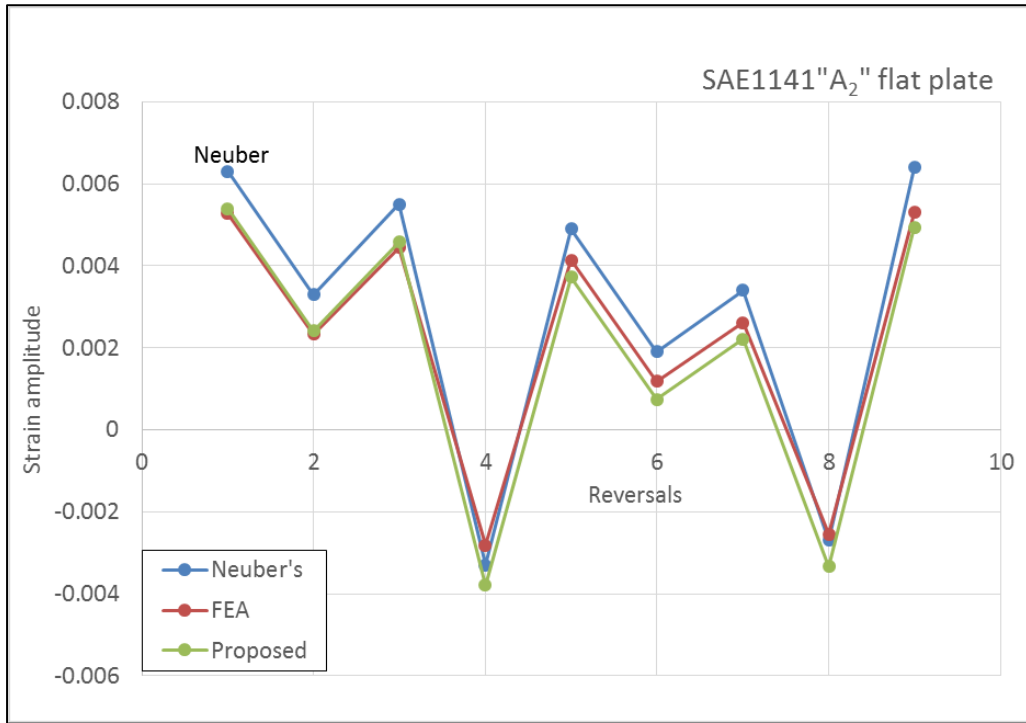


Figure 130 Notch Root Strain Amplitude vs Reversals for Flat Plate of SAE1141

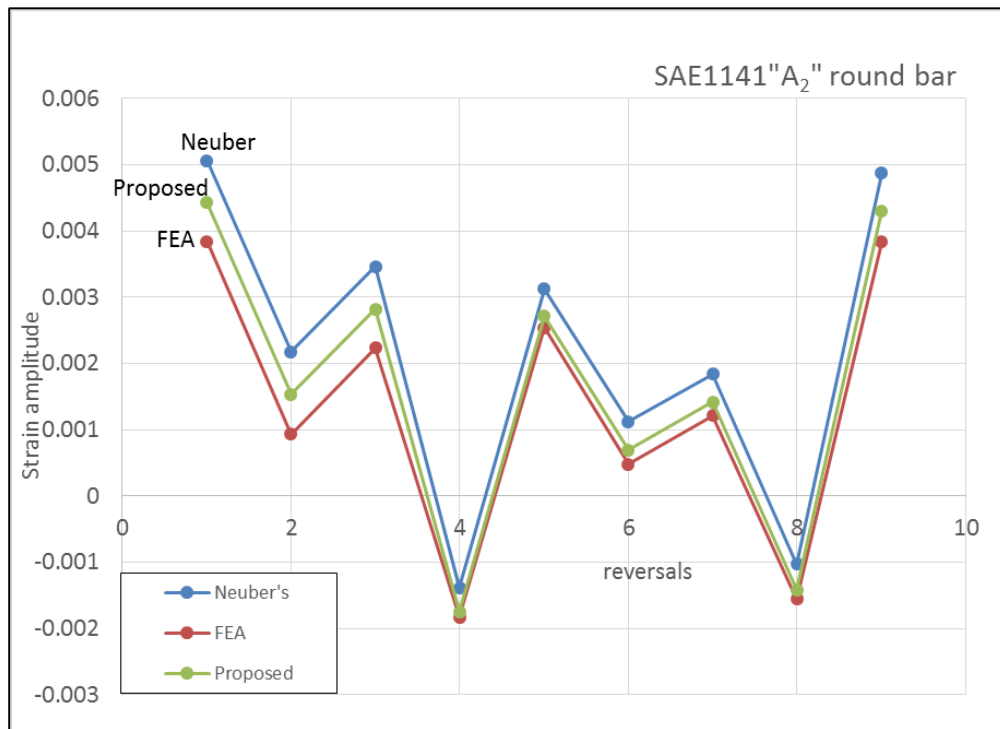


Figure 131 Notch Root Strain Amplitude vs Reversals for Round Bar of SAE1141

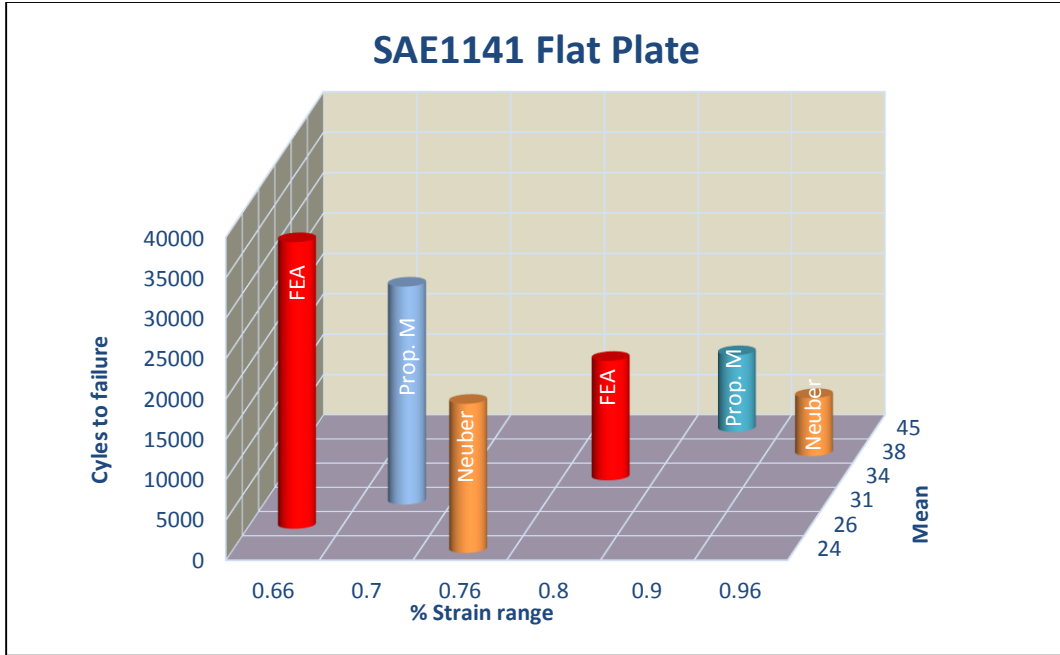


Figure 132 Cycles to Failure vs Strain Range and Mean Stress for SAE1141 Flat Plate

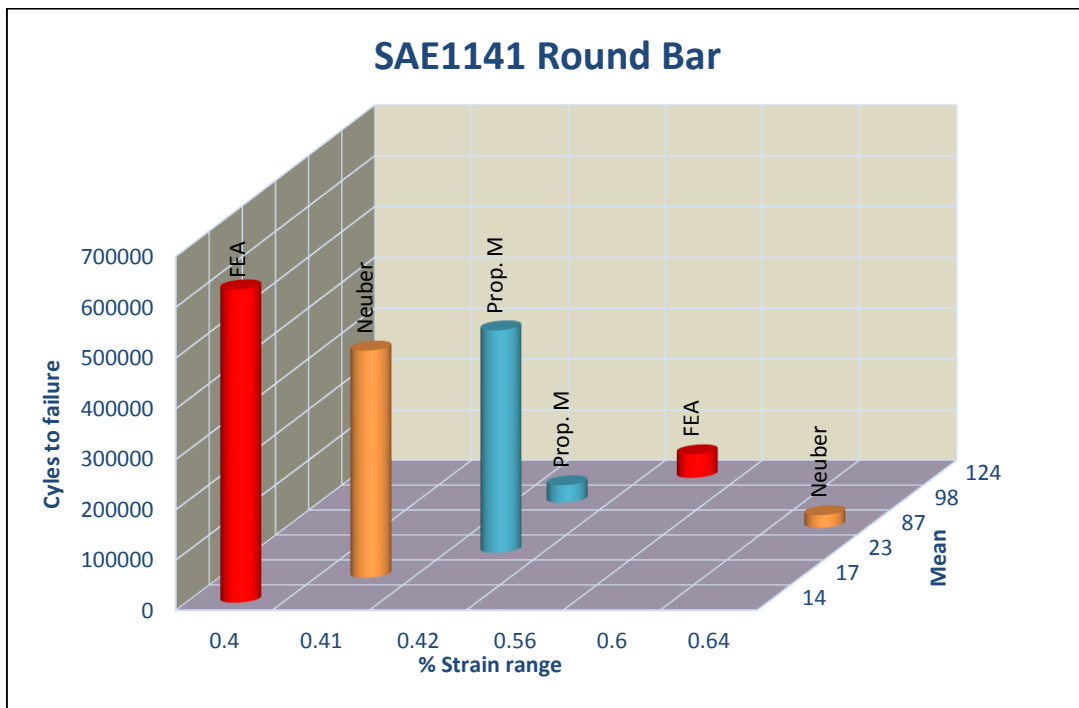


Figure 133 Cycles to Failure vs Strain Range and Mean Stress for SAE1141 Round Bar

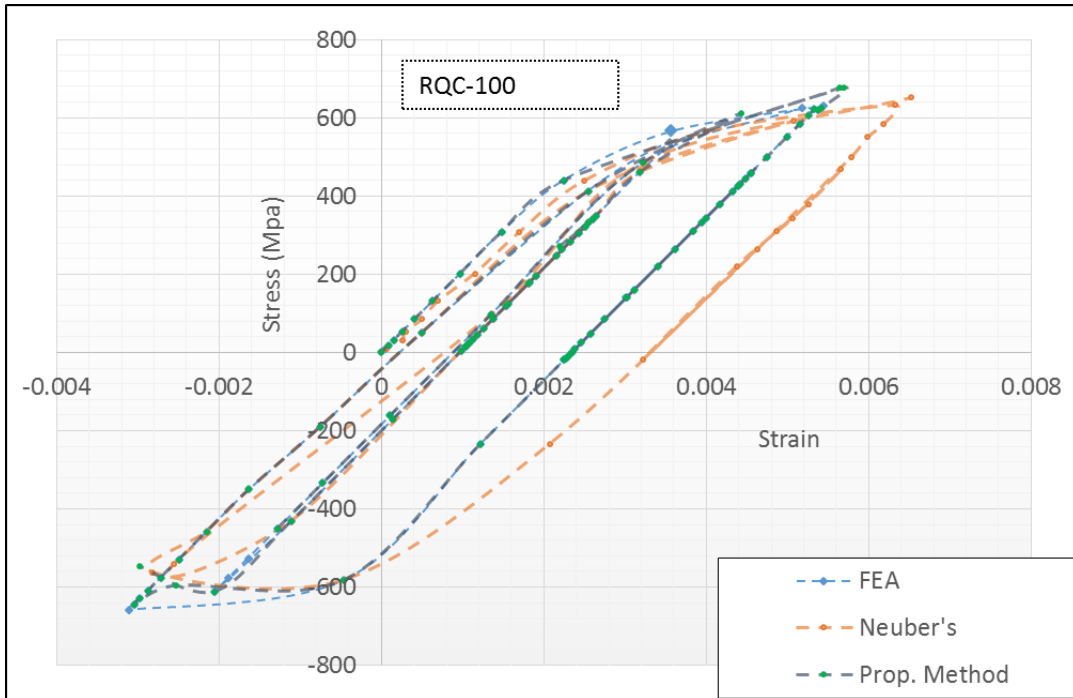


Figure 134 Hysteresis loops for RQC-100 Flat Plate

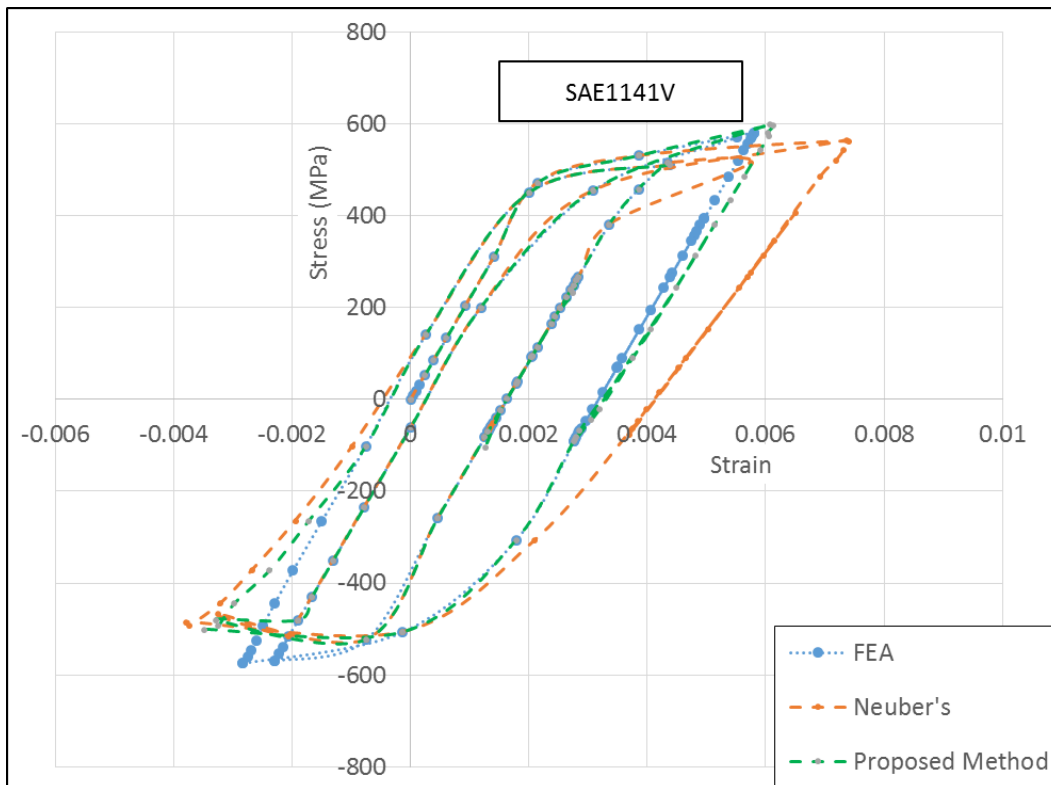


Figure 135 Hysteresis Loops for SAE1141V Flat Plate

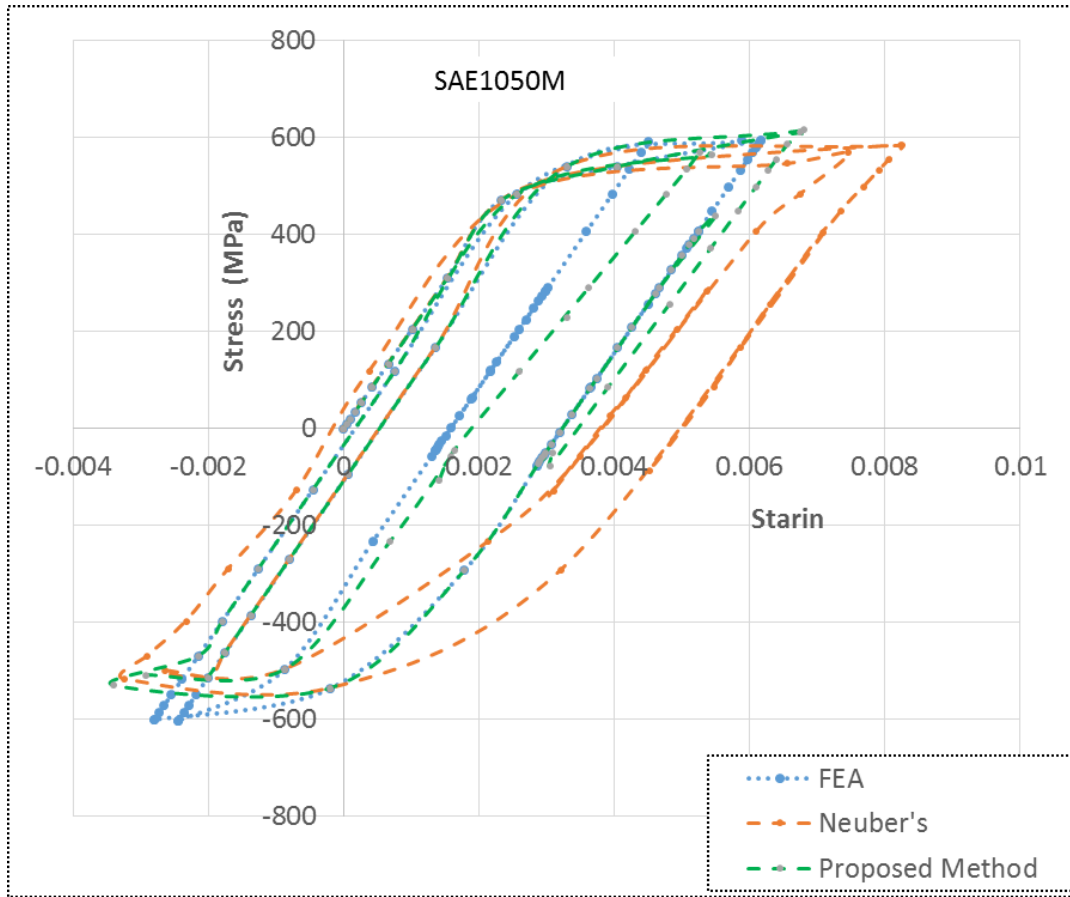


Figure 136 Hysteresis loop for SAE1050M Flat Plate

9 APPENDIX C

Fatigue test machines

Fatigue test machines may be classified based on different view-points such as; purpose of the test, type of stressing, operation characteristics, and type of load.

There is another classification for fatigue testing machines based on the purpose of the machine as [74]:

1. Machines for general purpose.
2. Machines for special purpose.
3. Equipments for testing parts and assemblies.

Figure 137 appendix C, schematically shows a rotating bending machine which produces a non-uniform bending moment along the specimen length. The other type of rotating bending machine is shown in Figure 138 appendix C, in this case a uniform bending moment along the test specimen. In both cases the load is stay constant regardless the changes in the material mechanical properties or crack initiation and propagation. This type of machines is called “constant load amplitude machines”.

Figure 139 appendix C, schematically shows a constant deflection amplitude cantilever bending machine, where a nonuniform bending moment is produced along the specimen, the load amplitude changes as the material mechanical properties changes, it increases as material harden and decreases as material soften or crack growth.

Axial loaded fatigue test machine is schematically shown in Figure 140 appendix C, this kind of machines is capable of applying both mean and alternating axial loads.

There are different types of machines have been designed over the years. The most important contribution of fatigue testing has been the closed-loop Servohydraulic test system [1], a modern Servohydraulic test system utilizing its own personal computer is shown in Figure 141 appendix C. The operational principal for this kind of machines is

based on generation of input signal of load, strain, or displacement using a function generator and applying this input through a hydraulic actuator, measuring the specimen response through a load cell, a clip gage or a linear variable differential transducer (LVDT), and comparing this with the specific input. The test data outputs are processed by a personal computer, the test frequency usually ranges from mHz to kHz.

These systems are capable of perform different types of tests, constant or variable amplitude, strain, displacement and stress intensity factor.

To perform a fatigue test a standard method should be followed. Standard fatigue test methods and procedures for metals are available from ASTM [4]. The International Organization for Standardization (ISO) draft standards on fatigue testing of metals are available through the ISO, Geneva, Switzerland.

Fatigue Test Specimens

There are many types and shapes of fatigue test specimens, Figure 142 appendix C, shows the specimens used to obtain total fatigue life, in this case no differentiation between crack nucleation and crack propagation. The surface of specimen has to be finely polished to minimize the surface roughness effects.

Specimen (a) is used for rotating bending test; specimen (b) and (c) are used for axial fatigue test. Specimen (d) for axial or bending test circumferential groove usually used to study the effect of stress concentration. Specimen (e) is a cantilever flat sheet specimen.

Specimens (g) to (j) are used for the study of fracture mechanics to study crack growth mechanisms in this case each specimen has a thin slit, notch, or groove at the middle with a very small root radius. The notched samples are subjected to a cyclic stress at a low stress intensity factor range to form a small fatigue crack at the root radius, then a real fatigue test can be applied.

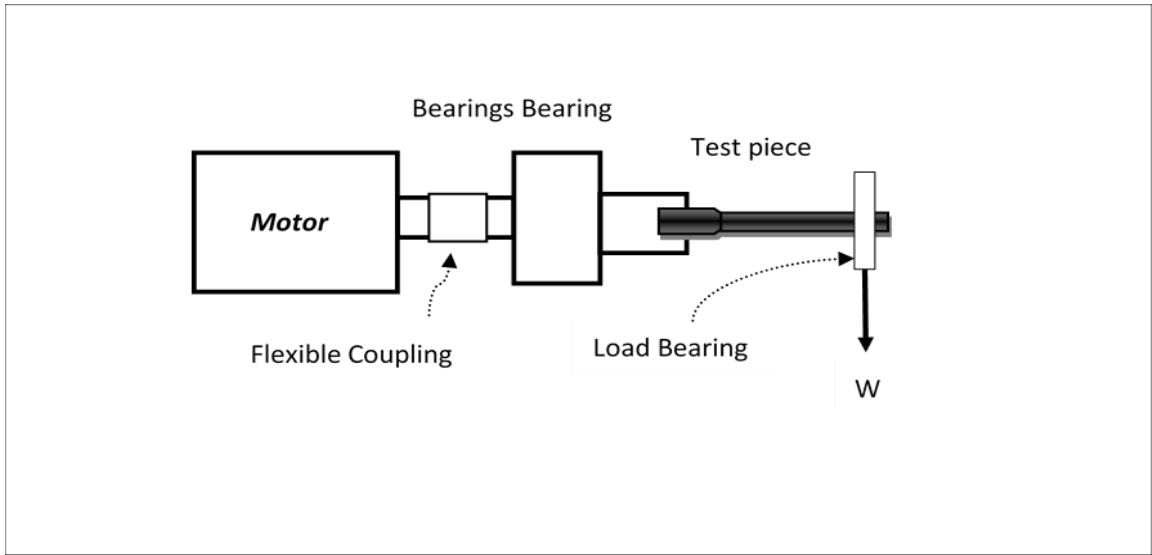


Figure 137 Nonuniform bending moment machine

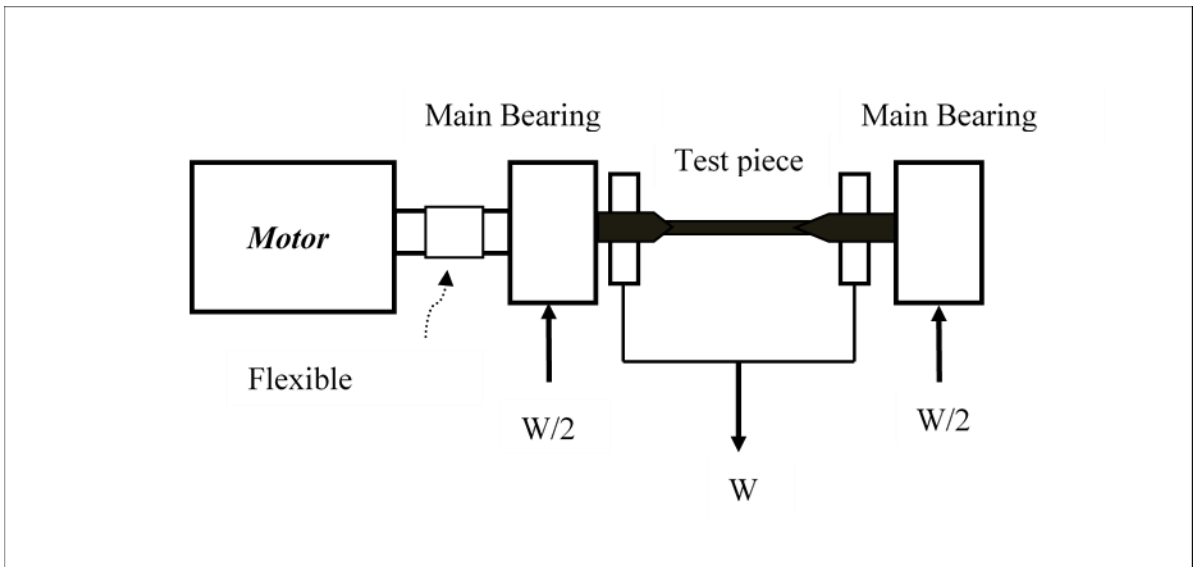


Figure 138 Uniform bending moment machine

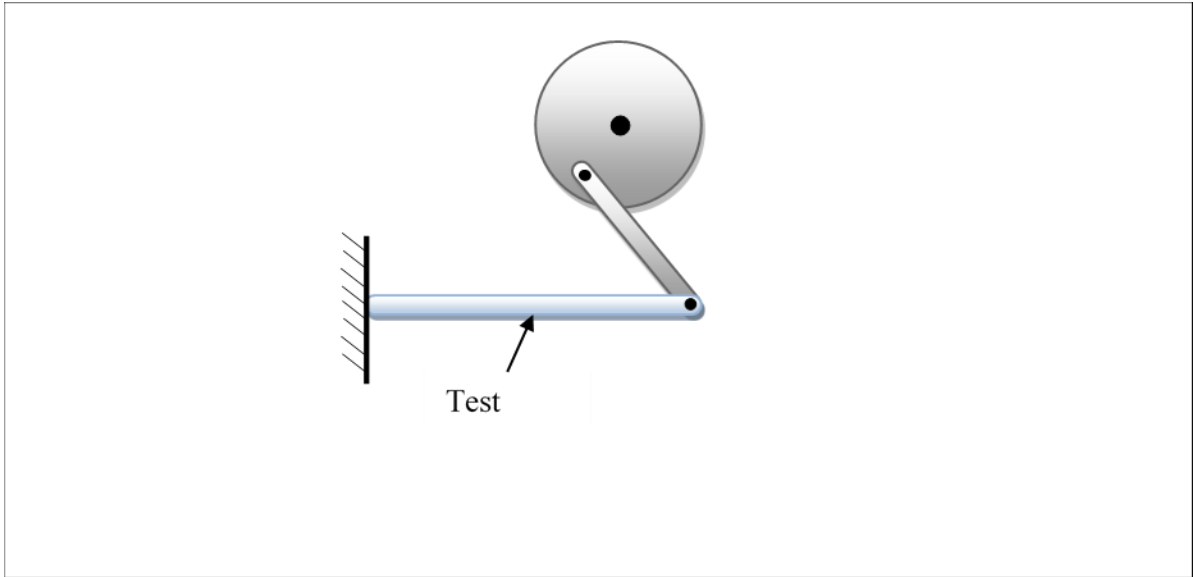


Figure 139 Constant deflection amplitude cantilever bending machine

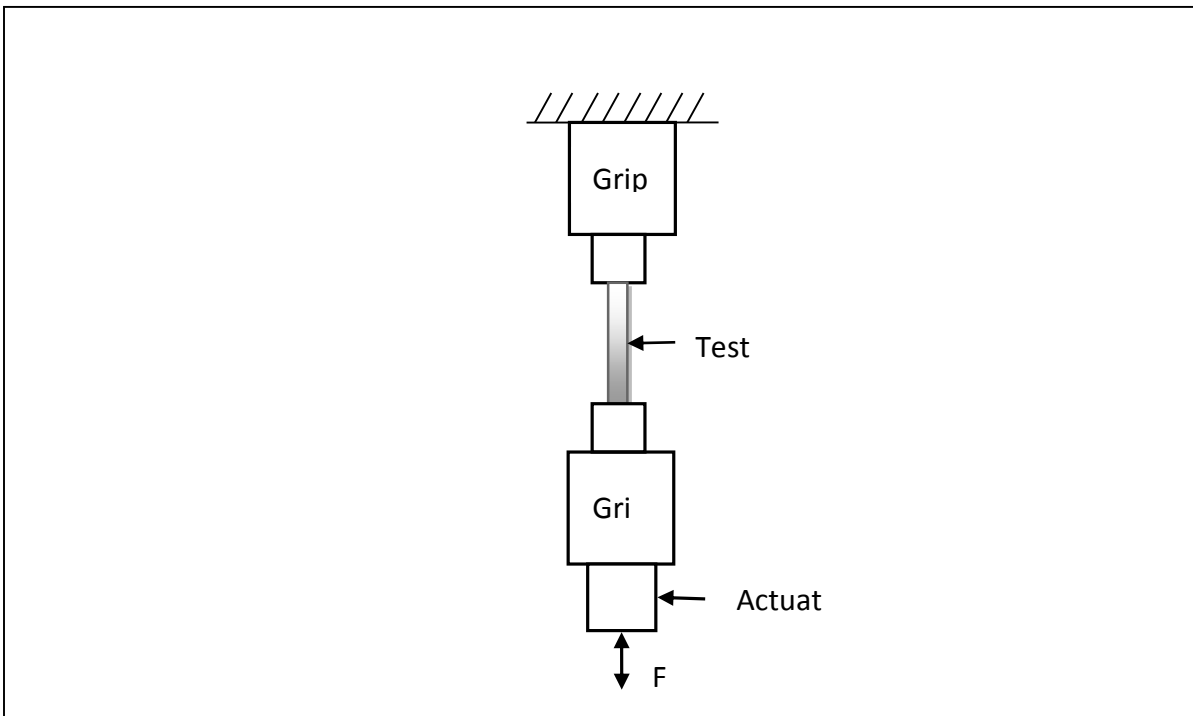


Figure 140 Axial loaded fatigue test machine



Figure 141 Closed-loop Servohydraulic test system including personal computer [74].

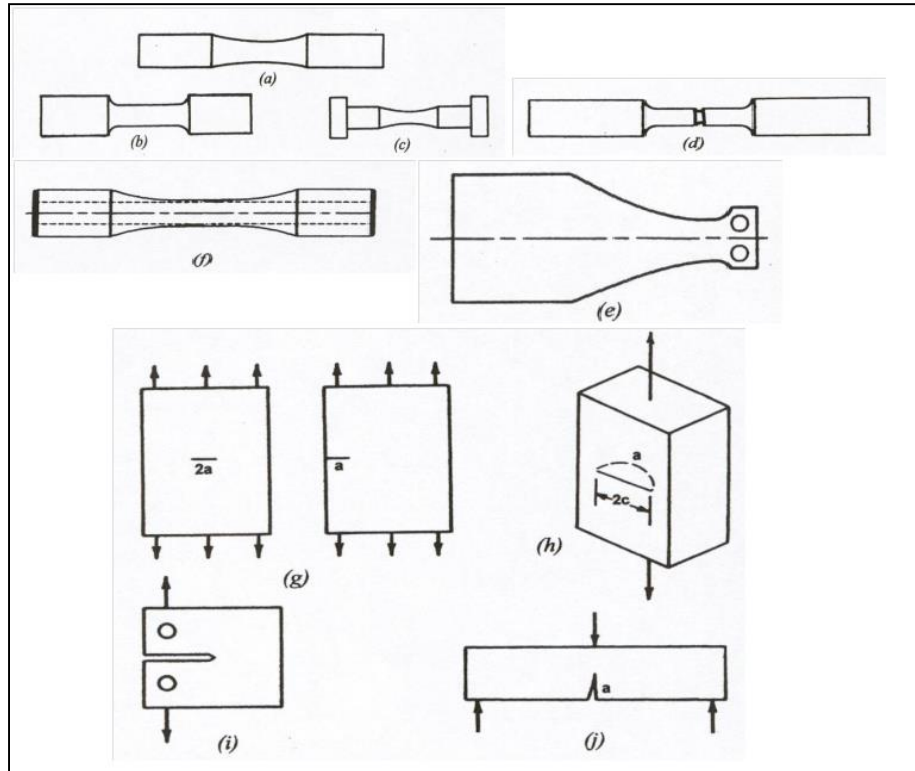


Figure 142 different types of fatigue test specimens [1].

10 REFERENCES

- [1] R. I. Stephens, A. Fatemi, R. R. Stephens and H. O. Fuchs, *Metal Fatigue in Engineering*, 2nd ed., New York, NY: John Wiley and Sons Inc., 2000.
- [2] C. H. R., *Mechanics of Materials*, 7th ed., Pearson Prentice Hall, New Jersey, 2008.
- [3] K. Serpe and R. Steven, *Manufacturing Engineering and Technology*, New Jersey: Pearson Prentice Hall Inc, 2006.
- [4] M. J., "Cyclic plastic strain energy and fatigue of metals," *International Friction damping and Cyclic Plasticity*, p. 45, 1945.
- [5] R. W. Langdraf and T. Endo, "Determination of cyclic stress-strain curve," *Journal of material science and engineering*, vol. 4, pp. 176-188, 1969.
- [6] A. B. Juli, J. C. Jess and L. H. James, *Fundamentals of metal fatigue analysis*, Englewood Cliff, New Jersey, 1990.
- [7] H. B. O., "The exponential law of endurance tests," *Proc. ASTM*, vol. 10, p. 625, 1910.
- [8] M. Roessle, A. Fatemi and A. Kosrovaneh, "Variation in cyclic deformation and strain-controlled fatigue properties using different curve fitting and measurement techniques," *SAE*, pp. 1-8, 1999.
- [9] J. H. Ong, "An evaluation of existing methods for the prediction of axial fatigue life from tensile data.," *International journal of fatigue*, vol. 15(1), pp. 9-13, 1993.
- [10] S. M. S and R. H. G., "Practical implementation of double linear damage," *Int. J. fract.*, vol. 17(2), p. 169, 1981.
- [11] N. S. K, W. P and H. T. T., "A stress-strain function for the fatigue of metals," *Journal of material science and engineering*, vol. 5, p. 169, 1970.
- [12] D. P. Walter , C. Karin and E. P. Joel , *Peterson's Stress Concentration Factors*, 2nd ed., Wiley, John & Sons, Incorporated, 1997, p. 544.
- [13] D. P. Walter and F. P. Deborah, *Stress Concentration Factor*, 3rd ed., John Wiley & Sons, 2008, p. 522.

- [14] M. Mitchell, "Fundamentals of modern fatigue analysis for design," *American Society for Metals*, pp. 385-437, 1979.
- [15] M. Roessle and A. Fatemi, "Strain-controlled fatigue properties of steels and some simple approximations," *International journal of fatigue*, vol. 22, pp. 495-511, 2000.
- [16] J. A. Baumel and T. Seeger, *Material data for cyclic loading*, Amsterdam: Elsevier Science, 1990.
- [17] JSMS, "Data book on fatigue strength of metallic materials," *Society of materials science and engineering*, Vols. 1(2,3), 1998.
- [18] S. L. Kwang and H. S. Ji, "Estimation methods for strain-life fatigue properties from hardness," *International Journal of fatigue*, vol. 28, pp. 386-400, 2006.
- [19] S. S. Manson, M. H. Hirschberg and R. W. Smith, "Fatigue behavior of materials under cycling in low and intermediate life range," *Technical Note D-1574*, 1963.
- [20] Z. L. Zang, Li, J and Q. Sun, "Two parameters describing cyclic hardening/softening behavior of metallic materials," *Journal of materials engineering*, vol. 18, pp. 237-244, 2009.
- [21] Z. P. Zhang , Y. J. Qiao, C. Li and J. Li, "Theoretical estimation to the cyclic strength coefficient and cyclic strain-hardening exponent for metallic materials," *Journal of materials engineering*, vol. 18, pp. 245-254, 2009.
- [22] R. Basan, M. franulovic and H. S. Smokvina, "Estimation of cyclic strain curves for low-alloy steel from hardness," *Journal for theory and practice in metallurgy*, vol. 49, pp. 83-86, 2010.
- [23] J. Li, Q. Sun, Z. Zhang and Y. Qiao, "Theoretical estimation to the cyclic yield strength and fatigue limit for alloy steel," *Mechanical research communications*, vol. 36, pp. 316-321, 2009.
- [24] American Iron and Steel Institute, "Bar Steel Fatigue Database," 2015. [Online]. Available: www.barsteelfatigue.autosteel.org. [Accessed 2012].
- [25] Society of Automotive Engineering, "Technical Report on Low Cycle Fatigue Properties Ferrous and Non-Ferrous," SAEJ1099, 2002.

- [26] J. Morrow, "Cyclic plastic strain energy and fatigue of metals, internal friction, damping and cyclic plasticity," *American Society for testing and materials*, pp. 45-87, 1964.
- [27] S. Manson, "Fatigue: a complex subject-some simple approximation.," Society of experimental stress analysis, Cleveland, 1965.
- [28] D. Raske and J. Morrow, "Mechanics of materials in low cycle fatigue testing," American Society for Testing and Materials, Philadelphia, 1969.
- [29] M. Mitchell, D. Socie and E. Caulfield, "Fundamentals of modern fatigue analysis," University of Illinois, 1977.
- [30] U. Muralidharan and S. Manson, "Modified universal slopes equation for estimation of fatigue characteristics," *Journal of Engineering Materials and Technology*, pp. 55-58, 1988.
- [31] J. Ong, "An improved technique for the prediction of axial fatigue life from tensile data," *International Journal of Fatigue*, pp. 213-219, 1993.
- [32] M. Meggiolaro and J. Castro, "Statistical evaluation of strain-life fatigue crack initiation prediction," *International Journal of Fatigue*, vol. 26, pp. 463-476, 2004.
- [33] J. Park and J. Song, "Detailed evaluation of methods for estimation of fatigue properties," *International Journal of Fatigue*, vol. 17, pp. 365-373, 1995.
- [34] W. Jeon and J. Song, "An expert system for estimation of fatigue properties of metallic materials," *International Journal of Fatigue*, vol. 24, pp. 685-698, 2002.
- [35] K. kim, X. Chen, C. Han and H. Lee, "estimation methods for fatigue properties of steels under axial and torsional loading," *International Journal of Fatigue*, vol. 24, pp. 783-793, 2002.
- [36] H. Neuber, "Theory of stress concentration shear-strained of prismatical bodies with arbitrary non-linear stress-strain law," *Journal of applied mechanics*, vol. 28, pp. 544-550, 1961.
- [37] T. H. Topper, R. M. Wetzel and J. Morrow, "Neuber's rule applied to fatigue of notched specimens," *Journal of Materials*, vol. 4, pp. 200-209, 1969.

- [38] J. Sharpe, N. W and K. C. Wang, "Evaluation of a modified monotonic Neuber relation," *Journal of Engineering Materials and Technology*, vol. 113, pp. 1-8, 1991.
- [39] J. Sharpe, N. W, C. H. Yang and R. L. Tregoning, "An Evaluation of the Neuber and Glinka relations for monotonic loading," *Journal of Applied Mechanics*, vol. 59, pp. 50-56, 1992.
- [40] J. Sharpe and N. W, "Elasto-plastic stress and strain concentrations," *Journal of Engineering Materials and Technology*, vol. 117, pp. 1-7, 1995.
- [41] S. M. Tipton, "Review of the development and use of Neuber's rule for failure analysis," in *SAE Trans., Sec5*, 1991.
- [42] N. E. Dowling, W. R. Brose and W. K. Wilson, "Notched member fatigue life prediction by local strain approach," *Advances in Mechanical Engineering*, vol. 6, pp. 55-84, 1977.
- [43] K. Molski and G. Glinka, "A method of elastic-plastic stress and strain calculation at a notch root," *Journal of material science and engineering*, pp. 93-100, 1981.
- [44] G. Glinka, "Energy density approach to calculation of inelastic strain-stress near notches and cracks," *Engineering fracture mechanics*, vol. 22(3), pp. 485-508, 1985.
- [45] M. Hoffmann and T. Seeger, "A generalized method for estimating multiaxial elastic-plastic notch stresses and strains, part 1," *Journal of Engineering Materials and Technology*, vol. 107, pp. 250-254, 1985.
- [46] M. Hoffmann and T. Seeger, "A generalized method for estimating multiaxial elastic-plastic notch stresses and strains, part2," *Journal of Engineering Materials and Technology*, vol. 107, pp. 255-260, 1985.
- [47] M. N. James, C. Dimitriou and H. D. Chandler, "Low cycle fatigue lives of notched components," *Fatigue & Fracture of Engineering Materials & Structures*, vol. 12, pp. 213-225, 1989.

- [48] A. Gowhari, R. A and S. J. Hardy, "Low cycle fatigue life predictions for hollow tubes with axially loaded axisymmetric internal projections," *Journal of Strain Analysis*, vol. 26, pp. 133-146, 1991.
- [49] J. Sharpe and N. W, "An interferometric strain/displacement measurement system.," *National and Space Administration*, 1989.
- [50] A. Tashkinov and M. Filatov, "Improved energy density method for inelastic notch tip strain calculation and its application for pressure vessel and piping design," *Journal of Pressure Vessels Piping*, vol. 53, pp. 183-194, 1993.
- [51] Y. L. Lee, Y. J. Chiang and H. H. Wong, "A constitutive model for estimating multiaxial notch strains," *Journal of Engineering Materials Technology*, vol. 117, pp. 33-40, 1995.
- [52] B. A and G. G, "Elastic-plastic stress-strain analysis of notches under non-proportional loading," *International conference of Biaxial/Multiaxial Fatigue and Fracture*, 1995.
- [53] Z. Zeng and A. Fatemi, "Elasto-plastic stress and strain behavior at notch roots under monotonic and cyclic loadings," *Journal of Strain Analysis*, vol. 36(3), pp. 287-300, 2001.
- [54] M. Stevan, "Fatigue life analysis of aircraft structural components," *Military Technical Institute (VTI), Ratka Resanvica*, pp. 15-21, 2005.
- [55] L. Samuelsson, "The supper-Neuber technique for correction on linear elastic FE results," in *International Congress of Aeronautical Sciences*, 2008.
- [56] H. Tanweer, M. Mujeebuddin and A. Zeesh, "Prediction of elastic-plastic behaviour of structures at notches," *Journal of Engineering Technology*, vol. 31, no. 3, 2012.
- [57] I. D. o. M. Engineering, "nptel," 2013. [Online]. Available: <http://www.nptel.in>. [Accessed 2015].
- [58] "Metal Yield," 2015. [Online]. Available: www.wikimedia.org. [Accessed 2012].
- [59] "wikipedia," 2012. [Online]. Available: http://en.wikipedia.org/wiki/Von_Mises_yield_criterion. [Accessed 2015].

- [60] P. W, "A New Method of Analysing Stresses and Strains in Work-Hardening Plastic Solids.," *Journal of applied mechanics*, vol. 23, pp. 493-496, 1956.
- [61] F. C and A. P, "A Mathematical Representation of the Multiaxial Bauschinger Effect," *Materials at High Temperature*, vol. 24(1), pp. 1-26, 1966.
- [62] M. Z, "On the description of anisotropic work-hardening," *Journal of mechanics and physics of solids*, vol. 15, pp. 163-175, 1967.
- [63] M. Z, "An attempt to describe the behavior of metals under cyclic loads using a more general work hardening model," *Acta Mechanica*, vol. 7, pp. 199-212, 1969.
- [64] Y. S. Garud, "A new approach to the evaluation of fatigue under multiaxial loadings," *Journal of engineering material and technology*, vol. 103, pp. 118-125, 1981.
- [65] C. C. Chu, "A three dimensional model of anisotropic hardening in metals and its application to the sheet metal forming," *journal of mechanics and physics of solids*, vol. 32, pp. 197-212, 1984.
- [66] N. Ohno and J. D. Wang, "Two Equivalent Forms of Nonlinear Kinematic Hardening Application to Nonisothermal Plasticity," *International Journal of Plasticity*, vol. 7, p. 637, 1991.
- [67] N. Ohno and J. D. Wang, "Kinematic Hardening Rules With Critical State of Dynamic Recovery, Part I: Formulation and Basic Feature for Ratcheting Behavior.," *International Journal of Plasticity*, vol. 9, pp. 375-390, 1993.
- [68] J. L. Chaboche, "On Some Modifications of Kinematic Hardening to Improve the Description of ratcheting Effect," *International Journal of Plasticity*, vol. 7, pp. 661-678, 1991.
- [69] Simulia, "ABAQUS analysis user's manual version 6.14," 2014. [Online]. [Accessed 2014].
- [70] Simulia, "fe-safe, Introduction to fe-safe," Simulia, Cincinnati (Mason), OH, 2015.
- [71] Baucio, Ed., ASM metals Reference book, 3rd ed., Material Park, OH: ASM International, 1993.

- [72] A. B. o. A. Standards, Metal test methods and analytical procedures, West Conshohocken, PA: ASTM, 2000.
- [73] C. R. Calladine, "Rapid method for estimating the greatest stress in a structure subjected to creep," *Journal of Mechanical Engineering*, vol. 178, pp. 198-206, 1964.
- [74] W. W, Fatigue testing and analysis of results, New York: Pergamon Press, 1961.
- [75] G. J. L, "The statistical treatment of fatigue experiments," *Elsevier Science*, 1964.
- [76] "Hard banding solution," 2015. [Online]. Available: www.hardbandingsolution.com. [Accessed 2012].